
Electronic Thesis and Dissertation Repository

8-21-2019 3:00 PM

Scaffold Design Considerations for Soft Tissue Regeneration

Madeleine M. Di Gregorio
The University of Western Ontario

Supervisor
Hamilton, Douglas W.
The University of Western Ontario

Graduate Program in Biomedical Engineering
A thesis submitted in partial fulfillment of the requirements for the degree in Master of
Engineering Science
© Madeleine M. Di Gregorio 2019

Follow this and additional works at: <https://ir.lib.uwo.ca/etd>



Part of the [Biomaterials Commons](#)

Recommended Citation

Di Gregorio, Madeleine M., "Scaffold Design Considerations for Soft Tissue Regeneration" (2019).
Electronic Thesis and Dissertation Repository. 6532.
<https://ir.lib.uwo.ca/etd/6532>

This Dissertation/Thesis is brought to you for free and open access by Scholarship@Western. It has been accepted for inclusion in Electronic Thesis and Dissertation Repository by an authorized administrator of Scholarship@Western. For more information, please contact wlsadmin@uwo.ca.

Abstract

Tissue engineering has emerged as a promising strategy for the replacement of degenerating or damaged tissues *in vivo*. Also known as regenerative medicine, integral to this therapeutic strategy is biomimetic scaffolds and the biomaterial structural components used to form them. In this study, three different biomaterial scaffolds for tissue engineering applications were fabricated: three-dimensional reverse embedded collagen scaffolds, polymer fusion printed polycaprolactone (PCL) scaffolds, and electrospun gelatin scaffolds. Three-dimensional collagen and PCL scaffolds promoted human adipose-derived stem/stromal cell (ASC) spreading, proliferation, and fibronectin deposition *in vitro*. Secondly, this study investigated the efficacy of exogenous galectin-3 delivery as a therapeutic in skin healing, given that galectin-3 has been implicated in several wound healing processes. Gelatin polymer blended with recombinant galectin-3 was electrospun into a protein delivery scaffold and employed in a murine model of cutaneous wound healing. Treatment of wounds with the galectin-3/gelatin scaffolds, or with topical galectin-3, did not enhance wound closure, re-epithelialization, or influence macrophage phenotypes *in vivo*.

Keywords

Wound Healing, Chronic Wound, Inflammation, Biomaterials, Tissue Engineering, Three-Dimensional Printing, Electrospinning, Collagen, Polycaprolactone, Gelatin, Galectin-3

Summary for Lay Audience

Following injury, the body's natural healing mechanisms mount a defense against invading pathogens and repair skin to close the wound. Factors such as disease and advanced age may reduce the body's ability to repair, resulting in a non-healing chronic wound. Chronic wounds pose a severe threat, causing pain, impaired limb function, prolonged infection, and may require hospitalization and limb amputation. Thus, research and design of biomaterials and tissue engineered scaffolds attempts to initiate healing and eventually restore tissue function. In this study, we use scaffold fabrication methods such as three-dimensional printing and polymer electrospinning to design materials that mimic the natural microenvironment and stimulate wound healing cell responses.

Co-Authorship Statement

This thesis was written by M.M. Di Gregorio with input, suggestions, and revisions from Dr. D.W. Hamilton. Experiments were designed by Dr. D.W. Hamilton. All studies were conducted by M.M. Di Gregorio.

Acknowledgements

I am sincerely thankful to Dr. Douglas Hamilton for his supervision of my research, mentorship, and support of my academic goals. Thank you for sharing your immense knowledge and showing patience and kindness during my graduate work. Production of this thesis would not have been possible without your guidance and encouragement. Thank you to my advisory committee members, Dr. Elizabeth Gillies and Dr. Amin Rizkalla, for valuable input regarding my project's organization and goals. This collaboration has been incredibly rewarding.

Thank you to all members of the Hamilton lab. It has been a pleasure to meet and work alongside an amazing group of scientists; I am thrilled to see what the future holds for each of you. JT and Georgia taught me animal studies. Adam taught me the fundamentals of electrospinning and was an excellent resource when I had questions. Sarah helped edit this thesis; Sanduni and Alex offered unlimited positivity and friendship. Thank you, Dr. John de Bruyn, for teaching me rheological testing. Thank you also to Dr. Rizkalla and Khalid for your collaboration and introducing me to polymer fusion 3D printing.

Thank you to my family especially; Dad, Oma and Nonno, for your endless encouragement and support. Sonja, my sister, who's work ethic is inspirational. Thank you, Hunter, for always being there for me, and for all the laughs.

Table of Contents

Abstract	ii
Keywords	ii
Summary for Lay Audience	iii
Co-Authorship Statement	iv
Acknowledgements	v
Table of Contents	vi
List of Tables	ix
List of Figures	x
List of Appendices	xi
List of Abbreviations	xii
1 Introduction	1
1.1 Cutaneous Wound Healing	1
1.1.1 Anatomy and Physiology of Skin.....	1
1.1.2 Acute Wound Healing	5
1.1.3 Chronic Wounds.....	9
1.1.4 Clinical Treatment of Chronic Wounds	11
1.2 Tissue Engineering and Regenerative Medicine	17
1.2.1 Biomaterial Scaffold Design Requirements	17
1.2.2 Three-Dimensional Bioprinting	18
1.2.3 Collagen-Based Biomaterials	19
1.2.4 Polycaprolactone-Based Biomaterials.....	20
1.2.5 Electrospinning.....	21
1.2.6 Stem Cell Therapy in Wound Healing	24
1.3 Galectin-3 as a Therapeutic for Chronic Wounds	26
1.3.1 Galectin-3 Overview	26
1.3.2 Roles in Inflammation	26
1.3.3 Roles in Angiogenesis	27
1.3.4 Roles in Re-Epithelialization	28
1.4 Hypothesis and Objectives.....	28
1.4.1 Rationale.....	28
1.4.2 Hypothesis.....	29
1.4.3 Objectives.....	29
1.5 References.....	31
2 Design and Validation of 3D Printed Scaffolds for Adipose Derived Stromal Cell Tissue Engineering	46
2.1 Introduction.....	46
2.2 Materials and Methods.....	47
2.2.1 Preparation of Gelatin Support Slurry.....	47

2.2.2	Gelatin Support Slurry Rheology.....	48
2.2.3	Gelatin Support Slurry Microparticle Morphology.....	49
2.2.4	Scaffold Computer-Aided Design.....	49
2.2.5	Printing of Porous Collagen Scaffolds.....	50
2.2.6	Printing of Porous Polycaprolactone Scaffolds.....	50
2.2.7	3D Printed Scaffold Morphology.....	51
2.2.8	Collagen Scaffold Hydrophilicity.....	51
2.2.9	Cell Isolation and Culture.....	51
2.2.10	<i>In Vitro</i> Proliferation Assay.....	52
2.2.11	<i>In Vitro</i> Cytoskeleton Morphology.....	52
2.2.12	<i>In Vitro</i> Fibronectin Detection.....	53
2.2.13	<i>In Vitro</i> Phenotype Study.....	53
2.3	Results.....	57
2.3.1	Preparation of 3D Printed Scaffolds.....	57
2.3.2	<i>In Vitro</i> Validation of 3D Printed Scaffolds as a Support for ASC Cell Growth.....	71
2.4	Discussion and Conclusion.....	87
2.5	References.....	90
3	<i>Investigating the Effects of Exogenous Galectin-3 in Murine Wound Healing.....</i>	93
3.1	Introduction.....	93
3.2	Materials and Methods.....	94
3.2.1	Electrospinning Galectin-3-Loaded Fibrous Gelatin Scaffolds.....	94
3.2.2	Scanning Electron Microscopy.....	95
3.2.3	Effect of Galectin-3 on Murine Wound Healing <i>In Vivo</i>	95
3.2.4	Murine Wound Healing Kinetics.....	96
3.2.5	Effect of Galectin-3 on Arginase I Enrichment During Wound Healing.....	97
3.3	Results.....	97
3.3.1	Preparation of Electrospun Galectin-3/Gelatin Scaffolds.....	97
3.3.2	<i>In Vivo</i> Effects of the Electrospun Galectin-3/Gelatin Scaffold.....	102
3.4	Discussion and Conclusion.....	118
3.5	References.....	121
4	<i>General Discussion.....</i>	124
4.1	Summary of Thesis Objectives.....	124
4.2	Summary of Fabricated Biomaterial Scaffolds.....	126
4.3	Galectin-3 to Modulate Inflammation <i>In Vivo</i>	128
4.4	Future Directions.....	130
4.4.1	Improving 3D Printed Scaffolds.....	130
4.4.2	Improving Electrospun Scaffolds.....	131
4.4.3	ASC Differentiation.....	132
4.4.4	Establishing <i>In Vitro</i> and <i>In Vivo</i> Effects of Galectin-3.....	132
4.5	Limitations of Results.....	134
4.5.1	Human Adipose Derived Stem/Stromal Cells.....	134
4.5.2	Murine Model of Wound Healing.....	135
4.6	Conclusion.....	136
4.7	References.....	138

5	<i>Appendices</i>	144
	Appendix A: Supplementary Rheological Results	144
	Appendix B: G-Code and FFF Files for Scaffolds	145
	Appendix C: Summary of Early Embedded Printing Attempts.....	163
	Appendix D: Autofluorescence of PCL Scaffolds.....	165
	Appendix E: Example of the Appearance of Individual Z Slices for Scaffold Confocal Microscopy .	166
	Appendix F: Arginase-I Immunofluorescent Staining of Day 9 Murine Wound Sections No Primary Antibody Negative Control.....	168
	Appendix G: Research Ethics Approvals	169
	<i>Curriculum Vitae</i>	171

List of Tables

Table 1. A summary of cutaneous cell types within the epidermis, dermis, and hypodermis.....	4
Table 2. Spatiotemporal coordination of normal wound healing.....	8
Table 3. Examples of clinically available moisture-retentive wound dressings.....	15

List of Figures

Figure 2.1. Preparation of the Sacrificial Support Slurry.....	55
Figure 2.2. Justification for Reverse Embedded Printing.....	59
Figure 2.3. Rheological Properties of the Gelatin Support Slurry.....	61
Figure 2.4. Effect of Blend Duration on Gelatin Microparticle Morphology.....	63
Figure 2.5. Collagen Scaffold Computer-Aided Design.....	65
Figure 2.6. Porous Collagen Scaffold Morphology.....	67
Figure 2.7. Polycaprolactone (PCL) Scaffold Morphology.....	69
Figure 2.8. ASC Proliferative Potential.....	73
Figure 2.9. ASC Cytoskeletal Morphology.....	75
Figure 2.10. ASC Cytoskeletal Morphology after 14 Days.....	78
Figure 2.11. Fibronectin Detection After 3 Days.....	80
Figure 2.12. Fibronectin Detection After 14 Days.....	83
Figure 2.13. ASC Phenotype Analysis.....	85
Figure 3.1. Effect of Gelatin on Electrospun Fiber Morphology.....	98
Figure 3.2. Refined Electrospun Fiber Morphology.....	100
Figure 3.3. Representative Images of Murine Full-Thickness Dermal Wounds.....	104
Figure 3.4. Quantification of Murine Wound Healing Kinetics.....	106
Figure 3.5. Masson's Trichrome Staining Following <i>In Vivo</i> Full-Thickness Wounding.....	108
Figure 3.6. Re-epithelialization and Epithelial Thickness Following <i>In Vivo</i> Full-Thickness Wounding.....	110
Figure 3.7. Example of Biological Variability in Masson's Trichrome Staining of Full-Thickness Wounds.....	112
Figure 3.8. Arginase I Enrichment of Full-Thickness Wounds.....	114
Figure 3.9. Arginase I-Positive Cell Density within the Wound Bed.....	116

List of Appendices

Appendix A: Supplementary Rheological Results	144
Appendix B: G-Code and FFF Files for Scaffolds	145
Appendix C: Summary of Early Embedded Printing Attempts.....	163
Appendix D: Autofluorescence of PCL Scaffolds.....	165
Appendix E: Example of the Appearance of Individual Z Slices for Scaffold Confocal Microscopy.	166
Appendix F: Arginase-I Immunofluorescent Staining of Day 9 Murine Wound Sections No Primary Antibody Negative Control.....	168
Appendix G: Research Ethics Approvals	169

List of Abbreviations

2D	Two-dimensional
3D	Three-dimensional
AMM	Amniotic mesenchymal stem cell
ANOVA	Analysis of variance
ADSC	Adipose-derived stem cell
AD-MSC	Adipose-derived mesenchymal stem cell
AMSC	Adipose MSC
ASC	Adipose-derived stem/stromal cell
Asc 2-P	Ascorbic acid 2-phosphate
AM	Additive manufacturing
BGP	β -glycerophosphate, glycerol 2-phosphate
BM	Bone marrow
BMDM	Bone marrow derived macrophage
BO	Bio-Oss
BSA	Bovine serum albumin
CAD	Computer-aided design
CCN2	Connective tissue growth factor 2
CKI	Cyclin-dependent kinase inhibitor
CSR	Controlled shear rate
CXCL	Chemokine ligand
c-Abl	Abelson tyrosine kinase
DCB	Decellularized bone
DFU	Diabetic foot ulcer
DMEM	Dulbecco's modified eagle medium
DMSO	Dimethyl sulfoxide
DNA	Deoxyribonucleic acid
ECM	Extracellular matrix
EGF	Epidermal growth factor
FBS	Fetal bovine serum
FDA	Federal Drug Association

FGF	Fibroblast growth factor
FRESH	Freeform reversible embedding of suspended hydrogel
GAG	Glycosaminoglycan
GSK-3 β	Glycogen synthase kinase-3 beta
G'	Storage modulus
G''	Loss modulus
HBOT	Hyperbaric oxygen therapy
HF	Hair follicle
HFSC	Hair follicle stem cell
IBMX	Isobutylmethylxanthine
IFN- γ	Interferon gamma
IFE	Interfollicular epidermis
IL	Interleukin
iNOS	Inducible nitric oxide synthase
LPS	Lipopolysaccharide
M1	Classical activated macrophage
M2/a	Alternative activated macrophage
M2b	Type 2 macrophage
M2c	Deactivated macrophage
M2d	M2-like macrophage
MCR	Modular compact rheometer
MMP	Matrix metalloproteinase
MRWD	Moisture-retentive wound dressing
MSC	Mesenchymal stem cell
NO	Nitric oxide
NPWT	Negative-pressure wound therapy
PBS	Phosphate buffered solution
PC	Progenitor cell
PCL	Poly(ϵ -caprolactone)
PCLDMA	Polycaprolactone dimethylacrylate
PDGF	Platelet derived growth factor

PEGDA	Poly(ethylene glycol) diacrylate
PEO	Poly ethylene oxide
PI	Propidium Iodide
PLA	Poly(lactic acid)
PLGA	Poly(lactic-co-glycolic)acid
PPAR γ	Peroxisome proliferator-activated receptor gamma
PSA	Prostate-specific antigen
PU	Pressure ulcer
PVA	Polyvinyl alcohol
RM	Regenerative medicine
RNA	Ribonucleic acid
ROI	Reactive oxygen intermediate
RPM	Revolutions per minute
RUNX2	Runt-related transcription factor 2
SC	Stem cell
SG	Sebaceous gland
SMA	Smooth muscle actin
SMC	Smooth muscle cell
STL	Stereolithography
SVF	Stromal vascular fraction
T3	Triiodothyronine
TCP	Tricalcium phosphate
TCPS	Tissue culture polystyrene
TBS	Tris-buffered saline
TE	Tissue engineering
TGF	Transforming growth factor
TIMP	Tissue inhibitor of matrix metalloproteinase
TNF	Tumor necrosis factor
TRM	Tissue resident memory
UV	Ultraviolet
VEGF	Vascular endothelial growth factor

VEGFR	Vascular endothelial growth factor receptor
VLU	Venous leg ulcer
V/V	Volume per volume
WT	Wild type
η	Viscosity
$ \eta^* $	Complex viscosity
τ	Shear stress

1 Introduction

1.1 Cutaneous Wound Healing

1.1.1 Anatomy and Physiology of Skin

Skin is part of the integumentary system and represents the largest organ of the human body.^{1,2} Skin is multifunction: it acts as a selectively permeable barrier to protect the body from harmful pathogens in the external environment; thermoregulation is achieved through blood vessel control and perspiration via sweat glands; cutaneous sensory receptors, including mechanoreceptors, nociceptors (pain) and thermoreceptors, mediate the body's interactions with the external environment.^{2,3} The epidermis, dermis, and subcutaneous hypodermis of skin are comprised of a variety of cell types with specific biological roles (Table 1).²

The epidermis is subdivided into five layers: the stratum basale, stratum spinosum, stratum granulosum, stratum lucidum, and stratum corneum.⁴⁻⁶ The epidermis is the outermost layer of skin and provides a cell-dense barrier between the body and the external environment. Keratin, the main structural protein found in the epidermis, is water insoluble and mechanically protects epithelial cells from damage or stress while preventing the invasion of foreign bodies.⁷ This water-resistant barrier is synthesized by keratinocytes, which are the dominant cell type within the epidermis, accounting for 95% of the cells located in this layer.⁸ Cornification, or keratinization, is the process by which proliferating keratinocytes of the basal layer undergo terminal differentiation into highly specialized corneocytes.^{9,10} In this process, keratinocytes migrate superficially, become flat, polyhedral, anucleated, and lose 55% of their water volume.³ Other cell types present in the epidermis include melanocytes, which produce melanosomes containing melanin.^{11,12} This protein provides skin with pigmentation and protects skin from ultraviolet radiation that can cause sunburn injury to skin, damage to nucleic DNA, and accelerated aging of skin.³ Merkel cells, also known as Merkel-Ranvier cells or tactile epithelial cells, are oval-shaped mechanoreceptors essential for light touch sensation in hairless skin of vertebrates.^{13,14} Langerhans cells also occupy the epidermis and act as antigen-presenting cells.¹⁵

The dermal layer confers pliability, elasticity, and tensile strength to skin.¹⁻³ These mechanical properties are achieved through a diverse arrangement of connective tissues, cell types, and structural components. The extracellular matrix (ECM) is a three-dimensional network consisting of extracellular fibrous proteins such as reticulin, elastin, fibronectin, laminin

and collagen, and hydrated gels of glycosaminoglycans (GAGs) linked to proteoglycans.^{2,3,16} The ECM occupies the interstitial space, providing structural support and biochemical cues to cells, while also acting as a compression buffer. The most abundant ECM protein is collagen (types I and III), which is synthesized by dermal fibroblasts and conveys structural integrity to the skin by resisting stress.³ In addition to fibroblasts, various leukocyte populations (including neutrophils and macrophages) can enter the dermis through the vascular networks in response to different stimuli. Blood vessels, lined with squamous endothelial cells, can become permeable allowing leukocytes and clotting proteins access to connective tissue.^{17,18} On the outside of blood vessels, pericytes wrap around capillaries and confer structural integrity to the vessel wall.¹⁹ Other components of the dermal layer include epidermally derived appendages such as hair follicles, nails, and sebaceous, sweat and mammary glands; also, dermal dendrocytes, mast cells, histiocytes, blood vessels, nerves, and lymphatics. The dermis is subdivided into the upper papillary dermis and lower reticular dermis, with distinctions in the structure and organization of collagen and elastin fibers between these sublayers. The dermal vasculature provides nutrition to the skin and assists the body in thermoregulation. Dilation and constriction of blood vessels leads to heat dissipation or conservation, respectively.²⁰ Thermoregulation is also controlled by arrector pili muscles (attached to hair follicles) and sweat glands.³ Piloerection, the erection or bristling of hairs, traps air close to the skin for an additional layer of insulation. Endothermic evaporation of sweat cools the surface of the skin.

The subcutaneous hypodermis consists primarily of fatty adipocytes but also contains fibrous septa of loose connective tissue, nerves, and blood vessels. Hypodermal fat lobules insulate and cushion the body, provide buoyancy, and store energy.³ In addition to adipocytes, fibroblasts and macrophages are also found in the hypodermis. Together, the epidermis, dermis, and hypodermis allow skin to maintain a physical barrier to the external environment; if this barrier is disrupted via injury to the skin, a spatiotemporally coordinated process is initiated in order to restore barrier function, maintain internal homeostasis and guard sterility.²¹

Skin cells are continually shed and replenished through desquamation, the shedding of the outermost layer of the stratum corneum. In this process, individual corneocytes are shed following degradation of cell-cell junctions known as corneodesmosomes.²² The rate of corneodesmosome degradation is highly regulated.²³ The self-perpetuating skin barrier is

maintained by permanently residing stem cells that sustain principal differentiated epidermal lineages, the interfollicular epidermis (IFE), sebaceous gland (SG), hair follicle (HF),^{24,25} and Merkel cell mechanoreceptors.²⁶ Through radiation dose-survival studies, it was proposed that stem cells comprise about 2-7% of basal layer cells²⁷ while another study of murine basal layer cells suggested a larger stem cell population, 10-12% of cells in the basal layer.²⁸ Maintenance of skin homeostasis is dependent on the ability of stem cells to replenish the turnover of apoptosing epithelial lineages.

Epithelial stem cells (SCs) reside in a specific microenvironment called the niche, where stem cell behaviour is influenced by cell-cell communication, cell-ECM interactions, and growth factors.²⁹ Cutaneous mesenchymal stem/stromal cells (MSCs) include dermal papilla cells (DPC) involved in hair follicle cycling,^{30,31} and the dermal sheath cells (DSC), which are capable of differentiating into wound healing fibroblasts that repair the dermis.³² Human FH-derived DPCs and DSCs have been shown to differentiate into adipogenic and osteogenic lineages *in vitro*, suggesting multi-lineage potential of these MSCs.³³ Hair follicle stem cells (HFSCs) reside in the follicle bulge and have been shown to give rise to IFE, HF, and SG lineages after transplantation.³⁴⁻³⁹ Under normal physiological conditions, however, lineage tracing in mice has shown that HFSCs only contribute to HF regeneration and not the SG, IFE, or infundibulum.⁴⁰⁻⁴⁵ In the IFE, a single basal layer of proliferative cells replenishes suprabasal terminally differentiated cells. This basal layer consists of a heterogeneous proliferative population of quiescent, long-lived IFE SCs and short-lived, differentiation-fated progenitor cells (PC).⁴⁶⁻⁵² Between the bulge and SG is the isthmus, where another pool of resident SCs maintain the isthmus, SG, SG ducts, and infundibulum.⁵³⁻⁵⁶ Epithelial SCs are normally confined to compartmental niches but can be activated and recruited to different regions during wound repair where these SCs contribute to regeneration of wounded skin.^{29,55,57-59}

Table 1. A summary of cutaneous cell types within the epidermis, dermis, and hypodermis.

	Cell Type	Function
Epidermis	Keratinocyte	Express involucrin and keratin; form barrier to external environment ⁹
	Merkel Cell	Mechanosensitive; Merkel cell-neurite complexes ¹⁴
	Melanocyte	Produce melanin pigment for skin colour ¹²
	Langerhans Cell	Capture microbial antigens to become antigen-presenting cells ¹⁵
	Tissue-resident memory (TRM) ($\alpha\beta$) T Cell	Rapid recognition of previously encountered pathogens ⁶⁰
	Epidermal-Resident ($\gamma\delta$) T Cell	Balance keratinocyte differentiation and proliferation with the destruction of infected or malignant cells ⁶¹
Dermis	Fibroblast	Secrete ECM, mainly collagen types I and III ⁶²
	Neutrophil	Phagocytosis and intracellular degradation, release of granules, and formation of neutrophil extracellular traps ⁶³
	Macrophage	Classical (M1) phagocytose foreign bodies, release pro-inflammatory cytokines ⁶⁴ Alternative (M2) induce proliferation and collagen production, release anti-inflammatory cytokines ⁶⁴
	Endothelial Cell	Line blood vessels (arteries, veins, capillaries and sinusoids) ¹⁸
	Pericyte	Contractile cells present at intervals along capillaries; attribute structural integrity and constrict during ischemia ¹⁹
	Dendrocyte	Antigen presentation ⁶⁵
	Mast Cell	Regulate vasodilation, vascular homeostasis, innate and adaptive immune responses, angiogenesis, and venom detoxification ⁶⁶
	Histiocyte	Connective tissue resident; phagocytosis and antigen presentation ⁶⁷
Hypodermis	Adipocyte	Store energy and cushion body ⁶⁸
	Mechanoreceptors*	Type 1 sense quivering and touch ¹³ Type 2 sense vibration and pressure ¹³
	Thermoreceptors*	Cold type sense temperatures < 30°C ¹³ Heat type sense temperatures 32-48°C ¹³
	Nociceptors*	Mechano sense significant pressure, inflammatory mediators, ischemia mediators ¹³ Polymodal sense inflammatory mediators ¹³
	Pruriceptors*	Sense histamine and inflammatory mediators ¹³

*Cutaneous sensory endings of the peripheral nervous system innervating the skin derive from the dorsal root ganglia and the trigeminal ganglia. Nerves in the skin form epidermal plexus from which some fibres cross the dermo-epidermal junction.¹³

1.1.2 Acute Wound Healing

Following injury, normal wound healing is achieved via four overlapping phases: hemostasis, inflammation, proliferation, and remodeling (Table 2). Thrombin, the principal enzyme involved in hemostasis, is produced primarily in the liver and circulates systemically in the blood plasma. This serine protease cleaves fibrinogen to create a polymerized fibrin matrix that captures circulating platelets to form a hemostatic plug and establish hemostasis.⁶⁹ Within the first hour post-injury, inflammatory cytokines such as interleukin (IL) -1 α , IL-1 β , IL-6, IL-8, tumor necrosis factor (TNF) - α , platelet derived growth factor (PDGF), and transforming growth factor (TGF) - β , are released by aggregated platelets to recruit early inflammatory cells and initiate healing.⁷⁰ When injury first occurs, vasoconstriction is induced locally to reduce blood loss. However, this is subsequently reversed to allow changes in blood flow, an increase in permeability of blood vessels, and the infiltration of fluid, proteins, and leukocytes from the circulatory system into the site of tissue damage.

Recruited leukocytes produce a chemotactic gradient that stimulates the migration of neutrophils, monocytes, smooth muscle cells (SMCs), and fibroblasts. Neutrophils, which comprise 60-70% of the leukocyte population, are part of the innate immune response and one of the first cell types to respond to injury. Neutrophils are granulocytes and lack immune memory; they function by releasing reactive oxygen species to produce toxic metabolites (hydrogen peroxide) that kill invading bacteria and certain fungal species, secreting serine proteases and matrix metalloproteinases (MMPs) to debride necrotic tissue, and phagocytosing dead bacteria and wound debris.⁷⁰ Neutrophils cannot renew their lysosomes and are short-lived, resulting in the formation of a white exudate called pus within the wound bed. Monocytes responding to paracrine signals, including TGF- β , differentiate into macrophages capable of phagocytosing debris and exhausted neutrophils. Macrophages that are classically activated (M1 polarization), typically by interferon (IFN) - γ or lipopolysaccharide (LPS) *in vitro*, produce pro-inflammatory cytokines, phagocytize microbes, express inducible nitric oxide synthase (iNOS), and produce nitric oxide (NO) or reactive oxygen intermediates (ROI) to protect against bacteria and viruses. Alternatively activated (M2) macrophages, typically activated by exposure to certain cytokines such as IL-4, IL-10, or IL-13, produce either polyamines to induce proliferation or proline to induce collagen production. These M2 macrophages secrete arginase I and anti-inflammatory cytokines, and consequently are associated with resolution of the inflammatory phase, pro-

regenerative wound healing and tissue repair. Following exhaustion of inflammatory cells, exocytotic release of a second wave of signaling molecules, including TGF- α , TGF- β , fibroblast growth factor (FGF) 2/basic FGF (bFGF), PDGF, and vascular endothelial growth factor (VEGF), recruits keratinocytes, fibroblasts, endothelial cells, and pericytes to initiate the overlap of late-stage inflammation with the proliferative stage of healing.⁷¹

During fibroplasia, fibroblasts proliferate and migrate into the wound bed, depositing collagen-rich ECM to slowly replace the fibrin clot with a permanent matrix.⁷² This ECM improves structural integrity of the damaged site and provides a supportive scaffold for neovascular growth (angiogenesis) and re-epithelialization.⁷³ Through cadherin-11-mediated adhesion between macrophages and fibroblastic cells, TGF- β -producing macrophages and TGF- β -activating myofibroblasts are held in close proximity, facilitating efficient myofibroblast activation and stimulating fibrosis.⁷⁴ Persistent fibroplasia leads to the accumulation of a dense fibrotic scar tissue.⁷² As ECM is deposited, re-epithelializing keratinocytes upregulate anti-fibrotic urokinase-type plasminogen activator, MMP-1 and MMP-3, and downregulate pro-fibrotic connective tissue growth factor 2 (CCN2), collagen I and II, fibronectin, plasminogen activator inhibitor-1, α -smooth muscle actin (α -SMA), and tissue inhibitor of matrix metalloproteinase (TIMP)-2/3.⁷⁵ Maturation of the granulation tissue, composed of the newly deposited collagen network and migrating endothelial cells and macrophages, is enhanced by angiogenesis and re-epithelialization.⁷⁶

Angiogenesis, vascular growth from pre-existing vasculature via endothelial cell migration, proliferation and vessel formation, re-establishes normoxia and nutrient supply to tissues.^{71,77} Post-injury hypoxic conditions promote the release of inflammatory mediators to increase vascular permeability and dilation, facilitating endothelial cell migration into the wounded tissue.^{78,79} Angiogenic factors, particularly VEGF-A and FGF-2/bFGF, promote endothelial cell proliferation and the formation of new capillary tubules in the developing granulation tissue to restore vascularization.⁸⁰⁻⁸³ To prevent excessive scar formation, wound progression through fibroplasia and angiogenesis must be tightly regulated. Proteolytic ECM remodeling decreases ECM density, decreases cell-ECM interactions (by cleaving matrix components such as collagen, fibronectin and laminin⁸⁴), and releases matrix-bound angiogenic factors to stimulate endothelial cell migration.⁸⁵

During re-epithelialization, epithelial cell proliferation and migration is initiated. Fibroblasts and macrophages release epidermal growth factor (EGF), TGF- α and FGF, initiating re-epithelialization.⁸⁶ Hemidesmosome links between the epidermis and the basement membrane separate, releasing cell-ECM linkages. Keratinocyte migration over the granulation tissue separates the eschar from viable tissue. Behind the migrating epithelial tongue, keratinocytes proliferate and mature, ultimately restoring the barrier function.⁸⁷ Macrophages secrete TGF- β that signals fibroblasts to migrate into the granulation tissue and produce new ECM components.⁸⁸ Macrophage-activated myofibroblasts, highly contractile cells, anchor to the ECM and contract the wound, pulling opposing edges together.^{86,87} Myofibroblast contractility is dependent on a positive feedback loop initiated by endogenous TGF- β and tensile forces, which increases the density of α -SMA enrichment in stress fibers, increases force production and tension development, and consequently upregulates TGF- β . Re-modeling of granulation tissue occurs as fibroblasts upregulate expression of collagen I, and MMPs degrade the temporary collagen III matrix. In the final stages of remodeling, the scar tissue consists of mainly an acellular matrix of parallel collagen I fiber bundles.^{87,89,90} The repaired tissue which has the composition of a scar does successfully restore barrier function, but possesses approximately 80% of the mechanical elasticity of unwounded skin.^{87,91} However, in certain instances, skin can remain compromised and demonstrate a reduced ability to heal.

Table 2. Spatiotemporal coordination of normal wound healing.

Post-Injury Period	Within Minutes	Within Hours	~3 Days	~1 Week	Weeks	Years
Wound Healing Stage	Hemostasis	Inflammation	Proliferation		Remodeling	
Active Cell Types	-Platelets	-Neutrophils -M1 macrophages -Mast cells	-Fibroblasts -M2 macrophages -Endothelial cells -Keratinocytes	-Myofibroblasts		
Major Events	-Vasoconstriction -Hemostatic plug formation -Chemotactic recruitment of inflammatory cells	-Inflammatory cell migration into the wound bed -Defense against foreign infection	-Granulation tissue -Fibroplasia -Randomly oriented ECM -Angiogenesis -Re-epithelialization	-Parallel collagen ECM -Contraction of wound bed -Scar management		

1.1.3 Chronic Wounds

Reduced ability to heal is often the result of a variety of morbidities including vascular insufficiency, diabetes, malnutrition, patient age, pressure, infection, and edema.⁷⁰ A persistent tissue injury that fails to proceed through the reparative process after 3 months is classified as a chronic (non-healing) wound.⁹² Such wounds become a significant burden to the patient, causing pain, impaired limb function, sepsis, hospitalization and the need for amputation. Worldwide, chronic wounds account for approximately 4% of the global healthcare expenditure.⁹³⁻⁹⁶ Within Canada, chronic wounds pose a significant burden to the Canadian healthcare system, costing on average \$10,000 to treat a single wound.⁹⁷ The most common chronic wound classifications are venous leg ulcers (VLUs), arterial ulcers, diabetic foot ulcers (DFUs) and pressure ulcers (PUs).

The largest class by occurrence is VLUs, caused by chronic venous insufficiency as a result of trauma, aging, obesity, pregnancy, phlebitis, deep vein thrombosis, congestive heart failure, and a history of ulcers.^{70,89} Arterial ulcers, formed following arterial disease and inadequate blood supply to the skin, are most commonly the manifestation of systemic atherosclerosis.^{98,99} DFUs affect approximately 10% of diabetics annually.⁸⁹ Hyperglycemia-induced impaired nerve function reduces sensation, causing foot deformity, limited joint mobility, and structurally compromised peripheries.⁹⁸ DFUs most frequently appear on the sole of the foot where peripheral neuropathy of the foot increases the risk of ulceration from repeated mechanical stress.¹⁰⁰ Finally, PUs are localized areas of necrotic tissue formed as a result of extended periods of soft tissue compression, causing localized hypoxia and ischemic-reperfusion injury. PUs, also called bedsores or decubitus ulcers, are associated with impaired mobility, decreased level of consciousness, diabetes mellitus, peripheral vascular disease, malnutrition, and fecal/urinary incontinence.¹⁰¹ With increasing prevalence of obesity, diabetes and atherosclerosis, as well as an aging population, the impact of chronic wounds on the healthcare system will continue to rise.

At the molecular level, chronic wounds are characterized by dysfunctional proteolytic activity and prolonged inflammation, bacterial infection, cellular senescence and constrained cell proliferation.¹⁰² Enrichment of proteases and reactive oxygen species leads to a deficient ECM structure, damages cell membranes leading to premature senescence, and interferes with the transcription of pro-inflammatory signaling molecules, up-regulating various MMPs and down-regulating antagonistic TIMPs.^{103,104} Prolonged inflammation and greater than normal

populations of neutrophils and macrophages are hallmarks of chronic wounds. Abundance of these inflammatory cells cause accumulation of proteolytic factors such as MMP-9, neutrophil elastase, and proteinase-3 within chronic wounds, indicating a disturbed balance between proteases and their inhibitors.¹⁰⁵ This imbalance can lead to the excessive breakdown of matrix, ultimately hindering re-epithelialization and angiogenesis.

During prolonged inflammation, neutrophils and macrophages release pro-inflammatory cytokines such as IL-1 β and TNF- α which advances further MMP and TIMP imbalance. Under normal conditions, pro-fibrotic macrophages release soluble factors (such as TGF- β , PDGF- β and galectin-3) to counteract the degradation of extracellular matrix by MMPs.¹⁰⁶ TGF- β , PDGF- β and galectin-3 increase the deposition of matrix and the release of TIMPs by myofibroblasts. Chronic wounds however represent a function of significantly increased neutrophil and pro-inflammatory macrophage populations. Thus, the switch from inflammation to proliferation, requiring downregulation of anti-inflammatory factors and initiation of fibroplasia, neoangiogenesis, and remodeling, is severely compromised in chronic wounds. In particular, the expression of IL-1 β and TNF- α is upregulated during pathological wound healing.^{86,107,108} These cytokines signal macrophages to release MMPs, and also suppress the synthesis of ECM proteins and TIMPs. A structurally immature ECM reduces or inhibits cellular migration, prolonging the wound healing process.^{86,107,108} This characteristic unbalanced proteolytic activity results in extreme degradation of ECM components, protease inhibitors, growth factors, and other wound repair mediators, creating a harsh microenvironment with abnormal biochemical and physical cues. Wound healing cell types rely on biochemical and physical signals in order for normal cellular activity to take place, which again delays the final stages of wound healing. Bacterial colonization of the affected tissue is an additional challenge resulting from compromised barrier function. This continuous bacterial presence contributes to a feedforward mechanism which elevates the proinflammatory response, preventing inflammatory resolution even further. Substantial bacterial presence generates a biofilm, a slippery buildup of bacteria, which impedes wound closure and blocks topical application of antibiotic treatments.^{105,109–111}

Angiogenesis normally ensures adequate nutrition and oxygenation during tissue healing. However, in the chronic wound microenvironment, antiangiogenic factors, for example myeloperoxidase, are upregulated while angiogenic stimulators, such as extracellular superoxide dismutase and VEGF, are diminished.¹¹² Proteolytic degradation of angiogenic factors and

pathological angiogenesis are possible mechanisms that lead to the development of inadequate capillary growth witnessed in chronic venous leg ulcers.^{113–116}

1.1.4 Clinical Treatment of Chronic Wounds

Medical intervention for a chronic wound includes debriding (cleaning) the affected region, removal of necrotic tissue, management of localized and systemic infection, application of bandages, mechanical off-loading to reduce shear forces on the skin and injury recurrence, and restoration of blood flow to the wounded tissue.¹¹⁷ Furthermore, the application of advanced multidisciplinary wound care strategies, such as combining pressure off-loading and revascularization with biomedical engineering approaches, has under certain circumstances significantly improved chronic wound healing outcomes.^{118–120}

Debridement involves the removal of unwanted calluses, necrotic tissue, foreign debris, and pathogens from the wound in order to minimize infection and expose underlying healthy tissue to the wound edge.⁹⁰ Surgical debridement is the preferred method and involves excising tissue with scissors or a scalpel. However, this procedure can be painful and may damage viable tissue depending on the surgeon's ability to distinguish regions of affected tissues from unaffected. Thus, a more accurate means of targeting only the nonviable tissue is by autolytic debridement, which degrades nonviable tissue via the catabolic action of endogenous enzymes. DuoDerm, a clinically available hydrocolloid dressing with autolytic properties, reduced pericapillary fibrin cuffs that can cause venous disease and chronic venous ulcers.¹²¹ Similarly, enzymatic debridement involves exogenous enzymes added exogenous to topical ointments to degrade and remove necrotic material from the wound bed.¹²² Collagenase, the sole enzymatic debriding agent approved by the Federal Drug Association (FDA), degrades bioactive fragments within the wound bed in order to increase endothelial cell and keratinocyte migration.¹²³ Lastly, biosurgical debridement involves the usage of medical grade maggots (*Lucilia sericata*, *Phaenicia sericata*, *Lucilia cuprina*) that ingest necrotic tissue.^{122,124–126}

Infection management includes the use of cleansing agents such as water, saline, or 0.5% acetic acid, and topical antimicrobials such as low-concentration povidone iodine, cadexomer iodine gel beads, metronidazole gel, silver, and medical grade manuka honey, to reduce bacterial growth.¹²² Unchecked bacterial invasion can be detrimental as infection spreads into adjacent

tissues, leading to necrotizing infection, gangrene, or deep abscesses with the need for amputation.¹²⁷

Covering a wound with dressings provides protection from infection, maintains moisture, absorbs exudate, and promotes tissue regeneration.^{89,122} Specifically, moisture-retentive wound dressings (MRWDs) limit moisture vapor transmission from the wound to less than 35 g/m²/hr, which promotes keratinocyte migration and wound healing.^{128–130} MRWDs can be fabricated from films, foams, hydrocolloids, alginates, and hydrogels.

MRWDs differ in their efficacy, advantages and disadvantages (Table 3). Films are comprised of thin, elastic sheets of polyurethane applied mainly to the site of acute surgical wounds.^{90,122} While films are gas permeable, transparent for visual inspection of wound progression, and exclude bacteria from entering the wound, they offer limited liquid drainage and can also damage tissue when removed. MRWD foams are moisture absorbent, comfortable to wear, and drape over tissue, but may require application of additional dressings to facilitate occlusion or drainage.^{90,122,131} Hydrocolloid dressings combine a foam or polyurethane film dressing with a hydrocolloid matrix that, when applied to wound exudate, forms a gel that promotes autolytic debridement and granulation tissue formation.^{90,122,131} However, hydrocolloids should not be employed for highly exudative or infected wounds as they may cause skin maceration.^{132,133} Alginate dressings are composed of sodium and calcium salts of alginic acid. Alginates have haemostatic properties, thus are highly absorbent and ideal for highly exudative wounds, but not for dry wounds.^{90,122,131} Lastly, hydrogels are macromolecular polymer gels that absorb wound exudate and stimulates autolytic debridement.^{90,122} Hydrogels may be applied to a range of wounds from mildly to highly exudative, but maceration can occur.¹³¹ These MRWDs are largely passive dressings, and the ideal clinical treatment of chronic wounds would also possess an ability to actively stimulate biological healing responses.

Bioengineered skin substitutes, in addition to retaining moisture, stimulate healing and are of interest in tissue engineering and regenerative medicine. Epidermis substitutes, including Epicel®, Epidex®, Myskin®, Bioseed®, and Cellspray®, are predominantly autogenic keratinocyte expansions formulated into delivery dressings or as suspensions that can be topically ejected or sprayed onto the wound site.¹³⁴ Dermal substitutes are 3D biomaterial matrices that match the native ECM in terms of structural, elastic, and mechanical properties. Acellular dermal substitutes, such as Oasis® and Alloderm®, are nonimmunogenic,

mechanically robust, and can be used off the shelf; however, these substitutes depend on host cell infiltration to initiate angiogenesis and remodeling.¹³⁴ In contrast, collagen-GAG cellular matrices such as Dermagraft® and OrCel® are pre-seeded with neonatal human foreskin fibroblasts and/or keratinocytes and have been shown to reduce wound contractility to allow re-epithelialization to restore a more natural tissue barrier.^{135,136} Bilayer skin substitutes contain both epidermal and dermal components. Apligraf® is an FDA-approved skin substitute consisting of an epidermal neonatal human foreskin keratinocyte layer and an underlying dermal bovine type I collagen layer seeded with neonatal human fetal fibroblasts.^{90,122} Apligraf® dressings already contain within them the cells responsible for the production and delivery of cytokines, growth factors and ECM components to the wound bed, however these bilayer substitutes are expensive and have a limited shelf life of 5-10 days.^{137,138}

Healing outcomes can also be influenced by employing adjuvant therapies in conjunction with standard medical practice. Negative-pressure wound therapy (NPWT) or vacuum-assisted closure therapy applies sub-atmospheric pressure to a local area of tissue damage through a specialized pump.¹³⁹ NPWT reduces tissue edema, improves circulation, promotes granulation tissue formation and inhibits bacterial growth.¹⁴⁰ Hyperbaric oxygen therapy (HBOT) involves briefly inhaling 100% oxygen while inside a pressurized chamber.¹⁴¹ Heightened blood and tissue oxygenation by HBOT improves oxygen delivery to hypoxic tissues and vasoconstricts surrounding healthy tissue, alleviating edema and permitting innate biological combating of infection and ischemia to ensue.¹⁴² Topical addition of growth factor formulations have also been used in chronic wound healing. For instance, a gel composition of recombinant PDGF (Regranex®/Becaplermin) has been employed to mediate cell division, migration and proliferation. Daily Becaplermin application significantly aided wound closure in PUs and in DFUs.^{143,144} However, there is increased risk of cancer mortality associated with excessive use (three or more dispensaries) of Becaplermin.¹⁴⁵ Notably, a significant limitation of topical growth factors is their rapid proteolytic degradation.¹⁴⁶

Current clinical strategies, including wound debridement, moisture-retentive dressings, and adjuvant therapies, have various disadvantages and do little to resolve a chronic wound. In Canada, 3.5 million individuals live with diabetes and DFUs will affect one quarter of these patients.^{95,147} DFUs are the most common cause of non-traumatic lower limb amputations, with 20% of DFU patients requiring amputation.⁸⁹ Furthermore, these amputations are associated with

a high of mortality rate; in Canada, 30% of patients with diabetes die within one year of amputation and 69% of patients within five years.^{96,148} Despite the multitude of wound healing products available, chronic wounds continue to be a significant burden on patients and the healthcare system. In recent years, attention has focused on development of biologically active and tissue mimetic technologies.

Table 3. Examples of clinically available moisture-retentive wound dressings.^{90,122,149,150}

Category	Advantages	Disadvantages	Examples
Films	<ul style="list-style-type: none"> -Suitable for flat, shallow wounds with low to medium exudates -Promote moist environment -Adhere to healthy skin but not to wound -Allow visual checks -May be left in place several days -Useful as secondary dressing 	<ul style="list-style-type: none"> -Provide no cushioning -Not for infected or heavily exuding wounds 	<p>Tegaderm (3M Healthcare), Polyskin II (Kendall Healthcare), Bioclusive (Johnson & Johnson Medical), Blisterfilm (The Kendall Co), Omniderm (Omikron Scientific Ltd), Proclude (ConvaTec), Mefilm (Mölnlycke Health Care), Carrafilm (Carrington Lab), and Transeal (DeRoyal)</p>
Foams	<ul style="list-style-type: none"> -Flat, shallow wounds (control of exudate depending on type of foam) -Provide a degree of cushioning 	<ul style="list-style-type: none"> -Need secondary dressing -Need to be replaced after 2 to 3 days 	<p>Polymem (Ferris Corp), Allevyn (Smith & Nephew United), Biopatch (Johnson & Johnson Medical), Curafoam (The Kendall Co), Flexzan (Dow Hickam), Hydrasorb (Tyco/Kendall Co), Lyofoam (ConvaTec), and Mepilex (Mölnlycke Health Care)</p>
Hydrocolloids	<ul style="list-style-type: none"> -Useful for flat, shallow wounds with low to medium exudate -Absorbent -Conformable -Suitable for heel, elbow, sacrum 	<ul style="list-style-type: none"> -May cause maceration -Need secondary dressing 	<p>Duoderm (ConvaTec), NuDerm (Johnson & Johnson Medical), Comfeel (Coloplast Sween, Inc), Hydrocol (Dow Hickam), Cutinova (Smith & Nephew), Replicare (Smith & Nephew United), and Tegasorb (3M)</p>
Alginates	<ul style="list-style-type: none"> -Useful in cavities and for undermining wounds -Highly absorbent 	<ul style="list-style-type: none"> -Need secondary dressing -Need to be changed daily 	<p>Algiderm (Bard), Algisite (Smith & Nephew), Algisorb (Calgon-Vestal), Algosteril (Johnson & Johnson Medical), Kaltostat (ConvaTec), Curasorb (The Kendall Co), Sorbsan (Dow</p>

			Hickam), Melgisorb (Mölnlycke Health Care), SeaSorb (Coloplast), and Kalginate (DeRoyal)
Hydrogels	<ul style="list-style-type: none"> -Supply moisture to wounds with low to medium exudate -Suitable for sloughy or necrotic wounds -Useful in flat wounds and cavities -May be left in place several days 	<ul style="list-style-type: none"> -Need secondary dressing -May cause maceration 	<ul style="list-style-type: none"> Vigilon (CR Bard), Nu-gel (Johnson & Johnson Medical), Tegagel (3M), FlexiGel (Smith & Nephew), Curagel (The Kendall Co), Clearsite (Conmed Corp), Curafil (The Kendall Co), Curasol (The Kendall Co), Carrasyn (Carrington Laboratories), Elasto-Gel (SW Technologies), Hypergel (Scott Health Care), Normgel (SCA Hygiene Products), 2nd Skin (Spenco Medical, Ltd), and Transigel (Smith & Nephew)

1.2 Tissue Engineering and Regenerative Medicine

Tissue engineering is an area of research that is focused on the combination of natural and synthetic scaffolds, cells, and biologically active molecules in an attempt to form biologically functional tissues. Similarly, regenerative medicine describes the use of engineered biological materials in conjunction with the body's innate proliferative mechanisms to expand cell populations and reconstruct tissues *in vivo*. Focuses of tissue engineering research include the development of bioengineered materials, skin substitutes, biomolecule delivery systems, and stem cell therapies.

1.2.1 Biomaterial Scaffold Design Requirements

Biomaterials can be considered natural or synthetic materials that are designed to interact with biological tissues for augmenting or replacing a native tissue. Tissue engineering scaffolds have the potential to mimic the native extracellular matrix at the nanoscale level, which is important for matrix production, neoangiogenesis and cellular ingrowth, leading to regeneration of tissues.¹⁵¹ Biomaterials must be biocompatible, nonimmunogenic, and if desirable, biodegradable; that is, a biomaterial should perform safely within the biological environment and any degradation products should be nontoxic. Scaffold structures should ideally mimic native ECM and display a fiber diameter of 50 to 500 nm, 90% porosity, and average pore size of 100 μm to facilitate mass transfer and cell infiltration.¹⁵²⁻¹⁵⁶ Various fabrication methods for construction of three-dimensional biomimetic scaffolds have been investigated, including electrospinning, phase-separation, freeze drying, and self-assembly.¹⁵⁷ However, the challenge of fabricating complex and functional tissues still exists. Current biomaterial fabrication methods are limited in the ability to control hierarchical architecture of scaffolds, formed by nanofibers and nanopores. The insufficient vascularization systems of biological substitutes results in limited diffusion properties of these biomimetic scaffolds.¹⁵⁷ As a consequence, biomaterial scaffolds contain a necrotic center where oxygen transport, nutrient deposit, and waste removal are limited, and viable cells do not penetrate. As such, a scaffold manufacturing technique with controlled material deposition is desirable in order to create complex architectures with optimized porosity.

1.2.2 Three-Dimensional Bioprinting

Additive manufacturing (AM), also known as three-dimensional (3D) printing, is a mechanized fabrication method that builds objects by repeatedly depositing material layer-by-layer. Adjacent layers fuse together during the process until the final object has been achieved. This technique first requires the creation of a 3D digital model that is generated using computer-aided design (CAD) software. Since building takes place layer-by-layer, the 3D model must be sliced into horizontal planes in order to generate a G-code, or programming language that will control the printer's extrusion path.¹⁵⁸ A basic 3D printer typically includes a movable print bed that can displace in the vertical (Z) direction and supports the print object, an ejector nozzle that moves in the horizontal (X, Y) plane, and the print material, which can be a wide range of materials, from plastics and metals to soft materials. G-code is sent to the printer and the object can be 3D printed.^{158,159} Advantages of 3D printing include the availability of low-cost hardware that is easily customizable, free, open-source software, and limited waste of print materials.¹⁶⁰

In 3D bioprinting, the print material is often referred to as a "bioink." Material properties to consider when choosing a bioink include the desired print resolution, ability for the printed device to be easily sterilized, shear strength and ability to recover scaffold shape, and the material stiffness. As is required for all biomaterials, bioinks need to display biological compatibility with cells and the body such that the biomaterial can adequately function in the biological environment while minimizing any foreign-body response mounted by the host immune system.¹⁶¹ Furthermore, optimized biomaterials should also exhibit the ability to be remodeled, biodegraded and bioadsorbed by cells, producing nontoxic degradation products.¹⁶¹ Commercially available bioinks include native structural extracellular matrix proteins such as collagen, gelatin, hyaluronic acid, and calcium phosphate.¹⁶²

Three-dimensional printing of soft materials, such as photocurable resins, polymer powders, or thermoplastic monofilaments, creates the additional challenge of apparent ink viscosity, which can cause the print material to flow out of its extruded shape.¹⁶³ One approach to 3D printing of soft materials is to eject the ink layer-by-layer into a secondary yield-stress support bath, embedding the print object in a granular medium. Embedding scaffold structures into a temporary, sacrificial support material is advantageous in that this technique allows for the printing of soft natural and synthetic materials that exhibit low viscosities prior to self-polymerization and gelation, allowing for the production of structures with complex architectures

and porous regions. Freeform reversible embedding of suspended hydrogels (FRESH), is a type of 3D printing that utilizes a support bath with reversible gelation properties, such that the bath can be liquified in order to liberate the 3D printed object post-printing.¹⁶⁴⁻¹⁶⁶

1.2.3 Collagen-Based Biomaterials

Twenty-nine collagen types have been identified which account for 33% of the protein in humans and 66% of the dry weight of skin.¹⁶⁷ Collagen types I-III, V, and XI have fibrillar quaternary structures. Collagen molecules are comprised of three polypeptide chains aligned in a parallel manner and coiled in a left-handed polyproline II-type (PPII) helix.¹⁶⁸ These chains arrange themselves further into a right-handed triple helix that is stabilized by interstrand hydrogen bonds and intrastrand non-covalent interactions.¹⁶⁹ Animal collagens arranged in triple helices, known as tropocollagen, form macroscopic fibers and extracellular matrix networks in tissue, bone, and basement membrane. Ninety percent of the total collagen content in human skin is type I collagen, and this type is most frequently employed for biomedical applications.¹⁷⁰

Biomaterial scaffolds fabricated using collagen have been applied extensively as a major component in dermal skin substitutes due to collagen's high biocompatibility, biodegradability, and molecular composition.¹⁷¹ Collagen extraction for biomedical application is commonly from bovine skin and tendons; porcine skin, intestine, or bladder mucosa; and rat tail sources.¹⁷² The quality and properties of extracted collagen depends on the source species and the tissue from which it was harvested. One risk associated with collagen derived from animal sources is allergic reaction and pathogen transmission.^{173,174} To overcome this complication, recombinant collagen can be produced via heterologous expression in mammalian, insect, yeast, or bacterial cells.¹⁷⁵⁻¹⁷⁷ Biorecognition of collagen is necessary since may cell-surface portions interact and bind to collagen. Cell-collagen communications are mediated by four different kinds of proteins: Pro-Hyp-Gly-recognizing receptors (for example, glycoprotein VI); integrin family receptors; integrin-type receptors that recognize cryptic motifs within collagen; and receptors with affinity for non-collagenous domains.^{178,179} Proteins containing Arg-Gly-Asp or similar integrin-recognition sequences, such as decorin and laminin, can bind to both collagen and integrins, promoting cell adhesion and proliferation.¹⁸⁰

Collagen types I-III are hydrolyzed by collagenases MMP-1, MMP-2, MMP-8, MMP-13, and MMP-14. Intrinsic biodegradability by endogenous collagenases makes exogenous collagen

ideal for use in biomedical applications. Exogenous degradation products of collagen types I-III have been shown to induce chemotaxis of human fibroblasts and is thought to promote regeneration of tissue structure and functionality.^{181,182} Collagen can be cross-linked via chemical cross-linking agents including formaldehyde, glutaraldehyde, carbodiimides, polyepoxy compounds, acyl azides, and hexamethylene diisocyanate;¹⁶⁷ physical cross-linking methods using ultraviolet light or dehydrothermal treatment;¹⁸³ and enzymatic cross-linking such as via tissue transglutaminase.¹⁸⁴ Although chemical cross-linking can enhance biomaterial stability, residual electrophilic reagents and compounds produced upon degradation *in vivo* can be cytotoxic. An advantage of cross-linking with enzymes is this method is benign and generates no cytotoxic byproducts.

Despite limitations such as immunogenicity of xenogeneic sources and high costs, the use of natural biological materials is of interest in biomaterial fabrication. For instance, collagen-based biomaterials have been demonstrated for a variety of applications, including neural stem cell scaffolds,¹⁸⁵ cartilage,^{186,187} osteochondral,¹⁸⁸ and skin.¹⁸⁹ Tissue substitutes comprised of natural biomaterials have garnered interest for applications in transdermal and topical formulation discovery, dermal toxicity studies, and autologous grafts for wound healing. Collagen-based biomaterials can be classified as either decellularized collagen matrices or more refined scaffolds based on the extent of their purification. Decellularized collagen matrices maintain the natural tissue properties and ECM structure; cellular matter is removed from collagen matrix by physical methods such as snap freezing or high pressure, chemical treatment with acid or alkali treatment, chelation with EDTA, or treatment with detergents or solutions of high osmolarity, and trypsin enzymatic digestion to produce the biomaterial.¹⁹⁰ In contrast, more refined scaffolds are fabricated via collagen protein extraction, purification, and polymerization. Natural collagen can dissolve in aqueous solutions depending on the extant cross-linking. Refined scaffolds require collagen to first be dissolved in aqueous solution; the most common solvent systems include a neutral NaCl solution, dilute acetic acid, or a solution of proteolytic enzymes.¹⁶⁷

1.2.4 Polycaprolactone-Based Biomaterials

In certain cases, the use of natural materials is not possible and thus synthetic materials have been proposed. Advantages of synthetic materials include high reproducibility, availability,

consistent quality, and tunable material properties.¹⁹¹ One such example of a widely employed synthetic material is polycaprolactone (poly(ϵ -caprolactone), PCL), a biocompatible polyester. PCL is a semi-crystalline, aliphatic polymer, having highly ordered molecular structure.¹⁹² The structure comprises of a repeating unit of one ester group and five methylene groups. Its melting temperature is above body temperature, thus within the body the semi-crystalline structure of PCL results in high toughness.¹⁹³ Advantages of PCL include its strength and durability, which are tunable, and its ease of fabrication while allowing for precise control of product architecture.¹⁹⁴

PCL is degraded in the body under physiological conditions via hydrolytic mechanisms. Due to its high molecular weight, the polyester has a slow degradation rate of approximately two years in the biological environment.^{195–197} PCL is biocompatible and non-toxic, while its durability means that PCL has less chance to induce immunological effects.¹⁹⁸ Physical properties of PCL are easily manipulated by compounding the polymer with secondary constituents. By using a copolymer of PCL with dl-lactide, a more flexible material with a faster degradation rate than the homopolymer can be achieved.¹⁹⁵ Moreover, the high degree of permeability has made PCL an important candidate for the development of drug delivery systems and in bone tissue regeneration.^{199–203}

PCL has been established as an important biomaterial. It has been approved by the Food and Drug Administration (FDA) for several medical applications, including suture materials and subdermal contraceptive implants.^{192,204,205} In dentistry, PCL has been employed as a root canal-filling material; PCL-filled roots demonstrated proper seals to protect against the aqueous environment.²⁰⁶ In wound healing, PCL was employed as wound-dressing material and delivery system for chemical antiseptic; PCL fibers were shown to exhibit desirable tensile properties following compounding with chlorhexidine diacetate while the antiseptic conferred antimicrobial properties, even at concentrations as low as 1% (w/w).²⁰⁷ Furthermore, PCL composites have been widely studied for applications in tissue engineering scaffolds that regenerate bone, ligament, cartilage, skin, nerve and vascular tissues.²⁰⁴

1.2.5 Electrospinning

In electrospinning, a polymer solution is ejected through a needle using an applied force from a syringe pump. An electric potential is applied to the needle through which the polymer

solution passes such that as each droplet accumulates at the tip of the needle, it experiences electrostatic repulsion between the surface charges of the droplet and Coulombic force exerted by the applied electric field.²⁰⁸ As charge accumulates on the surface of the droplet, a Taylor cone is formed. Once the electrostatic charge exceeds the surface tension of the polymer solution, a polymer jet is expelled and travels towards a grounded mandrel.²⁰⁸ The solvent evaporates, leaving a porous, nonwoven fiber mat deposited on the collector. Electrospinning allows for customization of scaffold morphology by varying parameters known to affect fiber shape and size, for instance the concentration and resultant viscosity of the polymer solution, solvent identity, distance from needle to collecting surface, applied voltage, flow rate, temperature, and humidity.^{209,210}

Electrospun nanofibrous scaffolds have been proposed as a novel alternate strategy to conventional wound dressings for management of chronic skin wounds.^{211,212} Electrospinning polymer solutions can also be supplemented with bioactive agents to improve scaffold biocompatibility, biodegradability, biorecognition, sterilizability, and mechanical properties.²¹³ Due to the high surface-area-to-volume ratio, nanoscale diameter, and highly porous structure of electrospun fibers, even distribution and controlled release of bioactive molecules is possible.²¹⁴ Immediate burst release with subsequent prolonged release of bioactive factors via passive diffusion occurs during degradation of polymer fibers.²¹⁵ Antimicrobial peptides, cytokines, and growth factors, are absent in chronic wounds, but could be delivered exogenously using a biomolecule delivery system.²¹⁶ For instance, electrospun polyvinyl alcohol (PVA)-silk nanofibers have previously been supplemented with EGF, bFGF, and the antimicrobial peptide LL-37. Biological gradients of these bioactive factors were established and tested using full-thickness excisional wounds on the dorsal surface of diabetic rabbits, demonstrating this combination of factors accelerated wound healing, lowered MMP expression, regulated ECM secretion, and reduced biofilm or bacterial colonization.²¹⁷

Several limitations of electrospun scaffolds have been identified however, including 1) the structure which is densely packed nanofibers, resulting in small pore sizes, 2) potential toxicity of residual solvents or cross-linking agents, and 3) difficulty with industrial upscaling.^{218–221} Small pore sizes and densely packed fibers result from the fabrication process where overlying layers compress underlying layers during electrospinning. As a result, cellular infiltration and ingrowth is inhibited, which in turn reduces vascularization and tissue

regeneration.²²² Pore size can be increased however, by changing the polymer solution flow rate, increasing the concentration of the polymer solution to produce thicker fibers, or selective and controlled heating of the electrospinning environment to facilitate solvent evaporation.^{214,223,224} However, while thicker fibers can counteract the limitation of pore size, increasing fiber diameter inhibits cellular adhesion and migration.²²⁵ Moreover, the use of organic solvents or chemical cross-linking agents is a common concern associated with blended electrospinning due to cytotoxicity²²⁰. Safe crosslinking options include enzymatic crosslinking, electrostatic crosslinking, or hydrogen bonding with sugars or polyphenols.²²⁶ However, these alternative cross-linking methods are associated with more complicated fabrication procedures and excessive degradation of bioactive factors loaded into the scaffold for slow release.²²⁶ Lastly, the soluble nature of most biomolecules often results in rapid release from the nanofibrous scaffolds, as fast as 70% released within 30 minutes, followed by degradation or aggregation due to the instability of these proteins against proteolysis, acidity, and heat in the wound microenvironment.^{227–229} Despite these challenges, electrospinning is a viable biomaterials technique due to the great potential for customization of scaffold morphology and material composition.

Electrospun nanofibrous scaffolds can be produced using natural and synthetic polymers.²³⁰ Natural polymers such as collagen, gelatin, silk, fibrinogen and chitin are biocompatible, biodegradable and abundant in the natural environment. However, natural polymers exhibit fragile structural properties, complicated processability, vulnerability to enzymatic degradation and potential immunogenicity. Weak mechanical properties and rapid degradation of natural polymers are overcome using cross-linking to improve scaffold stability. Chemical crosslinkers such as glutaraldehyde, formaldehyde, polyether oxide, hexamethylene diisocyanate and polyurethane, acyl azide and carbodiimides, and glycerol, and physical crosslinkers including drying, heating, and UV/gamma radiation, covalently bond amino acids on adjacent scaffold structures.

Gelatin is a natural polymer alternative to collagen for use in electrospun biomaterial scaffolds.²³¹ Gelatin, a derivative of collagen, is obtained by the denaturation of collagen in either acidic or basic processing. Type A gelatin is produced by acid pre-treatment of animal samples while type B gelatin is produced by alkaline pre-treatment.²³² Gelatin maintains biocompatibility and biodegradability at much lower production costs than collagen.²³²

Moreover, gelatin scaffolds have been shown to stimulate cellular adhesion, migration and proliferation, and accelerate wound healing.^{233–235}

1.2.6 Stem Cell Therapy in Wound Healing

Characteristics of stem cells (SCs) include the ability to self-renew, maintain long-term viability, and multipotent differentiation.²³⁶ SC therapies for the treatment of chronic wounds involves delivering adult stem and progenitor cells to the site of injury. Autologous SC transplant uses a person's own SCs while an allogeneic transplant uses stem cells from a donor. In wound healing, exogenous progenitor and stem cells have been employed to improve healing and scarring outcomes through SC differentiation and secretory activities. For instance, transplanted human amniotic mesenchymal stem cells (AMMs) into a diabetic murine excisional skin wound showed that AMMs promoted wound healing and increased re-epithelialization and cellularity; AMMs demonstrated engraftment and expression of keratinocyte-specific proteins *in vivo*, while the secretome was rich in angiogenic factors IGF-1, EGF and IL-8.²³⁷ A clinical study of autologous bone marrow (BM)-derived MSC intramuscular injection into the affected limb of 24 patients with non-healing ulcers demonstrated enhanced wound healing and improved clinical parameters such as painless walking.²³⁸ In a study of 41 type 2 diabetic patients with critical limb ischemia and foot ulcers, ulcer healing, limb perfusion, and painless walking were improved in groups injected intramuscularly with BM-MSCs compared to those that received BM-derived mononuclear cells or normal saline.²³⁹ Thus far, SC therapies for wound healing applications are limited to animal models and small clinical trials, but promising results warrant further investigation into the effective delivery of autologous and allogeneic stem and progenitor cells.²⁴⁰

Adipose-derived stem/stromal cells (ASCs) are MSCs derived from fat tissue and have garnered interest in SC therapy. ASCs have been shown to proliferate rapidly and differentiate *in vitro* toward the osteogenic, adipogenic, myogenic, and chondrogenic lineages.^{236,241,242} Moreover, ASCs are resistant to mechanical damage²⁴³ and easily harvested from the body by mechanical liposuction, manual aspiration (Coleman technique), or direct surgical excision.²⁴⁴ The stromal vascular fraction (SVF) derived from adipose tissue is heterogeneous, comprised of MSCs, pre-adipocytes, endothelial cells, pericytes, T cells, and alternative M2 macrophages.²⁴⁵ MSCs can be purified from the SVF by plastic adherence and sorting based on expression of cell

surface markers including CD44, CD90, CD105, CD166, and Stro-1.²⁴⁶ Notably, ASC phenotype is controversial and under speculation; the International Federation for Adipose Therapeutics and Science and the International Society for Cellular Therapy include ASC positivity for CD13, CD36, CD73, and CD10, and negativity for CD45, CD31 and CD106.²⁴⁷ Despite the need for a distinct set of quality control criteria that can define the standard ASC phenotype, ASCs are a promising focus for cell therapy.

In wound healing studies, ASCs injected locally into excisional wounds in diabetic rats with compromised healing abilities resulted in rescue of wound healing rates in diabetic rats almost equivalent to those of wild type rats.²⁴⁸ Moreover, ASCs appear to promote wound healing under ischemic conditions. Ischemia of rabbit ears was created by ligating two of three main arteries of the ear and subsequently wounding the ear; ASC therapy enhanced wound granulation in rabbit ears under ischemia.²⁴⁹ Radiation models of chronic wounds in rats and mice have demonstrated that ASCs administered directly into the irradiated region, intramuscularly into the irradiated limbs, or intravenously resulted in enhanced wound repair.^{250–252} ASCs within the subcutaneous adipose tissue niche are in close proximity to cutaneous wounds and are implemented in the wound healing process.²⁵³ ASCs exhibit great migration potential and may infiltrate the wound to foster wound repair. For instance, ASCs transplanted into the subretinal space of injured rat retinas migrated into the retinal pigmented epithelium after 4 weeks.²⁵⁴

ASCs are capable of affecting other cells through the release of hormones, cytokines, growth factors, and micro RNAs. Extracellular vesicles released by ASCs transport gene regulatory information that in turn affects angiogenesis, adipogenesis, and other cell pathways in recipient cells.²⁵⁵ Hormones released from ASCs have been shown to affect cancer cell proliferation.²⁵⁶ In diabetic rats, ASCs injected subcutaneously into full-thickness skin wounds stimulated angiogenesis and enhanced tissue regeneration after 8 weeks; ASCs amassed in the subdermal layer of the wound boundary and amplified angiogenesis via expression of von Willebrand factor and VEGF.²⁵⁷ Through co-culturing it was demonstrated that ASCs have an anti-inflammatory effect on monocyte-derived dendritic cells *in vitro*.²⁵⁸ Moreover, proliferation of lymphocytes was diminished following treatment with conditioned media from ASCs.²⁵⁹ *In vivo*, ASC-conditioned media applied topically to rodent wounds increased capillary density and wound closure kinetics.^{260,261} Together, these results implicate the ASC secretome in wound

healing processes, including tissue regeneration, angiogenesis, and inflammatory modulation, and are of significant interest for wound healing therapeutic strategies.

1.3 Galectin-3 as a Therapeutic for Chronic Wounds

1.3.1 Galectin-3 Overview

Galectin-3 is 250 amino acids in length, and is encoded by a single gene, LGALS3, located on chromosome 14.²⁶² Galectin-3 is defined as a matricellular protein and is a member of the beta-galactoside-binding protein family. It has been shown to play important roles in cell-cell adhesion, cell-matrix interactions, macrophage activation, angiogenesis, metastasis, and cell apoptosis. Implicated in several inflammatory and immunomodulatory processes, galectin-3 is of interest for applications in chronic wound treatment.

1.3.2 Roles in Inflammation

Galectin-3 can interact with a variety of inflammatory cell types including neutrophils, monocytes, and macrophages. Neutrophils, considered to be the first responders at the start of inflammation, eliminate foreign particles following injury. Treatment of neutrophils *in vitro* with recombinant human galectin-3 suggested that the matricellular protein was capable of activating neutrophils through its carbohydrate recognition domain.²⁶³ Similarly, in another study, galectin-3 increased exudate neutrophil activity corresponding to increased surface-bound protein, while activity of peripheral neutrophils was unaltered.²⁶⁴ In addition to increasing neutrophil activity, galectin-3 has also been shown to facilitate neutrophil adhesion to laminin *in vitro* and has been implicated in the recruitment of neutrophils during *in vivo* murine cutaneous infection.^{265,266}

Inflammation is also mediated by migrating monocytes that differentiate into macrophages.²⁶⁷ Galectin-3 affects monocyte migration *in vitro*, stimulating chemotaxis at high concentrations and chemokinesis at lower concentrations. A similar migratory effect from galectin-3 is also observed in macrophages.²⁶⁸ Monocyte and macrophage migration is increased in the presence of fibronectin, indicating that galectin-3 may mediate linkage of these cells to the ECM protein.²⁶⁹ Macrophages are known to clear exhausted neutrophils from the wound by phagocytosis.²⁶⁷ Galectin-3 may influence this process given that addition of exogenous galectin-3 increases apoptotic neutrophil uptake in macrophages *in vitro*. Moreover, it has been suggested that galectin-3 acts as an opsonin, physically linking phagocytic macrophages to neutrophils,

ensuring close proximity for easy ingestion of neutrophils.²⁷⁰ Regarding macrophage phenotype and activation phases, IFN- γ and LPS or TNF- α signals monocytes to undergo classical activation into M1-polarized macrophages, which are associated with inflammatory roles. M1 macrophages produce inducible nitric oxide synthase (iNOS) as well as pro-inflammatory cytokines. In mice, markers of M1 macrophages include iNOS, chemokine ligand 9 (CXCL9), CXCL 10, and CXCL11. Monocytes can also undergo alternative activation through stimulation with IL-4 or IL-13 into M2-polarized macrophages. M2 macrophages are associated with tissue remodeling and secrete arginase I and anti-inflammatory cytokines. M2 markers in mice include arginase I, Mrc I, Fizz I, Ym1, and Ym 2.^{88,267,271} A study investigating the effect of galectin-3 on macrophage activation in bone marrow-derived macrophages *in vitro* and in resident lung and recruited peritoneal macrophages *in vivo* demonstrated that macrophages derived from galectin-3 deficient mice exhibited diminished IL-4/IL-13-induced M2 macrophage polarization, suggesting that galectin-3 is involved in the regulation of alternative macrophage activation.²⁷²

1.3.3 Roles in Angiogenesis

Galectin-3 has been shown to induce angiogenesis. Capillary tube formation of human umbilical cord endothelial cells grown on a matrigel was stimulated with galectin-3 supplementation *in vitro*. *In vivo*, a galectin-3-loaded matrigel was able to induce angiogenesis in nude mice.²⁷³ Galectin-3 may modulate VEGF and FGF-2-mediated angiogenesis by activating focal adhesion kinase-mediated signaling pathways which control endothelial cell migration.²⁷⁴ The protein has also been implemented in angiogenesis and endothelial cell migration through integrin-linked kinase signaling.²⁷⁵ Galectin-3 binds vascular endothelial growth factor receptor 2 (VEGFR2), promoting its phosphorylation and preventing its internalization, thus increasing angiogenic processes of human umbilical cord endothelial cells *in vitro*.²⁷⁶ Similarly, galectin-3, together with galectin-1, can activate and prevent the internalization of VEGFR1, to again enhance angiogenesis.²⁷⁶ However, despite these findings, a study of murine cutaneous wound repair from our research group demonstrated that galectin-3 deficient mice exhibited no difference in vascular density or expression of angiogenic markers relative to wild-type mice.²⁷⁷

1.3.4 Roles in Re-Epithelialization

Surface expression of galectin-3 in type I and II alveolar epithelial cells was described in a model of irradiation-induced lung inflammation and repair.²⁷⁸ In corneal healing, re-epithelialization was reduced in galectin-3 deficient mice compared to wild-type counterparts.²⁷⁹ While galectin-3 did not alter the rate of epithelial cell proliferation, the protein may have influenced epithelial cell migration as elevated levels of galectin-3 were detected in the migrating epithelial tongue following injury.²⁷⁹ This influence was also seen in human corneal epithelial cells where galectin-3 promoted cell scattering, lamellipodia formation, and motility.²⁸⁰ Notably, in murine corneal healing the addition of exogenous galectin-3 increased re-epithelialization in wild type (WT) mice, but not galectin-3 deficient mice.²⁷⁹ Epithelial wounds in monkey corneal explants also exhibited enhanced re-epithelialization following human galectin-3 exogenous treatment.²⁸¹

Cutaneous wound healing models have demonstrated that keratinocytes from galectin-3 knockout mice exhibit a migratory defect, and that re-epithelialization, but not wound closure itself, is delayed in galectin-3 deficient mice.^{277,282} Overall, galectin-3 has been implicated in numerous wound healing processes including inflammation and contributing to re-epithelialization. As a result, topical delivery of this protein during the wound healing process is of interest to augment repair in challenged wound healing environments.

1.4 Hypothesis and Objectives

1.4.1 Rationale

Pathologies such as cutaneous chronic wounds are a challenge to treat clinically and new treatment strategies are desperately needed. Excessive inflammation, a deficient ECM structure and composition, cell senescence, and imbalance of signaling molecules contribute to a non-healing wound bed that persists beyond three months, leading to pain, impaired limb function, bacterial infection, and hospitalization. High mortality rates following lower limb amputation, necessitated by chronic wounds, indicate a severe need for a bioengineered scaffold that can resolve inflammation and serve as a temporary support for fibroplasia, neoangiogenesis, and re-epithelialization.

A three-dimensional scaffold more closely mimics the structure and function of native ECM and can be used in the delivery of bioactive molecules. The scaffold provides a site for cell

biorecognition and adhesion, necessary for cell infiltration and proliferation. Electrospinning and 3D printing are two means of biomimetic scaffold production. Electrospun scaffolds are highly nanofibrous and randomly organized, while 3D printed scaffolds allow for controlled material architecture and void pores.

Three-dimensional printing has gained interest in biomaterial engineering as an accessible means of scaffold fabrication with the opportunity for customized scaffold shape and porosity. Thus, our laboratory is interested in establishing a protocol for reproducible printing of soft materials which can be investigated for use in tissue engineering applications.

Electrospinning nanofibrous scaffolds is well-established in our laboratory.^{283,284} We have previously demonstrated that electrospun gelatin/galectin-3 scaffolds are biocompatible *in vitro*. The conditions under which galectin-3 might attenuate prolonged inflammation by modulating alternative M2 macrophage polarization remains to be elucidated.

1.4.2 Hypothesis

I hypothesize that scaffold design considerations will depend on their intended application. Firstly, I predict that 3D printed soft collagen scaffolds and rigid PCL scaffolds will exhibit desired architecture, porosity, and biocompatibility; these engineered scaffolds will support human adipose-derived stem/stromal cell (ASC) bioactivity *in vitro*. Secondly, I predict that local delivery of human recombinant galectin-3, either topically or using a gelatin scaffold, in a murine model of wound healing will cause the enrichment of pro-regenerative, arginase I-positive cells within the wound *in vivo*.

1.4.3 Objectives

The aims of this study were to investigate 3D printed and electrospun scaffolds for tissue engineering. Electrospun scaffolds are composed of nanofibers that are randomly organized, while 3D printed scaffolds allow for controlled deposition of print materials to ensure desired material architecture and void pores.

Aim 1: Three-Dimensional Bioprinting for Tissue Engineering

- Establish a protocol for soft collagen scaffold printing
- Polycaprolactone scaffold polymer fusion printing
- *In vitro* proof-of-concept scaffold performance and ASC phenotype analysis

Aim 2: Effects of Exogenous Galectin-3 in a Murine Wound Healing Model

- Electrospin galectin-3-loaded gelatin scaffolds
- Evaluate effects of exogenous galectin-3 *in vivo*

1.5 References

1. Wysocki, A. B. Skin anatomy, physiology, and pathophysiology. *Nurs. Clin. North Am.* **34**, 777–97, v (1999).
2. Kanitakis, J. Anatomy, histology and immunohistochemistry of normal human skin. *Eur. J. Dermatol. EJD* **12**, 390–399; quiz 400–401 (2002).
3. Kolarsick P. A. J., Kolarsick M. A., Goodwin C. Anatomy and Physiology of the Skin: Erratum. *J. Dermatol. Nurses' Assoc.* **3**, 366 (2011).
4. Kendall, M. A. F., Chong, Y.-F. & Cock, A. The mechanical properties of the skin epidermis in relation to targeted gene and drug delivery. *Biomaterials* **28**, 4968–4977 (2007).
5. Madison, K. C. Barrier Function of the Skin: “La Raison d’Être” of the Epidermis. *J. Invest. Dermatol.* **121**, 231–241 (2003).
6. Elias, P. M. The permeability barrier in mammalian epidermis. *J. Cell Biol.* **65**, 180–191 (1975).
7. Wickett, R. R. & Visscher, M. O. Structure and function of the epidermal barrier. *Am. J. Infect. Control* **34**, S98–S110 (2006).
8. Zaidi, Z. & Lanigan, S. W. *Dermatology in Clinical Practice*. (Springer-Verlag, 2010).
9. Eckert, R. L. & Rorke, E. A. Molecular biology of keratinocyte differentiation. *Environ. Health Perspect.* **80**, 109–116 (1989).
10. Eckhart, L., Lippens, S., Tschachler, E. & Declercq, W. Cell death by cornification. *Biochim. Biophys. Acta BBA - Mol. Cell Res.* **1833**, 3471–3480 (2013).
11. Gilchrist, B. A., Blog, F. B. & Szabo, G. Effects of Aging and Chronic Sun Exposure on Melanocytes in Human Skin. *J. Invest. Dermatol.* **73**, 141–143 (1979).
12. Yamaguchi, Y. & Hearing, V. J. Melanocytes and Their Diseases. *Cold Spring Harb. Perspect. Med.* **4**, (2014).
13. Boulais, N. & Misery, L. The epidermis: a sensory tissue. *Eur. J. Dermatol. EJD* **18**, 119–127 (2008).
14. Woo, S.-H., Lumpkin, E. A. & Patapoutian, A. Merkel cells and neurons keep in touch. *Trends Cell Biol.* **25**, 74–81 (2015).
15. Clayton, K., Vallejo, A. F., Davies, J., Sirvent, S. & Polak, M. E. Langerhans Cells—Programmed by the Epidermis. *Front. Immunol.* **8**, (2017).
16. McGrath, J. A., Eady, R. A. J. & Pope, F. M. Anatomy and Organization of Human Skin. 15
17. Wedmore, C. V. & Williams, T. J. Control of vascular permeability by polymorphonuclear leukocytes in inflammation. *Nature* **289**, 646–650 (1981).
18. Alberts, B. *et al.* Blood Vessels and Endothelial Cells. *Mol. Biol. Cell 4th Ed.* (2002).
19. Attwell, D., Mishra, A., Hall, C. N., O’Farrell, F. M. & Dalkara, T. What is a pericyte? *J. Cereb. Blood Flow Metab.* **36**, 451–455 (2016).
20. Romanovsky, A. A. Skin temperature: its role in thermoregulation. *Acta Physiol.* **210**, 498–507 (2014).
21. Rustin, M. H. A. Andrews’ Diseases of the Skin - Clinical Dermatology. *Postgrad. Med. J.* **66**, 984 (1990).
22. Jackson, S. M., Williams, M. L., Feingold, K. R. & Elias, P. M. Pathobiology of the stratum corneum. *West. J. Med.* **158**, 279–285 (1993).

23. Has, C. Peeling Skin Disorders: A Paradigm for Skin Desquamation. *J. Invest. Dermatol.* **138**, 1689–1691 (2018).
24. Fuchs, E., Tumber, T. & Guasch, G. Socializing with the Neighbors: Stem Cells and Their Niche. *Cell* **116**, 769–778 (2004).
25. Yan, X. & Owens, D. M. The skin: a home to multiple classes of epithelial progenitor cells. *Stem Cell Rev.* **4**, 113–118 (2008).
26. Woo, S.-H., Stumpfova, M., Jensen, U. B., Lumpkin, E. A. & Owens, D. M. Identification of epidermal progenitors for the Merkel cell lineage. *Dev. Camb. Engl.* **137**, 3965–3971 (2010).
27. Potten, C. S. Epidermal transit times. *Br. J. Dermatol.* **93**, 649–658 (1975).
28. Mackenzie, I. C. Retroviral Transduction of Murine Epidermal Stem Cells Demonstrates Clonal Units of Epidermal Structure. *J. Invest. Dermatol.* **109**, 377–383 (1997).
29. Gonzales, K. A. U. & Fuchs, E. Skin and Its Regenerative Powers: An Alliance between Stem Cells and Their Niche. *Dev. Cell* **43**, 387–401 (2017).
30. Rahmani, W. *et al.* Hair Follicle Dermal Stem Cells Regenerate the Dermal Sheath, Repopulate the Dermal Papilla, and Modulate Hair Type. *Dev. Cell* **31**, 543–558 (2014).
31. Sellheyer, K. & Krahl, D. Skin mesenchymal stem cells: Prospects for clinical dermatology. *J. Am. Acad. Dermatol.* **63**, 859–865 (2010).
32. Jahoda, C. A. & Reynolds, A. J. Hair follicle dermal sheath cells: unsung participants in wound healing. *The Lancet* **358**, 1445–1448 (2001).
33. Richardson, G. D. *et al.* Cultured Cells from the Adult Human Hair Follicle Dermis can be Directed Toward Adipogenic and Osteogenic Differentiation. *J. Invest. Dermatol.* **124**, 1090–1091 (2005).
34. Rochat, A., Kobayashi, K. & Barrandon, Y. Location of stem cells of human hair follicles by clonal analysis. *Cell* **76**, 1063–1073 (1994).
35. Blanpain, C., Lowry, W. E., Geoghegan, A., Polak, L. & Fuchs, E. Self-Renewal, Multipotency, and the Existence of Two Cell Populations within an Epithelial Stem Cell Niche. *Cell* **118**, 635–648 (2004).
36. Cotsarelis, G., Sun, T.-T. & Lavker, R. M. Label-retaining cells reside in the bulge area of pilosebaceous unit: Implications for follicular stem cells, hair cycle, and skin carcinogenesis. *Cell* **61**, 1329–1337 (1990).
37. Oshima, H., Rochat, A., Kedzia, C., Kobayashi, K. & Barrandon, Y. Morphogenesis and Renewal of Hair Follicles from Adult Multipotent Stem Cells. *Cell* **104**, 233–245 (2001).
38. Claudinot, S., Nicolas, M., Oshima, H., Rochat, A. & Barrandon, Y. Long-term renewal of hair follicles from clonogenic multipotent stem cells. *Proc. Natl. Acad. Sci.* **102**, 14677–14682 (2005).
39. Morris, R. J. *et al.* Enrichment for Living Murine Keratinocytes from the Hair Follicle Bulge with the Cell Surface Marker CD34. *J. Invest. Dermatol.* **120**, 501–511 (2003).
40. Youssef, K. K. *et al.* Identification of the cell lineage at the origin of basal cell carcinoma. *Nat. Cell Biol.* **12**, 299–305 (2010).
41. Jaks, V. *et al.* Lgr5 marks cycling, yet long-lived, hair follicle stem cells. *Nat. Genet.* **40**, 1291–1299 (2008).
42. Nowak, J. A., Polak, L., Pasolli, H. A. & Fuchs, E. Hair follicle stem cells are specified and function in early skin morphogenesis. *Cell Stem Cell* **3**, 33–43 (2008).
43. Howard, J. M., Nuguid, J. M., Ngole, D. & Nguyen, H. Tcf3 expression marks both stem and progenitor cells in multiple epithelia. *Dev. Camb. Engl.* **141**, 3143–3152 (2014).

44. Ito, M. *et al.* Wnt-dependent de novo hair follicle regeneration in adult mouse skin after wounding. *Nature* **447**, 316–320 (2007).
45. Levy, V., Lindon, C., Harfe, B. D. & Morgan, B. A. Distinct stem cell populations regenerate the follicle and interfollicular epidermis. *Dev. Cell* **9**, 855–861 (2005).
46. Clayton, E. *et al.* A single type of progenitor cell maintains normal epidermis. *Nature* **446**, 185–189 (2007).
47. Roy, E. *et al.* Bimodal behaviour of interfollicular epidermal progenitors regulated by hair follicle position and cycling. *EMBO J.* **35**, 2658–2670 (2016).
48. Lim, X. *et al.* Interfollicular epidermal stem cells self-renew via autocrine Wnt signaling. *Science* **342**, 1226–1230 (2013).
49. Doupé, D. P., Klein, A. M., Simons, B. D. & Jones, P. H. The ordered architecture of murine ear epidermis is maintained by progenitor cells with random fate. *Dev. Cell* **18**, 317–323 (2010).
50. Rompolas, P. *et al.* Spatiotemporal coordination of stem cell commitment during epidermal homeostasis. *Science* **352**, 1471–1474 (2016).
51. Mascré, G. *et al.* Distinct contribution of stem and progenitor cells to epidermal maintenance. *Nature* **489**, 257–262 (2012).
52. Sánchez-Danés, A. *et al.* Defining the clonal dynamics leading to mouse skin tumour initiation. *Nature* **536**, 298–303 (2016).
53. Horsley, V. *et al.* Blimp1 defines a progenitor population that governs cellular input to the sebaceous gland. *Cell* **126**, 597–609 (2006).
54. Snippert, H. J. *et al.* Lgr6 marks stem cells in the hair follicle that generate all cell lineages of the skin. *Science* **327**, 1385–1389 (2010).
55. Page, M. E., Lombard, P., Ng, F., Göttgens, B. & Jensen, K. B. The epidermis comprises autonomous compartments maintained by distinct stem cell populations. *Cell Stem Cell* **13**, 471–482 (2013).
56. Donati, G. *et al.* Wounding induces dedifferentiation of epidermal Gata6+ cells and acquisition of stem cell properties. *Nat. Cell Biol.* **19**, 603–613 (2017).
57. Ito, M. *et al.* Stem cells in the hair follicle bulge contribute to wound repair but not to homeostasis of the epidermis. *Nat. Med.* **11**, 1351–1354 (2005).
58. Jaks, V., Kasper, M. & Toftgård, R. The hair follicle—a stem cell zoo. *Exp. Cell Res.* **316**, 1422–1428 (2010).
59. Levy, V., Lindon, C., Zheng, Y., Harfe, B. D. & Morgan, B. A. Epidermal stem cells arise from the hair follicle after wounding. *FASEB J. Off. Publ. Fed. Am. Soc. Exp. Biol.* **21**, 1358–1366 (2007).
60. Park, C. O. & Kupper, T. S. The emerging role of resident memory T cells in protective immunity and inflammatory disease. *Nat. Med.* **21**, 688–697 (2015).
61. Cruz, M. S., Diamond, A., Russell, A. & Jameson, J. M. Human $\alpha\beta$ and $\gamma\delta$ T Cells in Skin Immunity and Disease. *Front. Immunol.* **9**, (2018).
62. Alberts, B. *et al.* Fibroblasts and Their Transformations: The Connective-Tissue Cell Family. *Mol. Biol. Cell 4th Ed.* (2002).
63. Rosales, C. Neutrophil: A Cell with Many Roles in Inflammation or Several Cell Types? *Front. Physiol.* **9**, (2018).
64. Mosser, D. M. & Edwards, J. P. Exploring the full spectrum of macrophage activation. *Nat. Rev. Immunol.* **8**, 958–969 (2008).
65. Headington, J. T. The dermal dendrocyte. *Adv. Dermatol.* **1**, 159–171 (1986).

66. Krystel-Whittemore, M., Dileepan, K. N. & Wood, J. G. Mast Cell: A Multi-Functional Master Cell. *Front. Immunol.* **6**, (2016).
67. Cline, M. J. Histiocytes and histiocytosis. *Blood* **84**, 2840–2853 (1994).
68. Ali, A. T., Hochfeld, W. E., Myburgh, R. & Pepper, M. S. Adipocyte and adipogenesis. *Eur. J. Cell Biol.* **92**, 229–236 (2013).
69. Eming, S. A., Martin, P. & Tomic-Canic, M. Wound repair and regeneration: Mechanisms, signaling, and translation. *Sci. Transl. Med.* **6**, 265sr6-265sr6 (2014).
70. Zhao, R., Liang, H., Clarke, E., Jackson, C. & Xue, M. Inflammation in Chronic Wounds. *Int. J. Mol. Sci.* **17**, 2085 (2016).
71. Greaves, N. S., Ashcroft, K. J., Baguneid, M. & Bayat, A. Current understanding of molecular and cellular mechanisms in fibroplasia and angiogenesis during acute wound healing. *J. Dermatol. Sci.* **72**, 206–217 (2013).
72. Xu, J. Extracellular matrix alters PDGF regulation of fibroblast integrins. *J. Cell Biol.* **132**, 239–249 (1996).
73. Clark, R. A. F. Fibrin and Wound Healing. *Ann. N. Y. Acad. Sci.* **936**, 355–367 (2006).
74. Lodyga, M. *et al.* Cadherin-11-mediated adhesion of macrophages to myofibroblasts establishes a profibrotic niche of active TGF- β . *Sci. Signal.* **12**, eaao3469 (2019).
75. Koskela, A., Engström, K., Hakelius, M., Nowinski, D. & Ivarsson, M. Regulation of fibroblast gene expression by keratinocytes in organotypic skin culture provides possible mechanisms for the antifibrotic effect of reepithelialization. *Wound Repair Regen. Off. Publ. Wound Heal. Soc. Eur. Tissue Repair Soc.* **18**, 452–459 (2010).
76. Eming, S. A., Hammerschmidt, M., Krieg, T. & Roers, A. Interrelation of immunity and tissue repair or regeneration. *Semin. Cell Dev. Biol.* **20**, 517–527 (2009).
77. Patan, S. Vasculogenesis and angiogenesis. *Cancer Treat. Res.* **117**, 3–32 (2004).
78. Kimura, H. & Esumi, H. Reciprocal regulation between nitric oxide and vascular endothelial growth factor in angiogenesis. *Acta Biochim. Pol.* **50**, 49–59 (2003).
79. Suri, C. *et al.* Increased vascularization in mice overexpressing angiopoietin-1. *Science* **282**, 468–471 (1998).
80. Sahni, A., Sporn, L. A. & Francis, C. W. Potentiation of endothelial cell proliferation by fibrin(ogen)-bound fibroblast growth factor-2. *J. Biol. Chem.* **274**, 14936–14941 (1999).
81. Kalebic, T., Garbisa, S., Glaser, B. & Liotta, L. A. Basement membrane collagen: degradation by migrating endothelial cells. *Science* **221**, 281–283 (1983).
82. Brooks, P. C., Clark, R. A. & Chersesh, D. A. Requirement of vascular integrin alpha v beta 3 for angiogenesis. *Science* **264**, 569–571 (1994).
83. Koolwijk, P. *et al.* Cooperative effect of TNFalpha, bFGF, and VEGF on the formation of tubular structures of human microvascular endothelial cells in a fibrin matrix. Role of urokinase activity. *J. Cell Biol.* **132**, 1177–1188 (1996).
84. Birkedal-Hansen, H. *et al.* Matrix Metalloproteinases: A Review. *Crit. Rev. Oral Biol. Med.* **4**, 197–250 (1993).
85. Birkedal-Hansen, H. Proteolytic remodeling of extracellular matrix. *Curr. Opin. Cell Biol.* **7**, 728–735 (1995).
86. Barrientos, S., Stojadinovic, O., Golinko, M. S., Brem, H. & Tomic-Canic, M. Growth factors and cytokines in wound healing. *Wound Repair Regen. Off. Publ. Wound Heal. Soc. Eur. Tissue Repair Soc.* **16**, 585–601 (2008).
87. Gurtner, G. C., Werner, S., Barrandon, Y. & Longaker, M. T. Wound repair and regeneration. *Nature* **453**, 314–321 (2008).

88. Rodero, M. P. & Khosrotehrani, K. Skin wound healing modulation by macrophages. *Int. J. Clin. Exp. Pathol.* **3**, 643–653 (2010).
89. Morton, L. M. & Phillips, T. J. Wound healing and treating wounds: Differential diagnosis and evaluation of chronic wounds. *J. Am. Acad. Dermatol.* **74**, 589–605; quiz 605–606 (2016).
90. Baltzis, D., Eleftheriadou, I. & Veves, A. Pathogenesis and treatment of impaired wound healing in diabetes mellitus: new insights. *Adv. Ther.* **31**, 817–836 (2014).
91. Singer, A. J. & Clark, R. A. Cutaneous wound healing. *N. Engl. J. Med.* **341**, 738–746 (1999).
92. Paz, J. C. & West, M. P. *Acute care handbook for physical therapists.* (2014).
93. Gottrup, F., Holstein, P., Jørgensen, B., Lohmann, M. & Karlsmar, T. A new concept of a multidisciplinary wound healing center and a national expert function of wound healing. *Arch. Surg. Chic. Ill 1960* **136**, 765–772 (2001).
94. Sen, C. K. *et al.* Human skin wounds: a major and snowballing threat to public health and the economy. *Wound Repair Regen. Off. Publ. Wound Heal. Soc. Eur. Tissue Repair Soc.* **17**, 763–771 (2009).
95. Hopkins, R. B., Burke, N., Harlock, J., Jegathisawaran, J. & Goeree, R. Economic burden of illness associated with diabetic foot ulcers in Canada. *BMC Health Serv. Res.* **15**, 13 (2015).
96. Available at: <https://www.woundscanada.ca/index.php/public/facts-stats-and-tools/statistics/>. (Accessed: 1st August 2019)
97. Woodbury, M. G. Risking Limbs, Wasting Money. **14**, 7 (2016).
98. Bonham, P. A. Assessment and management of patients with venous, arterial, and diabetic/neuropathic lower extremity wounds. *AACN Clin. Issues* **14**, 442–456; quiz 548–550 (2003).
99. Hirsch, A. T. *et al.* Peripheral arterial disease detection, awareness, and treatment in primary care. *JAMA* **286**, 1317–1324 (2001).
100. Alavi, A. *et al.* Diabetic foot ulcers: Part I. Pathophysiology and prevention. *J. Am. Acad. Dermatol.* **70**, 1.e1-18; quiz 19–20 (2014).
101. Maklebust, J. & Magnan, M. A. Risk factors associated with having a pressure ulcer: a secondary data analysis. *Adv. Wound Care J. Prev. Heal.* **7**, 25, 27–28, 31-34 passim (1994).
102. Acute Care Handbook for Physical Therapists, 4th Edition - 9781455728961. Available at: <https://evolve.elsevier.com/cs/product/9781455728961?role=student>. (Accessed: 1st August 2019)
103. Eming, S. A., Krieg, T. & Davidson, J. M. Inflammation in wound repair: molecular and cellular mechanisms. *J. Invest. Dermatol.* **127**, 514–525 (2007).
104. Wenk, J. *et al.* Selective pick-up of increased iron by deferoxamine-coupled cellulose abrogates the iron-driven induction of matrix-degrading metalloproteinase 1 and lipid peroxidation in human dermal fibroblasts in vitro: a new dressing concept. *J. Invest. Dermatol.* **116**, 833–839 (2001).
105. Eming, S. A. *et al.* Differential proteomic analysis distinguishes tissue repair biomarker signatures in wound exudates obtained from normal healing and chronic wounds. *J. Proteome Res.* **9**, 4758–4766 (2010).
106. Sindrilaru, A. *et al.* An unrestrained proinflammatory M1 macrophage population induced by iron impairs wound healing in humans and mice. *J. Clin. Invest.* **121**, 985–997 (2011).

107. Beidler, S. K. *et al.* Inflammatory cytokine levels in chronic venous insufficiency ulcer tissue before and after compression therapy. *J. Vasc. Surg.* **49**, 1013–1020 (2009).
108. Mustoe, T. A., O’Shaughnessy, K. & Kloeters, O. Chronic wound pathogenesis and current treatment strategies: a unifying hypothesis. *Plast. Reconstr. Surg.* **117**, 35S-41S (2006).
109. Roche, E. D. *et al.* Increasing the presence of biofilm and healing delay in a porcine model of MRSA-infected wounds. *Wound Repair Regen. Off. Publ. Wound Heal. Soc. Eur. Tissue Repair Soc.* **20**, 537–543 (2012).
110. Han, G. & Ceilley, R. Chronic Wound Healing: A Review of Current Management and Treatments. *Adv. Ther.* **34**, 599–610 (2017).
111. Frank, D. N. *et al.* Microbial diversity in chronic open wounds. *Wound Repair Regen. Off. Publ. Wound Heal. Soc. Eur. Tissue Repair Soc.* **17**, 163–172 (2009).
112. Krisp, C. *et al.* Proteome analysis reveals antiangiogenic environments in chronic wounds of diabetes mellitus type 2 patients. *Proteomics* **13**, 2670–2681 (2013).
113. Lauer, G. *et al.* Expression and proteolysis of vascular endothelial growth factor is increased in chronic wounds. *J. Invest. Dermatol.* **115**, 12–18 (2000).
114. Pastar, I. *et al.* Attenuation of the Transforming Growth Factor β –Signaling Pathway in Chronic Venous Ulcers. *Mol. Med.* **16**, 92–101 (2010).
115. Edsberg, L. E., Wyffels, J. T., Brogan, M. S. & Fries, K. M. Analysis of the proteomic profile of chronic pressure ulcers. *Wound Repair Regen. Off. Publ. Wound Heal. Soc. Eur. Tissue Repair Soc.* **20**, 378–401 (2012).
116. Leu, A. J., Leu, H. J., Franzeck, U. K. & Bollinger, A. Microvascular changes in chronic venous insufficiency--a review. *Cardiovasc. Surg. Lond. Engl.* **3**, 237–245 (1995).
117. Bekara, F. *et al.* New techniques for wound management: A systematic review of their role in the management of chronic wounds. *Arch. Plast. Surg.* **45**, 102–110 (2018).
118. Cavanagh, P. R. & Bus, S. A. Off-loading the diabetic foot for ulcer prevention and healing. *J. Vasc. Surg.* **52**, 37S-43S (2010).
119. Roth-Albin, I. *et al.* Outcomes Following Advanced Wound Care for Diabetic Foot Ulcers: A Canadian Study. *Can. J. Diabetes* **41**, 26–32 (2017).
120. Werdin, F., Tennenhaus, M., Schaller, H.-E. & Rennekampff, H.-O. Evidence-based Management Strategies for Treatment of Chronic Wounds. *Eplasty* **9**, (2009).
121. Mulder, G., Jones, R., Cederholm-Williams, S., Cherry, G. & Ryan, T. Fibrin cuff lysis in chronic venous ulcers treated with a hydrocolloid dressing. *Int. J. Dermatol.* **32**, 304–306 (1993).
122. Powers, J. G., Higham, C., Broussard, K. & Phillips, T. J. Wound healing and treating wounds: Chronic wound care and management. *J. Am. Acad. Dermatol.* **74**, 607–625; quiz 625–626 (2016).
123. Demidova-Rice, T. N., Geevarghese, A. & Herman, I. M. Bioactive peptides derived from vascular endothelial cell extracellular matrices promote microvascular morphogenesis and wound healing in vitro. *Wound Repair Regen. Off. Publ. Wound Heal. Soc. Eur. Tissue Repair Soc.* **19**, 59–70 (2011).
124. Davies, C. E. *et al.* Maggots as a wound debridement agent for chronic venous leg ulcers under graduated compression bandages: A randomised controlled trial. *Phlebology* **30**, 693–699 (2015).
125. Gilead, L., Mumcuoglu, K. Y. & Ingber, A. The use of maggot debridement therapy in the treatment of chronic wounds in hospitalised and ambulatory patients. *J. Wound Care* **21**, 78, 80, 82–85 (2012).

126. Prete, P. E. Growth effects of *Phaenicia sericata* larval extracts on fibroblasts: mechanism for wound healing by maggot therapy. *Life Sci.* **60**, 505–510 (1997).
127. Lipsky, B. A. *et al.* Specific guidelines for the treatment of diabetic foot infections 2011. *Diabetes Metab. Res. Rev.* **28**, 234–235 (2012).
128. Cordts, P. R. *et al.* A prospective, randomized trial of Unna's boot versus Duoderm CGF hydroactive dressing plus compression in the management of venous leg ulcers. *J. Vasc. Surg.* **15**, 480–486 (1992).
129. Ohlsson, P., Larsson, K., Lindholm, C. & Möller, M. A cost-effectiveness study of leg ulcer treatment in primary care. Comparison of saline-gauze and hydrocolloid treatment in a prospective, randomized study. *Scand. J. Prim. Health Care* **12**, 295–299 (1994).
130. Nemeth, A. J., Eaglstein, W. H., Taylor, J. R., Peerson, L. J. & Falanga, V. Faster healing and less pain in skin biopsy sites treated with an occlusive dressing. *Arch. Dermatol.* **127**, 1679–1683 (1991).
131. Skórkowska-Telichowska, K., Czemplik, M., Kulma, A. & Szopa, J. The local treatment and available dressings designed for chronic wounds. *J. Am. Acad. Dermatol.* **68**, e117–e126 (2013).
132. Bouza, C., Saz, Z., Muñoz, A. & Amate, J. M. Efficacy of advanced dressings in the treatment of pressure ulcers: a systematic review. *J. Wound Care* **14**, 193–199 (2005).
133. Singh, A. *et al.* Meta-analysis of randomized controlled trials on hydrocolloid occlusive dressing versus conventional gauze dressing in the healing of chronic wounds. *Asian J. Surg.* **27**, 326–332 (2004).
134. Greaves, N. S., Iqbal, S. A., Baguneid, M. & Bayat, A. The role of skin substitutes in the management of chronic cutaneous wounds. *Wound Repair Regen. Off. Publ. Wound Heal. Soc. Eur. Tissue Repair Soc.* **21**, 194–210 (2013).
135. Pham, C., Greenwood, J., Cleland, H., Woodruff, P. & Maddern, G. Bioengineered skin substitutes for the management of burns: a systematic review. *Burns J. Int. Soc. Burn Inj.* **33**, 946–957 (2007).
136. Compton, C. C., Butler, C. E., Yannas, I. V., Warland, G. & Orgill, D. P. Organized skin structure is regenerated in vivo from collagen-GAG matrices seeded with autologous keratinocytes. *J. Invest. Dermatol.* **110**, 908–916 (1998).
137. Bello, Y. M., Falabella, A. F. & Eaglstein, W. H. Tissue-engineered skin. Current status in wound healing. *Am. J. Clin. Dermatol.* **2**, 305–313 (2001).
138. Lepow, B. D., Downey, M., Yurgelon, J., Klassen, L. & Armstrong, D. G. Bioengineered tissues in wound healing: a progress report. *Expert Rev. Dermatol.* **6**, 255–262 (2011).
139. Armstrong, D. G., Lavery, L. A. & Diabetic Foot Study Consortium. Negative pressure wound therapy after partial diabetic foot amputation: a multicentre, randomised controlled trial. *Lancet Lond. Engl.* **366**, 1704–1710 (2005).
140. Limengka, Y. & Jeo, W. S. Spontaneous closure of multiple enterocutaneous fistula due to abdominal tuberculosis using negative pressure wound therapy: a case report. *J. Surg. Case Rep.* **2018**, rjy001 (2018).
141. Kaur, S., Pawar, M., Banerjee, N. & Garg, R. Evaluation of the efficacy of hyperbaric oxygen therapy in the management of chronic nonhealing ulcer and role of periwound transcutaneous oximetry as a predictor of wound healing response: A randomized prospective controlled trial. *J. Anaesthesiol. Clin. Pharmacol.* **28**, 70–75 (2012).
142. Kaur, S., Pawar, M., Banerjee, N. & Garg, R. Evaluation of the efficacy of hyperbaric oxygen therapy in the management of chronic nonhealing ulcer and role of periwound

- transcutaneous oximetry as a predictor of wound healing response: A randomized prospective controlled trial. *J. Anaesthesiol. Clin. Pharmacol.* **28**, 70–75 (2012).
143. Gilligan, A. M., Waycaster, C. R. & Milne, C. T. Cost Effectiveness of Becaplermin Gel on Wound Closure for the Treatment of Pressure Injuries. *Wounds Compend. Clin. Res. Pract.* **30**, 197–204 (2018).
 144. Waycaster, C. R., Gilligan, A. M. & Motley, T. A. Cost-Effectiveness of Becaplermin Gel on Diabetic Foot Ulcer Healing Changes in Wound Surface Area. *J. Am. Podiatr. Med. Assoc.* **106**, 273–282 (2016).
 145. Tecilazich, F., Dinh, T. L. & Veves, A. Emerging Drugs for the Treatment of Diabetic Ulcers. *Expert Opin. Emerg. Drugs* **18**, 207–217 (2013).
 146. Puppi, D., Piras, A. M., Detta, N., Dinucci, D. & Chiellini, F. Poly(lactic-co-glycolic acid) electrospun fibrous meshes for the controlled release of retinoic acid. *Acta Biomater.* **6**, 1258–1268 (2010).
 147. Singh, N., Armstrong, D. G. & Lipsky, B. A. Preventing foot ulcers in patients with diabetes. *JAMA* **293**, 217–228 (2005).
 148. Beyaz, S., Guler, Ü. Ö. & Simsek Bagir, G. Factors affecting lifespan following below-knee amputation in diabetic patients. *Acta Orthop. Traumatol. Turc.* **51**, (2017).
 149. Dhivya, S., Padma, V. V. & Santhini, E. Wound dressings – a review. *BioMedicine* **5**, (2015).
 150. Jones, V., Grey, J. E. & Harding, K. G. Wound dressings. *BMJ* **332**, 777–780 (2006).
 151. Wei, G. & Ma, P. X. Nanostructured Biomaterials for Regeneration. *Adv. Funct. Mater.* **18**, 3566–3582 (2008).
 152. Rho, K. S. *et al.* Electrospinning of collagen nanofibers: effects on the behavior of normal human keratinocytes and early-stage wound healing. *Biomaterials* **27**, 1452–1461 (2006).
 153. Smith, L. A. & Ma, P. X. Nano-fibrous scaffolds for tissue engineering. *Colloids Surf. B Biointerfaces* **39**, 125–131 (2004).
 154. Karande, T. S., Ong, J. L. & Agrawal, C. M. Diffusion in musculoskeletal tissue engineering scaffolds: design issues related to porosity, permeability, architecture, and nutrient mixing. *Ann. Biomed. Eng.* **32**, 1728–1743 (2004).
 155. Dubský, M. *et al.* Nanofibers prepared by needleless electrospinning technology as scaffolds for wound healing. *J. Mater. Sci. Mater. Med.* **23**, 931–941 (2012).
 156. Li, W.-J., Laurencin, C. T., Caterson, E. J., Tuan, R. S. & Ko, F. K. Electrospun nanofibrous structure: a novel scaffold for tissue engineering. *J. Biomed. Mater. Res.* **60**, 613–621 (2002).
 157. Lu, T., Li, Y. & Chen, T. Techniques for fabrication and construction of three-dimensional scaffolds for tissue engineering. *Int. J. Nanomedicine* **8**, 337–350 (2013).
 158. Conner, B. P. *et al.* Making sense of 3-D printing: Creating a map of additive manufacturing products and services. *Addit. Manuf.* **1–4**, 64–76 (2014).
 159. Berman, B. 3-D printing: The new industrial revolution. *Bus. Horiz.* **55**, 155–162 (2012).
 160. Weller, C., Kleer, R. & Piller, F. T. Economic implications of 3D printing: Market structure models in light of additive manufacturing revisited. *Int. J. Prod. Econ.* **164**, 43–56 (2015).
 161. Williams, D. F. On the mechanisms of biocompatibility. *Biomaterials* **29**, 2941–2953 (2008).
 162. Advanced BioMatrix. 3D Tissue Engineering.
 163. Truby, R. L. & Lewis, J. A. Printing soft matter in three dimensions. *Nature* **540**, 371–378 (2016).

164. Hinton, T. J. *et al.* Three-dimensional printing of complex biological structures by freeform reversible embedding of suspended hydrogels. *Sci. Adv.* **1**, e1500758 (2015).
165. Hinton, T. J., Hudson, A., Pusch, K., Lee, A. & Feinberg, A. W. 3D Printing PDMS Elastomer in a Hydrophilic Support Bath via Freeform Reversible Embedding. *ACS Biomater. Sci. Eng.* **2**, 1781–1786 (2016).
166. Hinton, T. J., Lee, A. & Feinberg, A. W. 3D bioprinting from the micrometer to millimeter length scales: Size does matter. *Curr. Opin. Biomed. Eng.* **1**, 31–37 (2017).
167. Chattopadhyay, S. & Raines, R. T. Review collagen-based biomaterials for wound healing. *Biopolymers* **101**, 821–833 (2014).
168. Shoulders, M. D. & Raines, R. T. Collagen Structure and Stability. *Annu. Rev. Biochem.* **78**, 929–958 (2009).
169. Okuyama, K. *et al.* Crystal structures of collagen model peptides with Pro-Hyp-Gly repeating sequence at 1.26 Å resolution: Implications for proline ring puckering. *Pept. Sci.* **76**, 367–377 (2004).
170. Tracy, L. E., Minasian, R. A. & Caterson, E. J. Extracellular Matrix and Dermal Fibroblast Function in the Healing Wound. *Adv. Wound Care* **5**, 119–136 (2016).
171. Liu, Y., Ma, L. & Gao, C. Facile fabrication of the glutaraldehyde cross-linked collagen/chitosan porous scaffold for skin tissue engineering. *Mater. Sci. Eng. C* **32**, 2361–2366 (2012).
172. Badylak, S. F. Xenogeneic extracellular matrix as a scaffold for tissue reconstruction. *Transpl. Immunol.* **12**, 367–377 (2004).
173. Maeda, M., Tani, S., Sano, A. & Fujioka, K. Microstructure and release characteristics of the minipellet, a collagen-based drug delivery system for controlled release of protein drugs. *J. Controlled Release* **62**, 313–324 (1999).
174. Koide, T. Designed triple-helical peptides as tools for collagen biochemistry and matrix engineering. *Philos. Trans. R. Soc. B Biol. Sci.* **362**, 1281–1291 (2007).
175. Pinkas, D. M., Ding, S., Raines, R. T. & Barron, A. E. Tunable, Post-translational Hydroxylation of Collagen Domains in Escherichia coli. *ACS Chem. Biol.* **6**, 320–324 (2011).
176. Olsen, D. *et al.* Recombinant collagen and gelatin for drug delivery. *Adv. Drug Deliv. Rev.* **55**, 1547–1567 (2003).
177. Buechter, D. D. *et al.* Co-translational Incorporation of Trans-4-Hydroxyproline into Recombinant Proteins in Bacteria. *J. Biol. Chem.* **278**, 645–650 (2003).
178. Orgel, J. P. R. O., San Antonio, J. D. & Antipova, O. Molecular and structural mapping of collagen fibril interactions. *Connect. Tissue Res.* **52**, 2–17 (2011).
179. Smethurst, P. A. *et al.* Structural Basis for the Platelet-Collagen Interaction the smallest motif within collagen that recognizes and activates platelet glycoprotein vi contains two glycine-proline-hydroxyproline triplets. *J. Biol. Chem.* **282**, 1296–1304 (2007).
180. Fiedler, L. R. *et al.* Decorin Regulates Endothelial Cell Motility on Collagen I through Activation of Insulin-like Growth Factor I Receptor and Modulation of $\alpha 2\beta 1$ Integrin Activity. *J. Biol. Chem.* **283**, 17406–17415 (2008).
181. Postlethwaite, A. E., Seyer, J. M. & Kang, A. H. Chemotactic attraction of human fibroblasts to type I, II, and III collagens and collagen-derived peptides. *Proc. Natl. Acad. Sci.* **75**, 871–875 (1978).

182. Yannas, I. V., Burke, J. F., Orgill, D. P. & Skrabut, E. M. Wound tissue can utilize a polymeric template to synthesize a functional extension of skin. *Science* **215**, 174–176 (1982).
183. Weadock, K. S., Miller, E. J., Bellincampi, L. D., Zawadsky, J. P. & Dunn, M. G. Physical crosslinking of collagen fibers: comparison of ultraviolet irradiation and dehydrothermal treatment. *J. Biomed. Mater. Res.* **29**, 1373–1379 (1995).
184. Khew, S. T., Yang, Q. J. & Tong, Y. W. Enzymatically crosslinked collagen-mimetic dendrimers that promote integrin-targeted cell adhesion. *Biomaterials* **29**, 3034–3045 (2008).
185. Lee, Y.-B. *et al.* Bio-printing of collagen and VEGF-releasing fibrin gel scaffolds for neural stem cell culture. *Exp. Neurol.* **223**, 645–652 (2010).
186. Ren, X. *et al.* Engineering zonal cartilage through bioprinting collagen type II hydrogel constructs with biomimetic chondrocyte density gradient. *BMC Musculoskelet. Disord.* **17**, 301 (2016).
187. Rhee, S., Puetzer, J. L., Mason, B. N., Reinhart-King, C. A. & Bonassar, L. J. 3D Bioprinting of Spatially Heterogeneous Collagen Constructs for Cartilage Tissue Engineering. *ACS Biomater. Sci. Eng.* **2**, 1800–1805 (2016).
188. Park, J. Y. *et al.* A comparative study on collagen type I and hyaluronic acid dependent cell behavior for osteochondral tissue bioprinting. *Biofabrication* **6**, 035004 (2014).
189. Lee, V. *et al.* Design and Fabrication of Human Skin by Three-Dimensional Bioprinting. *Tissue Eng. Part C Methods* **20**, 473–484 (2013).
190. Gilbert, T. W., Sellaro, T. L. & Badylak, S. F. Decellularization of tissues and organs. *Biomaterials* **27**, 3675–3683 (2006).
191. Perera Ayomi S. & Coppens Marc-Olivier. Re-designing materials for biomedical applications: from biomimicry to nature-inspired chemical engineering. *Philos. Trans. R. Soc. Math. Phys. Eng. Sci.* **377**, 20180268 (2019).
192. Bezwada, R. S. *et al.* Monocryl® suture, a new ultra-pliable absorbable monofilament suture. *Biomaterials* **16**, 1141–1148 (1995).
193. Abedalwafa, M. A., Wang, F., Wang, L. & Li, C. Biodegradable poly-epsilon-caprolactone (pcl) for tissue engineering applications: a review. in (2012).
194. Osathanon, T., Chanjavanakul, P., Kongdech, P., Clayhan, P. & Huynh, N. C.-N. Polycaprolactone-Based Biomaterials for Guided Tissue Regeneration Membrane. in *Periodontitis - A Useful Reference* (ed. Arjunan, P.) (InTech, 2017). doi:10.5772/intechopen.69153
195. Saad, B. & Suter, U. W. Biodegradable Polymeric Materials. in *Encyclopedia of Materials: Science and Technology* (eds. Buschow, K. H. J. *et al.*) 551–555 (Elsevier, 2001). doi:10.1016/B0-08-043152-6/00105-4
196. Lam, C. X. F., Hutmacher, D. W., Schantz, J.-T., Woodruff, M. A. & Teoh, S. H. Evaluation of polycaprolactone scaffold degradation for 6 months in vitro and in vivo. *J. Biomed. Mater. Res. A* **90A**, 906–919 (2009).
197. Lam, C. X., Teoh, S. H. & Hutmacher, D. W. Comparison of the degradation of polycaprolactone and polycaprolactone-(β -tricalcium phosphate) scaffolds in alkaline medium. *Polym. Int.* **56**, 718–728 (2007).
198. Shi, R. *et al.* Structure, physical properties, biocompatibility and in vitro/vivo degradation behavior of anti-infective polycaprolactone-based electrospun membranes for guided tissue/bone regeneration. *Polym. Degrad. Stab.* **109**, 293–306 (2014).

199. Ahn, S. H., Lee, H. J. & Kim, G. H. Polycaprolactone Scaffolds Fabricated with an Advanced Electrohydrodynamic Direct-Printing Method for Bone Tissue Regeneration. *Biomacromolecules* **12**, 4256–4263 (2011).
200. Meseguer-Olmo, L. *et al.* In-vivo behavior of Si-hydroxyapatite/polycaprolactone/DMB scaffolds fabricated by 3D printing. *J. Biomed. Mater. Res. A* **101A**, 2038–2048 (2013).
201. He, Y. *et al.* A new photocrosslinkable polycaprolactone-based ink for three-dimensional inkjet printing. *J. Biomed. Mater. Res. B Appl. Biomater.* **105**, 1645–1657 (2017).
202. Tay, B. Y. *et al.* Processing of polycaprolactone porous structure for scaffold development. *J. Mater. Process. Technol.* **182**, 117–121 (2007).
203. Sayyar, S. *et al.* Extrusion Printed Graphene/Polycaprolactone/Composites for Tissue Engineering. *Mater. Sci. Forum* **773–774**, 496–502 (2013).
204. Ulery, B. D., Nair, L. S. & Laurencin, C. T. Biomedical applications of biodegradable polymers. *J. Polym. Sci. Part B Polym. Phys.* **49**, 832–864 (2011).
205. Darney, P. D., Monroe, S. E., Klaisle, C. M. & Alvarado, A. Clinical evaluation of the Capronor contraceptive implant: Preliminary report. *Am. J. Obstet. Gynecol.* **160**, 1292–1295 (1989).
206. Álvarez, A. L., Espinar, F. O. & Méndez, J. B. The Application of Microencapsulation Techniques in the Treatment of Endodontic and Periodontal Diseases. *Pharmaceutics* **3**, 538–571 (2011).
207. Scaffaro, R. *et al.* Combining in the melt physical and biological properties of poly(caprolactone) and chlorhexidine to obtain antimicrobial surgical monofilaments. *Appl. Microbiol. Biotechnol.* **97**, 99–109 (2013).
208. Murugan, R. & Ramakrishna, S. Design Strategies of Tissue Engineering Scaffolds with Controlled Fiber Orientation. *Tissue Eng.* **13**, 1845–1866 (2007).
209. Tan, S.-H., Inai, R., Kotaki, M. & Ramakrishna, S. Systematic Parameter Study for Ultra-Fine Fiber Fabrication Via Electrospinning Process. *Polymer* **46**, 6128–6134 (2005).
210. Katti, D. S., Robinson, K. W., Ko, F. K. & Laurencin, C. T. Bioresorbable nanofiber-based systems for wound healing and drug delivery: optimization of fabrication parameters. *J. Biomed. Mater. Res. B Appl. Biomater.* **70**, 286–296 (2004).
211. Chong, E. J. *et al.* Evaluation of electrospun PCL/gelatin nanofibrous scaffold for wound healing and layered dermal reconstitution. *Acta Biomater.* **3**, 321–330 (2007).
212. Yin, H. *et al.* A bioengineered drug-Eluting scaffold accelerated cutaneous wound healing In diabetic mice. *Colloids Surf. B Biointerfaces* **145**, 226–231 (2016).
213. Khorshidi, S. *et al.* A review of key challenges of electrospun scaffolds for tissue-engineering applications. *J. Tissue Eng. Regen. Med.* **10**, 715–738 (2016).
214. Ji, W. *et al.* Bioactive electrospun scaffolds delivering growth factors and genes for tissue engineering applications. *Pharm. Res.* **28**, 1259–1272 (2011).
215. Yoo, H. S., Kim, T. G. & Park, T. G. Surface-functionalized electrospun nanofibers for tissue engineering and drug delivery. *Adv. Drug Deliv. Rev.* **61**, 1033–1042 (2009).
216. Falanga, V. Wound healing and its impairment in the diabetic foot. *Lancet Lond. Engl.* **366**, 1736–1743 (2005).
217. Chouhan, D., Janani, G., Chakraborty, B., Nandi, S. K. & Mandal, B. B. Functionalized PVA-silk blended nanofibrous mats promote diabetic wound healing via regulation of extracellular matrix and tissue remodelling. *J. Tissue Eng. Regen. Med.* **12**, e1559–e1570 (2018).

218. Wu, J. *et al.* Electrospun nanoYarn-CH scaffold and its application in tissue engineering. *Mater. Lett.* **89**, 146–149 (2012).
219. Luo, C. J., Stoyanov, S. D., Stride, E., Pelan, E. & Edirisinghe, M. Electrospinning versus fibre production methods: from specifics to technological convergence. *Chem. Soc. Rev.* **41**, 4708–4735 (2012).
220. Nam, J., Huang, Y., Agarwal, S. & Lannutti, J. Materials selection and residual solvent retention in biodegradable electrospun fibers. *J. Appl. Polym. Sci.* **107**, 1547–1554 (2008).
221. Persano, L., Camposeo, A., Tekmen, C. & Pisignano, D. Industrial Upscaling of Electrospinning and Applications of Polymer Nanofibers: A Review. *Macromol. Mater. Eng.* **298**, 504–520 (2013).
222. Yan, G. *et al.* Improving Nanofiber Production and Application Performance by Electrospinning at Elevated Temperatures. *Ind. Eng. Chem. Res.* **56**, 12337–12343 (2017).
223. Shabani, I., Haddadi-Asl, V., Seyedjafari, E. & Soleimani, M. Cellular infiltration on nanofibrous scaffolds using a modified electrospinning technique. *Biochem. Biophys. Res. Commun.* **423**, 50–54 (2012).
224. Rnjak-Kovacina, J. & Weiss, A. S. Increasing the pore size of electrospun scaffolds. *Tissue Eng. Part B Rev.* **17**, 365–372 (2011).
225. Chen, M., Patra, P. K., Warner, S. B. & Bhowmick, S. Role of fiber diameter in adhesion and proliferation of NIH 3T3 fibroblast on electrospun polycaprolactone scaffolds. *Tissue Eng.* **13**, 579–587 (2007).
226. Gould, L. J. Topical Collagen-Based Biomaterials for Chronic Wounds: Rationale and Clinical Application. *Adv. Wound Care* **5**, 19–31 (2016).
227. Lee, J., Yoo, J. J., Atala, A. & Lee, S. J. The effect of controlled release of PDGF-BB from heparin-conjugated electrospun PCL/gelatin scaffolds on cellular bioactivity and infiltration. *Biomaterials* **33**, 6709–6720 (2012).
228. Zamani, M., Prabhakaran, M. P. & Ramakrishna, S. Advances in drug delivery via electrospun and electrosprayed nanomaterials. *Int. J. Nanomedicine* **8**, 2997–3017 (2013).
229. Stephansen, K., Chronakis, I. S. & Jessen, F. Bioactive electrospun fish sarcoplasmic proteins as a drug delivery system. *Colloids Surf. B Biointerfaces* **122**, 158–165 (2014).
230. Zhang, X., Reagan, M. R. & Kaplan, D. L. Electrospun silk biomaterial scaffolds for regenerative medicine. *Adv. Drug Deliv. Rev.* **61**, 988–1006 (2009).
231. Malafaya, P. B., Silva, G. A. & Reis, R. L. Natural-origin polymers as carriers and scaffolds for biomolecules and cell delivery in tissue engineering applications. *Adv. Drug Deliv. Rev.* **59**, 207–233 (2007).
232. Hassiba, A. J. *et al.* Review of recent research on biomedical applications of electrospun polymer nanofibers for improved wound healing. *Nanomed.* **11**, 715–737 (2016).
233. Pezeshki-Modaress, M. *et al.* Gelatin/chondroitin sulfate nanofibrous scaffolds for stimulation of wound healing: In-vitro and in-vivo study. *J. Biomed. Mater. Res. A* **105**, 2020–2034 (2017).
234. Duan, H. *et al.* Engineering of epidermis skin grafts using electrospun nanofibrous gelatin/polycaprolactone membranes. *Int. J. Nanomedicine* **8**, 2077–2084 (2013).
235. Dubský, M. *et al.* Nanofibers prepared by needleless electrospinning technology as scaffolds for wound healing. *J. Mater. Sci. Mater. Med.* **23**, 931–941 (2012).
236. Zuk, P. Adipose-Derived Stem Cells in Tissue Regeneration: A Review. *ISRN Stem Cells* **2013**, 1–35 (2013).

237. Kim, S.-W., Zhang, H.-Z., Guo, L., Kim, J.-M. & Kim, M. H. Amniotic mesenchymal stem cells enhance wound healing in diabetic NOD/SCID mice through high angiogenic and engraftment capabilities. *PloS One* **7**, e41105 (2012).
238. Dash, N. R., Dash, S. N., Routray, P., Mohapatra, S. & Mohapatra, P. C. Targeting Nonhealing Ulcers of Lower Extremity in Human Through Autologous Bone Marrow-Derived Mesenchymal Stem Cells. *Rejuvenation Res.* **12**, 359–366 (2009).
239. Lu, D. *et al.* Comparison of bone marrow mesenchymal stem cells with bone marrow-derived mononuclear cells for treatment of diabetic critical limb ischemia and foot ulcer: A double-blind, randomized, controlled trial. *Diabetes Res. Clin. Pract.* **92**, 26–36 (2011).
240. Hu, M. S., Borrelli, M. R., Lorenz, H. P., Longaker, M. T. & Wan, D. C. Mesenchymal Stromal Cells and Cutaneous Wound Healing: A Comprehensive Review of the Background, Role, and Therapeutic Potential. *Stem Cells International* (2018). doi:10.1155/2018/6901983
241. Cho, S.-W. *et al.* Engineering of volume-stable adipose tissues. *Biomaterials* **26**, 3577–3585 (2005).
242. Zuk, P. A. *et al.* Human Adipose Tissue Is a Source of Multipotent Stem Cells. *Mol. Biol. Cell* **13**, 4279–4295 (2002).
243. Heimburg, D. von, Hemmrich, K., Zachariah, S., Staiger, H. & Pallua, N. Oxygen consumption in undifferentiated versus differentiated adipogenic mesenchymal precursor cells. *Respir. Physiol. Neurobiol.* **146**, 107–116 (2005).
244. Herold, C. *et al.* [Viability of autologous fat grafts harvested with the Coleman technique and the tissu trans system (shippert method): a comparative study]. *Handchir. Mikrochir. Plast. Chir. Organ Deutschsprachigen Arbeitsgemeinschaft Handchir. Organ Deutschsprachigen Arbeitsgemeinschaft Mikrochir. Peripher. Nerven Gefasse Organ V* **43**, 361–367 (2011).
245. Han, S., Sun, H. M., Hwang, K.-C. & Kim, S.-W. Adipose-Derived Stromal Vascular Fraction Cells: Update on Clinical Utility and Efficacy. *Crit. Rev. Eukaryot. Gene Expr.* **25**, 145–152 (2015).
246. Maleki, M., Ghanbarvand, F., Reza Behvarz, M., Ejtemaei, M. & Ghadirkhomi, E. Comparison of Mesenchymal Stem Cell Markers in Multiple Human Adult Stem Cells. *Int. J. Stem Cells* **7**, 118–126 (2014).
247. Bourin, P. *et al.* Stromal cells from the adipose tissue-derived stromal vascular fraction and culture expanded adipose tissue-derived stromal/stem cells: a joint statement of the International Federation for Adipose Therapeutics and Science (IFATS) and the International Society for Cellular Therapy (ISCT). *Cytotherapy* **15**, 641–648 (2013).
248. Maharlooei, M. K. *et al.* Adipose tissue derived mesenchymal stem cell (AD-MS) promotes skin wound healing in diabetic rats. *Diabetes Res. Clin. Pract.* **93**, 228–234 (2011).
249. Steinberg, J. P., Hong, S. J., Geringer, M. R., Galiano, R. D. & Mustoe, T. A. Equivalent Effects of Topically-Delivered Adipose-Derived Stem Cells and Dermal Fibroblasts in the Ischemic Rabbit Ear Model for Chronic Wounds. *Aesthet. Surg. J.* **32**, 504–519 (2012).
250. Tsumano, T. *et al.* A new mouse model of impaired wound healing after irradiation. *J. Plast. Surg. Hand Surg.* **47**, 83–88 (2013).
251. Huang, J. I. *et al.* Chondrogenic Potential of Multipotential Cells from Human Adipose Tissue: *Plast. Reconstr. Surg.* **113**, 585–594 (2004).

252. Ebrahimian T.G. *et al.* Cell Therapy Based on Adipose Tissue-Derived Stromal Cells Promotes Physiological and Pathological Wound Healing. *Arterioscler. Thromb. Vasc. Biol.* **29**, 503–510 (2009).
253. Kim, B.-S., Debye, B. & Beier, J. P. Adipose-derived stem cells in cutaneous wound repair. *Plast. Aesthetic Res.* **5**, 31 (2018).
254. Aboutaleb Kadkhodaeian, H. *et al.* Survival and Migration of Adipose-Derived Stem Cells Transplanted in the Injured Retina. *Exp. Clin. Transplant. Off. J. Middle East Soc. Organ Transplant.* **16**, 204–211 (2018).
255. Eirin, A. *et al.* MicroRNA and mRNA cargo of extracellular vesicles from porcine adipose tissue-derived mesenchymal stem cells. *Gene* **551**, 55–64 (2014).
256. Strong, A. L. *et al.* Leptin produced by obese adipose stromal/stem cells enhances proliferation and metastasis of estrogen receptor positive breast cancers. *Breast Cancer Res. BCR* **17**, (2015).
257. Kuo, Y.-R. *et al.* Adipose-Derived Stem Cells Accelerate Diabetic Wound Healing through the Induction of Autocrine and Paracrine Effects. *Cell Transplant.* **25**, 71–81 (2016).
258. Ivanova-Todorova, E. *et al.* Adipose tissue-derived mesenchymal stem cells are more potent suppressors of dendritic cells differentiation compared to bone marrow-derived mesenchymal stem cells. *Immunol. Lett.* **126**, 37–42 (2009).
259. DelaRosa, O. *et al.* Requirement of IFN- γ -Mediated Indoleamine 2,3-Dioxygenase Expression in the Modulation of Lymphocyte Proliferation by Human Adipose-Derived Stem Cells. *Tissue Eng. Part A* **15**, 2795–2806 (2009).
260. Lee, M. J. *et al.* Proteomic Analysis of Tumor Necrosis Factor- α -Induced Secretome of Human Adipose Tissue-Derived Mesenchymal Stem Cells. *J. Proteome Res.* **9**, 1754–1762 (2010).
261. Heo, S. C. *et al.* Tumor Necrosis Factor- α -Activated Human Adipose Tissue-Derived Mesenchymal Stem Cells Accelerate Cutaneous Wound Healing through Paracrine Mechanisms. *J. Invest. Dermatol.* **131**, 1559–1567 (2011).
262. Dunic, J., Dabelic, S. & Flögel, M. Galectin-3: An open-ended story. *Biochim. Biophys. Acta BBA - Gen. Subj.* **1760**, 616–635 (2006).
263. Yamaoka, A., Kuwabara, I., Frigeri, L. G. & Liu, F. T. A human lectin, galectin-3 (epsilon bp/Mac-2), stimulates superoxide production by neutrophils. *J. Immunol. Baltim. Md 1950* **154**, 3479–3487 (1995).
264. Karlsson, A., Follin, P., Leffler, H. & Dahlgren, C. Galectin-3 activates the NADPH-oxidase in exudated but not peripheral blood neutrophils. *Blood* **91**, 3430–3438 (1998).
265. Bhaumik, P., St-Pierre, G., Milot, V., St-Pierre, C. & Sato, S. Galectin-3 facilitates neutrophil recruitment as an innate immune response to a parasitic protozoa cutaneous infection. *J. Immunol. Baltim. Md 1950* **190**, 630–640 (2013).
266. Kuwabara, I. & Liu, F. T. Galectin-3 promotes adhesion of human neutrophils to laminin. *J. Immunol. Baltim. Md 1950* **156**, 3939–3944 (1996).
267. Brancato, S. K. & Albina, J. E. Wound macrophages as key regulators of repair: origin, phenotype, and function. *Am. J. Pathol.* **178**, 19–25 (2011).
268. Sano, H. *et al.* Human galectin-3 is a novel chemoattractant for monocytes and macrophages. *J. Immunol. Baltim. Md 1950* **165**, 2156–2164 (2000).
269. Danella Polli, C. *et al.* Monocyte Migration Driven by Galectin-3 Occurs through Distinct Mechanisms Involving Selective Interactions with the Extracellular Matrix. *ISRN Inflamm.* **2013**, (2013).

270. Karlsson, A. *et al.* Galectin-3 functions as an opsonin and enhances the macrophage clearance of apoptotic neutrophils. *Glycobiology* **19**, 16–20 (2009).
271. Martinez, F. O. & Gordon, S. The M1 and M2 paradigm of macrophage activation: time for reassessment. *F1000prime Rep.* **6**, 13 (2014).
272. MacKinnon, A. C. *et al.* Regulation of alternative macrophage activation by galectin-3. *J. Immunol. Baltim. Md 1950* **180**, 2650–2658 (2008).
273. Nangia-Makker, P. *et al.* Galectin-3 Induces Endothelial Cell Morphogenesis and Angiogenesis. *Am. J. Pathol.* **156**, 899–909 (2000).
274. Markowska, A. I., Liu, F.-T. & Panjwani, N. Galectin-3 is an important mediator of VEGF- and bFGF-mediated angiogenic response. *J. Exp. Med.* **207**, 1981–1993 (2010).
275. Wesley, U. V., Vemuganti, R., Ayvaci, E. R. & Dempsey, R. J. Galectin-3 enhances angiogenic and migratory potential of microglial cells via modulation of integrin linked kinase signaling. *Brain Res.* **1496**, 1–9 (2013).
276. Markowska, A. I., Jefferies, K. C. & Panjwani, N. Galectin-3 protein modulates cell surface expression and activation of vascular endothelial growth factor receptor 2 in human endothelial cells. *J. Biol. Chem.* **286**, 29913–29921 (2011).
277. Walker, J. T., Elliott, C. G., Forbes, T. L. & Hamilton, D. W. Genetic Deletion of Galectin-3 Does Not Impair Full-Thickness Excisional Skin Healing. *J. Invest. Dermatol.* **136**, 1042–1050 (2016).
278. Kasper, M. & Hughes, R. C. Immunocytochemical evidence for a modulation of galectin 3 (Mac-2), a carbohydrate binding protein, in pulmonary fibrosis. *J. Pathol.* **179**, 309–316 (1996).
279. Cao, Z. *et al.* Galectins-3 and -7, but not Galectin-1, Play a Role in Re-epithelialization of Wounds. *J. Biol. Chem.* **277**, 42299–42305 (2002).
280. Saravanan, C., Liu, F.-T., Gipson, I. K. & Panjwani, N. Galectin-3 promotes lamellipodia formation in epithelial cells by interacting with complex N-glycans on $\alpha 3\beta 1$ integrin. *J. Cell Sci.* **122**, 3684–3693 (2009).
281. Fujii, A., Shearer, T. R. & Azuma, M. Galectin-3 enhances extracellular matrix associations and wound healing in monkey corneal epithelium. *Exp. Eye Res.* **137**, 71–78 (2015).
282. Liu, W. *et al.* Galectin-3 regulates intracellular trafficking of EGFR through Alix and promotes keratinocyte migration. *J. Invest. Dermatol.* **132**, 2828–2837 (2012).
283. Hopfgartner, Adam. Development Of Granulation Tissue Mimetic Scaffolds For Skin Healing. (Western University).
284. McLeod, Karrington A. Design and Validation of Delivery Systems for Galectin-3 for Skin Healing Applications. (Western University).

2 Design and Validation of 3D Printed Scaffolds for Adipose Derived Stromal Cell Tissue Engineering

2.1 Introduction

Skin, the largest organ of the human body, is responsible for providing barrier protection as well as receiving sensation input from the external environment, and finally is responsible for thermal regulation of the body. Structurally, skin is comprised of three major layers, the epidermis, dermis and subcutaneous hypodermis.¹ Interestingly, the skin surface is not smooth but is laced with multiple networks of fine grooves called sulci cutis, which can be either deep or shallow. The slightly elevated areas that are surrounded by shallower areas of sulci cutis are called cristae cutis.² Sweat pores fed by the sweat glands open to the cristae cutis. The orientation of the sulci cutis, which differs depending on body location, is called the dermal ridge pattern. For instance, fingerprints and patterns on the palms of your hand and soles of your feet are formed by the sulci cutis. In addition, at the extracellular matrix level, skin contains significant topographical features; such biological topography provides important physical cues for oriented migration (contact guidance), cell orientation, spreading, contractility, migration and signaling.

Skin contains numerous stem and progenitor cell populations, which are self-renewing as skin constantly replaces itself following desquamation, the shedding of the outermost layer of skin. Non-pathologic desquamation of the skin occurs approximately every two weeks, when keratinocytes are individually shed unnoticeably.³ Humans keratinocytes turn over from stem cells to desquamation every 40-56 days,⁴ whereas in mice the estimated turnover time is much faster, 8-10 days.⁵ The continual regeneration of skin is maintained by permanently residing stem cells that sustain principal differentiated epidermal lineages, the interfollicular epidermis (IFE), sebaceous gland (SG), hair follicle (HF),^{6,7} and Merkel cell mechanoreceptors.⁸ Through radiation dose-survival studies, it was suggested that stem cells comprise about 2-7% of basal layer cells⁹ while another study of murine basal layer cells suggested a larger stem cell population, 10-12% of cells in the basal layer.¹⁰ Maintenance of skin homeostasis is dependent on the ability of stem cells to replenish the turnover of mature epithelial lineages.

Stem cell-based therapies employs the regenerative nature of stem and progenitor cells to treat disease or pathological conditions. In regenerative medicine, stem cells can be removed

from their natural environment, expanded to increase the population, and finally, implanted into a pathological tissue environment with or without a delivery scaffold. How stem and progenitor cells interact with their native microenvironment (stem cell niche), to establish and maintain their properties is crucial to tissue engineering applications particularly when the microenvironment is pathological in nature.¹¹ Of interest in tissue engineering is the cell population of adipose-derived stem/stromal cells (ASCs). ASCs have been shown to proliferate rapidly and differentiate *in vitro* towards adipogenic, osteogenic, chondrogenic and myogenic lineages.^{12,13} ASCs are found in the stromal vascular fraction along with pre-adipocytes, endothelial cells, pericytes, T cells, and alternative M2 macrophages.¹⁴ Following harvesting from the body by mechanical liposuction, manual aspiration, or surgical excision, enzymatic procedures, culture expansion with plastic adherence, and sorting using immunomagnetic beads coated with specific antibodies can be employed to isolate ASCs from contaminating cell types.¹⁵ ASCs have been implicated in tissue regeneration processes though their differentiation potential and secretion of bioactive molecules which signal and influence bioactivity of surrounding cells.¹⁶⁻²¹

A biomaterial for stem cell culture and delivery should provide biomimetic physical and chemical cues. Collagen type I composes 90% of the total collagen content in the skin, conferring compressive and tensile strength. Current approaches to the assembly of three-dimensional (3D) biomaterials use additive manufacturing (3D printing) to deposit materials layer by layer for controlled structure and architecture. Printing of biological hydrogels include syringe-based extrusion,^{22,23} printing with fibrin,^{24,25} gelatin,²⁶ and protein mixtures obtained from decellularized tissues.²⁷ However, 3D printed biological hydrogels and proteins must gel *in situ* in order to prevent their collapse or shape deformation; moreover the structural integrity of printed scaffolds remains to be studied *in vivo*.²⁸⁻³⁰ Direct printing into a secondary hydrogel that acts as a temporary support bath is of interest to preserve 3D printed architectures of soft biomaterials.^{31,32} In this study, 3D printed scaffolds are employed to assess *in vitro* ASC bioactivity and phenotype.

2.2 Materials and Methods

2.2.1 Preparation of Gelatin Support Slurry

A gelatin microparticle support slurry was adapted from Hinton *et al.*³¹ The preparation protocol is summarized in Figure 2.1. A 100 mL volume of 4% (w/v) type A 275 bloom porcine

gelatin powder (Advanced Biomatrix, San Diego, CA, USA) hydrate in 1X phosphate buffered solution (PBS) pre-heated to 45°C was prepared in a glass 500 mL mason jar (Ball Inc., Broomfield, CO, USA). The solution was mixed until gelatin had fully dissolved and then stored overnight at 4°C to produce a semi-rigid gelatin colloid. The following day, 100 mL of 1X PBS chilled to 4°C was transferred to the jar and a rubber spatula was used to gently dislodge the gelatin. The jar was overflowed with 4°C 1X PBS and a rubber sealing ring, Osterizer® Ice Crusher Blade (Sunbeam Products, Inc., Boca Raton, FL, USA), and threaded bottom cap were twisted onto the jar rim. The sealed jar was placed at -20°C until ice crystals began to form between the colloid and fluid layers, approximately 45 min. Immediately following removal from the -20°C freezer, the jar was inverted onto an Osterizer® Heritage Blend 400 (Sunbeam Products, Inc., Boca Raton, FL, USA) consumer-grade blender and the gelatin was blended to mechanically disrupt the gel for 60, 90, or 120 s. The gelatin slurry was placed on ice and aliquoted into 50 mL conical centrifuge tubes, also placed in ice. The slurry was centrifuged at 4000xg and 4°C for 5 min to separate the supernatant, composed of excess PBS and soluble gelatin, from the gelatin microparticle layer. The supernatant was poured off and 10 mL of 4°C 1X PBS was added to each conical centrifuge tube; all tubes were kept on ice to prevent the gelatin from melting. The slurry was vortexed briefly to resuspend the gelatin, and centrifugation followed by resuspension in fresh 1X PBS was repeated three more times. Once the supernatant had been completely cleared from the gelatin microparticle layer, 10 mL of fresh 4°C 1X PBS was added to each tube, tubes were vortexed, and stored in a 4°C fridge. To prepare the gelatin support slurry for use, it was recovered from the fridge, vortexed, then centrifuged at 4000xg and 4°C for 5 min. The supernatant was poured off and the slurry was scooped into a sterile 60 x 15 mm round polystyrene dish (Corning Inc. Life Sciences, Durham, NC, USA) using a metal spatula to prevent air bubble formation within the support slurry. The slurry surface was smoothed using a metal spatula and two light-duty tissues (VWR International, LLC, Radnor, PA, USA) were placed on top of the slurry to absorb residual liquid.

2.2.2 Gelatin Support Slurry Rheology

Gelatin slurries were prepared as described above and rheological properties of slurries blended for 60, 90, or 120 s (N=2, n=3) were measured. Approximately 5 cc of slurry was loaded

onto a Modular Compact Rheometer (MCR) 302 (Anton Paar GmbH, Graz, Austria) equipped with a 50 mm parallel plate measuring system equipped with a moisture trap to prevent samples from drying out. Samples were pre-sheared at 10 Hz for 5 min then subject to a 10 min wait period. Viscoelasticity was analyzed by frequency sweep from 0.1 to 100 rad/s at 1 mm separation and 3% strain. A second wait period was observed for 10 min. Viscosity was analyzed by controlled shear rate (CSR) flow testing from 0.01 to 30 Hz. The MCR 302 was held at 23°C for the duration of all rheological measurements as to accurately reflect the ambient temperature during 3D printing.

2.2.3 Gelatin Support Slurry Microparticle Morphology

To study gelatin microparticle morphology, support slurries were blended for 60, 90, or 120 s (N=2). Gelatin slurries were recovered from 4°C, vortexed, and diluted 1:4 in 4°C Immu-Mount mounting medium (Thermo Fisher Scientific, Waltham, MA, USA) containing 2.5% (v/v) blue dye (McCormick & Co., Inc., London, ON, Canada). Samples were mounted on a coverslip and imaged using a Nikon SMZ 1500 stereomicroscope (Nikon Instruments Inc, Melville, NY, USA) and CoolSNAP cf camera (Teledyne Photometrics, Tucson, AZ, USA). ImageJ software (National Institutes of Health, Bethesda, MD, USA) was employed to convert each image to 8-bit greyscale and adjust brightness, contrast, and thresholding. Particles were counted and analyzed, and the effect of blend time on gelatin microparticle area, perimeter, Feret diameter, and circularity was measured (n=250).

2.2.4 Scaffold Computer-Aided Design

Collagen scaffolds were designed using SolidWorks modeling program (Dassault Systèmes, Vélizy-Villacoublay, France) to generate a 10 x 10 x 0.5 mm rectangular prism stereolithography (STL) file. The 10 x 10 x 0.5 mm STL was uploaded in quadruplicate to Slic3r (open source GNU AGPL license) for Gcode generation. STLs were sliced using either a rectilinear or hexagonal/honeycomb infill pattern at 20% infill density.

Polycaprolactone (PCL) scaffolds were designed using Simplify3D (Cincinnati, Ohio, USA) slicing software. A 50 x 50 x 2 mm rectangular prism stereolithography (STL) file was sliced with a 50% density, rectilinear infill pattern.

2.2.5 Printing of Porous Collagen Scaffolds

A r3bEL mini bioprinter (SE3D, Santa Clara, CA, USA) was plugged into a 12V DC power adaptor and controlled using Pronterface free open-source software (Printrun software licensed under the GNU General Public License, version 3). Porous collagen scaffolds were printed using freeform reversible embedding as described by Hinton *et al.*³¹ Lifeink® 200 collagen bioink (Advanced Biomatrix) consisting of 35 mg/mL pH neutral type I collagen purified from bovine hide with physiological salt concentration, was loaded into a 5 mL syringe and centrifuged at 100xg and 4°C for 1 min. Any air collected at the top of the syringe was expelled, and the syringe was fitted with a stainless steel 30G blunt luer stub to serve as the printing nozzle. The syringe was manually primed until collagen ink filled the nozzle, then mounted into the syringe pump extruder of the bioprinter. A 60 x 15 mm round polystyrene dish containing gelatin microparticle support slurry prepared as described in section 2.2.1 was positioned on the bioprinter bed and secured with vinyl-coated laboratory tape (VWR) to prevent slippage during movement of the print bed. The nozzle tip was positioned at the center of the support bath in *x* and *y* dimensions, and approximately 2 mm from the bottom of the bath in the *z* (lateral) direction. G-code instructions were immediately initiated to avoid clogging the nozzle. All printing was completed at ambient temperatures (~23°C) over a period of 30 min and unused collagen ink was stored in the sealed syringe at 4°C immediately after printing. The polystyrene dish containing porous collagen scaffolds embedded within the gelatin support slurry was incubated at 37°C for 2 hr to melt the gelatin. Liquified gelatin was aspirated, and liberated collagen scaffolds were washed three times with PBS.

2.2.6 Printing of Porous Polycaprolactone Scaffolds

Low temperature polycaprolactone (PCL) 3D Filament (eSUN eMate, Shenzhen Esun Industrial Co., Ltd., Shenzhen, China) was fed into a F400-S (Fusion 3, Greensboro, NC, USA) operated using Duet Web Control (Creative Commons CC BY-SA 3.0 license). A 0.4 mm extrusion nozzle was heated to 90°C and the print bed to 30°C before execution of Gcode. Upon completion of printing, 6 mm diameter circular samples were cut using a biopsy punch (Integra Miltex, York, PA, USA) and functionalized using argon plasma treatment.

2.2.7 3D Printed Scaffold Morphology

Collagen and polycaprolactone scaffolds were prepared as described in sections 2.2.5 and 2.2.6 then imaged by digital camera and Nikon SMZ 1500 stereomicroscope to demonstrate scaffold architectures.

2.2.8 Collagen Scaffold Hydrophilicity

3D printed porous collagen scaffolds (N=4) were imaged using a Nikon SMZ 1500 stereomicroscope following printing, then incubated at 37°C in PBS for 14 days. Scaffolds were imaged again, and inner strut dimensions (n=45) were analyzed using ImageJ software to quantify the degree of swelling.

2.2.9 Cell Isolation and Culture

Human Research Ethics Board approval for this study was obtained from Western University (Appendix G). Subcutaneous adipose tissue samples were collected with informed consent a 67-year-old female undergoing lower limb amputation procedures at the London Health Sciences Centre (London, ON, Canada). Tissue samples were transported to the lab on ice in sterile, cation-free Dulbecco's phosphate buffered saline (DPBS; Sigma) supplemented with 20 mg/mL bovine serum albumin (BSA) and processed within 2 hr for adipose-derived stem/stromal cell (ASC) isolation. Adipose tissue was washed with PBS by shaking, then treated with a digestion solution consisting of 0.1% (w/v) collagenase type 1, 1% (w/v) CaCl₂, and 1% (w/v) BSA. Fat tissue was minced and incubated for 1 hr at 37°C. The sample was centrifuged for 5 min at 420xg and the liquid supernatant was aspirated off. The cellular pellet was resuspended in proliferation medium comprised of DMEM supplemented with 10% (v/v) fetal bovine serum (FBS; Thermo Fisher Scientific), and 3% (v/v) antibiotic-antimycotic (Life Technologies Inc., Burlington, ON, Canada) and cultured on tissue culture polystyrene (TCPS; Corning, New York) at 37°C (20% O₂ and 5% CO₂). After 24 hr, the media was replaced and adherent cells were expanded further. The culture medium was replaced every 3 days and cells were cryopreserved in freezing medium comprised of 80% FBS, 10% Dulbecco's Modified Eagle Medium (DMEM) and 10% dimethyl sulfoxide (DMSO) at passage one. ASCs were thawed and propagated on TCPS with 3rd passage cells used for all studies.

2.2.10 *In Vitro* Proliferation Assay

Collagen scaffolds in two architectures, rectilinear and hexagonal, and rectilinear PCL scaffolds were placed in a 24-well culture plate and ultraviolet (UV) treated for 2 hr. P3 ASCs were seeded onto each scaffold at 80,000 cells per well and cultured in proliferation medium comprised of DMEM supplemented with 10% (v/v) FBS and 3% (v/v) antibiotic-antimycotic (37°C, 20% O₂ and 5% CO₂). Cells were also seeded onto TCPS as a control. After 24 hr culturing on scaffolds, cells were stained using the iFluor 488 EdU proliferation assay (ab219801, Abcam). Cells were incubated with 40 μM EdU for 2 hr then fixed in 4% paraformaldehyde for 15 min at room temperature. Samples underwent two washes with PBS containing 3% BSA before permeabilization for 20 min. Samples were washed twice and incubated with a reaction mixture composed of 1:420 iFluor 488 azide, 20 mg/mL sodium ascorbate and 4 mM copper sulfate in 1X Tris-buffered saline (TBS). The reaction mixture was prepared fresh and used within 15 min of preparation. Samples were rocked to ensure even distribution of the reaction mixture, then incubated at room temperature for 30 min protected from light. Samples were washed once with PBS containing 3% BSA, then again in fresh PBS. Samples were then incubated with Hoechst 33342 (Trihydrochloride Trihydrate; Thermo Fisher Scientific) or propidium iodide (PI) at a dilution of 1:1000 for 1 hr at room temperature and subsequently washed with PBS three times. TCPS controls were imaged using an Axio Observer Z1 fluorescence microscope (Carl Zeiss) and 491/520 nm excitation/emission. Collagen and PCL scaffolds were imaged using z-stack acquisition on an LSM 800 confocal microscope (Zeiss). Images for each sample (n=10) were taken at 10X magnification and used to calculate the fraction of EdU-positive cells.

2.2.11 *In Vitro* Cytoskeleton Morphology

Collagen scaffolds in two architectures, rectilinear and hexagonal, and rectilinear PCL scaffolds were placed in a 24-well culture plate and UV treated for 2 hr. P3 ASCs were seeded onto each scaffold at 80,000 cells per well and cultured in proliferation medium comprised of DMEM supplemented with 10% (v/v) FBS and 3% (v/v) antibiotic-antimycotic (37°C, 20% O₂ and 5% CO₂). Cells were also seeded onto TCPS as a control. TGF-β1 (R&D Systems, Minneapolis, MN, USA) or bovine serum albumin (BSA) were added to the proliferation media at 10 ng/mL. After either 3 days or 14 days of culturing on scaffolds, cells were washed three

times with PBS, then fixed for 10 min in 4% paraformaldehyde at room temperature. Samples underwent three PBS washes then were permeabilized using 0.1% Triton X-100 for 5 min. Washes were repeated and cells were incubated with 10% horse serum for 30 min to block non-specific antibodies. Samples were incubated overnight at 4°C with a vinculin primary antibody (MAB3574, Millipore) at 1:1000 in 1% horse serum. The next day, samples were washed and incubated with 1:1000 Alexa Fluor 488 (Abcam), 1:1000 Hoechst 33342, and 1X rhodamine-conjugated phalloidin (ab235138, Abcam) for 1 hr at room temperature, protected from light. Samples were washed with PBS three times to remove unbound antibodies. TCPS controls were imaged using an Axio Observer Z1 fluorescence microscope (Carl Zeiss) and collagen and PCL scaffolds were imaged using z-stack acquisition on an LSM 800 confocal microscope (Zeiss). Images for each sample (n=10) were taken at 10X magnification.

2.2.12 *In Vitro* Fibronectin Detection

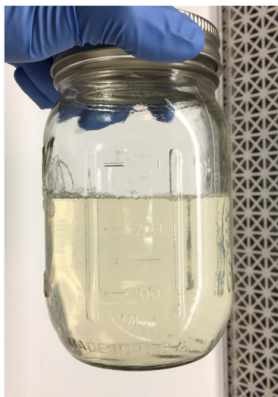
Collagen scaffolds in two architectures, rectilinear and hexagonal, and rectilinear PCL scaffolds were placed in a 24-well culture plate and UV treated for 2 hr (N=3). P3 ASCs were seeded onto each scaffold at 80,000 cells per well and cultured in proliferation medium comprised of DMEM supplemented with 10% (v/v) FBS and 3% (v/v) antibiotic-antimycotic (37°C, 20% O₂ and 5% CO₂). Cells were also seeded onto TCPS as a control. Transforming growth factor beta 1 (TGF-β₁) or bovine serum albumin (BSA) were added to the proliferation media at 10 ng/mL. After either 3 or 14 days of culturing on scaffolds, samples were treated using the immunofluorescent protocol described in section 2.2.11. A fibronectin primary antibody (sc 8422, Santa Cruz Biotechnology) was employed at 1:1000; the next day, samples were incubated with 1:1000 Alexa Fluor 488 (Abcam), 1:1000 Hoechst 33342, and 1X rhodamine-conjugated phalloidin. TCPS controls were imaged using an Axio Observer Z1 fluorescence microscope (Carl Zeiss) and collagen and PCL scaffolds were imaged using z-stack acquisition on an LSM 800 confocal microscope (Zeiss). Images for each sample (n=10) were taken at 10X magnification.

2.2.13 *In Vitro* Phenotype Study

Collagen scaffolds in two architectures, rectilinear and hexagonal, and rectilinear PCL scaffolds were placed in a 24-well culture plate and UV treated for 2 hr (N=3). P3 ASCs were

seeded onto each scaffold at 50,000 cells per well and cultured in either proliferation medium, osteogenic differentiation medium, or adipogenic differentiation medium. Cells were also seeded onto TCPS as a control. The proliferation medium was comprised of DMEM supplemented with 10% (v/v) FBS and 3% (v/v) antibiotic-antimycotic (37°C, 20% O₂ and 5% CO₂). Osteogenic differentiation medium, used to induce osteogenic lineage, was comprised of proliferative medium supplemented with 10 mM β-glycerophosphate and 50 μg/mL ascorbate 2-phosphate.³³ Adipogenic differentiation medium was comprised of serum-free DMEM media supplemented with 3% antibiotic-antimycotic, 33 μM biotin (vitamin B₇), 17 μM pantothenic acid (vitamin B₅), 66 nM insulin, 1 nM triiodothyronine (T3), and 10 μg/mL transferrin.^{20,34} For the first 3 days of culture, 1 μg/mL of troglitazone and 0.25 mM isobutylmethylxanthine (IBMX) were also included in the adipogenic media.^{20,34} After 21 days of culturing on scaffolds, samples were treated using the immunofluorescent protocol described previously. Primary detection antibodies for runt-related transcription factor 2 (RUNX2; EPR14334, abcam) and peroxisome proliferator-activated receptor gamma (PPARγ; A3409A, R&D Systems) were employed at 1:1000 and 1:400, respectively. Samples were subsequently incubated with Alexa Fluor 488 goat α mouse, Alexa Fluor 647 donkey α rabbit (Abcam), and Hoechst 33342, each at 1:1000 dilution. TCPS controls were imaged using an Axio Observer Z1 fluorescence microscope (Carl Zeiss) and collagen and PCL scaffolds were imaged using z-stack acquisition on an LSM 800 confocal microscope (Zeiss). Images for each sample (n=10) were taken at 10X magnification.

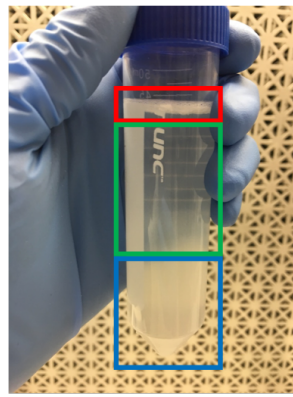
Figure 2.1. Preparation of the Sacrificial Support Slurry. A gelatin microparticle slurry was employed as a secondary, thermo-reversible support medium for 3D printing of collagen.



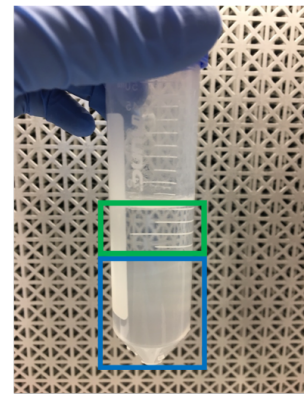
1. Gelatin solidified overnight at 4°C



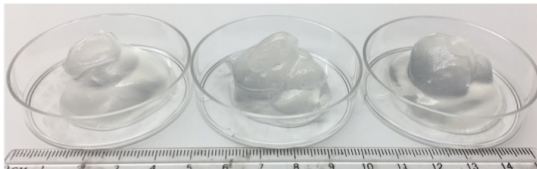
2. Gelatin blended for 120 s



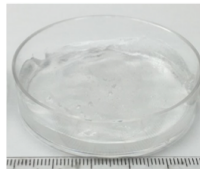
3. Soluble gelatin (red), PBS washing solution (green), and gelatin slurry (blue) after centrifugation



4. PBS washing solution (green) and gelatin slurry (blue) after final wash



5. Slurry product before smoothing



6. Final product ready for printing

2.3 Results

2.3.1 Preparation of 3D Printed Scaffolds

To manufacture collagen scaffolds for human ASC culturing, collagen bioink was printed by positive-displacement ejection from a syringe. Collagen bioink printed directly onto TCPS resulted in material flowing out of the deposited architecture (Figure 2.1). Moreover, following gelation, printed scaffolds adhered to the TCPS surface and could not be lifted off without further collapse of the scaffold shape. Collagen bioink was too viscous to direct print, thus reverse embedded printing was considered. Suspension of printed materials within a secondary, sacrificial material in order to preserve the desired print architecture and allow for easy scaffold liberation.

A gelatin microparticle slurry was adapted with modification from Hinton *et al.*^{31,32} and employed as a secondary, thermo-reversible support medium for 3D printing of collagen. Gelatin in PBS was mechanically blended for 60, 90, or 120 s to fabricate a temperature-sensitive microparticle slurry (Figure 2.2). Following centrifugation of blended particles, a white raft of soluble gelatin was apparent in all samples. Soluble gelatin was removed from all samples by repeated washes with cold PBS. Longer blend durations resulted in notably greater soluble gelatin content, indicative of gelatin melting during the longer period off ice. At 4°C the slurry remained a solid-like gel, however incubation at 37°C completely melted the gelatin to a liquid. Thus, materials embedded within the gelatin slurry could be easily removed by melting the gelatin. Gelatin slurries blended for 60, 90, or 120 s were subject to rheological testing to study deformation and flow (Figure 2.3). Independent of blend duration, all samples behave as a Bingham plastic fluid and displayed comparable viscoelasticity and viscosity ($p > 0.05$). At low stress, the slurry behaved as a solid, while at high stress it flowed as a viscous fluid. For all samples, the measured storage moduli (G') was greater than the loss moduli (G'' or E''), indicating that the gelatin slurry displayed more dominant gel-like structure than fluid-like. Supplementary rheological data is shown in Appendix A.

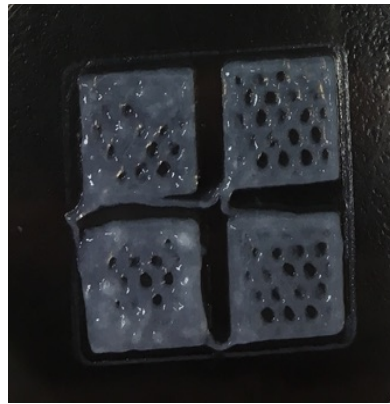
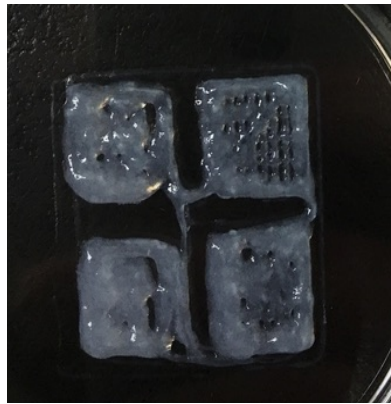
The effect of blend duration on gelatin microparticle morphology was investigated by blending gelatin samples for 60, 90, or 120 s, then observing suspended particles under a stereomicroscope (Figure 2.4). The mean particle area for slurries blended for 60, 90, or 120 s were $0.30 \pm 0.12 \text{ mm}^2$, $0.14 \pm 0.03 \text{ mm}^2$, and $0.04 \pm 0.01 \text{ mm}^2$, respectively. Significant differences in the particle area ($p < 0.05$), perimeter ($p < 0.01$) and Feret diameter ($p < 0.01$) were

observed between 60 s blended samples and 120 s blended samples. No significant differences involved the 90 s blended samples. All samples generated particles of comparable circularity, with reported index values of 0.74 ± 0.03 , 0.72 ± 0.02 , and 0.71 ± 0.03 for 60, 90, or 120 s blends (where 1.0 circularity index represents a perfect circle). Given that smaller particles would displace with higher resolution, 120 s blending was employed for all future embedded printing experiments.

For embedded printing of collagen bioinks, a 10 x 10 x 0.5 mm rectilinear prism STL was uploaded in quadruplicate to Slic3r for G-code generation (Figure 2.5). STLs were sliced using either a rectilinear or hexagonal (honeycomb) infill pattern at 20% infill density. A summary of early embedded printing attempts can be found in Appendix C. Rectilinear pores measured approximately 1 mm in diameter and exhibited interior angles of 90° . Hexagonal pores also measured approximately 1 mm in diameter and exhibited interior angles of 120° . The degree of scaffold swelling was assessed after two-week incubation in PBS at 37°C (Figure 2.6). Both infill patterns exhibited hydrophilicity, however while the hexagonal scaffold swelling was minimal enough to be considered not significant ($p > 0.05$), rectilinear swelling was significant ($p < 0.001$). This difference was likely a result of hexagonal struts being larger than their rectilinear counterparts, thus already containing free regions for water molecule infiltration, rather than being a difference in bioink hydrophilicity, since both architectures were printed using the same high concentration collagen type I bioink.

Polycaprolactone (PCL) scaffolds were printed using low temperature (90°C) polymer fusion printing. A 50 x 50 x 2 mm Rectangular prism CAD was sliced using rectilinear 50% density infill pattern from which 6 mm diameter circular samples were cut. The printed PCL construct displaced a rectilinear architecture with 90° interior angles where struts met, and struts approximately 0.4 mm in thickness.

Figure 2.2. Justification for Reverse Embedded Printing. Collagen bioink printed directly onto TCPS resulted in collapse of the scaffold architecture.



1 cm

Figure 2.3. Rheological Properties of the Gelatin Support Slurry. Gelatin slurries prepared by blending for 60, 90, or 120 s were subject to viscoelasticity and viscosity testing. A) Storage (G'), loss (G'') and complex viscosity ($|\eta^*|$) as a function of sweeping oscillatory angular frequency. B) Shear stress (τ) as a function of controlled shear rate (rotational speed) C) Viscosity (η) as a function of rotational shear rate. N=2, n=3, Two Way ANOVA, $p>0.05$. All data is represented as mean.

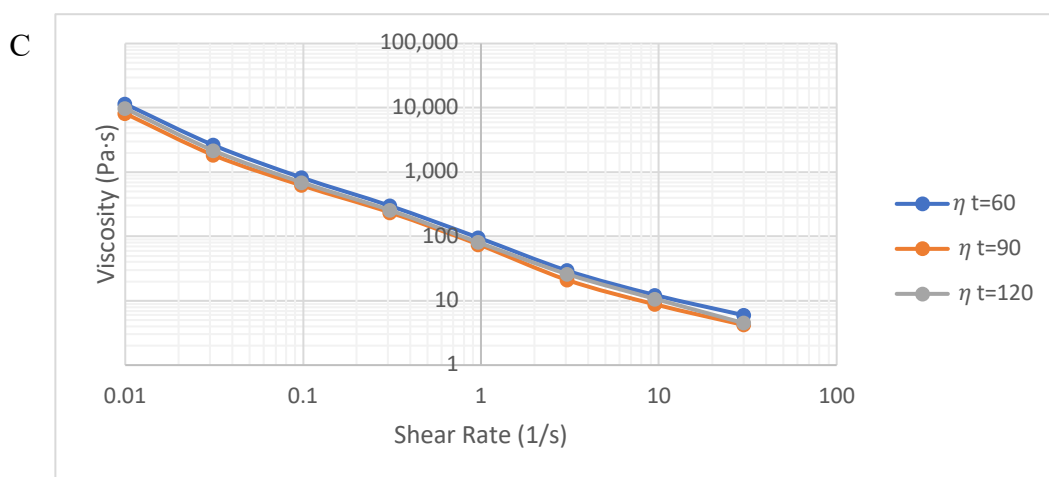
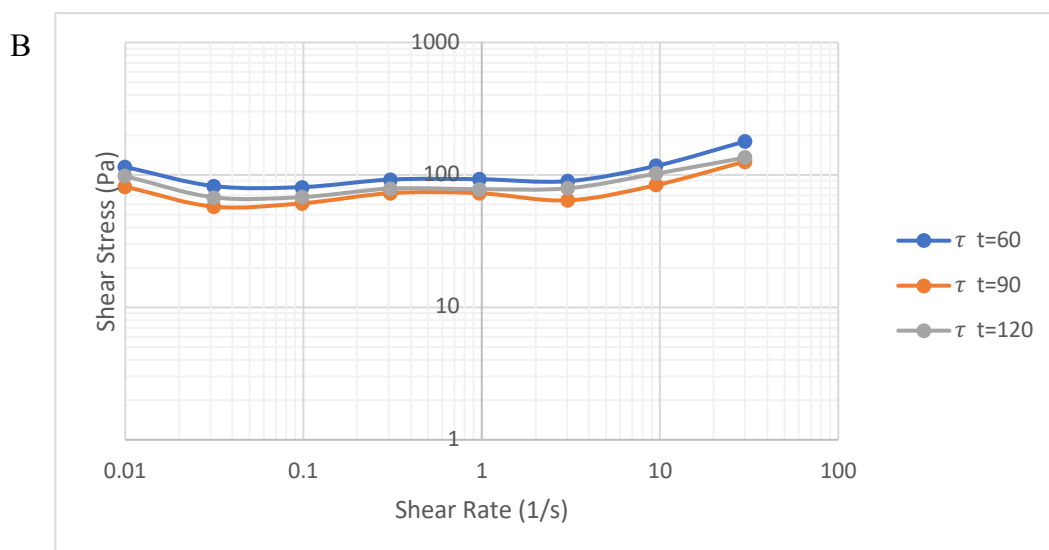
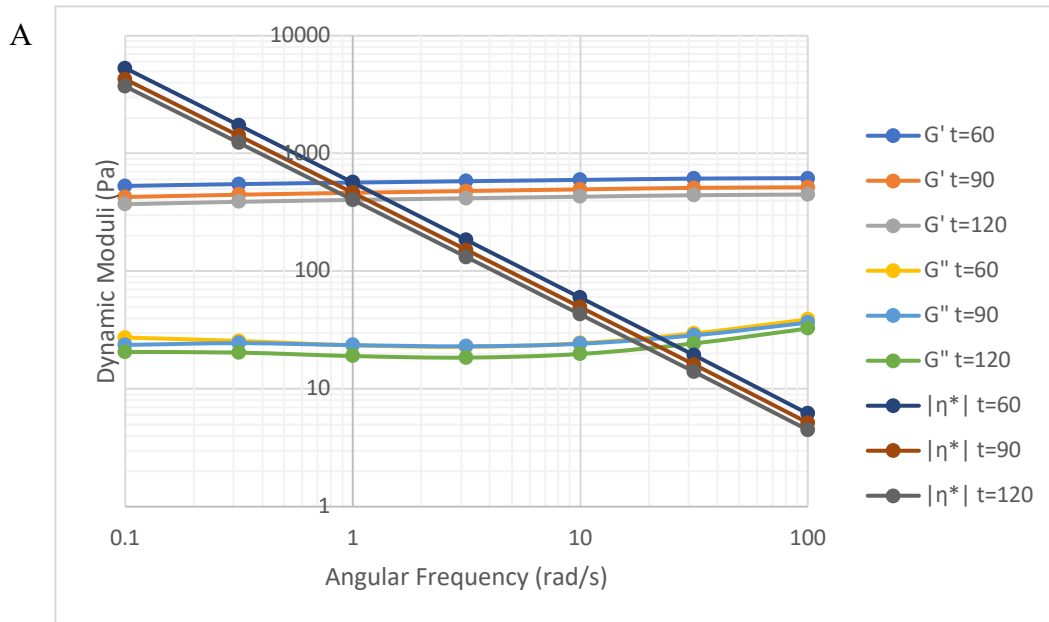
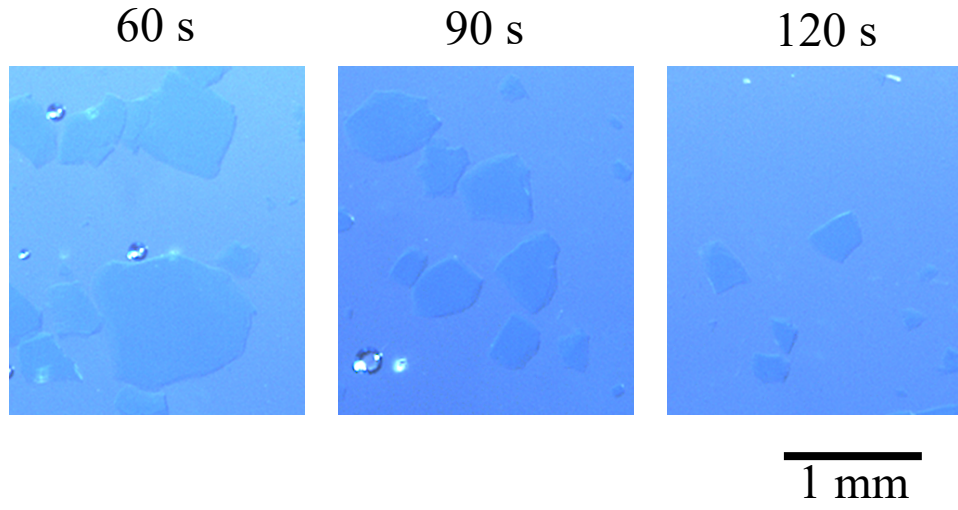


Figure 2.4. Effect of Blend Duration on Gelatin Microparticle Morphology. A)

Representative stereomicroscopic images of gelatin particles. B) Particle area, perimeter, Feret Diameter and circularity as a function of blend time. N=2, n=250, Two Way ANOVA with Tukey test, **p<0.01, *p<0.05. All data is represented as mean \pm SEM.

A



B

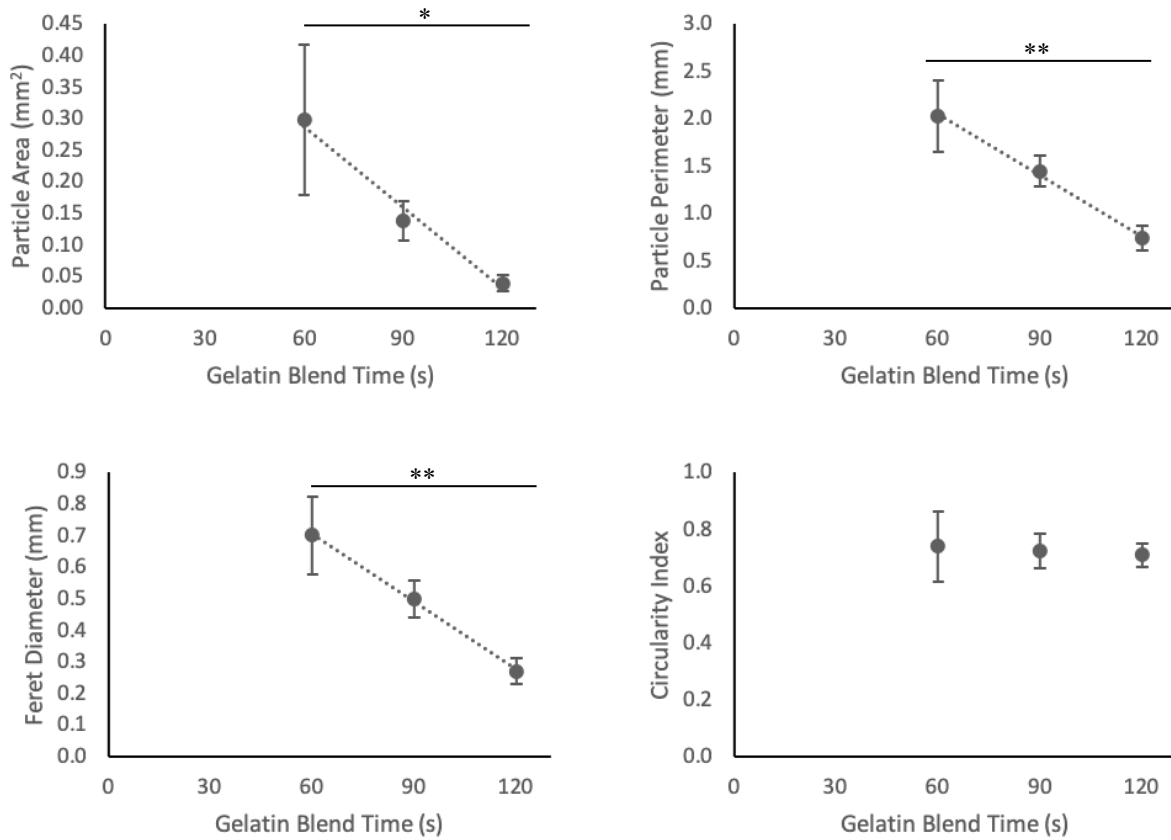
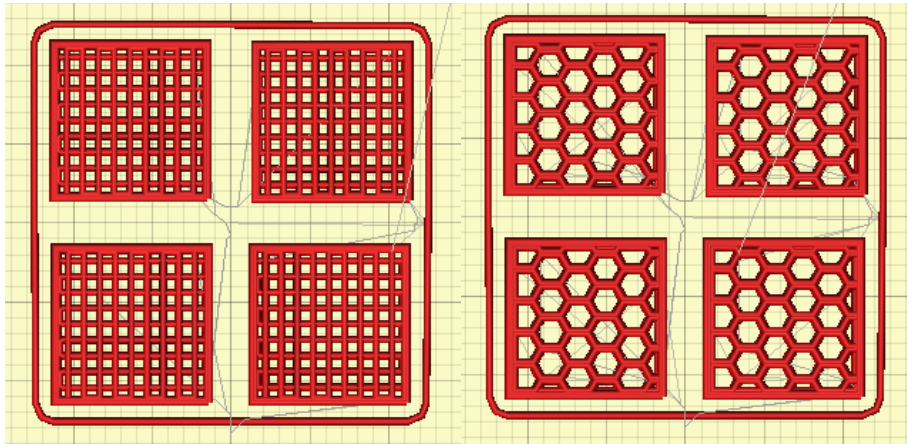
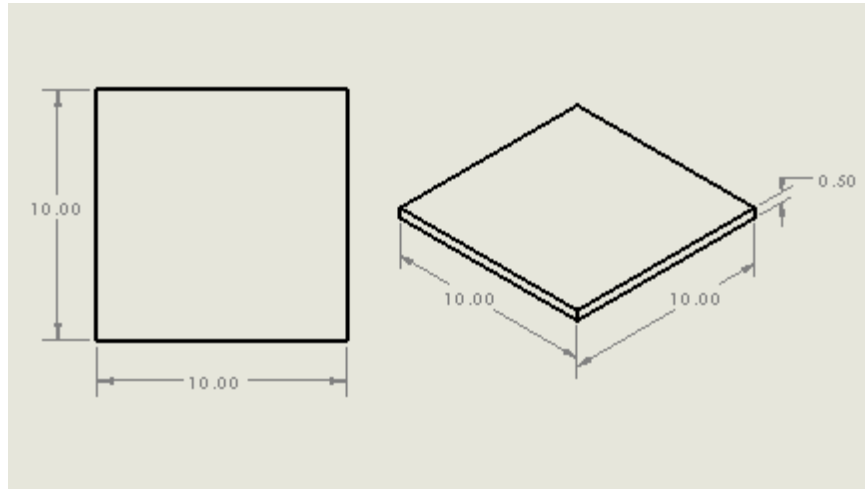


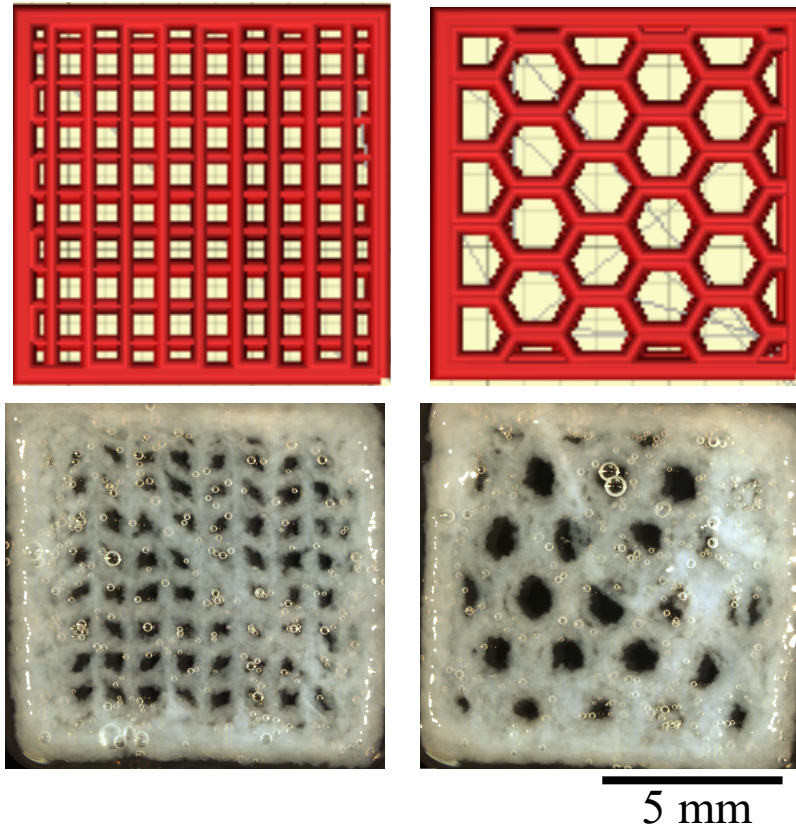
Figure 2.5. Collagen Scaffold Computer-Aided Design. A 10 x 10 x 0.5 mm rectilinear prism STL was uploaded in quadruplicate to Slic3r for G-code generation. STLs were sliced using either a rectilinear or hexagonal infill pattern at 20% infill density.



10 mm

Figure 2.6. Porous Collagen Scaffold Morphology. A) Scaffolds were successfully embedded within a gelatin support slurry and subsequently liberated. B) Scaffold swelling was assessed 2 weeks post-printing. N=4, Student's test, *** $p < 0.001$, ns=not significant at $p > 0.05$. All data is represented as mean \pm SEM.

A



B

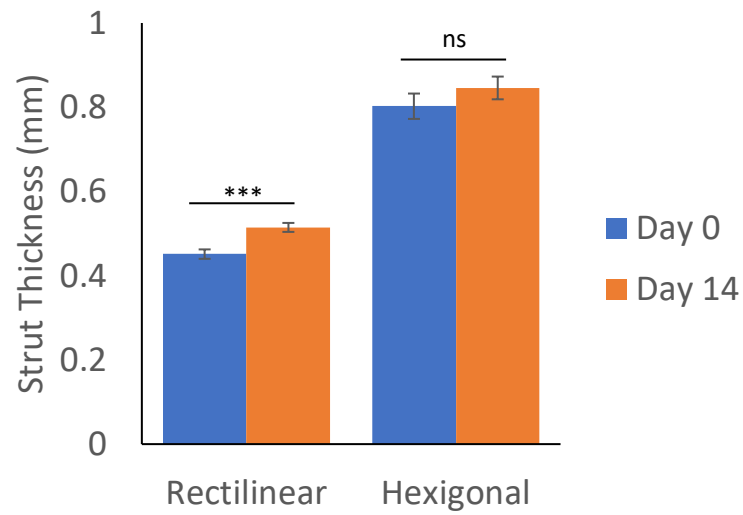
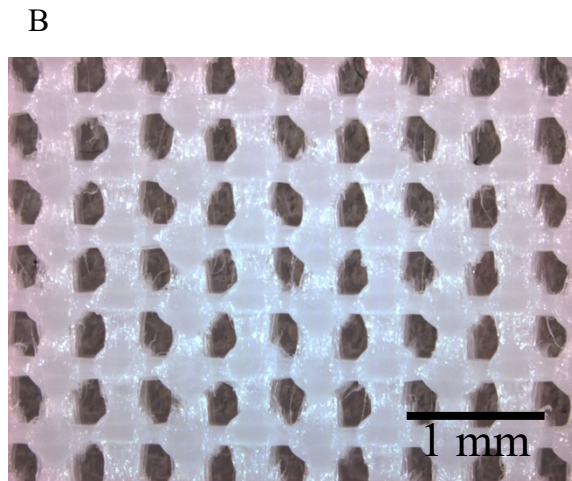
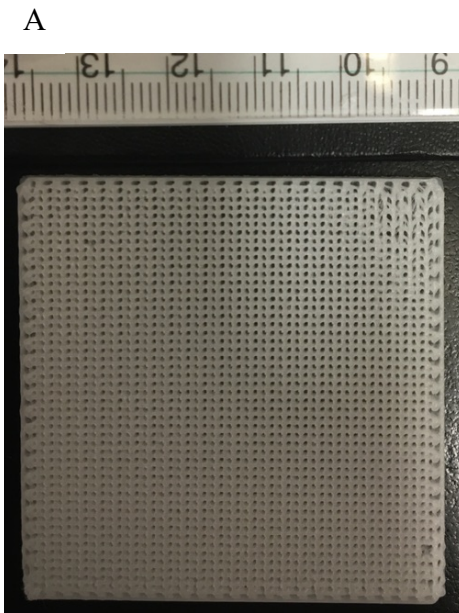


Figure 2.7. Polycaprolactone (PCL) Scaffold Morphology. A 50 x 50 x 2 mm Rectangular prism CAD was sliced using rectilinear 50% density infill pattern from which 6 mm diameter circular samples were cut. A) Digital photograph of the printed PCL construct. B) Stereomicroscopic image of the printed PCL showing scaffold architecture.



2.3.2 *In Vitro* Validation of 3D Printed Scaffolds as a Support for ASC Cell Growth

Three-dimensional printed scaffolds were assessed using human adipose-derived stem/stromal cells (ASCs) isolated from subcutaneous adipose tissue obtained from a female aged 67. In all studies, PCL rectilinear and collagen rectilinear and hexagonal 3D printed scaffolds were used.

Collagen and PCL scaffolds were first assessed using the EdU proliferation assay (Figure 2.8). Hoechst was used to counterstain DNA on TCPS and collagen scaffolds, while propidium iodide (PI) was used for PCL samples since this material auto fluoresces at 450 nm (Appendix D). ASCs seeded onto PCL scaffolds were over 90% EdU positive, and this difference was statistically significant when compared to collagen scaffolds of either architecture previously described, rectilinear or hexagonal ($p < 0.01$). While approximately 10% of cells seeded onto rectilinear or hexagonal collagen scaffolds were proliferating, it was significantly less than the control TCPS group ($p < 0.01$). ASC proliferation on PCL scaffolds compared to those cultured on TCPS was not significant ($p > 0.05$), likely as a result of low cell numbers present on PCL scaffolds themselves. Together, these results confirm that human ASCs are capable of proliferation, especially on a PCL scaffold.

ASC cytoskeletal morphology was assessed three days post-cell seeding on scaffolds and with media supplemented with transforming growth factor beta 1 (TGF- β 1) or bovine serum albumin (BSA) as a control (Figure 2.9). TGF- β 1 is a secreted cytokine that influences many cellular functions, including the control of cell growth, cell proliferation, cell differentiation, and apoptosis. The actin cytoskeleton was visualized as well as vinculin, a membrane-cytoskeletal linker protein. Qualitatively, TGF- β 1 increased cell density and spreading on all culturing surfaces, 3D scaffolds or 2D TCPS. Cells were seen to align along rectilinear or hexagonal geometries, and frequently were found stretched inside of pores, anchored to opposing struts on either side. Even in BSA control groups, cells plated on rigid PCL scaffolds exhibited robust cell spreading, an extensive actin network, and expression of vinculin; this contrasted with ASCs seeded onto soft collagen protein scaffolds, where cells appeared less spread.

ASC cytoskeletal morphology was also assessed 14 days post-seeding (Figure 2.10). Interestingly, ASCs cultured for 14 days on scaffolds exhibit a noticeable increase in cell density and spreading after 2 weeks, indicating a delayed cellular response and slower proliferative response. These results demonstrate that ASC activity can be stimulated using TGF- β 1 for rapid

(3 days) tissue regeneration while scaffolds alone are capable of maintaining viable ASCs for prolonged growth periods (2 weeks).

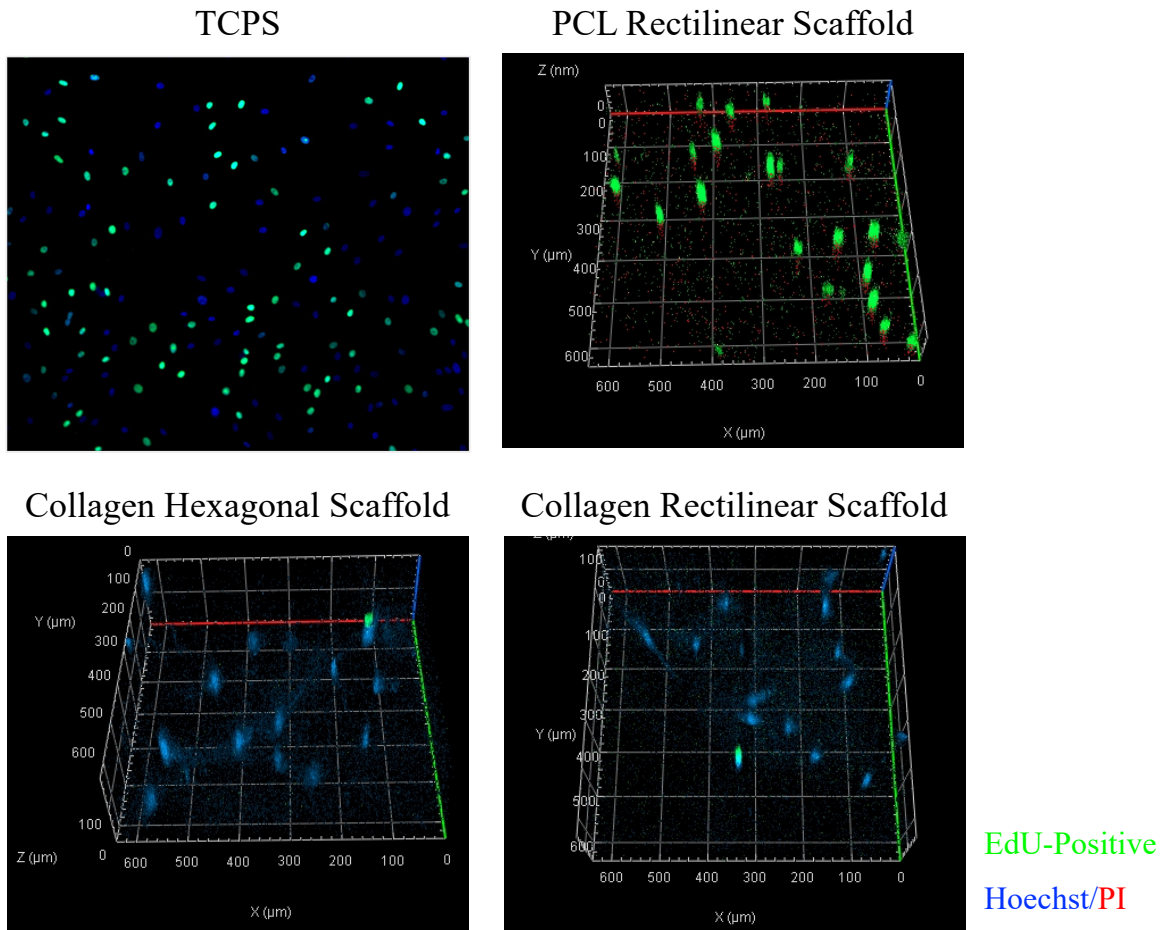
As an important component of tissue regeneration is the synthesis of new ECM, the presence of fibronectin was assessed three days post-cell seeding on scaffolds and with media supplemented with transforming growth factor beta 1 (TGF- β 1) or bovine serum albumin (BSA) as a control (Figure 2.11). Fibronectin is a high-molecular weight (~440 kDa) glycoprotein of the ECM that cells attach to through membrane-spanning receptor proteins, integrins. Fibronectin also binds to other extracellular matrix proteins such as collagen and fibrin. Consistent with previous findings, TGF- β 1 was sufficient to stimulate fibronectin production on all 3D scaffolds and the 2D TCPS. Between the BSA groups, printed collagen scaffolds appeared to increase fibronectin protein production in comparison with PCL scaffolds or 2D TCPS surfaces.

The presence of fibronectin was also evaluated 14 days post-seeding (Figure 2.12). By day 14, the presence of fibronectin was comparable to day 3 TGF- β 1 supplemented groups. The increase in fibronectin detected at day 14 suggests deposition of new fibronectin matrix by the ASCs. Fibronectin content appeared relatively uniform between PCL and collagen scaffolds by week 2. Taken together, these results have shown that ASCs can be stimulated with additional bioactive molecules and reinforces the strategy of using a biomaterial as a delivery system as well as a support structure for cells.

ASC phenotype was studied using adipogenic and osteogenic induction media types, as well as a proliferative media control. After 3-week culturing on PCL or collagen scaffolds, PPAR γ and RUNX2 expression was visualized by immunofluorescence (Figure 2.13). PPAR γ is a nuclear receptor mainly present in adipose tissue; it regulates fatty acid storage and stimulates lipid uptake. In contrast, RUNX2 is a transcription factor associated with osteoblast differentiation. Most ASCs appeared positive for PPAR γ , which was not affected by culturing in either osteogenic induction media or standard proliferative media. Varying the 3D scaffolding architecture did not appear to influence ASC phenotype, however this might be a caveat of ASCs derived from pathological lower limbs.

Figure 2.8. ASC Proliferative Potential. A) Hoechst was used to stain DNA on TCPS and collagen scaffolds, while propidium iodide (PI) was used for PCL samples. EdU-positive cells are indicative of cells that were in the process of cell division. B) The fraction of EdU-positive cells was quantified for TCPS, PCL rectilinear, and collagen rectilinear and hexagonal 3D printed scaffolds. N=3, n=10, Two Way ANOVA with Tukey test, **p<0.01. All data is represented as mean \pm SEM.

A



B

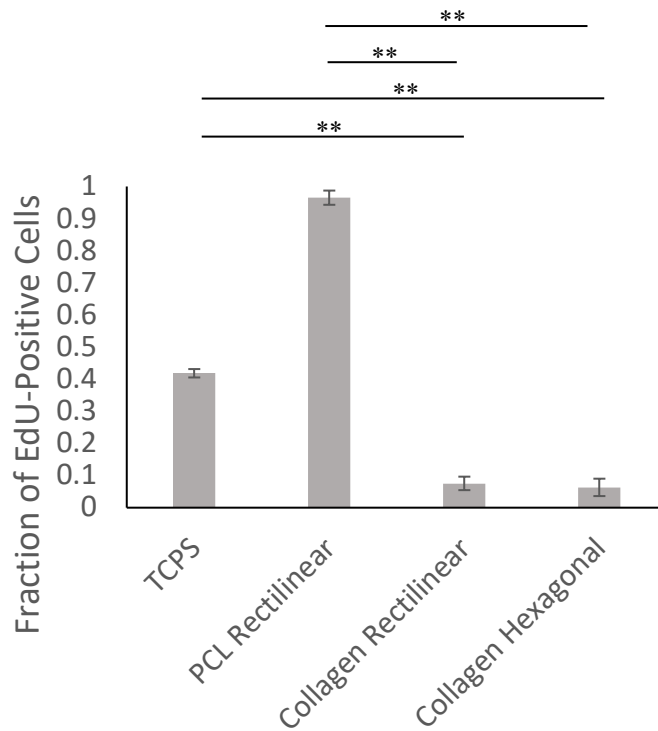
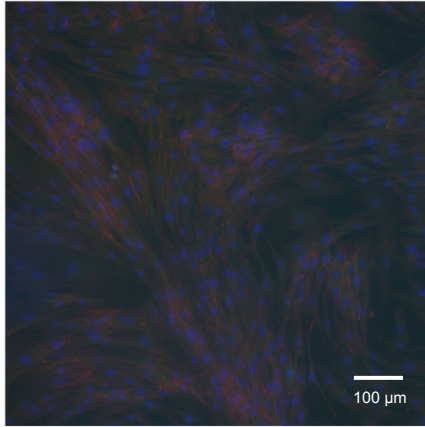


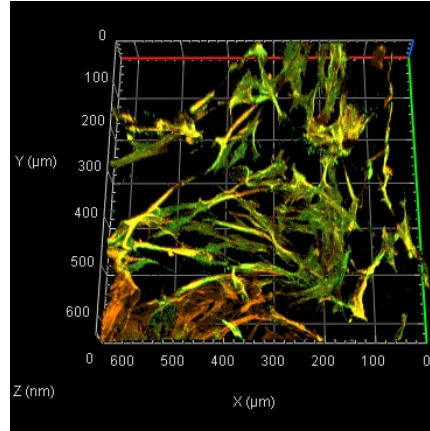
Figure 2.9. ASC Cytoskeletal Morphology. ASCs cultured on scaffolds or TCPS for 3 days with media supplemented with either A) 10 ng/mL BSA or B) 10 ng/mL TGF- β 1.

A

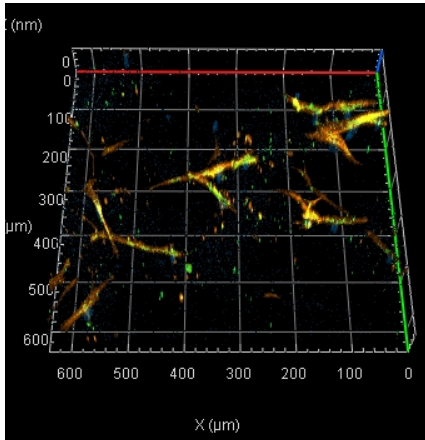
TCPS



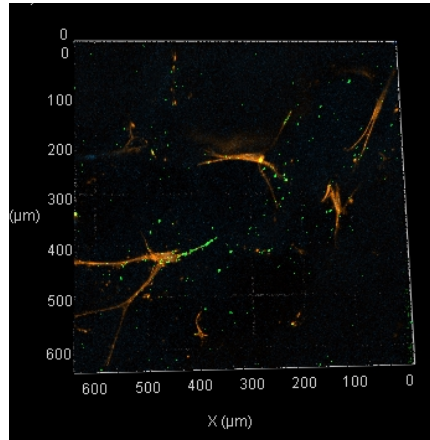
PCL Rectilinear Scaffold



Collagen Rectilinear Scaffold



Collagen Hexagonal Scaffold



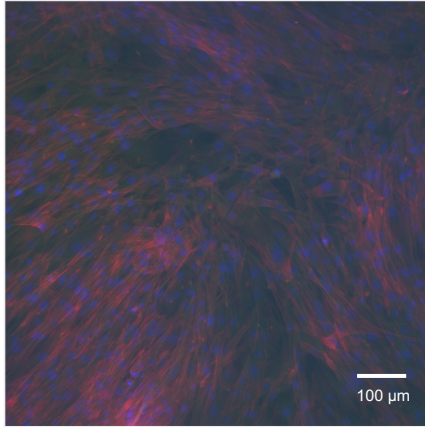
Hoechst

Vinculin

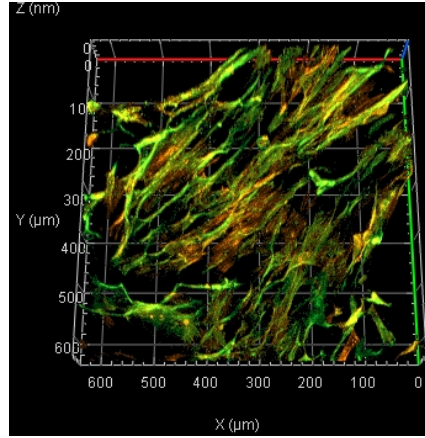
F-Actin

B

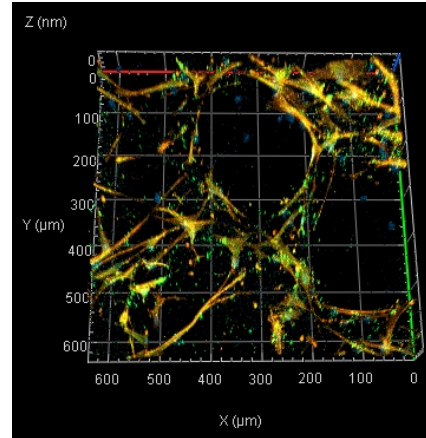
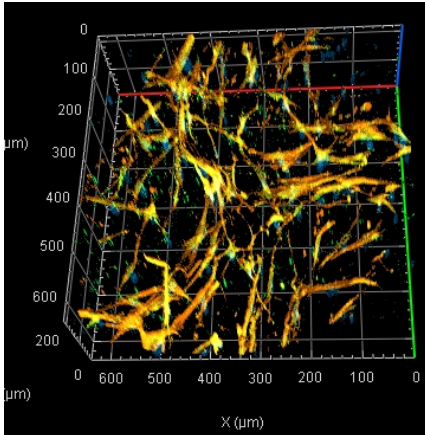
TCPS



PCL Rectilinear Scaffold



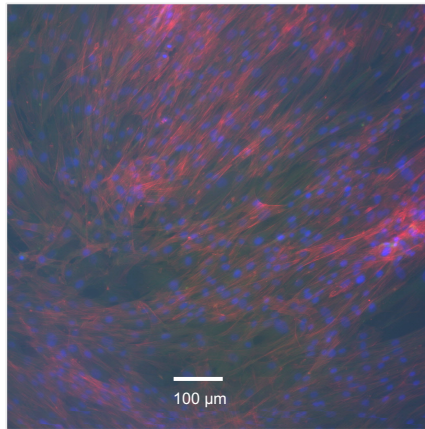
Collagen Rectilinear Scaffold Collagen Hexagonal Scaffold



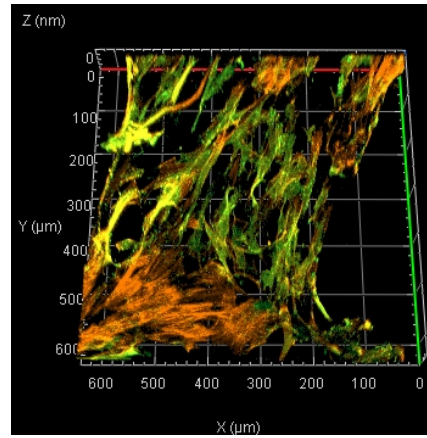
Hoechst
Vinculin
F-Actin

Figure 2.10. ASC Cytoskeletal Morphology after 14 Days. ASCs cultured on scaffolds or TCPS for 14 days with media supplemented with 10 ng/mL BSA.

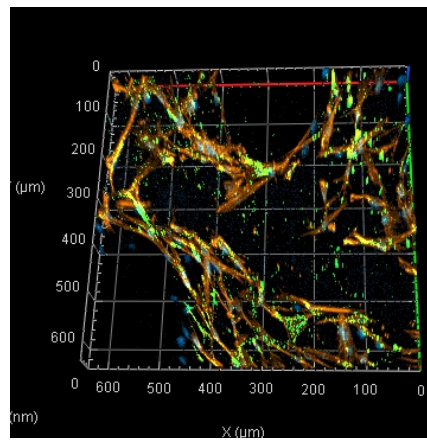
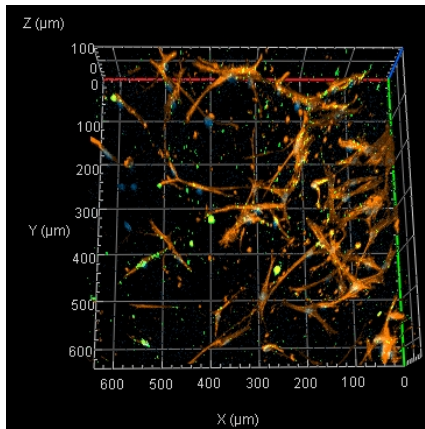
TCPS



PCL Rectilinear Scaffold



Collagen Rectilinear Scaffold Collagen Hexagonal Scaffold

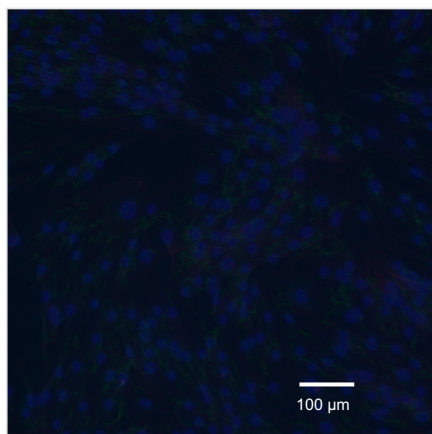


Hoechst
Vinculin
F-Actin

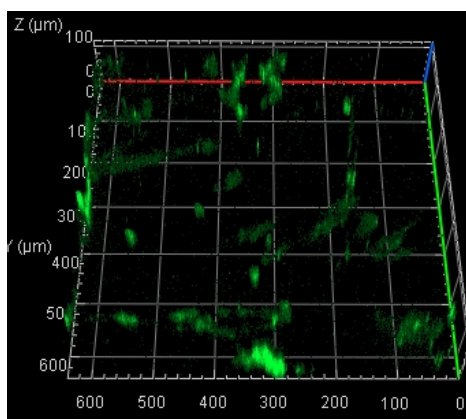
Figure 2.11. Fibronectin Detection After 3 Days. ASCs cultured on scaffolds or TCPS for 3 days with media supplemented with either A) 10 ng/mL BSA or B) 10 ng/mL TGF- β 1.

A

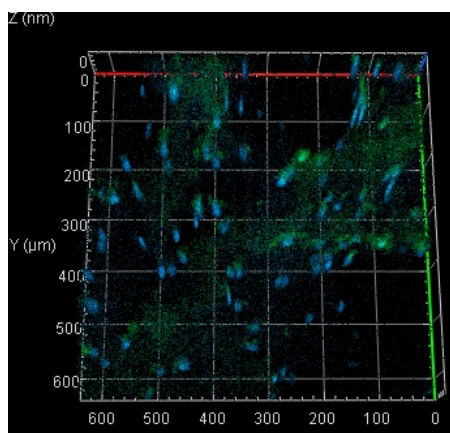
TCPS



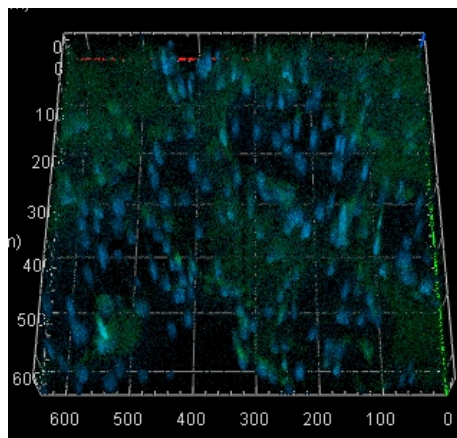
PCL Rectilinear Scaffold



Collagen Rectilinear Scaffold



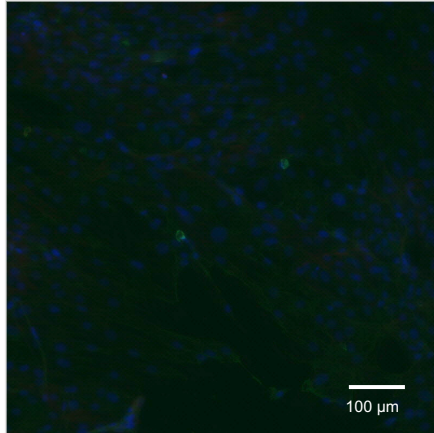
Collagen Hexagonal Scaffold



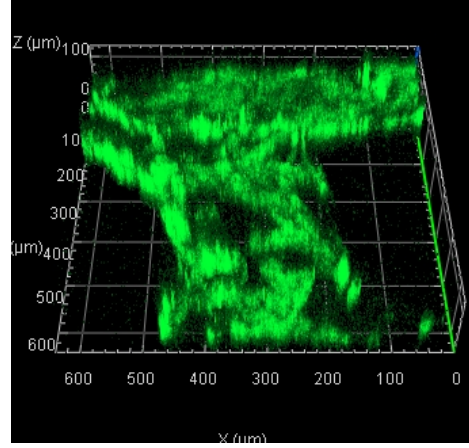
Hoechst
Fibronectin

B

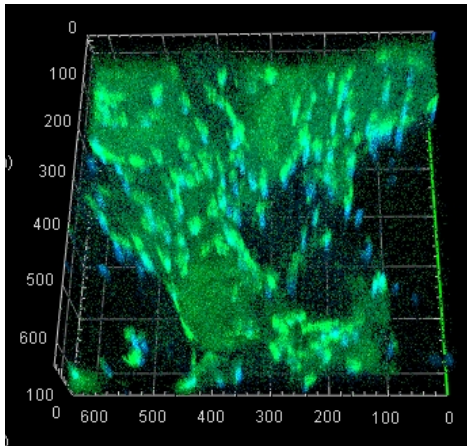
TCPS



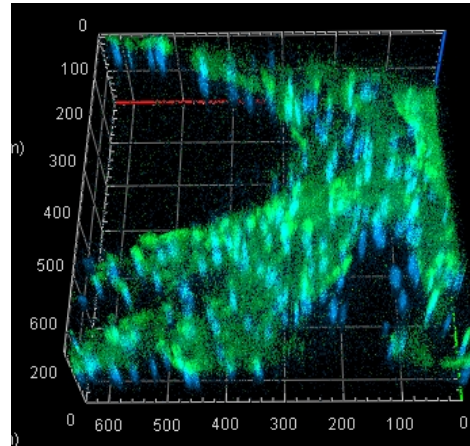
PCL Rectilinear Scaffold



Collagen Rectilinear Scaffold



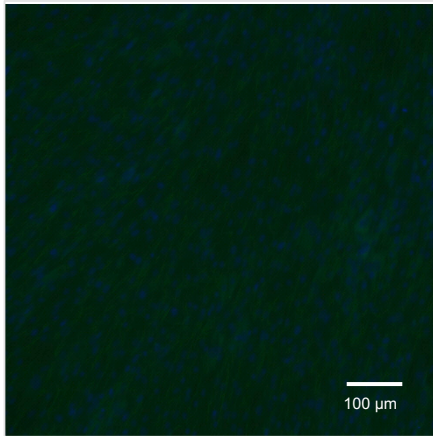
Collagen Hexagonal Scaffold



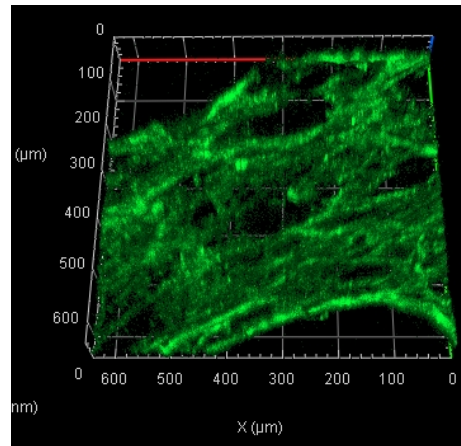
Hoechst
Fibronectin

Figure 2.12. Fibronectin Detection After 14 Days. ASCs cultured on scaffolds or TCPS for 14 days with media supplemented with 10 ng/mL BSA.

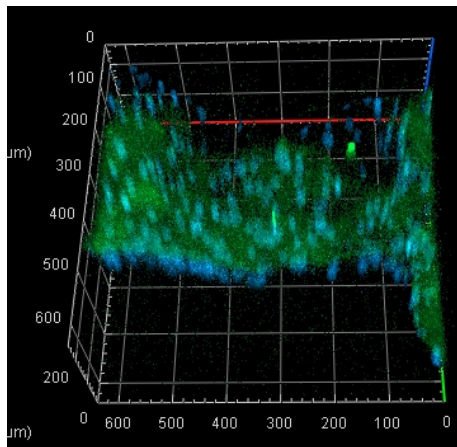
TCPS



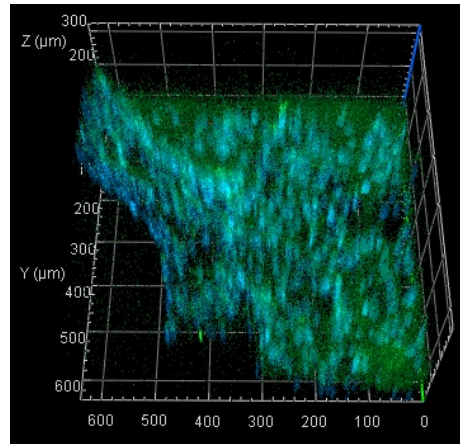
PCL Rectilinear Scaffold



Collagen Rectilinear Scaffold



Collagen Hexagonal Scaffold



Hoechst
Fibronectin

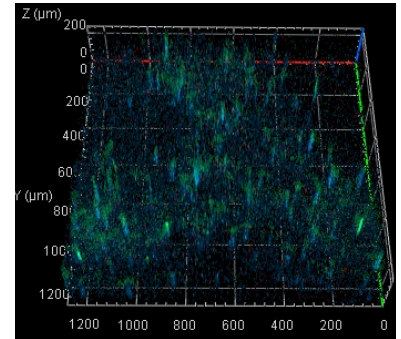
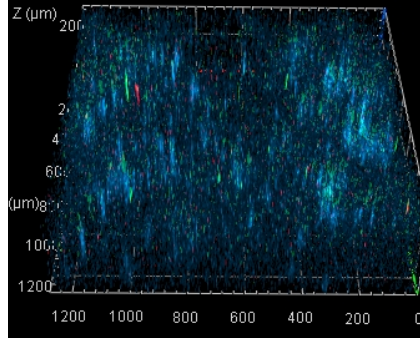
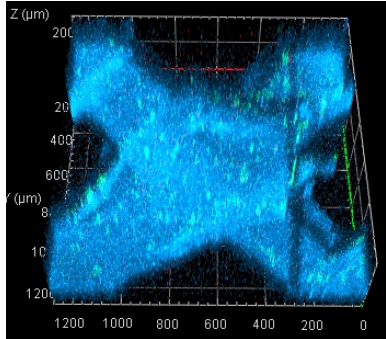
Figure 2.13. ASC Phenotype Analysis. ASC phenotype after culturing for 3 weeks in osteogenic induction media, adipogenic induction media, or proliferative media control.

PCL Rectilinear Scaffold

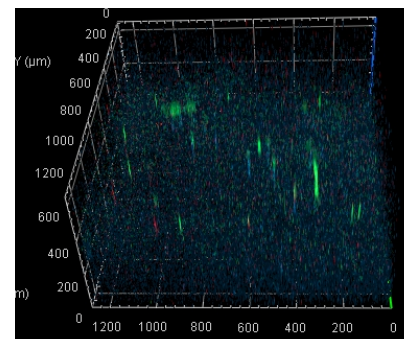
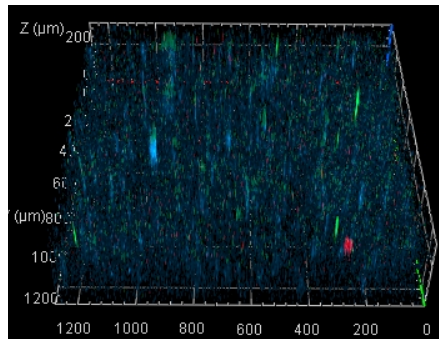
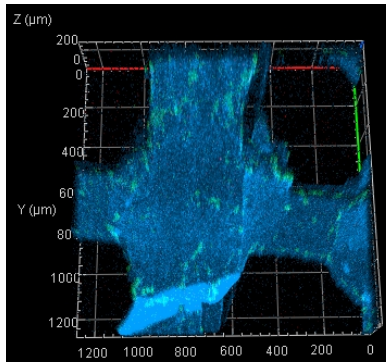
Collagen Rectilinear Scaffold

Collagen Hexagonal Scaffold

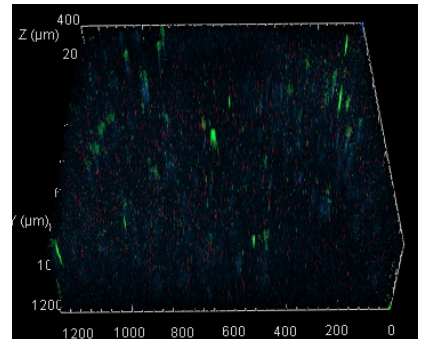
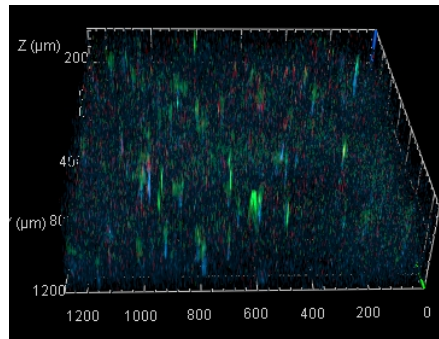
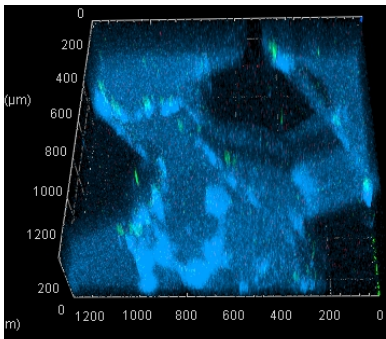
Proliferative Media



Osteogenic Media



Adipogenic Media



Hoechst

PPAR γ

RUNX2

2.4 Discussion and Conclusion

In this proof-of-concept tissue engineering study, soft collagen bioink scaffolds were reproducibly printed using a gelatin microparticle support bath. The gelatin support slurry was shear-sensitive and behaved similarly to a Bingham plastic fluid. Gelatin microparticle size was found to be dependent on the preparation method. Longer durations of mechanical blending resulted in smaller gelatin microparticles that displaced during embedded printing with higher resolution. Embedded printing has become a promising technique for the additive manufacture of viscous, soft materials such as elastomers, gels, and hydrogels.^{28,29} Specifically, the printing of biological hydrogels, composed of polysaccharides and proteins, are difficult to print because the biological materials must gel *in situ* after extrusion from the print nozzle. To be suited for bioprinting, a material must have appropriate mechanical fluid properties. If print materials are not fluid enough, or if they gel quickly, a blockage will form inside the small-diameter print nozzle and affect printing results. Fluid-like materials require surrounding support from a sacrificial material such that the printed object does not collapse or deform due to material viscosity and excess weight deposited layer-by-layer. Embedded printing of biological materials has been employed previously, such as in the fabrication of a sodium alginate coronary arterial tree with a perfusable, hollow lumen³¹ as well as the printing of perfusable polydimethylsiloxane (PDMS) tubes within a hydrophilic Carbopol gel support.³² Embedded printing of biologically relevant materials has the potential to precisely control microstructure and anisotropy during layer-by-layer assembly of 3D constructs.

Embedded printed collagen type I scaffolds and fusion printed PCL scaffolds were printed with reproducible quality and fidelity. Both material scaffolds were sterilizable, making them suitable for *in vitro* biological applications. Collagen and PCL scaffolds supported ASC proliferation, with the majority of ASCs seeded onto PCL scaffolds undergoing cell division. PCL scaffolds were quite rigid; the material has a documented Young's (elastic) modulus in the range of 340 to 365 MPa.³⁵ Matrix stiffness is known to regulate cell behavior (mechanosensation) and migration (durotaxis); stiff matrix environments have been shown to promote proliferative behavior in a variety of cell types, including hepatocytes, stellate cells, and fibroblasts.³⁶ Our findings are consistent in this regard, with ASCs demonstrating a robust proliferative response on PCL scaffolds compared to soft collagen protein scaffolds. Importantly,

cell proliferation for tissue engineering applications should be regulated to prevent pathological cell growth and tumor formation.³⁷

Cell response to the 3D printed scaffolds was evaluated by studying ASC cytoskeletal morphology and fibronectin deposition. On rectilinear PCL scaffolds, cells exhibited a high degree of spreading, a mature F-actin network, and interaction with the ECM via vinculin. However, fibronectin synthesis on PCL scaffolds appeared reduced compared to collagen scaffolds after 3 days of culturing. ASCs responded positively to TGF- β 1 treatment; independent of scaffold material or infill architecture, including this bioactive molecule in culture improved cell density, spreading, and fibronectin synthesis. This is expected, given that TGF- β 1 protein regulates cell proliferation, differentiation and growth, and can modulate expression and activation of other growth factors including interferon gamma and tumor necrosis factor alpha.³⁸ This study has demonstrated that ASC *in vitro* activity can be stimulated using TGF- β 1 for rapid (3 days) tissue regeneration while scaffolds alone are capable of maintaining viable ASCs for prolonged periods (2 weeks).

In this study, ASC phenotype appeared unaffected by scaffold material (PCL or collagen) or architecture (rectilinear or hexagonal). This may have been a caveat of using ASCs isolated from adipose tissue obtained from lower limb amputation. ASCs in this study were largely PPAR γ -positive, suggesting an adipogenic phenotype. Even when seeded onto TCPS, the majority of ASCs were PPAR γ -positive, with minimal RUNX2 expression detected (Results not published; ASC cultures reached hyperconfluency rapidly on TCPS, with culture decline and apoptosis occurring well before the 3-week experimental end point. In contrast, ASC differentiation on PCL and collagen scaffolds took approximately 3 weeks to obtain expression of PPAR γ and RUNX2). Three-dimensional geometry has been shown to successfully influence stem cell lineage. For example, mesenchymal stem cells (MSCs) seeded onto 3D printed poly(propylene fumarate) scaffolds demonstrated increased expression of early osteogenic markers when cultured onto cylindrical pores, while cubic pores influenced gene expression for MSCs undergoing adipogenesis and chondrogenesis.³⁹ Scaffold geometry of 3D-printed gelatin constructs, containing either 90° square shaped pores or 60° triangular pores, significantly influenced the differentiation and function of seeded hepatocytes.⁴⁰ In addition to pore geometry, pore size also influences cell behavior. PCL scaffolds printed into square, triangular, and rhomboidal pore geometries of varied pore diameters from 550 to 750 μ m were shown to

influence human MSC behaviors such as adhesion, viability and proliferation.⁴¹ Similarly, MSCs seeded onto either PCL or 300PEOT55PBT45 (PolyActive300/55/45) printed scaffolds presenting an axial gradient of pore size and total porosity displayed improved osteogenic differentiation.⁴²

In conclusion, 3D printing of biomaterials allows for rapid prototyping and precise control of construct geometry, microstructure, and anisotropy during layer-by-layer assembly. Relevant biomaterials will ideally be biocompatible, supporting cell adhesion, expansion, and viability. Biomaterials and their degradation products should be non-toxic and non-immunogenic. Furthermore, biomaterial properties should be closely matched to the tissues they are replacing. This study has demonstrated that soft collagen protein scaffolds stimulate fibronectin production *in vitro* and future work should be done to assess validity as a soft connective tissue substitute. Rigid PCL scaffolds in contrast support robust cell spreading and proliferation and should be investigated for implementation in the regeneration of stiff tissues (for example, bone), in long-term wound management applications (for example, management of non-healing wounds), and regions of repetitive mechanical loading that require stronger scaffold constructs (for example, wounds at the sole of the foot).

2.5 References

1. Kanitakis, J. Anatomy, histology and immunohistochemistry of normal human skin. *Eur. J. Dermatol. EJD* **12**, 390–399; quiz 400–401 (2002).
2. Uchida, S., Oiso, N., Suzuki, T. & Kawada, A. Dermoscopic Features of Hyperpigmented Dots in Crista Cutis in Two Siblings in a Japanese Family with Inherited Acanthosis Nigricans. *J. Cosmet. Dermatol. Sci. Appl.* **02**, 252–253 (2012).
3. Jackson, S. M., Williams, M. L., Feingold, K. R. & Elias, P. M. Pathobiology of the stratum corneum. *West. J. Med.* **158**, 279–285 (1993).
4. Halprin, K. M. Epidermal ‘turnover time’--a re-examination. *Br. J. Dermatol.* **86**, 14–19 (1972).
5. Potten, C. S., Saffhill, R. & Maibach, H. I. Measurement of the transit time for cells through the epidermis and stratum corneum of the mouse and guinea-pig. *Cell Tissue Kinet.* **20**, 461–472 (1987).
6. Fuchs, E., Tumber, T. & Guasch, G. Socializing with the Neighbors: Stem Cells and Their Niche. *Cell* **116**, 769–778 (2004).
7. Yan, X. & Owens, D. M. The skin: a home to multiple classes of epithelial progenitor cells. *Stem Cell Rev.* **4**, 113–118 (2008).
8. Woo, S.-H., Stumpfova, M., Jensen, U. B., Lumpkin, E. A. & Owens, D. M. Identification of epidermal progenitors for the Merkel cell lineage. *Dev. Camb. Engl.* **137**, 3965–3971 (2010).
9. Potten, C. S. Epidermal transit times. *Br. J. Dermatol.* **93**, 649–658 (1975).
10. Mackenzie, I. C. Retroviral Transduction of Murine Epidermal Stem Cells Demonstrates Clonal Units of Epidermal Structure. *J. Invest. Dermatol.* **109**, 377–383 (1997).
11. Jensen, U. B., Ghazizadeh, S. & Owens, D. M. Isolation and Characterization of Cutaneous Epithelial Stem Cells. in *Skin Stem Cells* (ed. Turksen, K.) **989**, 61–69 (Humana Press, 2013).
12. Cho, S.-W. *et al.* Engineering of volume-stable adipose tissues. *Biomaterials* **26**, 3577–3585 (2005).
13. Zuk, P. A. *et al.* Human Adipose Tissue Is a Source of Multipotent Stem Cells. *Mol. Biol. Cell* **13**, 4279–4295 (2002).
14. Han, S., Sun, H. M., Hwang, K.-C. & Kim, S.-W. Adipose-Derived Stromal Vascular Fraction Cells: Update on Clinical Utility and Efficacy. *Crit. Rev. Eukaryot. Gene Expr.* **25**, 145–152 (2015).
15. Rada, T., Reis, R. L. & Gomes, M. E. Novel method for the isolation of adipose stem cells (ASCs). *J. Tissue Eng. Regen. Med.* **3**, 158–159 (2009).
16. Rustad, K. C., Sorkin, M., Levi, B., Longaker, M. T. & Gurtner, G. C. Strategies for organ level tissue engineering. *Organogenesis* **6**, 151–157 (2010).
17. Kuo, Y.-R. *et al.* Adipose-Derived Stem Cells Accelerate Diabetic Wound Healing through the Induction of Autocrine and Paracrine Effects. *Cell Transplant.* **25**, 71–81 (2016).
18. Lee, C. *et al.* Adipose stem cells can secrete angiogenic factors that inhibit hyaline cartilage regeneration. *Stem Cell Res. Ther.* **3**, 35 (2012).
19. Ebrahimian T.G. *et al.* Cell Therapy Based on Adipose Tissue-Derived Stromal Cells Promotes Physiological and Pathological Wound Healing. *Arterioscler. Thromb. Vasc. Biol.* **29**, 503–510 (2009).
20. Flynn, L., Semple, J. L. & Woodhouse, K. A. Decellularized placental matrices for adipose tissue engineering. *J. Biomed. Mater. Res. A* **79A**, 359–369 (2006).

21. Haubner, F. *et al.* A Co-Culture Model of Fibroblasts and Adipose Tissue-Derived Stem Cells Reveals New Insights into Impaired Wound Healing After Radiotherapy. *Int. J. Mol. Sci.* **16**, 25947–25958 (2015).
22. Mannoor, M. S. *et al.* 3D Printed Bionic Ears. *Nano Lett.* **13**, 2634–2639 (2013).
23. Hockaday, L. A. *et al.* Rapid 3D printing of anatomically accurate and mechanically heterogeneous aortic valve hydrogel scaffolds. *Biofabrication* **4**, 035005 (2012).
24. Cui, X. & Boland, T. Human microvasculature fabrication using thermal inkjet printing technology. *Biomaterials* **30**, 6221–6227 (2009).
25. Xu, T. *et al.* Viability and electrophysiology of neural cell structures generated by the inkjet printing method. *Biomaterials* **27**, 3580–3588 (2006).
26. Kolesky, D. B. *et al.* 3D bioprinting of vascularized, heterogeneous cell-laden tissue constructs. *Adv. Mater. Deerfield Beach Fla* **26**, 3124–3130 (2014).
27. Pati, F. *et al.* Printing three-dimensional tissue analogues with decellularized extracellular matrix bioink. *Nat. Commun.* **5**, 3935 (2014).
28. Martin, I., Simmons, P. J. & Williams, D. F. Manufacturing challenges in regenerative medicine. *Sci. Transl. Med.* **6**, 232fs16 (2014).
29. Murphy, S. V. & Atala, A. 3D bioprinting of tissues and organs. *Nat. Biotechnol.* **32**, 773–785 (2014).
30. Sinha, G. Cell presses. *Nat. Biotechnol.* **32**, 716–719 (2014).
31. Hinton, T. J. *et al.* Three-dimensional printing of complex biological structures by freeform reversible embedding of suspended hydrogels. *Sci. Adv.* **1**, e1500758 (2015).
32. Hinton, T. J., Hudson, A., Pusch, K., Lee, A. & Feinberg, A. W. 3D Printing PDMS Elastomer in a Hydrophilic Support Bath via Freeform Reversible Embedding. *ACS Biomater. Sci. Eng.* **2**, 1781–1786 (2016).
33. Lee, H.-S. *et al.* Osteogenic differentiation of mesenchymal stem cells derived from bone marrow of patients with myeloproliferative disorders. *J. Formos. Med. Assoc. Taiwan Yi Zhi* **101**, 124–128 (2002).
34. Hauner, H., Skurk, T. & Wabitsch, M. Cultures of human adipose precursor cells. *Methods Mol. Biol. Clifton NJ* **155**, 239–247 (2001).
35. Eshraghi, S. & Das, S. Mechanical and microstructural properties of polycaprolactone scaffolds with one-dimensional, two-dimensional, and three-dimensional orthogonally oriented porous architectures produced by selective laser sintering. *Acta Biomater.* **6**, 2467–2476 (2010).
36. Wells, R. G. The role of matrix stiffness in regulating cell behavior. *Hepatology* **47**, 1394–1400 (2008).
37. Dzobo, K. *et al.* Advances in Regenerative Medicine and Tissue Engineering: Innovation and Transformation of Medicine. *Stem Cells Int.* **2018**, 1–24 (2018).
38. Derynck, R. *et al.* Human transforming growth factor- β complementary DNA sequence and expression in normal and transformed cells. *Nature* **316**, 701–705 (1985).
39. Ferlin, K. M., Prendergast, M. E., Miller, M. L., Kaplan, D. S. & Fisher, J. P. Influence of 3D printed porous architecture on mesenchymal stem cell enrichment and differentiation. *Acta Biomater.* **32**, 161–169 (2016).
40. Lewis, P. L., Green, R. M. & Shah, R. N. 3D-printed gelatin scaffolds of differing pore geometry modulate hepatocyte function and gene expression. *Acta Biomater.* **69**, 63–70 (2018).

41. Domingos, M. *et al.* The first systematic analysis of 3D rapid prototyped poly(ϵ -caprolactone) scaffolds manufactured through BioCell printing: the effect of pore size and geometry on compressive mechanical behaviour and *in vitro* hMSC viability. *Biofabrication* **5**, 045004 (2013).
42. Di Luca, A. *et al.* Gradients in pore size enhance the osteogenic differentiation of human mesenchymal stromal cells in three-dimensional scaffolds. *Sci. Rep.* **6**, 22898 (2016).

3 Investigating the Effects of Exogenous Galectin-3 in Murine Wound Healing

3.1 Introduction

Skin acts as a barrier between the external environment, facilitates sensation and thermoregulation. Following injury, normal wound healing involves four overlapping spatiotemporally coordinated events, hemostasis to halt bleeding, inflammation to clear the wound of debris and infectious bodies, proliferation of cells and re-epithelialization to restore skin barrier function.¹ However, factors such as advanced age, vascular insufficiency, limb trauma, obesity, and diabetes may result in a reduced ability to heal. If a wound persists beyond 12 weeks, it is classified as a non-healing chronic wound. The most common types of chronic wounds include venous ulcers, arterial ulcers, pressure ulcers, and diabetic ulcers.²

Chronic wounds are characterized by increased expression of pro-inflammatory cytokines such as interleukin-1 (IL-1), IL-6, and tissue necrosis factor alpha (TNF- α), combined with decreased levels of pro-regenerative cytokines including transforming growth factor beta (TGF- β) and vascular endothelial growth factor (VEGF).³ An imbalance of proteolytic activity leads to excessive degradation of the extracellular matrix, inhibiting cell migration and proliferation.⁴⁻⁶ Decreased levels of growth factors, such as keratinocyte growth factor, fibroblast growth factor 2 (FGF-2) and VEGF, further prevents progression towards proliferative and re-epithelialization stages.³ Chronic wound resolution thus depends on converting the pro-inflammatory microenvironment into a pro-fibrotic one.

Galectin-3, a matricellular protein and member of the lectin family, has been implicated in modulating the inflammatory phase of wound healing. *In vitro*, galectin-3 treatment increases monocyte and macrophage migration.⁷ Galectin-3 is important for macrophage linkage to neutrophils and increases neutrophil phagocytosis.⁸ Moreover, this protein is implicated in regulating alternative (M2) macrophage activation, an important process for inflammation resolution.⁹ Studies employing galectin-3 knockout mice have shown that macrophages derived from bone marrow of galectin-3 null animals display diminished ability to undergo alternative activation. Thus, the use of galectin-3 in modulating prolonged inflammation of a chronic wound is of interest. The context in which its regulatory activity is preserved, including therapeutic concentration range and delivery system, remains to be elucidated.

Blend electrospinning has previously been employed for the incorporation and delivery of proteins from a biomimetic nanofibrous scaffold. Electrospun scaffolds display high porosity and large surface area-to-volume ratios.^{10,11} Delivery of human recombinant galectin-3 via an electrospun gelatin scaffold in wound healing is of interest, as the scaffold facilitates effective delivery and distribution of the protein into the wound bed microenvironment.¹² In addition, the scaffold would act as a temporary extracellular matrix, directing tissue regeneration by providing a site for cell adhesion, proliferation, and migration into the wound bed. The goal of this research was to generate an electrospun gelatin scaffold loaded with recombinant galectin-3 and assess the effect of exogenous galectin-3 delivery in cutaneous wound healing.

3.2 Materials and Methods

3.2.1 Electrospinning Galectin-3-Loaded Fibrous Gelatin Scaffolds

A polymer solution consisting 50 µg/mL recombinant human galectin-3 (R&D Systems, Minneapolis, MN, USA) and 21% (w/v) Type B Bovine gelatin (Sigma-Aldrich, St. Louis, MO, USA) dissolved in 40% (v/v) acetic acid (Thermo Fisher Scientific, Waltham, MA, USA) was aspirated into a plastic 1cc Tuberculin syringe (Terumo, Shibuya, Tokyo, Japan) connected to PTFE capillarity tubing (Saint-Gobain Performance Plastics, France) fitted with a 20 gauge blunt-tip stainless steel needle. The tube and needle were primed by pushing the syringe plunger until the electrospinning solution began to drip from the needle. The syringe was secured in a pump (VWR International, Radnor, PA, USA) and the needle was connected to a high voltage DC power supply (Gamma High Voltage Research, Ormond Beach, FL, USA). The needle tip was positioned 10 cm from a grounded stainless steel rotating barrel. A piece of aluminum foil was wrapped around the rotating barrel and secured with electrical tape to act as the collecting surface. During electrospinning, a 15-kV voltage was applied as the electrospinning solution was pumped at a flowrate of 0.5 mL/hr. Scaffolds were electrospun onto the collection barrel rotating at 100 revolutions per minute (RPM) for 1.5 hours using a total volume of 0.75 mL of solution. Fibrous scaffolds were then crosslinked in a glass desiccator (VWR International) containing drierite (W.A. Hammond Drierite Co. Ltd, Xenia, OH, USA) using the vapour from a 5 mL solution consisting of 1.5% (v/v) glutaraldehyde (GTA) (Sigma-Aldrich, St. Louis, MO, USA) in anhydrous ethyl alcohol (Commercial Alcohols, Brampton, ON). The desiccator was held under

vacuum for 20 min and scaffolds were stored in the sealed desiccator for 48 hr. Following crosslinking, scaffolds were transferred to sealed plastic containers with desiccant at 4°C.

3.2.2 Scanning Electron Microscopy

Gelatin scaffolds (N=3) were electrospun using gelatin polymer solutions of 20, 21, 25, and 30% (w/v) concentration. An 8 mm diameter circular sample was collected per scaffold using a biopsy punch (Integra Miltex, York, PA, USA). Scaffold samples were fixed onto 15 mm aluminum stubs using adhesive carbon discs and sputter coated with osmium (OPC-80T, Filgen Inc., Japan), then imaged using a Hitachi 4300-N scanning electron microscope (Hitachi Ltd., Japan) at the Biotron Integrated Microscopy Facility (Western University). Images were acquired at 1000X, 3000X, and 5000X magnifications at an accelerating voltage of 4 kV. ImageJ software (National Institutes of Health, Bethesda, MD, USA) was employed to assess the diameter of fibers (n=250) from 5 images taken at the same magnification.

3.2.3 Effect of Galectin-3 on Murine Wound Healing *In Vivo*

Galectin-3-loaded fibrous gelatin scaffolds were recovered from storage at 4°C and 8 mm diameter circular samples were collected using a biopsy punch (Integra Miltex, York, PA, USA). Each scaffold was separated from its tinfoil base and quenched in 0.1 M glycine (Sigma-Aldrich, St. Louis, MO, USA) for 1 hr at 23°C to remove residual glutaraldehyde. Scaffolds underwent three 15 min PBS rinses then were stored overnight at 4°C. Prior to implantation, scaffolds were exposed to ultraviolet (UV) treatment for 2 hr.

All animal procedures followed protocols approved by the University Council on Animal Care at Western University. Nine male wild type (WT) (C57BL/6J; 000664) mice (The Jackson Laboratory, Sacramento, CA, USA), 14 weeks of age at the time of surgery, were employed. Approximately 30 min prior to surgery, 0.05 mg/kg of buprenorphine was administered to each mouse as a pre-emptive analgesic. Animals were anaesthetized using 90 mg/kg ketamine and 5 mg/kg xylazine, with inhalation of 3% isoflurane in oxygen as needed. Hair was shaved from the back of the animal and 1 cc of Nair cream (Church & Dwight Co., Inc., Ewing, NJ, USA) was applied topically for 5 min to remove remaining hair by chemical depilation. The Nair cream was wiped off and the underlying murine skin was rinsed with warm water, then dried. Povidone

iodine was used to clean the area. Four full-thickness dermal wounds measuring 6 mm in diameter were created using a sterile biopsy punch (Integra Miltex, York, PA, USA). Each wound was assigned one of four treatment conditions: empty (control), implantation of a 21% (w/v) gelatin electrospun scaffold containing 50 µg/mL galectin-3, or daily topical application of 10 µL of galectin-3 at a concentration of either 12.5 µg/mL or 25 µg/mL in PBS. Treatments were rotated clockwise in each mouse to eliminate positional effects on wound healing. Following completion of the surgical procedure, atipamezole was administered at a dose of 1 mg/kg. Animals were given buprenorphine again 12 hr post-surgery.

Mice were sacrificed using carbon dioxide exposure as follows: three mice on day 3, three mice on day 7, and two mice on day 9 post-surgery (one animal was sacrificed early and excluded from the study due to impaired recovery 1-day post-surgery). Wound tissue samples were harvested immediately and fixed in 10% neutral buffered formalin (Sigma-Aldrich, St. Louis, MO, USA) for 24 hr at 4 °C. Tissues were transferred to 70% ethanol (Commercial Alcohols) and were paraffin embedded at the Molecular Pathology Core Facility (Robarts Research Institute, London, ON, Canada). Serial 5 µm sections were taken from the center of the wounds.

3.2.4 Murine Wound Healing Kinetics

On days 0, 3, 5, 7, and 9 post-surgery, each animal was lightly anesthetized by inhalation of 3% isoflurane in oxygen, and the back area containing the dermal biopsy wounds was imaged by digital camera. A ruler was placed next to the animal and included in the digital photographs for scale documentation. Wound bed area was quantified using ImageJ software (National Institutes of Health, Bethesda, MD, USA).

Serial 5 µm wound sections were stained with Masson's Trichrome at the Molecular Pathology Core Facility (Robarts Research Institute, London, ON, Canada) and imaged at 5X magnification using an Axio Imager M1 light microscope (Carl Zeiss AG, Oberkochen, Germany). Images were stitched together, and epithelial tongue length and epithelial tongue thickness were evaluated. Epithelial tongue length was measured as the distance from the tip of the epithelial tongue to the unwounded dermis. Epithelial tongue thickness was evaluated as the epithelial tongue area divided by the epithelial tongue length.

3.2.5 Effect of Galectin-3 on Arginase I Enrichment During Wound Healing

Serial 5 µm wound sections were rehydrated, rinsed with PBS for 5 min and subjected to enzymatic antigen retrieval for 15 min at 37°C. Samples were again rinsed in PBS for 5 min at room temperature and blocked using 10% horse serum in PBS for 30 min at room temperature in a humidified chamber. Sections were incubated in primary chicken antibody against arginase I (ABS535; MilliporeSigma, Burlington, MA, USA) diluted at 1:25 in 10% horse serum overnight at 4°C. Sections were rinsed in PBS for 5 min and incubated with Alexa Fluor 488 goat anti-chicken (Abcam, Cambridge, United Kingdom) at a dilution of 1:500 and Hoechst 33342 (Trihydrochloride Trihydrate; Thermo Fisher Scientific) at a dilution of 1:1000 in 10% horse serum for 1 hr at room temperature, protected from light. Sections were rinsed thoroughly in PBS, mounted using Immu-Mount (Thermo Fisher Scientific) mounting medium, sealed with glass coverslips, and imaged using an Axio Observer Z1 fluorescence microscope (Carl Zeiss) using the appropriate filters. Negative controls were also stained without the addition of primary antibodies. These negative control slides were imaged to set the threshold values for the detection of fluorescence (Appendix F). ImageJ software was used to quantify the number of arginase I-positive cells in the wound bed at days 7 and 9 (N=2, n=5).

3.3 Results

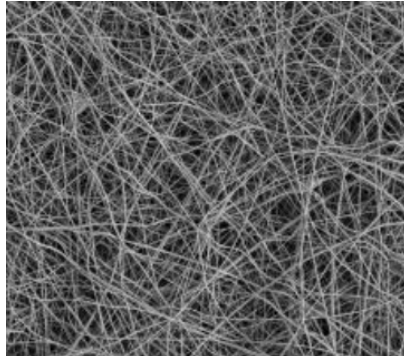
3.3.1 Preparation of Electrospun Galectin-3/Gelatin Scaffolds

The effect of gelatin concentration on electrospun fiber morphology was assessed by spinning gelatin polymer solutions at three concentrations, 20%, 25%, and 30% (Figure 3.1). As the concentration of gelatin increased, the resulting fiber diameter also increased. The majority of fibers spun from 30% weight gelatin ranged in diameter from 500-2000 nm in diameter, but there was significant variation in fiber size, with some fibers measuring over 4000 nm in diameter. At 25% weight, the majority of fibers were within the range of 300-500 nm, while lowering the gelatin to 20% resulted in fibers 100-200 nm in diameter. Fiber diameter was refined using 21% weight gelatin in the electrospinning polymer solution, resulting in a tighter distribution of fibers around 200 nm in diameter (Figure 3.2). Fibers spun from 21% gelatin displayed a mean diameter of 181 ± 40 nm.

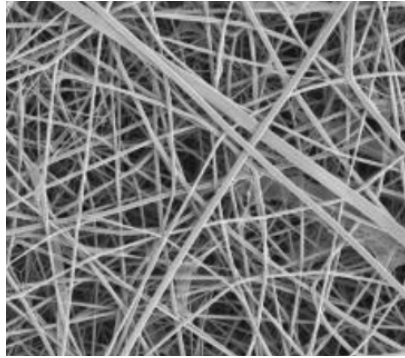
Figure 3.1. Effect of Gelatin on Electrospun Fiber Morphology. A) Representative scanning electron microscopy images for scaffolds spun from 20%, 25% and 30% gelatin polymer solutions are shown. B) Quantified frequency distribution of fiber diameters for 20%, 25% and 30% gelatin scaffolds.

A

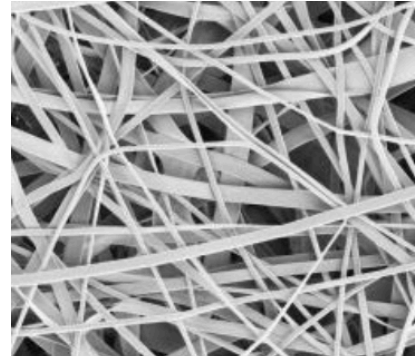
20% Gelatin



25% Gelatin



30% Gelatin



10 μm

B

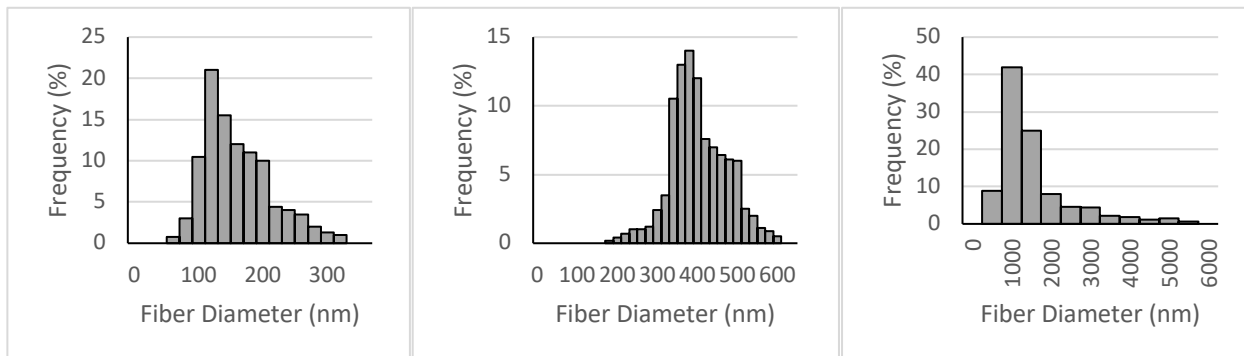
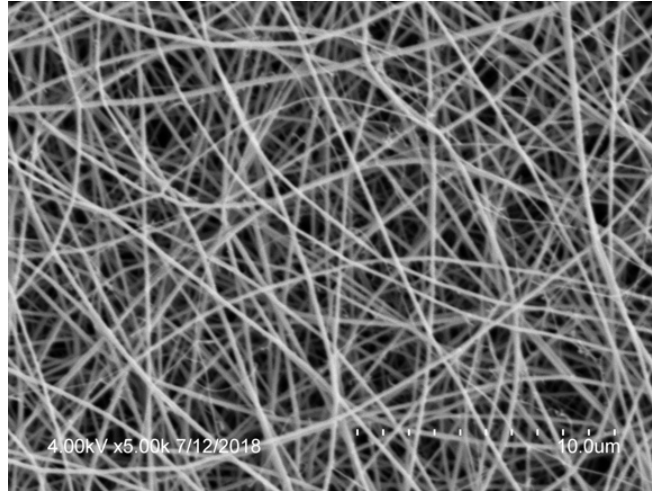


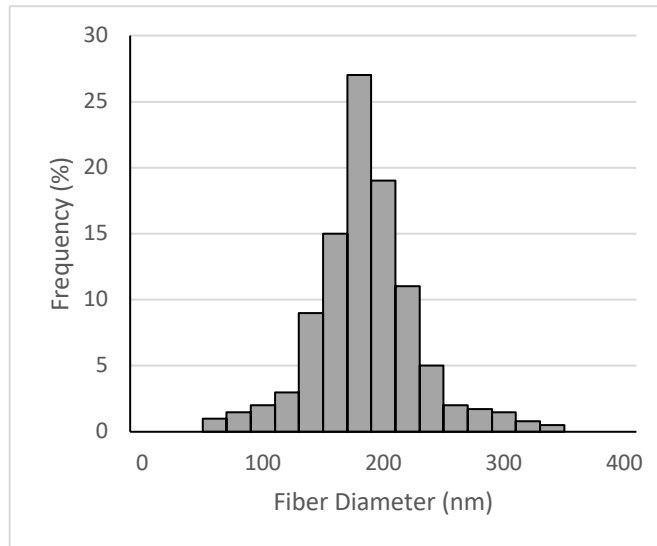
Figure 3.2. Refined Electrospun Fiber Morphology. A) Representative scanning electron microscopy image of 21% gelatin electrospun fibers. B) Quantification of fiber diameters. Fibers spun from 21% gelatin displayed a mean diameter of 181 ± 40 nm.

A

21% Gelatin



B



3.3.2 *In Vivo* Effects of the Electrospun Galectin-3/Gelatin Scaffold

To investigate the effects of exogenous recombinant galectin-3 in murine wound healing, full-thickness dermal wounds were created on the backs of wild type mice. Independent of treatment, all dermal wounds appeared much smaller by day 9 post-wounding (Figure 3.3). The wound area was measured on days 0, 3, 5, 7 and 9 to calculate wound closure kinetics (Figure 3.4). No differences between each of the treatment groups and the experimental control (empty wound) were observed at all time points assessed. Wound closure increased steadily over the 9-day period for all wounds assessed, independent of treatment. These results demonstrated that neither implantation of a galectin-3/gelatin electrospun scaffold, nor daily topical delivery of galectin-3, delayed wound closure *in vivo*.

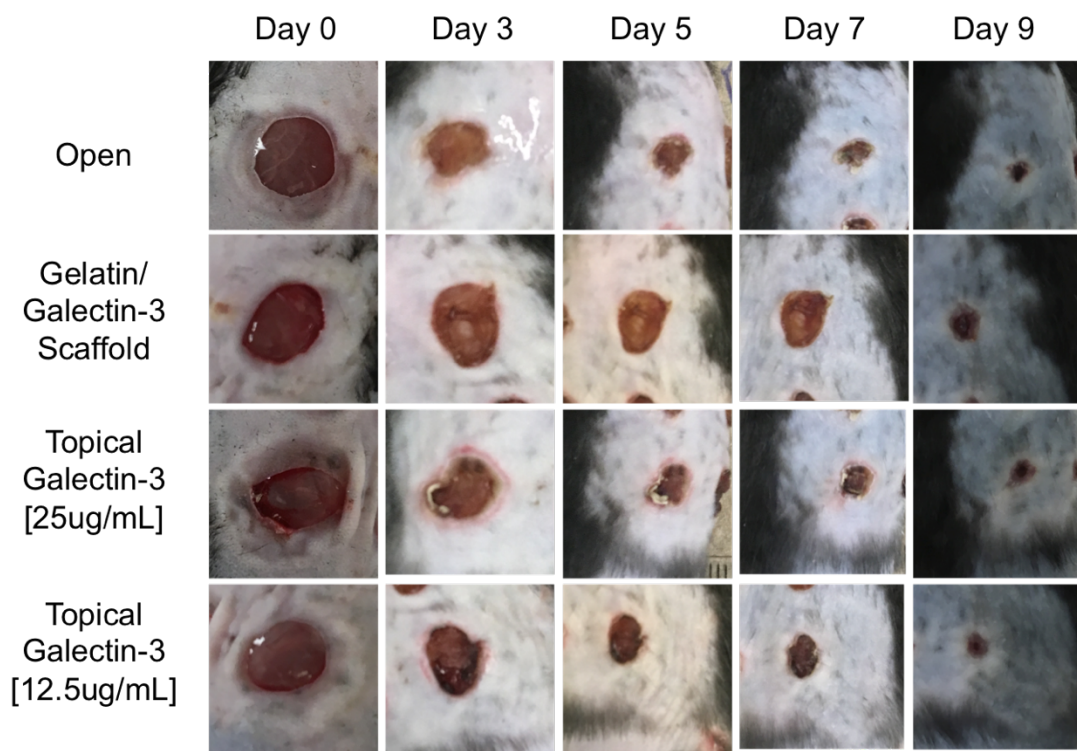
Since exogenous delivery of galectin-3, either by slow release from an electrospun scaffold or by topical application did not affect wound healing kinetics, re-epithelialization of the wound was studied. Masson's trichrome staining for sections obtained from days 7 and 9 post-wounding revealed a great amount of variation between biological replicates, regardless of wound treatment group (Figure 3.5). Wounds re-epithelialized at the same mean rate, and no differences were found between epithelial tongue length or thickness between treatment groups (Figure 3.6). Variation between biological replicates for all treatment groups was apparent. For instance, focusing specifically on the topical galectin-3 (12.5 µg/mL) experimental treatment, a thick tongue and fully re-epithelialized wound was observed for one animal (Figure 3.7A), while another day 7 replicate exhibited a much thinner tongue and significantly less re-epithelialization of the wound (Figure 3.7B). Day 9 animals were similar with one displaying full migration of the epithelial tongue (Figure 3.7C) while another displayed minimal re-epithelialization (Figure 3.7D). While one day 7 animal exhibited a thick epithelial tongue re-epithelializing the wound, both day 9 animals of this group exhibited noticeably thinner epithelial tongues, indicating that the enhanced re-epithelialization observed in a single day 7 mouse was likely not a result of the galectin-3 topical treatment of the wound but rather random occurrence.

The influence of exogenous galectin-3 from an electrospun galectin-3/gelatin scaffold and by daily topical application on macrophage polarity during full-thickness wound healing was also investigated. While qualitatively it appeared that increasing galectin-3 concentration at the wound led to more arginase I-positive macrophages (Figure 3.8), quantification revealed that the

mean density of arginase I-positive cells in the wounds was not different between treatment conditions at day 9 (Figure 3.9).

Figure 3.3. Representative Images of Murine Full-Thickness Dermal Wounds. Full thickness excisional wounds measuring 6 mm in diameter were treated with implantation of an electrospun scaffold composed of 21% gelatin blended with galectin-3 (50 µg/mL), daily topical treatment of galectin-3 in PBS (12.5 µg/mL or 25 µg/mL) or left empty (control). Representative images of the four conditions are shown at days 0, 3, 5, 7 and 9 post-wounding.

Day Post-Wound



10 mm

Figure 3.4. Quantification of Murine Wound Healing Kinetics. Full thickness excisional wounds measuring 6 mm in diameter were treated with implantation of an electrospun scaffold composed of 21% gelatin blended with galectin-3 (50 µg/mL), daily topical treatment of galectin-3 in PBS (12.5 µg/mL or 25 µg/mL), or left empty (control). Percentage of wound area closure was calculated over a 9-day period. Data is represented as mean ± SEM.

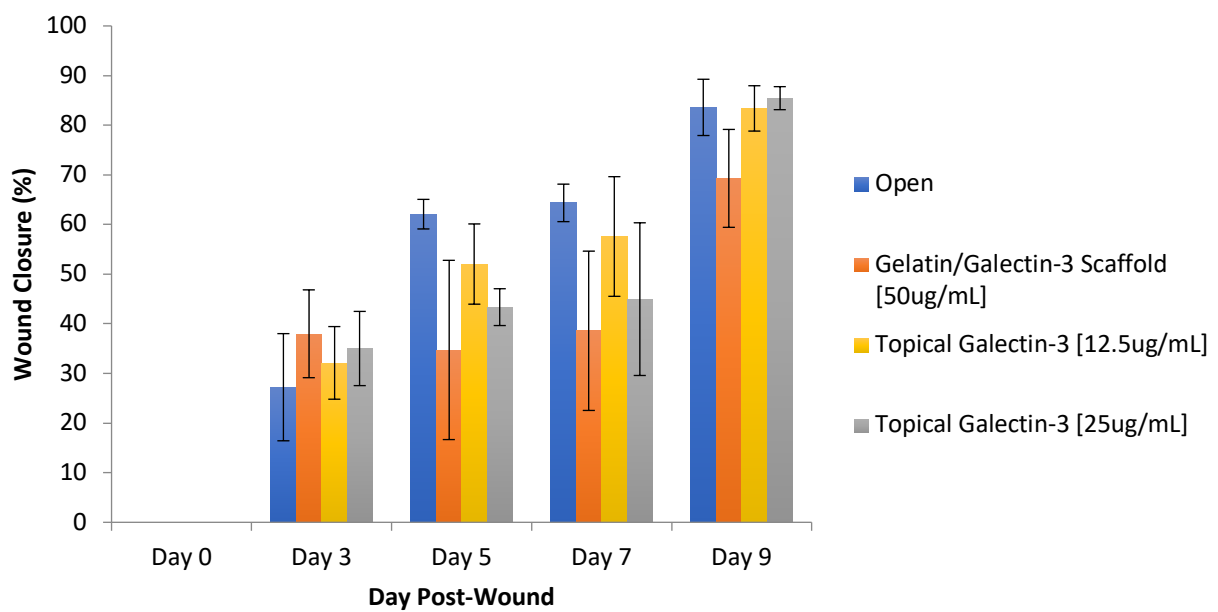
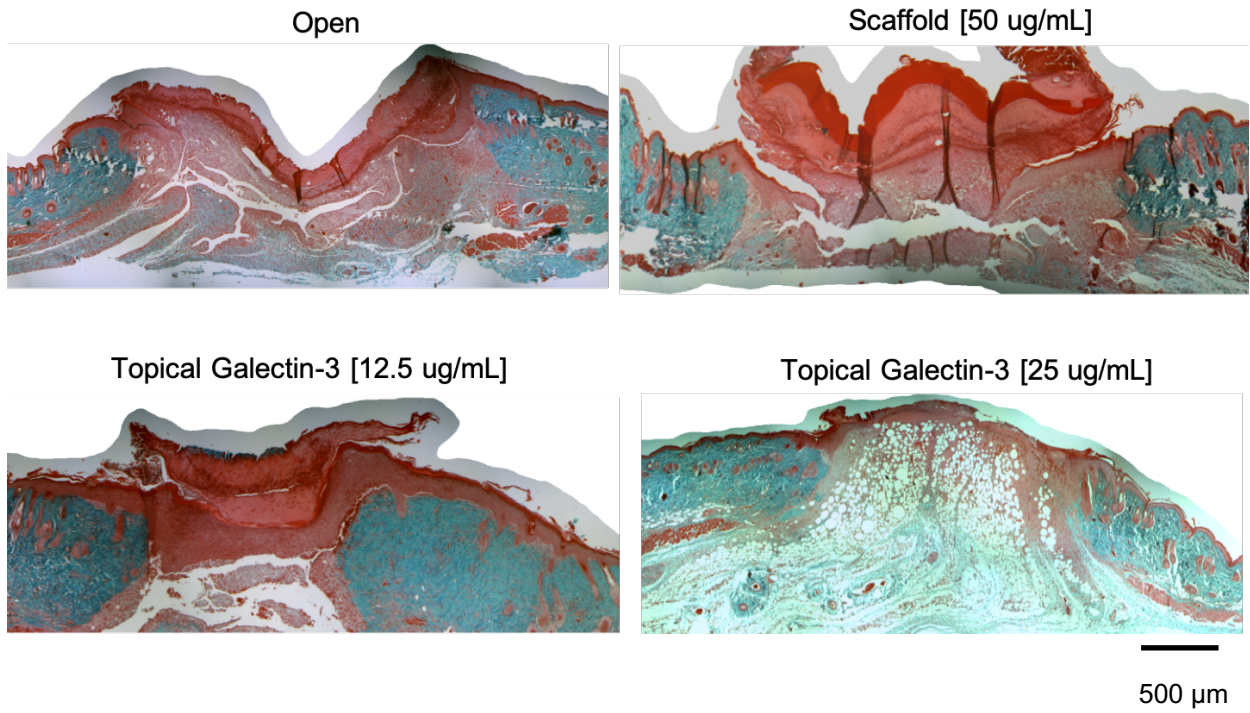


Figure 3.5. Masson's Trichrome Staining Following *In Vivo* Full-Thickness Wounding. Full thickness excisional wounds measuring 6 mm in diameter were treated with implantation of an electrospun scaffold composed of 21% gelatin blended with galectin-3 (50 µg/mL), daily topical treatment of galectin-3 in PBS (12.5 µg/mL or 25 µg/mL concentration), or left empty (control). Sections show the wound edge for each condition and the epithelial tongue. A) Sections from day 7 post-wounding. B) Sections from day 9 post-wounding.

A



B

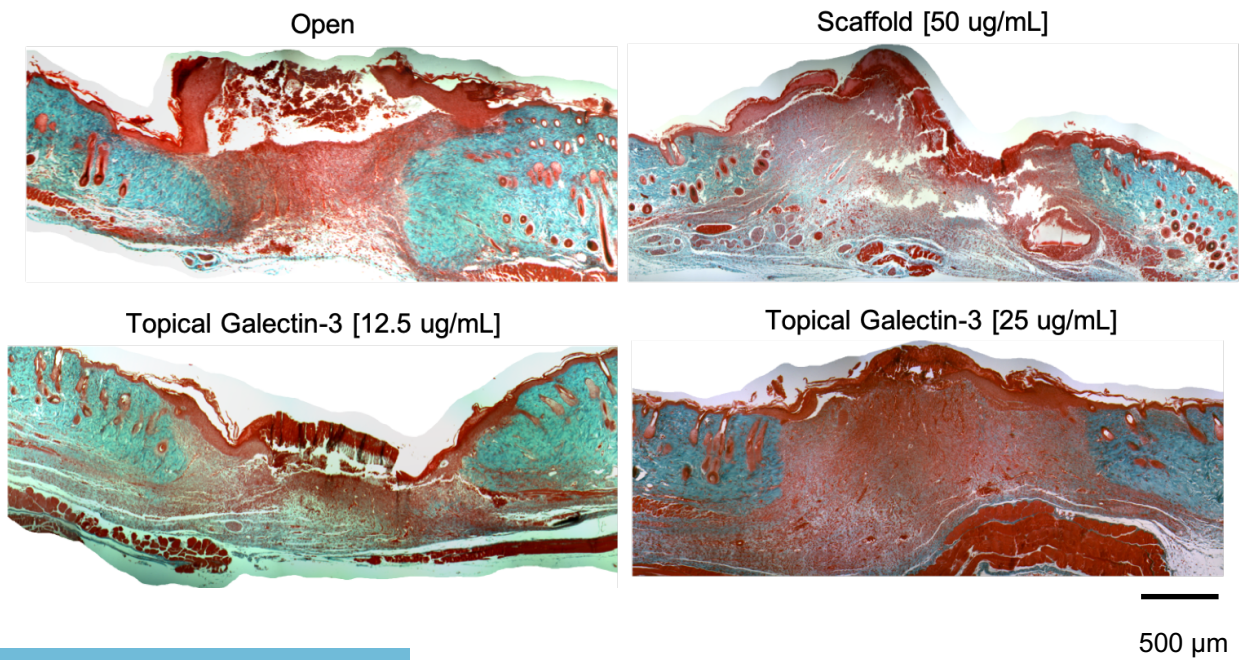
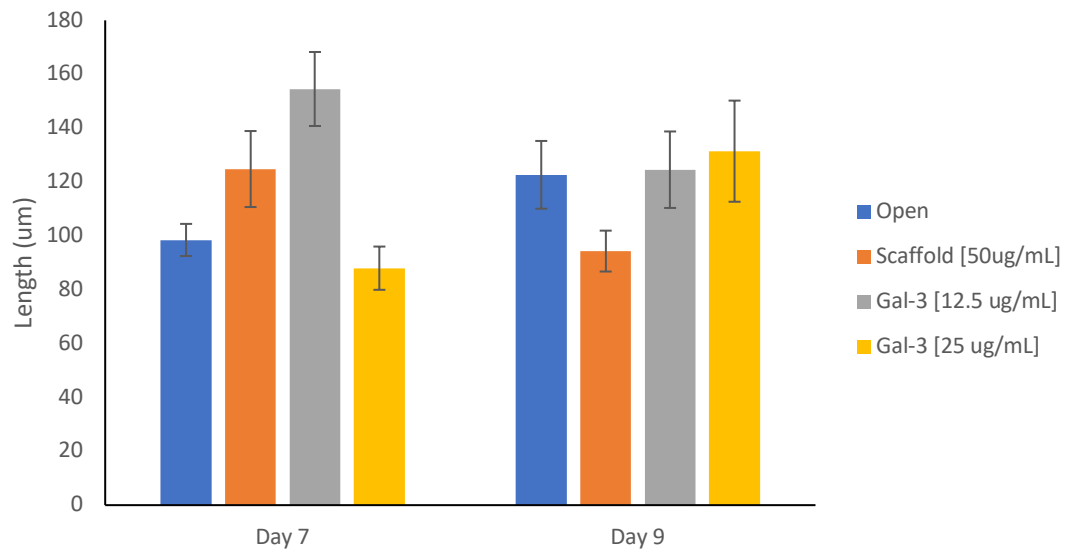


Figure 3.6. Re-epithelialization and Epithelial Thickness Following *In Vivo* Full-Thickness Wounding. Full thickness excisional wounds measuring 6 mm in diameter were treated with implantation of an electrospun scaffold composed of 21% gelatin blended with galectin-3 (50 $\mu\text{g}/\text{mL}$), daily topical treatment of galectin-3 in PBS (12.5 $\mu\text{g}/\text{mL}$ or 25 $\mu\text{g}/\text{mL}$), or left empty (control). A) Epithelial tongue length was calculated at days 7 and 9 post-wounding. B) Epithelial tongue thickness was calculated at days 7 and 9 post-wounding. All data is represented as mean \pm SEM.

A



B

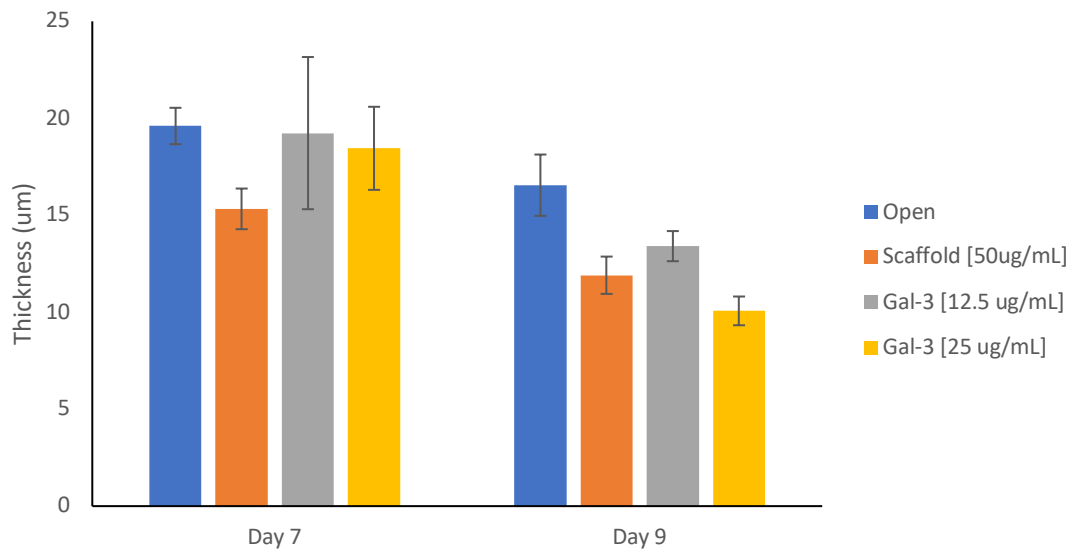
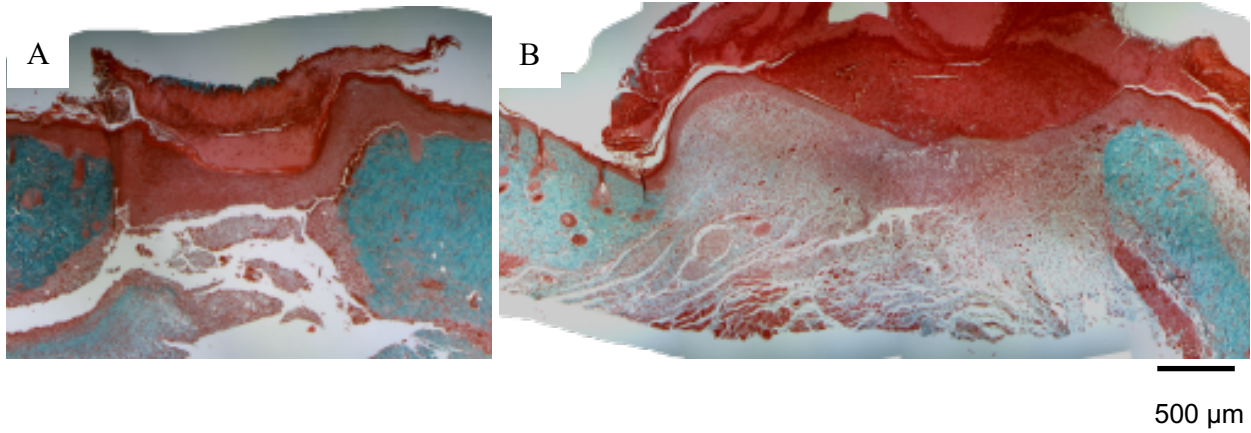


Figure 3.7. Example of Biological Variability in Masson's Trichrome Staining of Full-Thickness Wounds. All wounds shown were treated with daily topical application of galectin-3 in PBS (12.5 µg/mL concentration). A and B) Two biological replicates from day 7 post-wounding. C and D) Two biological replicates from day 9 post-wounding.

Day 7: Topical Galectin-3 [12.5 µg/mL]



Day 9: Topical Galectin-3 [12.5 µg/mL]

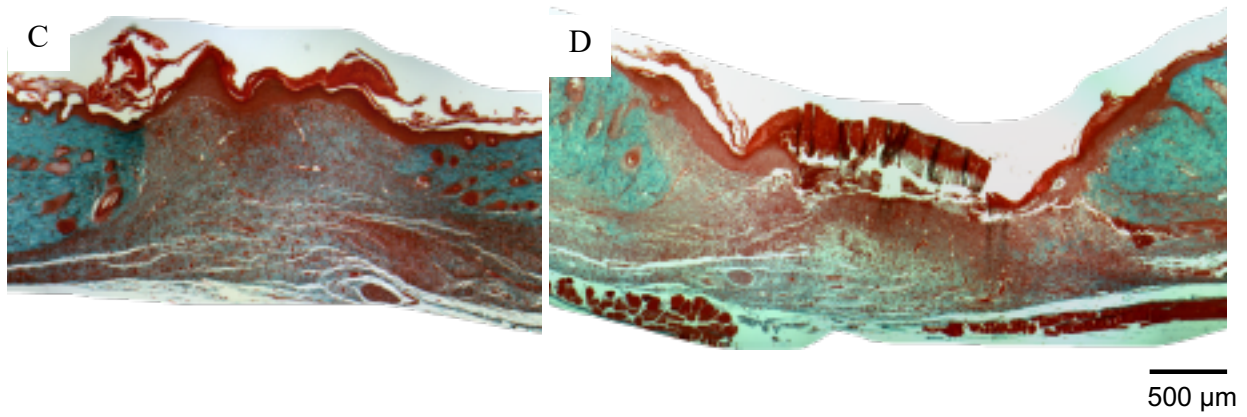
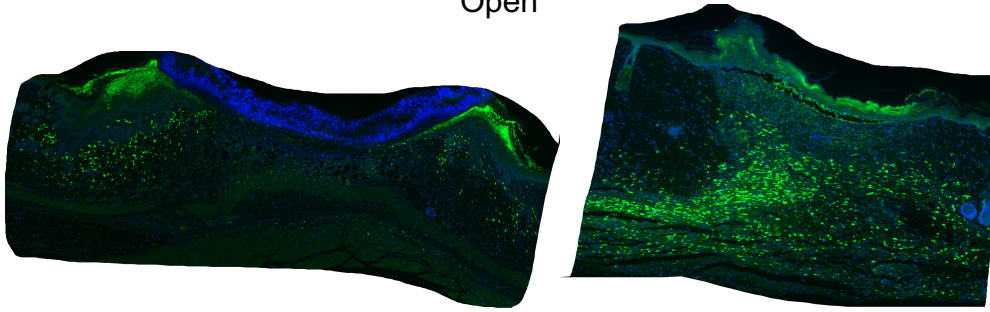
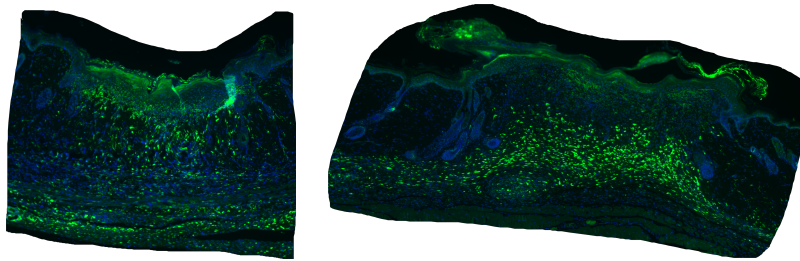


Figure 3.8. Arginase I Enrichment of Full-Thickness Wounds. Full thickness excisional wounds measuring 6 mm in diameter were treated with implantation of an electrospun scaffold composed of 21% gelatin blended with galectin-3 (50 µg/mL), daily topical treatment of galectin-3 in PBS (12.5 µg/mL or 25 µg/mL concentration), or left empty (control). Sections show the relative amounts of arginase I-positive cells (green) in the wound bed for each treatment condition. Cell nuclei are shown in blue. Two biological replicates are shown for each treatment.

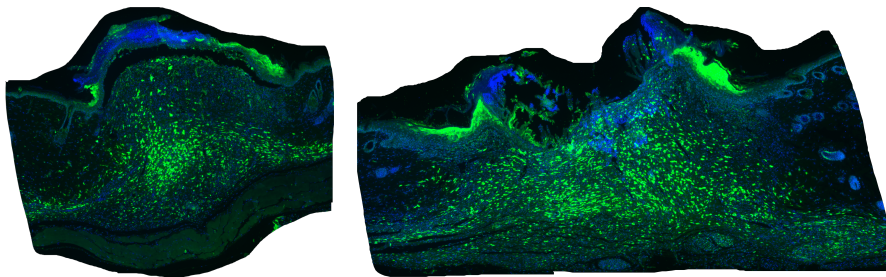
Open



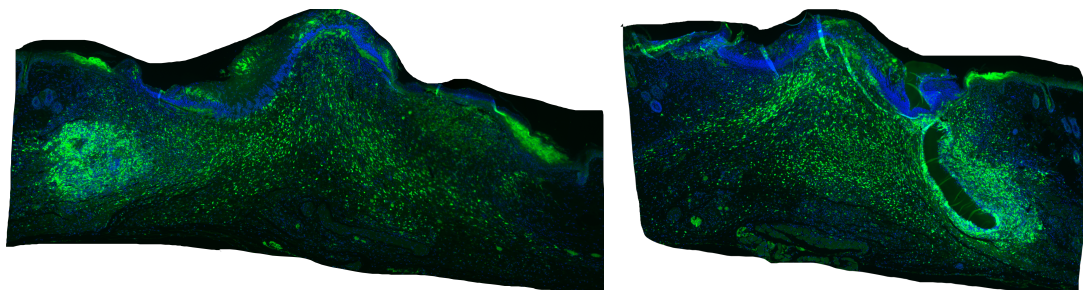
Topical Galectin-3 [12.5 µg/mL]



Topical Galectin-3 [25 µg/mL]

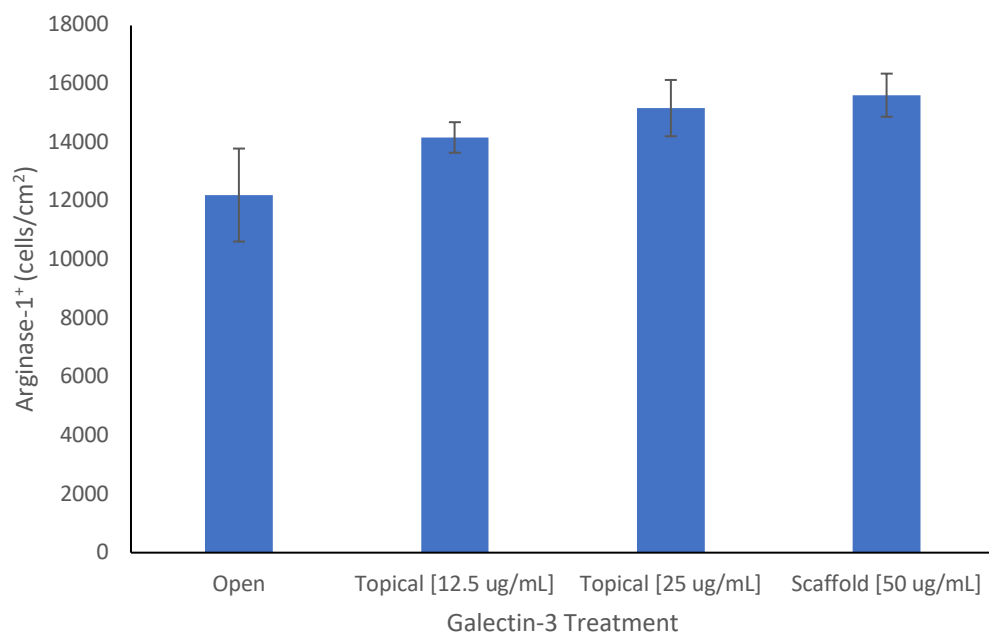


Galectin-3/Gelatin Scaffold [50 µg/mL]



500 µm

Figure 3.9. Arginase I-Positive Cell Density within the Wound Bed. Full thickness excisional wounds measuring 6 mm in diameter were treated with implantation of an electrospun scaffold composed of 21% gelatin blended with galectin-3 (50 $\mu\text{g}/\text{mL}$), daily topical treatment of galectin-3 in PBS (12.5 $\mu\text{g}/\text{mL}$ or 25 $\mu\text{g}/\text{mL}$), or left empty (no scaffold control, daily topical PBS). Density of arginase I-positive cells was quantified from 5 sections. All data is represented as mean \pm SEM.



3.4 Discussion and Conclusion

Prolonged inflammation, a hallmark of chronic wounds, halts progression to proliferative and re-epithelialization phases, preventing wound resolution and restoration of the epithelial barrier.³ Galectin-3 has been indicated in wound healing processes, including monocyte migration,⁷ alternative macrophage activation,⁹ and increased re-epithelialization in corneal wounds.^{13,14} However, the efficacy of exogenous galectin-3 in treating skin wounds appeared to be tissue- and context-specific. Based on its described functions, we hypothesized that local delivery of galectin-3 could regulate macrophage activation and increase re-epithelialization in skin healing. An electrospun gelatin scaffold was employed for the localized delivery of galectin-3. Electrospun nanofibers exhibit a large surface area for distribution of the protein.^{15,16} Type B bovine gelatin is derived from collagen¹⁷ and has suitable biorecognizable properties.^{18,19} While electrospinning of collagen has demonstrated loss of collagen's tertiary structure,²⁰ gelatin has been widely employed with results showing biocompatibility and functionality. Electrospun gelatin scaffolds have been shown to enhance wound closure in a full thickness wound healing model in rats.²¹⁻²⁴ Electrospun gelatin scaffolds, both alone and mixed with other polymers, have also been employed for the delivery of growth factors and bioactive molecules.²⁵⁻²⁷ Moreover, the biodegradability of gelatin can be tuned using glutaraldehyde crosslinking, wherein the aldehyde groups react with lysine or hydroxylysine residues to form aldimine linkages.^{28,29} Subsequent glycine quenching of the scaffolds blocks unreacted aldehyde groups.³⁰ The electrospinning polymer solution was prepared by dissolving type B bovine gelatin in 40% (v/v) acetic acid. Acetic acid has been used for the electrospinning of collagen, resulting in fiber diameters distributed around 100-200 nm.^{31,32} By electrospinning with acetic acid, the use of highly cytotoxic and protein structure damaging fluoroalcohols is avoided.³³

Our lab has previously demonstrated the refinement of scaffold manufacturing protocols to create bead-free and ribbon-free fibers with diameters measuring within the range of the native extracellular matrix.^{34,35} The polymer solution flowrate, collector distance, and the concentration of the polymer have all previously been reported to influence the resulting electrospun fiber diameter and morphology.^{18,36,37} As a result, 0.5 mL/hr was selected for electrospinning since this flowrate decreases the amount of time required for electrospinning as well as the duration that galectin-3 is exposed to the solvent. A collector distance of 10 cm was selected for electrospinning as this facilitates a wider distribution of fibers on the rotating mandrel,

maximizing scaffold surface area. Consistent with other studies, this thesis has demonstrated that increasing the concentration of gelatin results in increased fiber diameter.^{24,30,38} By using a 21% gelatin polymer solution, electrospun scaffolds exhibited ribbon-like fibers within the range of collagen fibril sizes found in human tissues.¹⁰ Electrospun scaffolds exhibit densely packed nanofibers and small sized pores, which is not ideal. Scaffolds with pores 100 μm in diameter and overall scaffold porosity of 90% has been shown to support the infiltration of cells from the surface of the scaffold.³⁹ Porosity can be improved using salt or sacrificial secondary polymers, which are deposited during the electrospinning process and subsequently removed.^{40,41}

Our lab has shown that macrophage polarization was not affected by treatment with an electrospun scaffold containing 6.7 $\mu\text{g}/\text{mL}$ galectin-3 in murine full-thickness wound healing.³⁴ Thus, we sought to elucidate the conditions where galectin-3 can affect macrophage polarization *in vivo*. In this thesis, recombinant human galectin-3 was added to the electrospinning gelatin solution to a final concentration of 50 $\mu\text{g}/\text{mL}$, while daily topical delivery was also investigated using 12.5 $\mu\text{g}/\text{mL}$ and 25 $\mu\text{g}/\text{mL}$ galectin-3 solutions in PBS. These concentrations are much higher than those needed to achieve effects *in vitro*, where concentrations as low as 1 $\mu\text{g}/\text{mL}$ have been used to enhance keratinocyte migration⁴² and 0.001-0.01 μM (0.026152-0.26152 $\mu\text{g}/\text{mL}$) to create a concentration-dependent effect on monocyte recruitment.⁴³ Additionally, while 6.3 $\mu\text{g}/\text{mL}$ galectin-3 promoted human keratinocyte migration, use of 50 $\mu\text{g}/\text{mL}$ limited migration *in vitro*.⁴⁴ However, galectin-3 activity is understood to be context-specific, and *in vivo* activity is not always accurately reflected *in vitro*. The use of galectin-3/gelatin scaffolds and topical deliver of galectin-3 did not alter wound closure kinetics during the 9-day period. In contrast to our findings, the use of gelatin scaffolds alone has been reported to increase wound closure in full-thickness skin healing in rats.²¹ However, several factors could have contributed to these discrepancies including the use of rats instead of mice, the difference in size of the initial wounds, and the use of TegadermTM (3M) secondary bandaging to cover the wounds.²¹

During the proliferative/epithelialization stages of wound healing, keratinocyte proliferation and migration over the dermis restores the epithelial barrier.¹ Studies of dermal healing have demonstrated that galectin-3 deficient mice exhibit impaired re-epithelialization, which manifests in decreased length of the epithelial tongue, and therefore decreased re-epithelialization at days 2⁴² and 7⁴⁵ post-wounding. However, when recombinant human galectin-3 was added to wounds of wildtype mice topically or using a gelatin scaffold, no

differences in epithelial thickness were observed at days 7 and 9 post-wounding. This result was consistent with previous reports showing no defect in epithelial thickness in galectin-3 knockout mice.^{42,45} In contrast, studies of corneal healing have shown that exogenous human recombinant galectin-3 can increase re-epithelialization in mice¹³ and in monkey corneal explants,¹⁴ highlighting the issue of the context-dependent roles of matricellular proteins.⁴⁶

During the inflammatory phase, monocytes are recruited to the wound by chemoattractants and differentiate into macrophages.⁴⁷ Macrophages mediate wound healing through the release of regulatory molecules.⁴⁸ Classically activated (M1) macrophages produce nitric oxide and secrete proinflammatory cytokines including TNF- α , IL-1, IL-6, and IL-12, while alternatively activated macrophages (M2) are implicated in tissue remodeling and secrete TGF- β .⁴⁹ Control of macrophage activation and whether macrophages can switch between M1 and M2 phenotypes is incompletely understood. Galectin-3 has previously been implicated in macrophage function.^{8,9,43} Thus, we sought to investigate whether galectin-3 treatment using topical galectin-3 and galectin-3/gelatin scaffolds could increase the number of M2 polarized macrophages. While day 9 wound sections qualitatively appeared to contain denser M2 macrophage populations, quantification showed no differences in M2 macrophage density across the four treatment groups. This result was unexpected given that bone marrow derived macrophages (BMDMs) from galectin-3 knockout mice show a defect in IL-4 and IL-13 M2 macrophage polarization *in vivo* and *in vitro*.⁹ However, this study did not investigate the effects of exogenous galectin-3 addition, therefore there is no indication galectin-3 would be sufficient in rescuing the deficient M2 polarization of BMDMs in galectin-3 null mice. It is possible that exogenous galectin-3 alone is not sufficient in upregulating the expression of surface-bound galectin-3, the secretion of galectin-3 or upregulating CD98 which are each implicated in the suggested autocrine loop that controls M2 activation.⁹ Moreover, human and murine galectin-3 are only 80% similar homologously,⁵⁰ which might contribute to the lack of functionality of exogenous human galectin-3 in murine wound healing.

In conclusion, blend electrospun galectin-3/gelatin scaffolds have been developed which do not delay wound healing in a full-thickness murine model. Use of topical galectin-3 and galectin-3/gelatin scaffolds did not affect wound closure, epithelial thickness, or re-epithelialization, or influence the density of M2 macrophages in the wound. Future work should explore the contexts in which *in vivo* inflammation can be modulated.

3.5 References

1. Gurtner, G. C., Werner, S., Barrandon, Y. & Longaker, M. T. Wound repair and regeneration. *Nature* **453**, 314–321 (2008).
2. Morton, L. M. & Phillips, T. J. Wound healing and treating wounds: Differential diagnosis and evaluation of chronic wounds. *J. Am. Acad. Dermatol.* **74**, 589–605; quiz 605–606 (2016).
3. Brem, H. & Tomic-Canic, M. Cellular and molecular basis of wound healing in diabetes. *J. Clin. Invest.* **117**, 1219–1222 (2007).
4. Zhao, R., Liang, H., Clarke, E., Jackson, C. & Xue, M. Inflammation in Chronic Wounds. *Int. J. Mol. Sci.* **17**, 2085 (2016).
5. Blakytyn, R. & Jude, E. The molecular biology of chronic wounds and delayed healing in diabetes. *Diabet. Med. J. Br. Diabet. Assoc.* **23**, 594–608 (2006).
6. Wlaschek, M. & Scharffetter-Kochanek, K. Oxidative stress in chronic venous leg ulcers. *Wound Repair Regen. Off. Publ. Wound Heal. Soc. Eur. Tissue Repair Soc.* **13**, 452–461 (2005).
7. Sano, H. *et al.* Human galectin-3 is a novel chemoattractant for monocytes and macrophages. *J. Immunol. Baltim. Md 1950* **165**, 2156–2164 (2000).
8. Karlsson, A., Follin, P., Leffler, H. & Dahlgren, C. Galectin-3 activates the NADPH-oxidase in exudated but not peripheral blood neutrophils. *Blood* **91**, 3430–3438 (1998).
9. MacKinnon, A. C. *et al.* Regulation of alternative macrophage activation by galectin-3. *J. Immunol. Baltim. Md 1950* **180**, 2650–2658 (2008).
10. Xie, J., Li, X. & Xia, Y. Putting Electrospun Nanofibers to Work for Biomedical Research. *Macromol. Rapid Commun.* **29**, 1775–1792 (2008).
11. Zhong, S. P., Zhang, Y. Z. & Lim, C. T. Tissue scaffolds for skin wound healing and dermal reconstruction. *Wiley Interdiscip. Rev. Nanomed. Nanobiotechnol.* **2**, 510–525 (2010).
12. Barondes, S. H. *et al.* Galectins: a family of animal beta-galactoside-binding lectins. *Cell* **76**, 597–598 (1994).
13. Cao, Z. *et al.* Galectins-3 and -7, but not Galectin-1, Play a Role in Re-epithelialization of Wounds. *J. Biol. Chem.* **277**, 42299–42305 (2002).
14. Fujii, A., Shearer, T. R. & Azuma, M. Galectin-3 enhances extracellular matrix associations and wound healing in monkey corneal epithelium. *Exp. Eye Res.* **137**, 71–78 (2015).
15. Moura, L. I. F. *et al.* Neurotensin-loaded collagen dressings reduce inflammation and improve wound healing in diabetic mice. *Biochim. Biophys. Acta* **1842**, 32–43 (2014).
16. Ji, W. *et al.* Bioactive electrospun scaffolds delivering growth factors and genes for tissue engineering applications. *Pharm. Res.* **28**, 1259–1272 (2011).
17. Malafaya, P. B., Silva, G. A. & Reis, R. L. Natural-origin polymers as carriers and scaffolds for biomolecules and cell delivery in tissue engineering applications. *Adv. Drug Deliv. Rev.* **59**, 207–233 (2007).
18. Murugan, R. & Ramakrishna, S. Design Strategies of Tissue Engineering Scaffolds with Controlled Fiber Orientation. *Tissue Eng.* **13**, 1845–1866 (2007).
19. Kim, H. N. *et al.* Nanotopography-guided tissue engineering and regenerative medicine. *Adv. Drug Deliv. Rev.* **65**, 536–558 (2013).
20. Zeugolis, D. I. *et al.* Electro-spinning of pure collagen nano-fibres - just an expensive way to make gelatin? *Biomaterials* **29**, 2293–2305 (2008).
21. Dubský, M. *et al.* Nanofibers prepared by needleless electrospinning technology as scaffolds for wound healing. *J. Mater. Sci. Mater. Med.* **23**, 931–941 (2012).

22. Gomes, S. R. *et al.* In vitro and in vivo evaluation of electrospun nanofibers of PCL, chitosan and gelatin: a comparative study. *Mater. Sci. Eng. C Mater. Biol. Appl.* **46**, 348–358 (2015).
23. Powell, H. M. & Boyce, S. T. Fiber density of electrospun gelatin scaffolds regulates morphogenesis of dermal-epidermal skin substitutes. *J. Biomed. Mater. Res. A* **84**, 1078–1086 (2008).
24. Zha, Z., Teng, W., Markle, V., Dai, Z. & Wu, X. Fabrication of gelatin nanofibrous scaffolds using ethanol/phosphate buffer saline as a benign solvent. *Biopolymers* **97**, 1026–1036 (2012).
25. Montero, R. B., Vazquez-Padron, R. I., Pham, S. M., D'Ippolito, G. & Andreopoulos, F. M. Electrospun Gelatin Constructs with Tunable Fiber Orientation Promote Directed Angiogenesis. *Open J. Regen. Med.* **03**, 1–12 (2014).
26. Shan, Y.-H. *et al.* Silk fibroin/gelatin electrospun nanofibrous dressing functionalized with astragaloside IV induces healing and anti-scar effects on burn wound. *Int. J. Pharm.* **479**, 291–301 (2015).
27. Han, F. *et al.* Performance of a multilayered small-diameter vascular scaffold dual-loaded with VEGF and PDGF. *Biomaterials* **34**, 7302–7313 (2013).
28. Olde Damink, L. H. H. *et al.* Glutaraldehyde as a crosslinking agent for collagen-based biomaterials. *J. Mater. Sci. Mater. Med.* **6**, 460–472 (1995).
29. Akin, H. & Hasirci, N. Preparation and characterization of crosslinked gelatin microspheres. *J. Appl. Polym. Sci.* **58**, 95–100 (1995).
30. Montero, R. B. *et al.* bFGF-containing electrospun gelatin scaffolds with controlled nano-architectural features for directed angiogenesis. *Acta Biomater.* **8**, 1778–1791 (2012).
31. Liu, T., Teng, W. K., Chan, B. P. & Chew, S. Y. Photochemical crosslinked electrospun collagen nanofibers: synthesis, characterization and neural stem cell interactions. *J. Biomed. Mater. Res. A* **95**, 276–282 (2010).
32. Erencia, M., Cano, F., Tornero, J. A., Macanás, J. & Carrillo, F. Resolving the electrospinnability zones and diameter prediction for the electrospinning of the gelatin/water/acetic acid system. *Langmuir ACS J. Surf. Colloids* **30**, 7198–7205 (2014).
33. Gast, K., Siemer, A., Zirwer, D. & Damaschun, G. Fluoroalcohol-induced structural changes of proteins: some aspects of cosolvent-protein interactions. *Eur. Biophys. J. EBJ* **30**, 273–283 (2001).
34. McLeod, K. Design and Validation of Delivery Systems for Galectin-3 for Skin Healing Applications. *Electron. Thesis Diss. Repos.* (2017).
35. Hopfgartner, Adam. Development Of Granulation Tissue Mimetic Scaffolds For Skin Healing. (Western University).
36. Pezeshki-Modaress, M., Mirzadeh, H. & Zandi, M. Gelatin-GAG electrospun nanofibrous scaffold for skin tissue engineering: fabrication and modeling of process parameters. *Mater. Sci. Eng. C Mater. Biol. Appl.* **48**, 704–712 (2015).
37. Subbiah, T., Bhat, G. S., Tock, R. W., Parameswaran, S. & Ramkumar, S. S. Electrospinning of nanofibers. *J. Appl. Polym. Sci.* **96**, 557–569 (2005).
38. Song, J.-H., Kim, H.-E. & Kim, H.-W. Production of electrospun gelatin nanofiber by water-based co-solvent approach. *J. Mater. Sci. Mater. Med.* **19**, 95–102 (2008).
39. Zhu, X., Cui, W., Li, X. & Jin, Y. Electrospun fibrous mats with high porosity as potential scaffolds for skin tissue engineering. *Biomacromolecules* **9**, 1795–1801 (2008).
40. Nam, J., Huang, Y., Agarwal, S. & Lannutti, J. Materials selection and residual solvent retention in biodegradable electrospun fibers. *J. Appl. Polym. Sci.* **107**, 1547–1554 (2008).

41. Skotak, M., Ragusa, J., Gonzalez, D. & Subramanian, A. Improved cellular infiltration into nanofibrous electrospun cross-linked gelatin scaffolds templated with micrometer-sized polyethylene glycol fibers. *Biomed. Mater. Bristol Engl.* **6**, 055012 (2011).
42. Liu, W. *et al.* Galectin-3 regulates intracellular trafficking of EGFR through Alix and promotes keratinocyte migration. *J. Invest. Dermatol.* **132**, 2828–2837 (2012).
43. Danella Polli, C. *et al.* Monocyte Migration Driven by Galectin-3 Occurs through Distinct Mechanisms Involving Selective Interactions with the Extracellular Matrix. *ISRN Inflamm.* **2013**, (2013).
44. Kariya, Y., Kawamura, C., Tabei, T. & Gu, J. Bisecting GlcNAc residues on laminin-332 down-regulate galectin-3-dependent keratinocyte motility. *J. Biol. Chem.* **285**, 3330–3340 (2010).
45. Walker, J. T., Elliott, C. G., Forbes, T. L. & Hamilton, D. W. Genetic Deletion of Galectin-3 Does Not Impair Full-Thickness Excisional Skin Healing. *J. Invest. Dermatol.* **136**, 1042–1050 (2016).
46. Hamilton, D. *et al.* Cell–matrix interactions governing skin repair: matricellular proteins as diverse modulators of cell function. *Res. Rep. Biochem.* **73** (2015). doi:10.2147/RRBC.S57407
47. Singer, A. J. & Clark, R. A. Cutaneous wound healing. *N. Engl. J. Med.* **341**, 738–746 (1999).
48. Brancato, S. K. & Albina, J. E. Wound macrophages as key regulators of repair: origin, phenotype, and function. *Am. J. Pathol.* **178**, 19–25 (2011).
49. Rodero, M. P. & Khosrotehrani, K. Skin wound healing modulation by macrophages. *Int. J. Clin. Exp. Pathol.* **3**, 643–653 (2010).
50. Haudek, K. C. *et al.* Dynamics of galectin-3 in the nucleus and cytoplasm. *Biochim. Biophys. Acta* **1800**, 181–189 (2010).

4 General Discussion

4.1 Summary of Thesis Objectives

Aim 1: Three-Dimensional Bioprinting for Tissue Engineering

Establish a protocol for soft collagen printing

In this thesis, collagen bioink scaffolds were printed by positive-displacement extrusion and embedded into a gelatin microparticle support bath. Optimization of the gelatin slurry preparation protocol was performed. Gelatin microparticle size was found to be dependent on the preparation method. Thus, longer durations of mechanical blending resulted in smaller gelatin microparticles that displaced during embedded printing with higher resolution. Rheological testing of the gelatin slurry demonstrated a shear-sensitive support slurry that behaved similarly to a Bingham plastic fluid. Computer-aided design was employed to generate 3D scaffold rectangular prisms (10 x 10 x 0.5 mm) which were sliced using rectilinear and hexagonal infill patterns at 20% density. Scaffolds were printed using a high concentration bovine type I collagen bioink and exhibited high print fidelity and reproducibility.

Polycaprolactone scaffold printing

Computer-aided design was employed to generate a 3D scaffold rectangular prism (50 x 50 x 2 mm) which was sliced using a rectilinear infill pattern at 50% density. Polycaprolactone (poly(ϵ -caprolactone); PCL) constructs were printed using low temperature polymer fusion printing. From the printed construct, 6 mm diameter circular samples were cut and functionalized by argon plasma treatment.

In vitro proof-of-concept ASC biocompatibility and differentiation

Three-dimensional printed scaffolds were assessed *in vitro* using human adipose-derived stromal cells (ASCs). ASCs seeded onto PCL scaffolds showed the greatest proliferative potential (96% of cells), while ASCs on either rectilinear or hexagonal collagen scaffolds exhibited less EdU incorporation (~10% of cells). Treatment of ASCs with TGF- β 1 stimulated cell spreading, and fibronectin production after 3 days post-seeding. In the absence of TGF- β 1, scaffolds supported bioactivity and after 14 days on scaffolds, ASCs exhibited increased cell density, spreading, and fibronectin deposition. Together, these results demonstrated that ASC

activity can be stimulated using TGF- β 1 for rapid (3 days) tissue regeneration while scaffolds alone are capable of maintaining viable ASCs for prolonged growth periods (2 weeks). Lastly, ASC phenotype was assessed after treatment with osteogenic and adipogenic induction factors for 3 weeks. ASCs demonstrated a PPAR γ -positive phenotype.

Aim 2: Effects of Exogenous Galectin-3 in a Murine Wound Healing Model

Electrospin galectin-3-loaded gelatin scaffolds

The effect of gelatin concentration on electrospun fiber morphology was assessed by spinning gelatin polymer solutions at three concentrations, 20%, 25%, and 30%. The majority of fibers spun from 30% weight gelatin ranged in diameter from 500-2000 nm in diameter, with significant variation in fiber size. At 25% weight, the majority of fibers were within the range of 300-500 nm, while lowering the gelatin to 20% resulted in fibers 100-200 nm in diameter. Fiber diameter was refined using 21% weight gelatin in the electrospinning polymer solution, resulting in electrospun fibers with a mean diameter of 181 ± 40 nm.

Evaluate effects of exogenous galectin-3 *in vivo*

To investigate the effects of exogenous recombinant galectin-3 on murine wound healing, full-thickness excisional dermal wounds were created on the backs of wild type mice. Wounds were treated with either 21% gelatin electrospun scaffold containing 50 μ g/mL recombinant galectin-3, daily topical application of galectin-3 at either 12.5 or 25 μ g/mL, or no treatment (control). All dermal wounds healed with reduction in size by day 9 post-wounding. The wound area was measured on days 0, 3, 5, 7 and 9 to calculate wound closure kinetics, but no differences were observed between treatments. Epithelial tongue length and thickness was quantified at days 7 and 9 post-wounding; however, no differences were evident between any conditions. Macrophage polarization within the wound was quantified and the mean density of arginase I-positive macrophages in the wounds was found not to be statistically significant between treatment conditions. Thus, treatment of murine full-thickness dermal wounds, either using a galectin-3/gelatin electrospun scaffold or by daily topical galectin-3, did not delay wound healing or re-epithelialization, but did not influence arginase I enrichment within the wounds.

4.2 Summary of Fabricated Biomaterial Scaffolds

Tissue engineering (TE) has emerged as a promising strategy for the replacement of degenerating or damaged tissues *in vivo*. Also known as regenerative medicine (RM), integral to this therapeutic strategy is biomimetic scaffolds and the biomaterial structural components used to form them. The scaffold needs to have mechanical properties strong enough to withstand the biological forces of the native environment, for example, compression, tension, and shear/torsion forces.¹ Biomaterials should exhibit elasticity such that the scaffold returns to its normal shape after deformation. Moreover, the architectural design should facilitate mass transfer within the scaffold for the exchange of gases, nutrients, and waste, and prevention of necrotic zones.² Further, biomaterials chosen must exhibit biocompatibility, and depending on the biomaterial device itself, biodegradability and bioabsorbability.³ That is, the biomaterial and its degradation products must be non-toxic and non-immunogenic. Clearly, design and fabrication of a biomaterial scaffold is complex, and various fabrication methods have been investigated to fulfill TE requirements.

Controlling scaffold architecture allows the fabrication of scaffolds that are highly porous and provide physical topographic cues to the cell surface. Current approaches to the assembly of three-dimensional (3D) biomaterials employ additive manufacturing (3D printing) to deposit materials layer-by-layer for controlled structure and architecture. Polymer fusion printing is of interest in TE for the fabrication of scaffolds using synthetic materials. For instance, polycaprolactone (poly(ϵ -caprolactone), PCL), a polyester, has been employed for TE applications due to its biocompatibility.⁴⁻⁶ PCL has a slow degradation rate of approximately two years in the biological environment.⁷⁻⁹ However, by using copolymers such as PCL with dl lactide, a more flexible material with a faster degradation rate than the homopolymer can be achieved.⁷ Moreover, the high degree of permeability has made PCL an important candidate for the development of drug delivery systems and in bone tissue regeneration.^{4,10-13} In contrast to synthetic biomaterials, scaffolds synthesized from natural biological materials are highly compatible with the host environment, being of biological origin. Hydrogel printing, including syringe-based extrusion,^{14,15} printing with fibrin,^{16,17} gelatin,¹⁸ type I collagen,¹⁹ and protein mixtures obtained from decellularized tissues,²⁰ has been established as a promising TE strategy. However, due to their viscosity, printing of soft materials poses the challenge of printed materials flowing out of their desired architecture. To overcome this, hydrogels and proteins

must gel *in situ* in order to prevent their collapse or shape deformation.^{21–23} Embedded printing into a secondary hydrogel that acts as a temporary support bath has been proposed.^{24,25}

In this thesis, fusion printed PCL scaffolds and embedded printed collagen scaffolds were employed to assess *in vitro* biocompatibility using human adipose-derived stem/stromal cells (ASCs). ASCs are multipotent, with adipogenic, chondrogenic, neurogenic and osteogenic differentiation described.^{26–29} Collagen, being the main structural component of the extracellular matrix,³⁰ has a biological molecular composition and is biodegradable.³¹ Independent of the 3D architectural pattern (rectilinear or hexagonal), collagen scaffolds stimulated ASC fibronectin production *in vitro* while PCL scaffolds supported robust ASC spreading and proliferation. These differences in cell responses indicated that polymer fusion printing and hydrogel embedded printing methods should be employed depending on the TE application. Collagen's ability to be remodeled and degraded has warranted further investigation into its employment as a soft connective tissue substitute.^{32,33} The scaffold should serve as a temporary cell support that is slowly replaced by newly synthesized matrix components in order to mediate regeneration of the tissue. In contrast, PCL scaffolds supported ASC proliferation and their rigid structure is well suited for applications where stronger scaffold constructs are required, such as in bone regeneration and also wound healing at the sole of the foot, where repetitive mechanical loading would damage soft scaffolds. Future research is needed to validate the RM potential of printed collagen and PCL scaffolds *in vivo*.

TE constructs that are not pre-seeded with cells rely on the migration of native cells to infiltrate and populate the scaffold. In this study, ASC phenotype was positive for PPAR γ expression. Therefore, future research is needed to determine under which conditions ASCs isolated from pathological tissues can be derived towards adipogenic and osteogenic lineages. Experiments should be performed with a greater number of patient samples to improve sample size and also with non-pathologically sourced ASCs. ASCs were responsive to biomolecule stimulation using TGF- β 1, thus elucidating mechanisms of slow release of this molecule might enhance the outcomes of 3D printed collagen and PCL scaffolds.

While 3D printed collagen and PCL exhibited controlled material deposition and thus scaffold architecture, these constructs were limited in their ability to mimic nanofiber morphology. The extracellular matrix (ECM), comprised of collagen fibers and associated glycoproteins and polysaccharides, fills the interstitial space and supports cell adhesion.

Collagen fibers, the main structural component of the ECM, are typically 100-200 nm in diameter.³⁰ Cell anchorage is achieved through focal adhesion complexes where transmembrane receptors, such as integrins, link the cytoskeleton to the ECM.³⁴ Three-dimensional printed struts exhibit much greater diameters, in the range of 0.4-1 mm, depending on the print nozzle. Higher print resolution could improve scaffold morphology, but employment of a smaller-diameter nozzle would create new challenges, mainly nozzle blockage. Thus, other methods of scaffold production are required to produce scaffolds with nanofibrous strut dimensions.

Polymer electrospinning, in contrast to 3D bioprinting, allows for the fabrication of nanofibrous scaffolds. Electrospun scaffolds display high porosity and large surface area-to-volume ratios,^{35,36} facilitating effective delivery and distribution of incorporated bioactive factors.³⁷ However, in electrospinning, pore size is not controlled, resulting in densely-packed nanofibers. In this thesis, electrospun gelatin scaffolds did not delay healing *in vivo*, but did not enhance wound closure or re-epithelialization states. Future research should attempt to improve electrospun scaffold porosity. One possible strategy is the incorporation of salt agents or sacrificial secondary polymers within the electrospinning solution, which can be subsequently leached out of the scaffold, resulting in greater void regions.^{38,39}

Together, this thesis has demonstrated that each scaffold fabrication method has its advantages and limitations. Bioprinting allows for controlled scaffold architecture and porosity, but printing resolution is low, on the scale of approximately 400-1000 μm . Higher scaffold resolution can be achieved using electrospun fibers, which exhibit diameters in the range of 100-200 nm. However, electrospun scaffolds are randomly organized and densely packed, limiting the potential for cell infiltration. Design of a TE scaffold must take into consideration the desired physical properties in order to choose a suitable material and fabrication method.

4.3 Galectin-3 to Modulate Inflammation *In Vivo*

Chronic wounds are halted at the inflammatory stage of healing, presenting decreased levels of growth factors such as TGF- β and VEGF and increased levels of expression of inflammatory cytokines, such as IL-1, IL-6, and TNF- α , which increase local inflammation further.⁴⁰ Several underlying factors, such as impaired re-epithelialization, angiogenesis, and granulation tissue formation, imbalances in proteolytic activity, persistent bacterial colonization and the formation of biofilms, and the accumulation of oxidative stress at the wound site, disrupt

the normal wound healing process.^{40,41} Regardless of wound management and intervention, including wound debridement, treatment of infection, application of wound dressings to control exudate and moisture, mechanical off-loading to reduce pressure ulcer recurrence, and tissue revascularization, chronic wounds remain a significant burden on patients and the healthcare system.⁴² Current available therapies offer low clinical efficacy in the resolution of continuous inflammation, keeping the wound in a pro-inflammatory non-healing state.^{41,43} Thus, a therapeutic strategy capable of artificially shifting the wound microenvironment from pro-inflammatory to pro-fibrotic is of interest.

In normal wound healing, macrophages are implicated in the regulation of fibrosis, and release signaling molecules such as TGF- β , PDGF- β and galectin 3 to increase myofibroblast matrix synthesis and release of tissue inhibitors of metalloproteinases (TIMPs).⁴⁴ Macrophages are a heterogeneous population of myeloid cells that exhibit distinct physiological roles. Macrophages respond to pathogens and modulate the adaptive immune response, including the induction and resolution of inflammation, tissue repair, and homeostasis. Macrophages exhibit plasticity in their polarization towards classical M1 (pro-inflammatory) or alternative M2 (anti-inflammatory) phenotypes, depending on the types of stimuli present. For instance, M1 macrophages are induced by stimulation with interferon gamma (IFN γ) and lipopolysaccharides (LPS).^{45,46} M2 macrophages can be further classified into four speculated subdivisions based on the stimuli and the achieved transcriptional changes. Alternative activated macrophages (M2a) are activated by Interleukin (IL)-4 or IL-13, type 2 macrophages (M2b) are believed to be activated by immune complexes and LPS, deactivated macrophages (M2c) may be activated by glucocorticoids or IL-10, while M2-like macrophages (M2d) may be activated by adenosines or IL-6.^{45,46} Macrophage phenotype, whether classical (M1) pro-inflammatory or alternative (M2) anti-inflammatory, determines physiological roles and therefore also the expressed proteome of the macrophage.

Galectin-3 gene and protein expression is higher in M2 polarized macrophages.⁴⁷ The protein functions during the regulation of M2 macrophage polarization⁴⁸ and as a chemoattractant for monocytes and macrophages,^{49,50} implicating galectin-3 as a potential therapeutic target for inflammatory regulation during skin healing. This thesis has shown that delivery of galectin-3, via an electrospun scaffold or topical application, does not enhance M2 macrophage density at the wound. Biological activity of galectin-3 described in the literature is

highly context-specific, leading to discrepancies in its roles during inflammation. For example, a study by Mackinnon *et al.* found that expression and secretion of galectin-3 was suppressed in bone marrow-derived macrophages exposed to 100 ng/mL LPS.⁴⁸ In contrast, Novak *et al.* reported a significant increase in galectin-3 expression from human blood-monocyte derived macrophages exposed to 100 ng/mL LPS and 20 ng/mL IFN γ .⁴⁷ Moreover, *in vitro* effects of galectin-3 do not always translate *in vivo* since important factors including cell maturation, matrix composition and chemoattractants, are often absent from *in vitro* studies.

In this thesis, exogenous galectin-3 did not significantly influence murine wound healing, re-epithelialization or inflammation. Treatment of full-thickness excisional wounds with recombinant human galectin-3, delivered by an electrospun gelatin scaffold or topically applied, did not delay cutaneous wound healing *in vivo* after 9 days. Galectin-3 treatment did not affect epithelial tongue length or thickness at days 7 or 9 post-wounding. Arginase I-positive cell density was also unaffected by exogenous galectin-3 treatment. As such, galectin-3 in a recombinant, extracellular presence may not be an effective therapeutic for the clinical treatment of chronic skin wounds. Future experiments may assess the efficacy of other bioactive constituents, such as TGF- β and IL-4,^{51,52} in shifting the chronic wound microenvironment from pro-inflammatory to pro-fibrotic.⁵³

4.4 Future Directions

4.4.1 Improving 3D Printed Scaffolds

Collagen protein scaffolds were printed from a high concentration type I collagen bioink. The Young's modulus of the bioink, reported by Advanced Biomatrix, was approximately 1050 Pa after 30 min *in situ* gelation. In future studies, the softness of this gel could be tuned by mixing the collagen bioink with a second component to increase scaffold stiffness. For instance, by adding methacrylated type I bovine collagen bioink, gels could be prepared at various concentrations and UV crosslinked after printing to provide tunable gel stiffness. Increasing *in situ* gelation may affect ASC bioactivity on the scaffolds and improve cell adhesion, spreading and proliferation.

Osteo-inductivity of synthetic PCL scaffolds should be investigated further. Future experiments employing fusion printed PCL scaffolds should investigate improving scaffold biocompatibility via mineral functionalization. For instance, PCL scaffolds containing mineral

additives, such as Bio-Oss (BO) or decellularized bone matrix (DCB), have demonstrated enhanced calcium content, collagen I deposition, osteocalcin expression of ASCs after 3 weeks.⁵⁴ Improving the osteo-inductive properties of PCL scaffolds might improve their efficacy in tissue engineering applications. A second future direction to improve printed PCL scaffold efficacy is by employing a PCL composite. For instance, future work should study photocrosslinkable polycaprolactone dimethylacrylate (PCLDMA) and poly(ethylene glycol) diacrylate (PEGDA), which can be mixed together to prepare an ink for ink-jet 3D printing.¹¹ This PCLDMA/PEGDA ink has been shown to improve material properties and the quality of the resultant scaffolds.¹¹ However, a nitrogen atmosphere is needed during printing, thus our current bioprinter set-up would require modification.

4.4.2 Improving Electrospun Scaffolds

Research in our lab has previously demonstrated that electrospun galectin-3/gelatin scaffolds were biocompatible *in vitro*; electrospun scaffolds supported the adhesion, proliferation, and fibronectin secretion of human dermal fibroblasts.⁵⁵ Electrospun galectin-3/gelatin scaffolds generated in this thesis exhibited fibers within the desired 100-200 nm diameter range, but were densely packed. Within a TE scaffold, large pore sizes are necessary to ensure the penetration of cells.^{56,57} One technique to improve scaffold pore size is to co-electrospin polymer fibers with sacrificial fibers that can subsequently be removed.⁵⁸ For instance, the co-electrospinning of gelatin scaffolds with sacrificial polyethylene glycol fibers has been shown to generate pores ranging 10-100 μm in diameter.³⁹ Likewise, poly-ethylene oxide (PEO) is another sacrificial material candidate as it is highly water soluble, facilitating easy removal following gelatin crosslinking.⁵⁸ This method has been employed for the blend electrospinning of a collagen/PCL scaffold with PEO as the sacrificial fiber component. Soaking the scaffold in water, dissolved PEO fibers, resulting in a scaffold with improved void pores for cell infiltration.⁵⁹ This scaffold design demonstrated complete infiltration of scaffolds after 4 weeks in a model of neoangiogenesis in rats.⁵⁹ Moreover, micropores can be generated by simply piercing the electrospun scaffold with a micro-diameter needle. For instance, using an acupuncture needle, 160 μm pores were created in a 70:30 collagen/PCL electrospun scaffold.^{60,61} When implanted into full-thickness skin wounds on the backs of Sprague-Dawley rats, the microporous scaffolds promoted faster skin regeneration *in vivo* than unprocessed

electrospun scaffolds.⁶⁰ Pre-seeding of these microporous scaffolds with fibroblasts further promoted tissue regeneration following wounding.⁶¹ In comparison to other methods for increasing scaffold pore size, the generation of a stamp/press device with a defined needle diameter and scaffold piercing capabilities offers a technically straightforward and cost-effective approach for introducing organized and reproducible micropores into electrospun scaffolds. Improving porosity in the electrospun scaffolds could enhance cell infiltration *in vivo* during murine wound healing, facilitating fibrosis, vascularization, and re-epithelialization.

4.4.3 ASC Differentiation

ASC multipotency has been widely explored, leading to the generation of various classifications of the cells including adipose-derived stem cells (ADSCs), adipose-derived adult stem cells, adipose-derived mesenchymal stem cells (AD-MSCs), adipose MSCs (AMSCs), and adipose stromal/stem cells (ASCs). To avoid further confusion, the International Society for Cellular Therapy proposed classifying all plastic-adherent cells derived from mesenchymal tissues and showing multipotency as mesenchymal stromal cells, regardless of tissue source. The term stem cell should be reserved for cells showing definitive stem cell characteristics, including adherence to tissue culture plastic, multipotency, and long-term self-renewal capacity.⁶² Future experiments should study the culturing conditions which will enhance the differentiation potential of ASCs on 3D printed scaffolds. This potentially might be achieved through the co-culturing of ASCs with differentiated cells, for example fibroblasts,⁶³ chondrocytes,⁶⁴ endothelial cells,⁶⁵ or Schwann cells.⁶⁶

4.4.4 Establishing *In Vitro* and *In Vivo* Effects of Galectin-3

This thesis has demonstrated that treatment of murine wounds with recombinant human galectin-3, delivered by an electrospun scaffold or topically applied, did not statistically influence wound healing kinetics, re-epithelialization, or M2 macrophage number. The lyophilized protein used in this study has been tested for *in vitro* bioactivity using rabbit erythrocytes to evaluate galectin-3-mediated agglutination.⁶⁷ Galectin-3 bioactivity has also been confirmed by studying cell viability following treatment of acute T-cell leukemia cell lines with galectin-3, a treatment known to induce apoptosis in T-cells.^{47,68}

The findings of this thesis suggest galectin-3 in an exogenous form does not influence acute wound healing processes. Research from our laboratory has shown that galectin-3 knockout mice display closure kinetics of full thickness excisional wounds comparable to that of wildtype groups.⁶⁹ Moreover, the bioactivity of galectin-3 is possibly influenced by post-translational modifications, including cleavage and phosphorylation of the protein.⁷⁰ Cleavage of galectin-3 by MMPs, prostate-specific antigen (PSA), and parasite-originating proteases has been shown to produce intact carbohydrate-recognition domain and N-terminal peptides of variable sizes that retained lectin binding activity but lost multivalence.^{70,71} Moreover, phosphorylation of serine and tyrosine by Abelson tyrosine kinase (c-Abl), cyclin-dependent kinase inhibitor (CKI), and glycogen synthase kinase-3 beta (GSK-3 β) could regulate galectin-3 localization and associated signal transduction.^{70,72} Thus, galectin-3 contains several domains through which protein multivalence, localization, and ligand interactions can be modified; absence of these modifications may render recombinant human galectin-3 inactive in the extracellular environment.

As previously discussed, interleukin 4 (IL-4) and IL-13 treatment of bone marrow derived macrophages from galectin-3 knockout mice resulted in reduced arginase I activity.⁴⁸ *In vitro* analysis of exogenous galectin-3 is required to better understand the influence of the protein on macrophage polarization in a controlled experimental environment. THP-1, an immortalized monocyte-like cell line, could be employed to identify the effects of exogenous recombinant human galectin-3 on upregulating M2 macrophage markers, including TGF- β and the mannose receptor in human monocytes.^{48,73} Such experiments might indicate whether galectin-3 can direct monocyte differentiation towards an M2 phenotype, and under which treatment concentrations galectin-3 bioactivity is optimized.^{49,74} Once the bioactivity of galectin-3 is better understood *in vitro*, investigation of its role *in vivo* via topical delivery could once again be pursued. If galectin-3 does influence M2 macrophage density *in vivo*, future work should also investigate the role of galectin-3 at various time points post-wounding, given that galectin-3 expression is highest day 1 following wounding in wildtype mice.⁷⁵

4.5 Limitations of Results

4.5.1 Human Adipose Derived Stem/Stromal Cells

In this thesis, human adipose derived stem/stromal cells (ASCs) were cultured onto 3D printed scaffolds to study material biocompatibility and the influence of a scaffold on ASC lineage commitment. Initially known as processed lipoaspirate cells or PLA cells,⁷⁶ ASCs can be isolated from human lipoaspirates and, similar to mesenchymal stem cells (MSCs), can be differentiated *in vitro* using lineage-specific factors toward osteogenic, adipogenic, myogenic, and chondrogenic phenotypes.²⁹ Adipose tissue is easily isolated by tissue resection, ultrasonic-assisted lipoplasty, syringe extraction, or suction-assisted lipoplasty (commonly known as liposuction).⁷⁷ From adipose tissue, the stromal vascular fraction (SVF), composed of red blood cells, fibroblasts, endothelial cells, smooth muscle cells, pericytes and pre-adipocytes, can be isolated using enzymatic digestion.^{78,79} Further processing and culturing of the SVF eliminates contaminating cell populations and results in an adherent, multi-potent pre-adipocyte population. Due to their availability and multi-potency, ASCs have been employed in a variety of regenerative models. *In vitro* bone tissue regeneration has been demonstrated using porous poly(lactic-co-glycolic)acid- β -tricalcium phosphate (PLGA- β -TCP) scaffolds,⁸⁰ polylactic acid (PLA)/ β -tricalcium phosphate (β -TCP) composite scaffolds,⁸¹ and polycaprolactone-tricalcium phosphate (mPCL-TCP) scaffolds with matrix components, either fibrin glue or lyophilized collagen.⁸² Similarly, *in vitro* cartilage tissue regeneration,⁸³⁻⁸⁵ adipose differentiation,^{29,86,87} and epidermal differentiation⁸⁸⁻⁹⁰ have also been validated.

Despite previous findings, differentiation of multiple lineages was not observed in this thesis. ASCs in this study were derived from human adipose tissue originating from the lower limb of a 67-year-old woman, and lineage appeared already committed towards an adipogenic phenotype. This finding was independent of ASC treatment with lineage-specific factors for osteogenic commitment, such as glycerol 2-phosphate (commonly known as β -glycerophosphate; BGP) and ascorbic acid 2-phosphate (Asc 2-P). This result was unexpected given that BGP and Asc 2-P are well established osteogenic lineage inducing factors. Reports have shown that MSC isolated from bone marrow exhibit rapid growth and osteogenic differentiation following treatment with 10 mM BGP.⁹¹ Likewise Asc 2-P treatment significantly improved nascent cell growth at both high and low concentrations (0.25-1.0 mM), and also increased expression of osteoblast differentiation markers, including collagen synthesis and alkaline phosphatase

activity.⁹² Osteogenic differentiation has been noted to take 4-6 weeks in previous studies, therefore the 3 week experimental time point of this thesis may have been insufficient. Moreover, this thesis employed ASCs of pathological origin, whereas other reports employed healthy human or animal ASCs. Thus, future work is needed to elucidate the differentiation potential of ASCs originating from pathological, amputated limbs in order to justify their use in regenerative medicine.

4.5.2 Murine Model of Wound Healing

Human chronic skin wounds represent a complex pathological environment with observed heterogeneity among populations. Chronic wounds can arise from a number of factors including malnutrition, advanced age, infection, diabetes, vascular insufficiency, prolonged pressure and edema contribute to amplified inflammation and a non-healing wound.⁴¹ Thus, a major limitation to this thesis is the employment of an animal model that cannot fully imitate the complexity of human chronic wounds.⁹³ This study utilizes a wild type mouse (*Mus musculus*) model of full-thickness dermal wound healing. While murine models are simple to maintain and economically accessible, important differences between murine and human skin healing exist.⁹⁴ Mice have small bodies which limits modeling of wound sizes relevant for humans, and also have a short life expectancy which limits studies of “chronic” wounds in mice.^{95,96}

With regards to wound healing, murine wounds close mainly by contraction via the subcutaneous panniculus carnosus, a layer of striated muscle.⁹⁷ This contrasts with human wounds closure which is achieved through cell migration over granulation tissue and re-epithelialization. In the dermis and epidermis, human and murine skin have unvarying layers of cells, however these layers greatly diverge in physiology. While human skin is over 100 μm thick, firm, and adherent to basal tissues, murine skin is less than 25 μm thick and is unattached and loose.⁹⁷⁻⁹⁹ The epidermis is comprised of 5-10 cell layers in humans but only 2-3 in mice.¹⁰⁰ Humans and mice also differ in the role of specific niches of skin stem cells. For instance, murine skin is densely populated by hair follicles while the majority of human epidermis is classified as interfollicular, exhibiting sparse and uneven hair follicle distribution.^{97,100} In a study of split-thickness skin grafting, scalp donor sites rich in hair follicles healed faster than thigh sites which had fewer hair follicles.¹⁰¹ This difference is due to the important roles hair follicle stem cells play in cutaneous repair,¹⁰²⁻¹⁰⁴ where up to a quarter of newly formed

epidermis is derived from hair follicle stem or progenitor cells.¹⁰² Overall, caution must be exercised when translating murine findings to pre-clinical studies.

Moreover, in this thesis, the validity of the mouse studies conducted was limited by the low number of mice used for each condition and at each time point. Three mice were sacrificed at day 3 post-wounding, three mice at day 7, and two mice at day 9. The inclusion of a larger sample size of mice may have eliminated the significant variability observed in the study, thereby improving the power of the study. All mice were age and sex matched, in addition to being wildtype. Thus, this model of healing was unchallenged and does not accurately reflect the impeded healing associated with human chronic wounds. Additionally, observation of wound area for closure kinetics was affected by the overlaying eschar which concealed healing wounds. In calculations of the wound area, the eschar area was also included, thus measured wound areas could have appeared larger. In order to directly observe the underlying healing tissues, it would have been necessary to remove the eschar. However, this manipulation could potentially disrupt the underlying tissues and thus was not executed.

4.6 Conclusion

This thesis has demonstrated fabrication of three different biomaterial scaffolds for tissue engineering applications, three-dimensional reverse embedding of collagen scaffolds, polymer fusion printing of PCL scaffolds, and electrospinning of gelatin scaffolds. Bioprinting of soft collagen scaffolds required embedding the print within a secondary gelatin support slurry to facilitate *in situ* gelation. Preparation and validation of the gelatin support slurry demonstrated that gelatin microparticle morphology was dependent on mechanical blend treatment, and that the prepared slurry behaved as a Bingham plastic fluid. Collagen scaffolds of rectilinear or hexagonal infill patterning stimulated ASC fibronectin deposition. Rectilinear PCL scaffolds promoted ASC adhesion, spreading, and proliferation responses. While collagen and PCL scaffolds exhibit *in vitro* biocompatibility, ASC phenotype was uninfluenced by 3D versus 2D culturing conditions, collagen or PCL scaffold material, or rectilinear versus hexagonal geometric cues. These scaffolds should be investigated further regarding *in vivo* efficacy for RM applications. Gelatin polymer blended with recombinant galectin-3 was electrospun into a protein delivery scaffold and employed in a murine model of cutaneous wound healing. Treatment of wounds with the galectin-3/gelatin scaffolds, or with topical galectin-3, did not

enhance wound closure, re-epithelialization, or influence macrophage phenotypes in the wound. Future directions include elucidating the conditions where galectin-3 might modulate inflammation *in vivo* and considering other target molecules such as TGF- β and IL-4.

4.7 References

1. LeVeau, B. F. & Bernhardt, D. B. Developmental biomechanics. Effect of forces on the growth, development, and maintenance of the human body. *Phys. Ther.* **64**, 1874–1882 (1984).
2. Hollister, S. J. Porous scaffold design for tissue engineering. *Nat. Mater.* **4**, 518–524 (2005).
3. Williams, D. F. On the mechanisms of biocompatibility. *Biomaterials* **29**, 2941–2953 (2008).
4. Ahn, S. H., Lee, H. J. & Kim, G. H. Polycaprolactone Scaffolds Fabricated with an Advanced Electrohydrodynamic Direct-Printing Method for Bone Tissue Regeneration. *Biomacromolecules* **12**, 4256–4263 (2011).
5. Domingos, M. *et al.* The first systematic analysis of 3D rapid prototyped poly(ϵ -caprolactone) scaffolds manufactured through BioCell printing: the effect of pore size and geometry on compressive mechanical behaviour and *in vitro* hMSC viability. *Biofabrication* **5**, 045004 (2013).
6. Eshraghi, S. & Das, S. Mechanical and microstructural properties of polycaprolactone scaffolds with one-dimensional, two-dimensional, and three-dimensional orthogonally oriented porous architectures produced by selective laser sintering. *Acta Biomater.* **6**, 2467–2476 (2010).
7. Saad, B. & Suter, U. W. Biodegradable Polymeric Materials. in *Encyclopedia of Materials: Science and Technology* (eds. Buschow, K. H. J. *et al.*) 551–555 (Elsevier, 2001). doi:10.1016/B0-08-043152-6/00105-4
8. Lam, C. X. F., Hutmacher, D. W., Schantz, J.-T., Woodruff, M. A. & Teoh, S. H. Evaluation of polycaprolactone scaffold degradation for 6 months *in vitro* and *in vivo*. *J. Biomed. Mater. Res. A* **90A**, 906–919 (2009).
9. Lam, C. X., Teoh, S. H. & Hutmacher, D. W. Comparison of the degradation of polycaprolactone and polycaprolactone-(β -tricalcium phosphate) scaffolds in alkaline medium. *Polym. Int.* **56**, 718–728 (2007).
10. Meseguer-Olmo, L. *et al.* In-vivo behavior of Si-hydroxyapatite/polycaprolactone/DMB scaffolds fabricated by 3D printing. *J. Biomed. Mater. Res. A* **101A**, 2038–2048 (2013).
11. He, Y. *et al.* A new photocrosslinkable polycaprolactone-based ink for three-dimensional inkjet printing. *J. Biomed. Mater. Res. B Appl. Biomater.* **105**, 1645–1657 (2017).
12. Tay, B. Y. *et al.* Processing of polycaprolactone porous structure for scaffold development. *J. Mater. Process. Technol.* **182**, 117–121 (2007).
13. Sayyar, S. *et al.* Extrusion Printed Graphene/Polycaprolactone/Composites for Tissue Engineering. *Mater. Sci. Forum* **773–774**, 496–502 (2013).
14. Mannoor, M. S. *et al.* 3D Printed Bionic Ears. *Nano Lett.* **13**, 2634–2639 (2013).
15. Hockaday, L. A. *et al.* Rapid 3D printing of anatomically accurate and mechanically heterogeneous aortic valve hydrogel scaffolds. *Biofabrication* **4**, 035005 (2012).
16. Cui, X. & Boland, T. Human microvasculature fabrication using thermal inkjet printing technology. *Biomaterials* **30**, 6221–6227 (2009).
17. Xu, T. *et al.* Viability and electrophysiology of neural cell structures generated by the inkjet printing method. *Biomaterials* **27**, 3580–3588 (2006).
18. Kolesky, D. B. *et al.* 3D bioprinting of vascularized, heterogeneous cell-laden tissue constructs. *Adv. Mater. Deerfield Beach Fla* **26**, 3124–3130 (2014).

19. Filardo, G. *et al.* Patient-specific meniscus prototype based on 3D bioprinting of human cell-laden scaffold. *Bone Jt. Res.* **8**, 101–106 (2019).
20. Pati, F. *et al.* Printing three-dimensional tissue analogues with decellularized extracellular matrix bioink. *Nat. Commun.* **5**, 3935 (2014).
21. Martin, I., Simmons, P. J. & Williams, D. F. Manufacturing challenges in regenerative medicine. *Sci. Transl. Med.* **6**, 232fs16 (2014).
22. Murphy, S. V. & Atala, A. 3D bioprinting of tissues and organs. *Nat. Biotechnol.* **32**, 773–785 (2014).
23. Sinha, G. Cell presses. *Nat. Biotechnol.* **32**, 716–719 (2014).
24. Hinton, T. J. *et al.* Three-dimensional printing of complex biological structures by freeform reversible embedding of suspended hydrogels. *Sci. Adv.* **1**, e1500758 (2015).
25. Hinton, T. J., Hudson, A., Pusch, K., Lee, A. & Feinberg, A. W. 3D Printing PDMS Elastomer in a Hydrophilic Support Bath via Freeform Reversible Embedding. *ACS Biomater. Sci. Eng.* **2**, 1781–1786 (2016).
26. Deslex, S., Negrel, R., Vannier, C., Etienne, J. & Ailhaud, G. Differentiation of human adipocyte precursors in a chemically defined serum-free medium. *Int. J. Obes.* **11**, 19–27 (1987).
27. Hauner, H. *et al.* Promoting effect of glucocorticoids on the differentiation of human adipocyte precursor cells cultured in a chemically defined medium. *J. Clin. Invest.* **84**, 1663–1670 (1989).
28. Gimble, J. M. & Guilak, F. Differentiation potential of adipose derived adult stem (ADAS) cells. *Curr. Top. Dev. Biol.* **58**, 137–160 (2003).
29. Zuk, P. A. *et al.* Human adipose tissue is a source of multipotent stem cells. *Mol. Biol. Cell* **13**, 4279–4295 (2002).
30. Tracy, L. E., Minasian, R. A. & Caterson, E. J. Extracellular Matrix and Dermal Fibroblast Function in the Healing Wound. *Adv. Wound Care* **5**, 119–136 (2016).
31. Liu, Y., Ma, L. & Gao, C. Facile fabrication of the glutaraldehyde cross-linked collagen/chitosan porous scaffold for skin tissue engineering. *Mater. Sci. Eng. C* **32**, 2361–2366 (2012).
32. Gould, L. J. Topical Collagen-Based Biomaterials for Chronic Wounds: Rationale and Clinical Application. *Adv. Wound Care* **5**, 19–31 (2016).
33. Rhee, S., Puetzer, J. L., Mason, B. N., Reinhart-King, C. A. & Bonassar, L. J. 3D Bioprinting of Spatially Heterogeneous Collagen Constructs for Cartilage Tissue Engineering. *ACS Biomater. Sci. Eng.* **2**, 1800–1805 (2016).
34. Hynes, R. O. Integrins: Versatility, modulation, and signaling in cell adhesion. *Cell* **69**, 11–25 (1992).
35. Xie, J., Li, X. & Xia, Y. Putting Electrospun Nanofibers to Work for Biomedical Research. *Macromol. Rapid Commun.* **29**, 1775–1792 (2008).
36. Zhong, S. P., Zhang, Y. Z. & Lim, C. T. Tissue scaffolds for skin wound healing and dermal reconstruction. *Wiley Interdiscip. Rev. Nanomed. Nanobiotechnol.* **2**, 510–525 (2010).
37. Barondes, S. H. *et al.* Galectins: a family of animal beta-galactoside-binding lectins. *Cell* **76**, 597–598 (1994).
38. Nam, J., Huang, Y., Agarwal, S. & Lannutti, J. Materials selection and residual solvent retention in biodegradable electrospun fibers. *J. Appl. Polym. Sci.* **107**, 1547–1554 (2008).

39. Skotak, M., Ragusa, J., Gonzalez, D. & Subramanian, A. Improved cellular infiltration into nanofibrous electrospun cross-linked gelatin scaffolds templated with micrometer-sized polyethylene glycol fibers. *Biomed. Mater. Bristol Engl.* **6**, 055012 (2011).
40. Brem, H. & Tomic-Canic, M. Cellular and molecular basis of wound healing in diabetes. *J. Clin. Invest.* **117**, 1219–1222 (2007).
41. Zhao, R., Liang, H., Clarke, E., Jackson, C. & Xue, M. Inflammation in Chronic Wounds. *Int. J. Mol. Sci.* **17**, 2085 (2016).
42. Bekara, F. *et al.* New techniques for wound management: A systematic review of their role in the management of chronic wounds. *Arch. Plast. Surg.* **45**, 102–110 (2018).
43. Velnar, T., Bailey, T. & Smrkolj, V. The wound healing process: an overview of the cellular and molecular mechanisms. *J. Int. Med. Res.* **37**, 1528–1542 (2009).
44. Forbes, S. J. & Rosenthal, N. Preparing the ground for tissue regeneration: from mechanism to therapy. *Nat. Med.* **20**, 857–869 (2014).
45. Huang, X., Li, Y., Fu, M. & Xin, H.-B. Polarizing Macrophages In Vitro. *Methods Mol. Biol. Clifton NJ* **1784**, 119–126 (2018).
46. Mantovani, A. *et al.* The chemokine system in diverse forms of macrophage activation and polarization. *Trends Immunol.* **25**, 677–686 (2004).
47. Novak, R., Dabelic, S. & Dumic, J. Galectin-1 and galectin-3 expression profiles in classically and alternatively activated human macrophages. *Biochim. Biophys. Acta* **1820**, 1383–1390 (2012).
48. MacKinnon, A. C. *et al.* Regulation of alternative macrophage activation by galectin-3. *J. Immunol. Baltim. Md 1950* **180**, 2650–2658 (2008).
49. Sano, H. *et al.* Human galectin-3 is a novel chemoattractant for monocytes and macrophages. *J. Immunol. Baltim. Md 1950* **165**, 2156–2164 (2000).
50. Jia, W., Kidoya, H., Yamakawa, D., Naito, H. & Takakura, N. Galectin-3 accelerates M2 macrophage infiltration and angiogenesis in tumors. *Am. J. Pathol.* **182**, 1821–1831 (2013).
51. McCartney-Francis, N. L. & Wahl, S. M. TGF- β and macrophages in the rise and fall of inflammation. in *TGF- β and Related Cytokines in Inflammation* (eds. Breit, S. N. & Wahl, S. M.) 65–90 (Birkhäuser Basel, 2001). doi:10.1007/978-3-0348-8354-2_4
52. Transforming growth factor beta: the good, the bad, and the ugly. *J. Exp. Med.* **180**, 1587–1590 (1994).
53. Martinez, F. O. & Gordon, S. The M1 and M2 paradigm of macrophage activation: time for reassessment. *F1000prime Rep.* **6**, 13 (2014).
54. Nyberg, E., Rindone, A., Dorafshar, A. & Grayson, W. L. Comparison of 3D-Printed Poly- ϵ -Caprolactone Scaffolds Functionalized with Tricalcium Phosphate, Hydroxyapatite, Bio-Oss, or Decellularized Bone Matrix. *Tissue Eng. Part A* **23**, 503–514 (2016).
55. McLeod, K. Design and Validation of Delivery Systems for Galectin-3 for Skin Healing Applications. *Electron. Thesis Diss. Repos.* (2017).
56. Karande, T. S., Ong, J. L. & Agrawal, C. M. Diffusion in musculoskeletal tissue engineering scaffolds: design issues related to porosity, permeability, architecture, and nutrient mixing. *Ann. Biomed. Eng.* **32**, 1728–1743 (2004).
57. Zhu, X., Cui, W., Li, X. & Jin, Y. Electrospun fibrous mats with high porosity as potential scaffolds for skin tissue engineering. *Biomacromolecules* **9**, 1795–1801 (2008).
58. Wu, J. & Hong, Y. Enhancing cell infiltration of electrospun fibrous scaffolds in tissue regeneration. *Bioact. Mater.* **1**, 56–64 (2016).

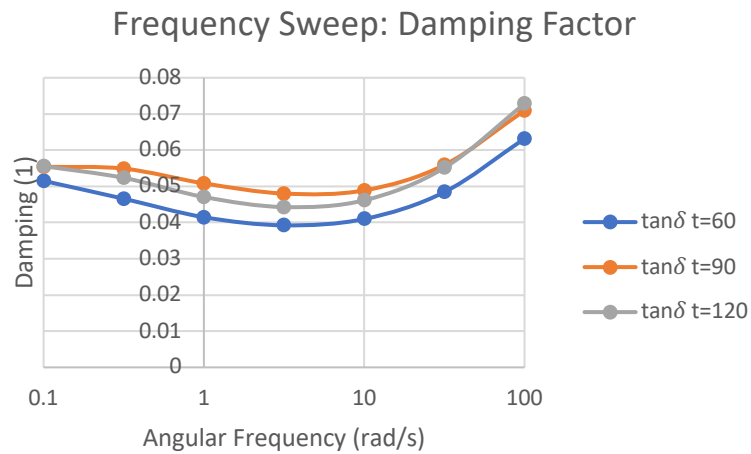
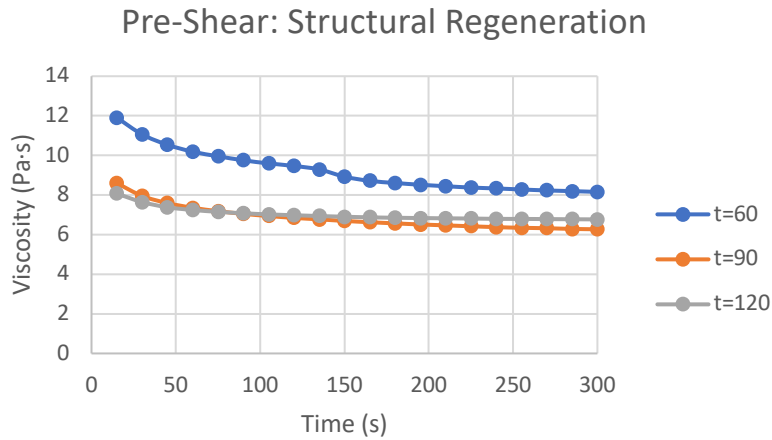
59. Klumpp, D. *et al.* Three-dimensional vascularization of electrospun PCL/collagen-blend nanofibrous scaffolds in vivo. *J. Biomed. Mater. Res. A* **100**, 2302–2311 (2012).
60. Bonvallet, P. P. *et al.* Microporous dermal-like electrospun scaffolds promote accelerated skin regeneration. *Tissue Eng. Part A* **20**, 2434–2445 (2014).
61. Bonvallet, P. P. *et al.* Microporous Dermal-Mimetic Electrospun Scaffolds Pre-Seeded with Fibroblasts Promote Tissue Regeneration in Full-Thickness Skin Wounds. *PLoS ONE* **10**, (2015).
62. Horwitz, E. M. *et al.* Clarification of the nomenclature for MSC: The International Society for Cellular Therapy position statement. *Cytotherapy* **7**, 393–395 (2005).
63. Haubner, F. *et al.* A Co-Culture Model of Fibroblasts and Adipose Tissue-Derived Stem Cells Reveals New Insights into Impaired Wound Healing After Radiotherapy. *Int. J. Mol. Sci.* **16**, 25947–25958 (2015).
64. Lee, C. *et al.* Adipose stem cells can secrete angiogenic factors that inhibit hyaline cartilage regeneration. *Stem Cell Res. Ther.* **3**, 35 (2012).
65. Volz, A.-C. Completely defined co-culture of adipogenic differentiated ASCs and microvascular endothelial cells. *ALTEX* 464–476 (2018). doi:10.14573/altex.1802191
66. Wei, Y. *et al.* Schwann-like cell differentiation of rat adipose-derived stem cells by indirect co-culture with Schwann cells in vitro: Schwann-like cell differentiation of rat ADSCs. *Cell Prolif.* **43**, 606–616 (2010).
67. Hadari, Y. R. *et al.* Galectin-8 binding to integrins inhibits cell adhesion and induces apoptosis. *J. Cell Sci.* **113 (Pt 13)**, 2385–2397 (2000).
68. Fukumori, T. *et al.* CD29 and CD7 mediate galectin-3-induced type II T-cell apoptosis. *Cancer Res.* **63**, 8302–8311 (2003).
69. Walker, J. T., Elliott, C. G., Forbes, T. L. & Hamilton, D. W. Genetic Deletion of Galectin-3 Does Not Impair Full-Thickness Excisional Skin Healing. *J. Invest. Dermatol.* **136**, 1042–1050 (2016).
70. Gao, X., Liu, J., Liu, X., Li, L. & Zheng, J. Cleavage and phosphorylation: important post-translational modifications of galectin-3. *Cancer Metastasis Rev.* **36**, 367–374 (2017).
71. Saraswati, S. *et al.* Galectin-3 is a substrate for prostate specific antigen (PSA) in human seminal plasma. *The Prostate* **71**, 197–208 (2011).
72. Balan, V., Nangia-Makker, P., Kho, D. H., Wang, Y. & Raz, A. Tyrosine-phosphorylated Galectin-3 Protein Is Resistant to Prostate-specific Antigen (PSA) Cleavage. *J. Biol. Chem.* **287**, 5192–5198 (2012).
73. Brancato, S. K. & Albina, J. E. Wound macrophages as key regulators of repair: origin, phenotype, and function. *Am. J. Pathol.* **178**, 19–25 (2011).
74. Danella Polli, C. *et al.* Monocyte Migration Driven by Galectin-3 Occurs through Distinct Mechanisms Involving Selective Interactions with the Extracellular Matrix. *ISRN Inflamm.* **2013**, (2013).
75. Walker, J. T. *et al.* Cell–matrix interactions governing skin repair: matricellular proteins as diverse modulators of cell function. *Research and Reports in Biochemistry* (2015). doi:10.2147/RRBC.S57407
76. Zuk, P. A. *et al.* Multilineage cells from human adipose tissue: implications for cell-based therapies. *Tissue Eng.* **7**, 211–228 (2001).
77. Zhu, M., Heydarkhan-Hagvall, S., Hedrick, M., Benhaim, P. & Zuk, P. Manual isolation of adipose-derived stem cells from human lipoaspirates. *J. Vis. Exp. JoVE* e50585 (2013). doi:10.3791/50585

78. Poznanski, W. J., Waheed, I. & Van, R. Human fat cell precursors. Morphologic and metabolic differentiation in culture. *Lab. Investig. J. Tech. Methods Pathol.* **29**, 570–576 (1973).
79. Rodbell, M. METABOLISM OF ISOLATED FAT CELLS. I. EFFECTS OF HORMONES ON GLUCOSE METABOLISM AND LIPOLYSIS. *J. Biol. Chem.* **239**, 375–380 (1964).
80. Hao, W. *et al.* Collagen I Gel Can Facilitate Homogenous Bone Formation of Adipose-Derived Stem Cells in PLGA- β -TCP Scaffold. *Cells Tissues Organs* **187**, 89–102 (2008).
81. Haimi, S. *et al.* Growth and Osteogenic Differentiation of Adipose Stem Cells on PLA/Bioactive Glass and PLA/ β -TCP Scaffolds. *Tissue Eng. Part A* **15**, 1473–1480 (2009).
82. Leong, D. T., Nah, W. K., Gupta, A., Hutmacher, D. W. & Woodruff, M. A. The Osteogenic Differentiation of Adipose Tissue-Derived Precursor Cells in a 3D Scaffold/Matrix Environment. (2008). Available at: <https://www.ingentaconnect.com/content/ben/cddt/2008/00000005/00000004/art00006>.
83. Lin, Y. *et al.* Molecular and cellular characterization during chondrogenic differentiation of adipose tissue-derived stromal cells in vitro and cartilage formation in vivo. *J. Cell. Mol. Med.* **9**, 929–39 (2005).
84. Cheng, N.-C., Estes, B. T., Awad, H. A. & Guilak, F. Chondrogenic Differentiation of Adipose-Derived Adult Stem Cells by a Porous Scaffold Derived from Native Articular Cartilage Extracellular Matrix. *Tissue Eng. Part A* **15**, 231–241 (2009).
85. Yoon, I.-S. *et al.* Proliferation and chondrogenic differentiation of human adipose-derived mesenchymal stem cells in porous hyaluronic acid scaffold. *J. Biosci. Bioeng.* **112**, 402–408 (2011).
86. Ogawa, R. *et al.* Adipogenic differentiation by adipose-derived stem cells harvested from GFP transgenic mice-including relationship of sex differences. *Biochem. Biophys. Res. Commun.* **319**, 511–517 (2004).
87. Sirico, M. L. *et al.* Human Mature Adipocytes Express Albumin and This Expression Is Not Regulated by Inflammation. *Mediators Inflamm.* **2012**, 1–8 (2012).
88. Trottier, V., Marceau-Fortier, G., Germain, L., Vincent, C. & Fradette, J. IFATS Collection: Using Human Adipose-Derived Stem/Stromal Cells for the Production of New Skin Substitutes: ifats collection: using human adipose-derived stem/stromal cells for the production of new skin substitutes. *Stem Cells* **26**, 2713–2723 (2008).
89. Li, H., Xu, Y., Fu, Q. & Li, C. Effects of Multiple Agents on Epithelial Differentiation of Rabbit Adipose-Derived Stem Cells in 3D Culture. *Tissue Eng. Part A* **18**, 1760–1770 (2012).
90. Du, Y. *et al.* Adipose-derived stem cells differentiate to keratocytes in vitro. *Mol. Vis.* **16**, 2680–2689 (2010).
91. SHIMA, W. N. *et al.* Rapid growth and osteogenic differentiation of mesenchymal stem cells isolated from human bone marrow. *Exp. Ther. Med.* **9**, 2202–2206 (2015).
92. Takamizawa, S. *et al.* Effects of ascorbic acid and ascorbic acid 2-phosphate, a long-acting vitamin C derivative, on the proliferation and differentiation of human osteoblast-like cells. *Cell Biol. Int.* **28**, 255–265 (2004).
93. Nunan, R., Harding, K. G. & Martin, P. Clinical challenges of chronic wounds: searching for an optimal animal model to recapitulate their complexity. *Dis. Model. Mech.* **7**, 1205–1213 (2014).
94. Zomer, H. D. & Trentin, A. G. Skin wound healing in humans and mice: Challenges in translational research. *J. Dermatol. Sci.* **90**, 3–12 (2018).

95. Dutta, S. & Sengupta, P. Men and mice: Relating their ages. *Life Sci.* **152**, 244–248 (2016).
96. Cibelli, J. *et al.* Strategies for improving animal models for regenerative medicine. *Cell Stem Cell* **12**, 271–274 (2013).
97. Gerber, P. A. *et al.* The top skin-associated genes: a comparative analysis of human and mouse skin transcriptomes. *Biol. Chem.* **395**, 577–591 (2014).
98. Wong, V. W., Sorkin, M., Glotzbach, J. P., Longaker, M. T. & Gurtner, G. C. Surgical approaches to create murine models of human wound healing. *J. Biomed. Biotechnol.* **2011**, 969618 (2011).
99. Abdullahi, A., Amini-Nik, S. & Jeschke, M. G. Animal models in burn research. *Cell. Mol. Life Sci. CMLS* **71**, 3241–3255 (2014).
100. Pasparakis, M., Haase, I. & Nestle, F. O. Mechanisms regulating skin immunity and inflammation. *Nat. Rev. Immunol.* **14**, 289–301 (2014).
101. Martinot, V., Mitchell, V., Fevrier, P., Duhamel, A. & Pellerin, P. Comparative study of split thickness skin grafts taken from the scalp and thigh in children. *Burns J. Int. Soc. Burn Inj.* **20**, 146–150 (1994).
102. Ito, M. *et al.* Wnt-dependent de novo hair follicle regeneration in adult mouse skin after wounding. *Nature* **447**, 316–320 (2007).
103. Ito, M. & Cotsarelis, G. Is the Hair Follicle Necessary for Normal Wound Healing? *J. Invest. Dermatol.* **128**, 1059–1061 (2008).
104. Oshimori, N. & Fuchs, E. Paracrine TGF- β signaling counterbalances BMP-mediated repression in hair follicle stem cell activation. *Cell Stem Cell* **10**, 63–75 (2012).

5 Appendices

Appendix A: Supplementary Rheological Results



Appendix B: G-Code and FFF Files for Scaffolds

Collagen Rectilinear Scaffolds

; external perimeters extrusion width =
0.16mm
; perimeters extrusion width = 0.22mm
; infill extrusion width = 0.22mm
; solid infill extrusion width = 0.22mm
; top infill extrusion width = 0.22mm

G21 ; set units to millimeters
G90 ; use absolute coordinates
M83 ; use relative distances for
extrusion

G1 Z0.160 F180.000
G1 X12.511 Y-0.145 F180.000
G1 X12.529 Y1.407 E0.02113 F90.000
G1 X12.529 Y11.407 E0.13615
G1 X12.146 Y12.256 E0.01268
G1 X11.401 Y12.540 E0.01086
G1 X-1.389 Y12.609 E0.17414
G1 X-11.395 Y12.609 E0.13623
G1 X-12.244 Y12.227 E0.01268
G1 X-12.529 Y11.476 E0.01094
G1 X-12.529 Y1.468 E0.13626
G1 X-12.438 Y-11.484 E0.17633
G1 X-12.050 Y-12.330 E0.01268
G1 X-11.304 Y-12.609 E0.01084
G1 X-1.303 Y-12.609 E0.13616
G1 X11.247 Y-12.597 E0.17086
F90.000
G1 X12.095 Y-12.214 E0.01268
G1 X12.379 Y-11.477 E0.01076
G1 X12.510 Y-0.169 E0.15396
G1 X11.185 Y1.616 F180.000
G1 X11.185 Y11.197 E0.13044 F90.000
G1 X1.605 Y11.197 E0.13044
G1 X1.605 Y1.616 E0.13044
G1 X11.161 Y1.616 E0.13011
G1 X11.315 Y1.487 F180.000
G1 X11.315 Y11.327 E0.12595 F90.000
G1 X1.475 Y11.327 E0.12595
G1 X1.475 Y1.487 E0.12595
G1 X11.291 Y1.487 E0.12564
G1 X11.235 Y1.625 F180.000
G1 X11.098 Y12.438 F180.000
G1 X1.712 Y2.438 E0.12780 F90.000
G1 X1.712 Y3.444 E0.01369
G1 X11.098 Y3.444 E0.12780
G1 X11.098 Y4.449 E0.01369
G1 X1.712 Y4.449 E0.12780
G1 X1.712 Y5.454 E0.01369
G1 X11.098 Y5.454 E0.12780
G1 X11.098 Y6.460 E0.01369
G1 X1.712 Y6.460 E0.12780
G1 X1.712 Y7.465 E0.01369
G1 X11.098 Y7.465 E0.12780
G1 X11.098 Y8.470 E0.01369
G1 X1.712 Y8.470 E0.12780
G1 X1.712 Y9.476 E0.01369
G1 X11.098 Y9.476 E0.12780
G1 X11.098 Y10.481 E0.01369
G1 X1.712 Y10.481 E0.12780
G1 X0.395 Y0.992 F180.000
G1 X-0.003 Y0.992 F180.000
G1 X0.000 Y1.061 F180.000

G1 X-0.395 Y1.061 F180.000
G1 X-1.605 Y1.685 F180.000
G1 X-1.605 Y11.266 E0.13044 F90.000
G1 X-11.185 Y11.266 E0.13044
G1 X-11.185 Y1.685 E0.13044
G1 X-1.629 Y1.685 E0.13011
G1 X-1.475 Y1.556 F180.000
G1 X-1.475 Y11.396 E0.12595 F90.000
G1 X-11.315 Y11.396 E0.12595
G1 X-11.315 Y1.556 E0.12595
G1 X-1.499 Y1.556 E0.12564
G1 X-1.555 Y1.694 F180.000
G1 X-1.692 Y2.507 F180.000
G1 X-11.078 Y2.507 E0.12780 F90.000
G1 X-11.078 Y3.513 E0.01369
G1 X-1.692 Y3.513 E0.12780
G1 X-1.692 Y4.518 E0.01369
G1 X-11.078 Y4.518 E0.12780
G1 X-11.078 Y5.523 E0.01369
G1 X-1.692 Y5.523 E0.12780
G1 X-1.692 Y6.529 E0.01369
G1 X-11.078 Y6.529 E0.12780
G1 X-11.078 Y7.534 E0.01369
G1 X-1.692 Y7.534 E0.12780
G1 X-1.692 Y8.539 E0.01369
G1 X-11.078 Y8.539 E0.12780
G1 X-11.078 Y9.545 E0.01369
G1 X-1.692 Y9.545 E0.12780
G1 X-1.692 Y10.550 E0.01369
G1 X-11.078 Y10.550 E0.12780
G1 X-0.981 Y0.476 F180.000
G1 X-0.369 Y0.045 F180.000
G1 X-0.035 Y-0.768 F180.000
G1 X-0.035 Y-0.792 F180.000
G1 X-0.304 Y-1.061 F180.000
G1 X-1.514 Y-11.266 F180.000
G1 X-1.514 Y-1.685 E0.13044 F90.000
G1 X-11.095 Y-1.685 E0.13044
G1 X-11.095 Y-11.266 E0.13044
G1 X-1.538 Y-11.266 E0.13011
G1 X-1.384 Y-11.396 F180.000
G1 X-1.384 Y-1.556 E0.12595 F90.000
G1 X-11.224 Y-1.556 E0.12595
G1 X-11.224 Y-11.396 E0.12595
G1 X-1.408 Y-11.396 E0.12564
G1 X-1.464 Y-11.257 F180.000
G1 X-1.601 Y-10.444 F180.000
G1 X-10.987 Y-10.444 E0.12780
F90.000
G1 X-10.987 Y-9.438 E0.01369
G1 X-1.601 Y-9.438 E0.12780
G1 X-1.601 Y-8.433 E0.01369
G1 X-10.987 Y-8.433 E0.12780
G1 X-10.987 Y-7.428 E0.01369
G1 X-1.601 Y-7.428 E0.12780
G1 X-1.601 Y-6.423 E0.01369
G1 X-10.987 Y-6.423 E0.12780
G1 X-10.987 Y-5.417 E0.01369
G1 X-1.601 Y-5.417 E0.12780
G1 X-1.601 Y-4.412 E0.01369
G1 X-10.987 Y-4.412 E0.12780
G1 X-10.987 Y-3.407 E0.01369
G1 X-1.601 Y-3.407 E0.12780
G1 X-1.601 Y-2.401 E0.01369

G1 X-10.987 Y-2.401 E0.12780
G1 X-0.304 Y-11.890 F180.000
G1 X-0.023 Y-12.171 F180.000
G1 X-0.002 Y-13.297 F180.000
G1 X0.831 Y-12.464 F180.000
G1 X11.036 Y-11.254 F180.000
G1 X11.036 Y-1.673 E0.13044 F90.000
G1 X1.455 Y-1.673 E0.13044
G1 X1.455 Y-11.254 E0.13044
G1 X11.012 Y-11.254 E0.13011
G1 X11.166 Y-11.384 F180.000
G1 X11.166 Y-1.544 E0.12595 F90.000
G1 X1.326 Y-1.544 E0.12595
G1 X1.326 Y-11.384 E0.12595
G1 X11.142 Y-11.384 E0.12564
G1 X11.086 Y-11.245 F180.000
G1 X10.949 Y-10.432 F180.000
G1 X1.562 Y-10.432 E0.12780 F90.000
G1 X1.562 Y-9.426 E0.01369
G1 X10.949 Y-9.426 E0.12780
G1 X10.949 Y-8.421 E0.01369
G1 X1.562 Y-8.421 E0.12780
G1 X1.562 Y-7.416 E0.01369
G1 X10.949 Y-7.416 E0.12780
G1 X10.949 Y-6.410 E0.01369
G1 X1.562 Y-6.410 E0.12780
G1 X1.562 Y-5.405 E0.01369
G1 X10.949 Y-5.405 E0.12780
G1 X10.949 Y-4.400 E0.01369
G1 X1.562 Y-4.400 E0.12780
G1 X1.562 Y-3.395 E0.01369
G1 X10.949 Y-3.395 E0.12780
G1 X10.949 Y-2.389 E0.01369
G1 X1.562 Y-2.389 E0.12780
G1 Z0.260 F180.000
G1 X11.660 Y-0.464 F180.000
G1 X12.042 Y-0.081 F180.000
G1 X12.319 Y-0.103 F180.000
G1 X12.513 Y0.050 F180.000
G1 X12.529 Y1.407 E0.01266 F180.000
G1 X12.529 Y11.407 E0.09329
G1 X12.146 Y12.256 E0.00869
G1 X11.401 Y12.540 E0.00744
G1 X-1.389 Y12.609 E0.11932
G1 X-11.395 Y12.609 E0.09335
G1 X-12.244 Y12.227 E0.00869
G1 X-12.529 Y11.476 E0.00750
G1 X-12.529 Y1.468 E0.09336
G1 X-12.438 Y-11.484 E0.12082
G1 X-12.050 Y-12.330 E0.00869
G1 X-11.304 Y-12.609 E0.00743
G1 X-1.303 Y-12.609 E0.09330
G1 X11.247 Y-12.597 E0.11708
F180.000
G1 X12.095 Y-12.214 E0.00869
G1 X12.379 Y-11.477 E0.00737
G1 X12.513 Y0.026 E0.10732
G1 X12.319 Y-0.103 F180.000
G1 X12.319 Y-0.103 F180.000
G1 X11.809 Y0.407 F180.000
G1 X11.145 Y1.656 F180.000
G1 X11.145 Y11.157 E0.12161
F180.000
G1 X1.645 Y11.157 E0.12161

G1 X1.645 Y1.656 E0.12161
G1 X11.121 Y1.656 E0.12130
G1 X11.315 Y1.487 F180.000
G1 X11.315 Y11.327 E0.08679
F180.000
G1 X1.475 Y11.327 E0.08679
G1 X1.475 Y1.487 E0.08679
G1 X11.291 Y1.487 E0.08657
G1 X11.235 Y1.625 F180.000
G1 X2.321 Y1.797 F180.000
G1 X2.321 Y11.036 E0.11826 F180.000
G1 X3.326 Y11.036 E0.01287
G1 X3.326 Y1.797 E0.11826
G1 X4.331 Y1.797 E0.01287
G1 X4.331 Y11.036 E0.11826
G1 X5.337 Y11.036 E0.01287
G1 X5.337 Y1.797 E0.11826
G1 X6.342 Y1.797 E0.01287
G1 X6.342 Y11.036 E0.11826
G1 X7.347 Y11.036 E0.01287
G1 X7.347 Y1.797 E0.11826
G1 X8.353 Y1.797 E0.01287
G1 X8.353 Y11.036 E0.11826
G1 X9.358 Y11.036 E0.01287
G1 X9.358 Y1.797 E0.11826
G1 X10.363 Y1.797 E0.01287
G1 X10.363 Y11.036 E0.11826
G1 X0.395 Y0.992 F180.000
G1 X-0.003 Y0.992 F180.000
G1 X0.000 Y1.061 F180.000
G1 X-0.395 Y1.061 F180.000
G1 X-1.645 Y1.725 F180.000
G1 X-1.645 Y11.226 E0.12161
F180.000
G1 X-11.145 Y11.226 E0.12161
G1 X-11.145 Y1.725 E0.12161
G1 X-1.669 Y1.725 E0.12130
G1 X-1.475 Y1.556 F180.000
G1 X-1.475 Y11.396 E0.08679
F180.000
G1 X-11.315 Y11.396 E0.08679
G1 X-11.315 Y1.556 E0.08679
G1 X-1.499 Y1.556 E0.08657
G1 X-1.555 Y1.694 F180.000
G1 X-10.469 Y1.866 F180.000
G1 X-10.469 Y11.105 E0.11826
F180.000
G1 X-9.464 Y11.105 E0.01287
G1 X-9.464 Y1.866 E0.11826
G1 X-8.459 Y1.866 E0.01287
G1 X-8.459 Y11.105 E0.11826
G1 X-7.453 Y11.105 E0.01287
G1 X-7.453 Y1.866 E0.11826
G1 X-6.448 Y1.866 E0.01287
G1 X-6.448 Y11.105 E0.11826
G1 X-5.443 Y11.105 E0.01287
G1 X-5.443 Y1.866 E0.11826
G1 X-4.438 Y1.866 E0.01287
G1 X-4.438 Y11.105 E0.11826
G1 X-3.432 Y11.105 E0.01287
G1 X-3.432 Y1.866 E0.11826
G1 X-2.427 Y1.866 E0.01287
G1 X-2.427 Y11.105 E0.11826
G1 X-0.981 Y0.476 F180.000
G1 X-0.369 Y0.045 F180.000
G1 X-0.035 Y-0.768 F180.000
G1 X-0.035 Y-0.792 F180.000
G1 X-0.304 Y-1.061 F180.000
G1 X-1.554 Y-11.226 F180.000
G1 X-1.554 Y-1.725 E0.12161 F180.000

G1 X-11.054 Y-1.725 E0.12161
G1 X-11.054 Y-11.226 E0.12161
G1 X-1.578 Y-11.226 E0.12130
G1 X-1.384 Y-11.396 F180.000
G1 X-1.384 Y-1.556 E0.08679 F180.000
G1 X-11.224 Y-1.556 E0.08679
G1 X-11.224 Y-11.396 E0.08679
G1 X-1.408 Y-11.396 E0.08657
G1 X-1.464 Y-11.257 F180.000
G1 X-10.379 Y-11.085 F180.000
G1 X-10.379 Y-1.846 E0.11826
F180.000
G1 X-9.373 Y-1.846 E0.01287
G1 X-9.373 Y-11.085 E0.11826
G1 X-8.368 Y-11.085 E0.01287
G1 X-8.368 Y-1.846 E0.11826
G1 X-7.363 Y-11.085 E0.01287
G1 X-7.363 Y-11.085 E0.11826
G1 X-6.357 Y-11.085 E0.01287
G1 X-6.357 Y-1.846 E0.11826
G1 X-5.352 Y-11.085 E0.11826
G1 X-5.352 Y-11.085 E0.11826
G1 X-4.347 Y-11.085 E0.01287
G1 X-4.347 Y-1.846 E0.11826
G1 X-3.341 Y-11.085 E0.11826
G1 X-3.341 Y-11.085 E0.11826
G1 X-2.336 Y-11.085 E0.01287
G1 X-2.336 Y-1.846 E0.11826
G1 X-0.304 Y-11.890 F180.000
G1 X-0.023 Y-12.171 F180.000
G1 X-0.002 Y-13.297 F180.000
G1 X0.831 Y-12.464 F180.000
G1 X10.996 Y-11.214 F180.000
G1 X10.996 Y-1.713 E0.12161
F180.000
G1 X1.495 Y-1.713 E0.12161
G1 X1.495 Y-11.214 E0.12161
G1 X10.972 Y-11.214 E0.12130
G1 X11.166 Y-11.384 F180.000
G1 X11.166 Y-1.544 E0.08679
F180.000
G1 X1.326 Y-1.544 E0.08679
G1 X1.326 Y-11.384 E0.08679
G1 X11.142 Y-11.384 E0.08657
G1 X11.086 Y-11.245 F180.000
G1 X2.171 Y-11.073 F180.000
G1 X2.171 Y-1.834 E0.11826 F180.000
G1 X3.176 Y-1.834 E0.01287
G1 X3.176 Y-11.073 E0.11826
G1 X4.182 Y-11.073 E0.01287
G1 X4.182 Y-1.834 E0.11826
G1 X5.187 Y-1.834 E0.01287
G1 X5.187 Y-11.073 E0.11826
G1 X6.192 Y-11.073 E0.01287
G1 X6.192 Y-1.834 E0.11826
G1 X7.198 Y-1.834 E0.01287
G1 X7.198 Y-11.073 E0.11826
G1 X8.203 Y-11.073 E0.01287
G1 X8.203 Y-1.834 E0.11826
G1 X9.208 Y-1.834 E0.01287
G1 X9.208 Y-11.073 E0.11826
G1 X10.214 Y-11.073 E0.01287
G1 X10.214 Y-1.834 E0.11826
G1 Z0.360 F180.000
G1 X11.660 Y-0.464 F180.000
G1 X11.660 Y-0.028 F180.000
G1 X11.809 Y-0.041 F180.000
G1 X11.809 Y0.407 F180.000
G1 X11.145 Y1.656 F180.000

G1 X11.145 Y11.157 E0.12161
F180.000
G1 X1.645 Y11.157 E0.12161
G1 X1.645 Y1.656 E0.12161
G1 X11.121 Y1.656 E0.12130
G1 X11.315 Y1.487 F180.000
G1 X11.315 Y11.327 E0.08679
F180.000
G1 X1.475 Y11.327 E0.08679
G1 X1.475 Y1.487 E0.08679
G1 X11.291 Y1.487 E0.08657
G1 X11.235 Y1.625 F180.000
G1 X11.025 Y2.438 F180.000
G1 X1.786 Y2.438 E0.11826 F180.000
G1 X1.786 Y3.444 E0.01287
G1 X11.025 Y3.444 E0.11826
G1 X11.025 Y4.449 E0.01287
G1 X1.786 Y4.449 E0.11826
G1 X1.786 Y5.454 E0.01287
G1 X11.025 Y5.454 E0.11826
G1 X11.025 Y6.460 E0.01287
G1 X1.786 Y6.460 E0.11826
G1 X1.786 Y7.465 E0.01287
G1 X11.025 Y7.465 E0.11826
G1 X11.025 Y8.470 E0.01287
G1 X1.786 Y8.470 E0.11826
G1 X1.786 Y9.476 E0.01287
G1 X11.025 Y9.476 E0.11826
G1 X11.025 Y10.481 E0.01287
G1 X1.786 Y10.481 E0.11826
G1 X0.395 Y0.992 F180.000
G1 X-0.003 Y0.992 F180.000
G1 X0.000 Y1.061 F180.000
G1 X-0.395 Y1.061 F180.000
G1 X-1.645 Y1.725 F180.000
G1 X-1.645 Y11.226 E0.12161
F180.000
G1 X-11.145 Y11.226 E0.12161
G1 X-11.145 Y1.725 E0.12161
G1 X-1.669 Y1.725 E0.12130
G1 X-1.475 Y1.556 F180.000
G1 X-1.475 Y11.396 E0.08679
F180.000
G1 X-11.315 Y11.396 E0.08679
G1 X-11.315 Y1.556 E0.08679
G1 X-1.499 Y1.556 E0.08657
G1 X-1.555 Y1.694 F180.000
G1 X-10.469 Y1.866 F180.000
G1 X-10.469 Y11.105 E0.11826
F180.000
G1 X-9.464 Y11.105 E0.01287
G1 X-9.464 Y1.866 E0.11826
G1 X-8.459 Y1.866 E0.01287
G1 X-8.459 Y11.105 E0.11826
G1 X-7.453 Y11.105 E0.01287
G1 X-7.453 Y1.866 E0.11826
G1 X-6.448 Y1.866 E0.01287
G1 X-6.448 Y11.105 E0.11826
G1 X-5.443 Y11.105 E0.01287
G1 X-5.443 Y1.866 E0.11826
G1 X-4.438 Y1.866 E0.01287
G1 X-4.438 Y11.105 E0.11826
G1 X-3.432 Y11.105 E0.01287
G1 X-3.432 Y1.866 E0.11826
G1 X-2.427 Y1.866 E0.01287
G1 X-2.427 Y11.105 E0.11826
G1 X-0.981 Y0.476 F180.000
G1 X-0.369 Y0.045 F180.000
G1 X-0.035 Y-0.768 F180.000
G1 X-0.035 Y-0.792 F180.000
G1 X-0.304 Y-1.061 F180.000
G1 X-1.554 Y-11.226 F180.000
G1 X-1.554 Y-1.725 E0.12161 F180.000

G1 X-0.304 Y-1.061 F180.000
G1 X-1.554 Y-11.226 F180.000
G1 X-1.554 Y-1.725 E0.12161 F180.000
G1 X-11.054 Y-1.725 E0.12161
G1 X-11.054 Y-11.226 E0.12161
G1 X-1.578 Y-11.226 E0.12130
G1 X-1.384 Y-11.396 F180.000
G1 X-1.384 Y-1.556 E0.08679 F180.000
G1 X-11.224 Y-1.556 E0.08679
G1 X-11.224 Y-11.396 E0.08679
G1 X-1.408 Y-11.396 E0.08657
G1 X-1.464 Y-11.257 F180.000
G1 X-1.675 Y-10.444 F180.000
G1 X-10.914 Y-10.444 E0.11826 F180.000
G1 X-10.914 Y-9.438 E0.01287
G1 X-1.675 Y-9.438 E0.11826
G1 X-1.675 Y-8.433 E0.01287
G1 X-10.914 Y-8.433 E0.11826
G1 X-10.914 Y-7.428 E0.01287
G1 X-1.675 Y-7.428 E0.11826
G1 X-1.675 Y-6.423 E0.01287
G1 X-10.914 Y-6.423 E0.11826
G1 X-10.914 Y-5.417 E0.01287
G1 X-1.675 Y-5.417 E0.11826
G1 X-1.675 Y-4.412 E0.01287
G1 X-10.914 Y-4.412 E0.11826
G1 X-10.914 Y-3.407 E0.01287
G1 X-1.675 Y-3.407 E0.11826
G1 X-1.675 Y-2.401 E0.01287
G1 X-10.914 Y-2.401 E0.11826
G1 X-0.304 Y-11.890 F180.000
G1 X-0.023 Y-12.171 F180.000
G1 X-0.002 Y-13.297 F180.000
G1 X0.831 Y-12.464 F180.000
G1 X10.996 Y-11.214 F180.000
G1 X10.996 Y-1.713 E0.12161 F180.000
G1 X1.495 Y-1.713 E0.12161
G1 X1.495 Y-11.214 E0.12161
G1 X10.972 Y-11.214 E0.12130
G1 X11.166 Y-11.384 F180.000
G1 X11.166 Y-1.544 E0.08679 F180.000
G1 X1.326 Y-1.544 E0.08679
G1 X1.326 Y-11.384 E0.08679
G1 X11.142 Y-11.384 E0.08657
G1 X11.086 Y-11.245 F180.000
G1 X10.875 Y-10.432 F180.000
G1 X1.636 Y-10.432 E0.11826 F180.000
G1 X1.636 Y-9.426 E0.01287
G1 X10.875 Y-9.426 E0.11826
G1 X10.875 Y-8.421 E0.01287
G1 X1.636 Y-8.421 E0.11826
G1 X1.636 Y-7.416 E0.01287
G1 X10.875 Y-7.416 E0.11826
G1 X10.875 Y-6.410 E0.01287
G1 X1.636 Y-6.410 E0.11826
G1 X1.636 Y-5.405 E0.01287
G1 X10.875 Y-5.405 E0.11826
G1 X10.875 Y-4.400 E0.01287
G1 X1.636 Y-4.400 E0.11826
G1 X1.636 Y-3.395 E0.01287
G1 X10.875 Y-3.395 E0.11826
G1 X10.875 Y-2.389 E0.01287
G1 X1.636 Y-2.389 E0.11826
G1 Z0.460 F180.000
G1 X11.660 Y-0.464 F180.000
G1 X11.660 Y-0.028 F180.000

G1 X11.809 Y-0.041 F180.000
G1 X11.809 Y0.407 F180.000
G1 X11.145 Y1.656 F180.000
G1 X11.145 Y11.157 E0.12161 F180.000
G1 X1.645 Y11.157 E0.12161
G1 X1.645 Y1.656 E0.12161
G1 X11.121 Y1.656 E0.12130
G1 X11.315 Y1.487 F180.000
G1 X11.315 Y11.327 E0.08679 F180.000
G1 X1.475 Y11.327 E0.08679
G1 X1.475 Y1.487 E0.08679
G1 X11.291 Y1.487 E0.08657
G1 X11.235 Y1.625 F180.000
G1 X2.321 Y1.797 F180.000
G1 X2.321 Y11.036 E0.11826 F180.000
G1 X3.326 Y11.036 E0.01287
G1 X3.326 Y1.797 E0.11826
G1 X4.331 Y1.797 E0.01287
G1 X4.331 Y11.036 E0.11826
G1 X5.337 Y11.036 E0.01287
G1 X5.337 Y1.797 E0.11826
G1 X6.342 Y1.797 E0.01287
G1 X6.342 Y11.036 E0.11826
G1 X7.347 Y11.036 E0.01287
G1 X7.347 Y1.797 E0.11826
G1 X8.353 Y1.797 E0.01287
G1 X8.353 Y11.036 E0.11826
G1 X9.358 Y11.036 E0.01287
G1 X9.358 Y1.797 E0.11826
G1 X10.363 Y1.797 E0.01287
G1 X10.363 Y11.036 E0.11826
G1 X0.395 Y0.992 F180.000
G1 X-0.003 Y0.992 F180.000
G1 X0.000 Y1.061 F180.000
G1 X-0.395 Y1.061 F180.000
G1 X-1.645 Y1.725 F180.000
G1 X-1.645 Y11.226 E0.12161 F180.000
G1 X-11.145 Y11.226 E0.12161
G1 X-11.145 Y1.725 E0.12161
G1 X-1.669 Y1.725 E0.12130
G1 X-1.475 Y1.556 F180.000
G1 X-1.475 Y11.396 E0.08679 F180.000
G1 X-11.315 Y11.396 E0.08679
G1 X-11.315 Y1.556 E0.08679
G1 X-1.499 Y1.556 E0.08657
G1 X-1.555 Y1.694 F180.000
G1 X-10.469 Y1.866 F180.000
G1 X-10.469 Y11.105 E0.11826 F180.000
G1 X-9.464 Y11.105 E0.01287
G1 X-9.464 Y1.866 E0.11826
G1 X-8.459 Y1.866 E0.01287
G1 X-8.459 Y11.105 E0.11826
G1 X-7.453 Y11.105 E0.01287
G1 X-7.453 Y1.866 E0.11826
G1 X-6.448 Y1.866 E0.01287
G1 X-6.448 Y11.105 E0.11826
G1 X-5.443 Y11.105 E0.01287
G1 X-5.443 Y1.866 E0.11826
G1 X-4.438 Y1.866 E0.01287
G1 X-4.438 Y11.105 E0.11826
G1 X-3.432 Y11.105 E0.01287
G1 X-3.432 Y1.866 E0.11826
G1 X-2.427 Y1.866 E0.01287
G1 X-2.427 Y11.105 E0.11826
G1 X-0.981 Y0.476 F180.000

G1 X-0.369 Y0.045 F180.000
G1 X-0.035 Y-0.768 F180.000
G1 X-0.035 Y-0.792 F180.000
G1 X-0.304 Y-1.061 F180.000
G1 X-1.554 Y-11.226 F180.000
G1 X-1.554 Y-1.725 E0.12161 F180.000
G1 X-11.054 Y-1.725 E0.12161
G1 X-11.054 Y-11.226 E0.12161
G1 X-1.578 Y-11.226 E0.12130
G1 X-1.384 Y-11.396 F180.000
G1 X-1.384 Y-1.556 E0.08679 F180.000
G1 X-11.224 Y-1.556 E0.08679
G1 X-11.224 Y-11.396 E0.08679
G1 X-1.408 Y-11.396 E0.08657
G1 X-1.464 Y-11.257 F180.000
G1 X-10.379 Y-11.085 F180.000
G1 X-10.379 Y-1.846 E0.11826 F180.000
G1 X-9.373 Y-1.846 E0.01287
G1 X-9.373 Y-11.085 E0.11826
G1 X-8.368 Y-11.085 E0.01287
G1 X-8.368 Y-1.846 E0.11826
G1 X-7.363 Y-1.846 E0.01287
G1 X-7.363 Y-11.085 E0.11826
G1 X-6.357 Y-11.085 E0.01287
G1 X-6.357 Y-1.846 E0.11826
G1 X-5.352 Y-1.846 E0.01287
G1 X-5.352 Y-11.085 E0.11826
G1 X-4.347 Y-11.085 E0.01287
G1 X-4.347 Y-1.846 E0.11826
G1 X-3.341 Y-1.846 E0.01287
G1 X-3.341 Y-11.085 E0.11826
G1 X-2.336 Y-11.085 E0.01287
G1 X-2.336 Y-1.846 E0.11826
G1 X-0.304 Y-11.890 F180.000
G1 X-0.023 Y-12.171 F180.000
G1 X-0.002 Y-13.297 F180.000
G1 X0.831 Y-12.464 F180.000
G1 X10.996 Y-11.214 F180.000
G1 X10.996 Y-1.713 E0.12161 F180.000
G1 X1.495 Y-1.713 E0.12161
G1 X1.495 Y-11.214 E0.12161
G1 X10.972 Y-11.214 E0.12130
G1 X11.166 Y-11.384 F180.000
G1 X11.166 Y-1.544 E0.08679 F180.000
G1 X1.326 Y-1.544 E0.08679
G1 X1.326 Y-11.384 E0.08679
G1 X11.142 Y-11.384 E0.08657
G1 X11.086 Y-11.245 F180.000
G1 X10.875 Y-10.432 F180.000
G1 X1.636 Y-10.432 E0.11826 F180.000
G1 X1.636 Y-9.426 E0.01287
G1 X10.875 Y-9.426 E0.11826
G1 X10.875 Y-8.421 E0.01287
G1 X1.636 Y-8.421 E0.11826
G1 X1.636 Y-7.416 E0.01287
G1 X10.875 Y-7.416 E0.11826
G1 X10.875 Y-6.410 E0.01287
G1 X1.636 Y-6.410 E0.11826
G1 X1.636 Y-5.405 E0.01287
G1 X10.875 Y-5.405 E0.11826
G1 X10.875 Y-4.400 E0.01287
G1 X1.636 Y-4.400 E0.11826
G1 X1.636 Y-3.395 E0.01287
G1 X10.875 Y-3.395 E0.11826
G1 X10.875 Y-2.389 E0.01287
G1 X1.636 Y-2.389 E0.11826
G1 Z0.460 F180.000
G1 X11.660 Y-0.464 F180.000
G1 X11.660 Y-0.028 F180.000

```

G1 Z150 F200 S1
G1 X20 Y40 F12000
; filament used = 35.4mm (0.0cm3)

; avoid_crossing_perimeters = 1
; bed_shape = -60x-65,60x-65,60x65,-60x65
; bed_temperature = 0
; before_layer_gcode =
; bridge_acceleration = 0
; bridge_fan_speed = 100
; brim_width = 0
; complete_objects = 0
; cooling = 0
; default_acceleration = 0
; disable_fan_first_layers = 1
; duplicate_distance = 6
; end_gcode = G1 E-20 F3000\nG1 Z150 F200 S1 \nG1 X20 Y40 F12000
; extruder_clearance_height = 20
; extruder_clearance_radius = 20
; extruder_offset = 0x0
; extrusion_axis = E
; extrusion_multiplier = 0.5
; fan_always_on = 0
; fan_below_layer_time = 60
; filament_colour = #FFFFFFF
; filament_diameter = 1
; first_layer_acceleration = 0
; first_layer_bed_temperature = 0
; first_layer_extrusion_width = 0
; first_layer_speed = 50%
; first_layer_temperature = 0
; gcode_arcs = 0
; gcode_comments = 0
; gcode_flavor = reprap
; infill_acceleration = 0
; infill_first = 0
; layer_gcode =
; max_fan_speed = 100
; max_print_speed = 80
; max_volumetric_speed = 0
; min_fan_speed = 35
; min_print_speed = 10
; min_skirt_length = 0
; notes =
; nozzle_diameter = 0.16

```

```

;
only_retract_when_crossing_perimeters = 1
; ooze_prevention = 0
; output_filename_format = [input_filename_base].gcode
; perimeter_acceleration = 0
; post_process =
; pressure_advance = 0
; resolution = 0
; retract_before_travel = 2
; retract_layer_change = 1
; retract_length = 0
; retract_length_toolchange = 0
; retract_lift = 0
; retract_restart_extra = 0
; retract_restart_extra_toolchange = 0
; retract_speed = 30
; skirt_distance = 1
; skirt_height = 2
; skirts = 1
; slowdown_below_layer_time = 30
; spiral_vase = 0
; standby_temperature_delta = -5
; start_gcode =
; temperature = 0
; threads = 4
; toolchange_gcode =
; travel_speed = 3
; use_firmware_retraction = 0
; use_relative_e_distances = 1
; use_volumetric_e = 0
; vibration_limit = 0
; wipe = 0
; z_offset = 0
; dont_support_bridges = 1
; extrusion_width = 0
; first_layer_height = 0.16
; infill_only_where_needed = 0
; interface_shells = 0
; layer_height = 0.1
; raft_layers = 0
; seam_position = aligned
; support_material = 0
; support_material_angle = 0
; support_material_contact_distance = 0.2

```

```

; support_material_enforce_layers = 0
; support_material_extruder = 1
; support_material_extrusion_width = 0
; support_material_interface_extruder = 1
; support_material_interface_layers = 3
; support_material_interface_spacing = 0
; support_material_interface_speed = 100%
; support_material_pattern = honeycomb
; support_material_spacing = 2.5
; support_material_speed = 3
; support_material_threshold = 60
; xy_size_compensation = 0
; bottom_solid_layers = 0
; bridge_flow_ratio = 1
; bridge_speed = 3
; external_fill_pattern = rectilinear
; external_perimeter_extrusion_width = 0
; external_perimeter_speed = 50%
; external_perimeters_first = 0
; extra_perimeters = 1
; fill_angle = 0
; fill_density = 20%
; fill_pattern = rectilinear
; gap_fill_speed = 3
; infill_every_layers = 1
; infill_extruder = 1
; infill_extrusion_width = 0
; infill_overlap = 0%
; infill_speed = 3
; overhangs = 0
; perimeter_extruder = 1
; perimeter_extrusion_width = 0
; perimeter_speed = 3
; perimeters = 2
; small_perimeter_speed = 3
; solid_infill_below_area = 70
; solid_infill_every_layers = 0
; solid_infill_extruder = 1
; solid_infill_extrusion_width = 0
; solid_infill_speed = 3
; thin_walls = 1
; top_infill_extrusion_width = 0
; top_solid_infill_speed = 50
; top_solid_layers = 0

```

Collagen Hexagonal Scaffolds

```

; external_perimeters_extrusion_width = 0.16mm
; perimeters_extrusion_width = 0.22mm
; infill_extrusion_width = 0.22mm
; solid_infill_extrusion_width = 0.22mm
; top_infill_extrusion_width = 0.22mm

```

```

G21 ; set units to millimeters
G90 ; use absolute coordinates
M83 ; use relative distances for extrusion
G1 Z0.160 F180.000
G1 X12.511 Y-0.145 F180.000
G1 X12.529 Y1.407 E0.02113 F90.000
G1 X12.529 Y11.407 E0.13615
G1 X12.146 Y12.256 E0.01268
G1 X11.401 Y12.540 E0.01086
G1 X-1.389 Y12.609 E0.17414
G1 X-11.395 Y12.609 E0.13623

```

```

G1 X-12.244 Y12.227 E0.01268
G1 X-12.529 Y11.476 E0.01094
G1 X-12.529 Y1.468 E0.13626
G1 X-12.438 Y-11.484 E0.17633
G1 X-12.050 Y-12.330 E0.01268
G1 X-11.304 Y-12.609 E0.01084
G1 X-1.303 Y-12.609 E0.13616
G1 X11.247 Y-12.597 E0.17086 F90.000
G1 X12.095 Y-12.214 E0.01268
G1 X12.379 Y-11.477 E0.01076
G1 X12.510 Y-0.169 E0.15396
G1 X11.185 Y1.616 F180.000
G1 X11.185 Y11.197 E0.13044 F90.000
G1 X1.605 Y11.197 E0.13044
G1 X1.605 Y1.616 E0.13044
G1 X11.161 Y1.616 E0.13011
G1 X11.315 Y11.487 F180.000
G1 X11.315 Y11.327 E0.12595 F90.000
G1 X1.475 Y11.327 E0.12595

```

```

G1 X1.475 Y1.487 E0.12595
G1 X11.291 Y1.487 E0.12564
G1 X11.235 Y1.625 F180.000
G1 X10.468 Y2.467 F180.000
G1 X11.018 Y2.467 E0.00749 F90.000
G1 X11.018 Y2.668 E0.00274
G1 X10.468 Y2.668 E0.00749
G1 X10.004 Y3.472 E0.01264
G1 X8.727 Y3.472 E0.01739
G1 X8.263 Y2.668 E0.01264
G1 X6.986 Y2.668 E0.01739
G1 X6.521 Y3.472 E0.01264
G1 X5.244 Y3.472 E0.01739
G1 X4.780 Y2.668 E0.01264
G1 X3.503 Y2.668 E0.01739
G1 X3.039 Y3.472 E0.01264
G1 X1.772 Y3.472 E0.01725
G1 X1.772 Y1.784 E0.02299
G1 X3.109 Y1.784 E0.01820
G1 X3.503 Y2.467 E0.01074

```

G1 X4.780 Y2.467 E0.01739
G1 X5.175 Y1.784 E0.01074
G1 X6.591 Y1.784 E0.01929
G1 X6.986 Y2.467 E0.01074
G1 X8.263 Y2.467 E0.01739
G1 X8.657 Y1.784 E0.01074
G1 X10.074 Y1.784 E0.01929
G1 X10.468 Y2.467 E0.01074
G1 X3.503 Y4.477 F180.000
G1 X4.780 Y4.477 E0.01739 F90.000
G1 X5.244 Y3.673 E0.01264
G1 X6.521 Y3.673 E0.01739
G1 X6.986 Y4.477 E0.01264
G1 X8.263 Y4.477 E0.01739
G1 X8.727 Y3.673 E0.01264
G1 X10.004 Y3.673 E0.01739
G1 X10.468 Y4.477 E0.01264
G1 X11.018 Y4.477 E0.00749
G1 X11.018 Y4.679 E0.00274
G1 X10.468 Y4.679 E0.00749
G1 X10.004 Y5.483 E0.01264
G1 X8.727 Y5.483 E0.01739
G1 X8.263 Y4.679 E0.01264
G1 X6.986 Y4.679 E0.01739
G1 X6.521 Y5.483 E0.01264
G1 X5.244 Y5.483 E0.01739
G1 X4.780 Y4.679 E0.01264
G1 X3.503 Y4.679 E0.01739
G1 X3.039 Y5.483 E0.01264
G1 X1.772 Y5.483 E0.01725
G1 X1.772 Y3.673 E0.02464
G1 X3.039 Y3.673 E0.01725
G1 X3.503 Y4.477 E0.01264
G1 X3.503 Y6.488 F180.000
G1 X4.780 Y6.488 E0.01739 F90.000
G1 X5.244 Y5.684 E0.01264
G1 X6.521 Y5.684 E0.01739
G1 X6.986 Y6.488 E0.01264
G1 X8.263 Y6.488 E0.01739
G1 X8.727 Y5.684 E0.01264
G1 X10.004 Y5.684 E0.01739
G1 X10.468 Y6.488 E0.01264
G1 X11.018 Y6.488 E0.00749
G1 X11.018 Y6.689 E0.00274
G1 X10.468 Y6.689 E0.00749
G1 X10.004 Y7.493 E0.01264
G1 X8.727 Y7.493 E0.01739
G1 X8.263 Y6.689 E0.01264
G1 X6.986 Y6.689 E0.01739
G1 X6.521 Y7.493 E0.01264
G1 X5.244 Y7.493 E0.01739
G1 X4.780 Y6.689 E0.01264
G1 X3.503 Y6.689 E0.01739
G1 X3.039 Y7.493 E0.01264
G1 X1.772 Y7.493 E0.01725
G1 X1.772 Y5.684 E0.02464
G1 X3.039 Y5.684 E0.01725
G1 X3.503 Y6.488 E0.01264
G1 X3.503 Y8.499 F180.000
G1 X4.780 Y8.499 E0.01739 F90.000
G1 X5.244 Y7.694 E0.01264
G1 X6.521 Y7.694 E0.01739
G1 X6.986 Y8.499 E0.01264
G1 X8.263 Y8.499 E0.01739
G1 X8.727 Y7.694 E0.01264
G1 X10.004 Y7.694 E0.01739
G1 X10.468 Y8.499 E0.01264
G1 X11.018 Y8.499 E0.00749
G1 X11.018 Y8.700 E0.00274
G1 X10.468 Y8.700 E0.00749

G1 X10.004 Y9.504 E0.01264
G1 X8.727 Y9.504 E0.01739
G1 X8.263 Y8.700 E0.01264
G1 X6.986 Y8.700 E0.01739
G1 X6.521 Y9.504 E0.01264
G1 X5.244 Y9.504 E0.01739
G1 X4.780 Y8.700 E0.01264
G1 X3.503 Y8.700 E0.01739
G1 X3.039 Y9.504 E0.01264
G1 X1.772 Y9.504 E0.01725
G1 X1.772 Y7.694 E0.02464
G1 X3.039 Y7.694 E0.01725
G1 X3.503 Y8.499 E0.01264
G1 X3.503 Y10.509 F180.000
G1 X4.780 Y10.509 E0.01739 F90.000
G1 X5.244 Y9.705 E0.01264
G1 X6.521 Y9.705 E0.01739
G1 X6.986 Y10.509 E0.01264
G1 X8.263 Y10.509 E0.01739
G1 X8.727 Y9.705 E0.01264
G1 X10.004 Y9.705 E0.01739
G1 X10.468 Y10.509 E0.01264
G1 X11.018 Y10.509 E0.00749
G1 X11.018 Y10.710 E0.00274
G1 X10.468 Y10.710 E0.00749
G1 X10.284 Y11.030 E0.00502
G1 X8.447 Y11.030 E0.02501
G1 X8.263 Y10.710 E0.00502
G1 X6.986 Y10.710 E0.01739
G1 X6.801 Y11.030 E0.00502
G1 X4.964 Y11.030 E0.02501
G1 X4.780 Y10.710 E0.00502
G1 X3.503 Y10.710 E0.01739
G1 X3.319 Y11.030 E0.00502
G1 X1.772 Y11.030 E0.02106
G1 X1.772 Y9.705 E0.01803
G1 X3.039 Y9.705 E0.01725
G1 X3.503 Y10.509 E0.01264
G1 X0.395 Y0.992 F180.000
G1 X-0.003 Y0.992 F180.000
G1 X0.000 Y1.061 F180.000
G1 X-0.395 Y1.061 F180.000
G1 X-1.605 Y1.685 F180.000
G1 X-1.605 Y11.266 E0.13044 F90.000
G1 X-11.185 Y11.266 E0.13044
G1 X-11.185 Y1.685 E0.13044
G1 X-1.629 Y1.685 E0.13011
G1 X-1.475 Y1.556 F180.000
G1 X-1.475 Y11.396 E0.12595 F90.000
G1 X-11.315 Y11.396 E0.12595
G1 X-11.315 Y1.556 E0.12595
G1 X-1.499 Y1.556 E0.12564
G1 X-1.555 Y1.694 F180.000
G1 X-2.322 Y2.536 F180.000
G1 X-1.772 Y2.536 E0.00749 F90.000
G1 X-1.772 Y2.737 E0.00274
G1 X-2.322 Y2.737 E0.00749
G1 X-2.786 Y3.541 E0.01264
G1 X-4.063 Y3.541 E0.01739
G1 X-4.528 Y2.737 E0.01264
G1 X-5.804 Y2.737 E0.01739
G1 X-6.269 Y3.541 E0.01264
G1 X-7.546 Y3.541 E0.01739
G1 X-8.010 Y2.737 E0.01264
G1 X-9.287 Y2.737 E0.01739
G1 X-9.751 Y3.541 E0.01264
G1 X-11.018 Y3.541 E0.01725
G1 X-11.018 Y1.853 E0.02299
G1 X-9.681 Y1.853 E0.01820
G1 X-9.287 Y2.536 E0.01074

G1 X-8.010 Y2.536 E0.01739
G1 X-7.616 Y1.853 E0.01074
G1 X-6.199 Y1.853 E0.01929
G1 X-5.804 Y2.536 E0.01074
G1 X-4.528 Y2.536 E0.01739
G1 X-4.133 Y1.853 E0.01074
G1 X-2.716 Y1.853 E0.01929
G1 X-2.322 Y2.536 E0.01074
G1 X-9.287 Y4.547 F180.000
G1 X-8.010 Y4.547 E0.01739 F90.000
G1 X-7.546 Y3.742 E0.01264
G1 X-6.269 Y3.742 E0.01739
G1 X-5.804 Y4.547 E0.01264
G1 X-4.528 Y4.547 E0.01739
G1 X-4.063 Y3.742 E0.01264
G1 X-2.786 Y3.742 E0.01739
G1 X-2.322 Y4.547 E0.01264
G1 X-1.772 Y4.547 E0.00749
G1 X-1.772 Y4.748 E0.00274
G1 X-2.322 Y4.748 E0.00749
G1 X-2.786 Y5.552 E0.01264
G1 X-4.063 Y5.552 E0.01739
G1 X-4.528 Y4.748 E0.01264
G1 X-5.804 Y4.748 E0.01739
G1 X-6.269 Y5.552 E0.01264
G1 X-7.546 Y5.552 E0.01739
G1 X-8.010 Y4.748 E0.01264
G1 X-9.287 Y4.748 E0.01739
G1 X-9.751 Y5.552 E0.01264
G1 X-11.018 Y5.552 E0.01725
G1 X-11.018 Y3.742 E0.02464
G1 X-9.751 Y3.742 E0.01725
G1 X-9.287 Y4.547 E0.01264
G1 X-9.287 Y6.557 F180.000
G1 X-8.010 Y6.557 E0.01739 F90.000
G1 X-7.546 Y5.753 E0.01264
G1 X-6.269 Y5.753 E0.01739
G1 X-5.804 Y6.557 E0.01264
G1 X-4.528 Y6.557 E0.01739
G1 X-4.063 Y5.753 E0.01264
G1 X-2.786 Y5.753 E0.01739
G1 X-2.322 Y6.557 E0.01264
G1 X-1.772 Y6.557 E0.00749
G1 X-1.772 Y6.758 E0.00274
G1 X-2.322 Y6.758 E0.00749
G1 X-2.786 Y7.562 E0.01264
G1 X-4.063 Y7.562 E0.01739
G1 X-4.528 Y6.758 E0.01264
G1 X-5.804 Y6.758 E0.01739
G1 X-6.269 Y7.562 E0.01264
G1 X-7.546 Y7.562 E0.01739
G1 X-8.010 Y6.758 E0.01264
G1 X-9.287 Y6.758 E0.01739
G1 X-9.751 Y7.562 E0.01264
G1 X-11.018 Y7.562 E0.01725
G1 X-11.018 Y5.753 E0.02464
G1 X-9.751 Y5.753 E0.01725
G1 X-9.287 Y6.557 E0.01264
G1 X-9.287 Y8.568 F180.000
G1 X-8.010 Y8.568 E0.01739 F90.000
G1 X-7.546 Y7.764 E0.01264
G1 X-6.269 Y7.764 E0.01739
G1 X-5.804 Y8.568 E0.01264
G1 X-4.528 Y8.568 E0.01739
G1 X-4.063 Y7.764 E0.01264
G1 X-2.786 Y7.764 E0.01739
G1 X-2.322 Y8.568 E0.01264
G1 X-1.772 Y8.568 E0.00749
G1 X-1.772 Y8.769 E0.00274
G1 X-2.322 Y8.769 E0.00749

G1 X-2.786 Y9.573 E0.01264
G1 X-4.063 Y9.573 E0.01739
G1 X-4.528 Y8.769 E0.01264
G1 X-5.804 Y8.769 E0.01739
G1 X-6.269 Y9.573 E0.01264
G1 X-7.546 Y9.573 E0.01739
G1 X-8.010 Y8.769 E0.01264
G1 X-9.287 Y8.769 E0.01739
G1 X-9.751 Y9.573 E0.01264
G1 X-11.018 Y9.573 E0.01725
G1 X-11.018 Y7.764 E0.02464
G1 X-9.751 Y7.764 E0.01725
G1 X-9.287 Y8.568 E0.01264
G1 X-9.287 Y10.578 F180.000
G1 X-8.010 Y10.578 E0.01739 F90.000
G1 X-7.546 Y9.774 E0.01264
G1 X-6.269 Y9.774 E0.01739
G1 X-5.804 Y10.578 E0.01264
G1 X-4.528 Y10.578 E0.01739
G1 X-4.063 Y9.774 E0.01264
G1 X-2.786 Y9.774 E0.01739
G1 X-2.322 Y10.578 E0.01264
G1 X-1.772 Y10.578 E0.00749
G1 X-1.772 Y10.779 E0.00274
G1 X-2.322 Y10.779 E0.00749
G1 X-2.506 Y11.099 E0.00502
G1 X-4.343 Y11.099 E0.02501
G1 X-4.528 Y10.779 E0.00502
G1 X-5.804 Y10.779 E0.01739
G1 X-5.989 Y11.099 E0.00502
G1 X-7.826 Y11.099 E0.02501
G1 X-8.010 Y10.779 E0.00502
G1 X-9.287 Y10.779 E0.01739
G1 X-9.471 Y11.099 E0.00502
G1 X-11.018 Y11.099 E0.02106
G1 X-11.018 Y9.774 E0.01803
G1 X-9.751 Y9.774 E0.01725
G1 X-9.287 Y10.578 E0.01264
G1 X-0.981 Y0.476 F180.000
G1 X-0.369 Y0.045 F180.000
G1 X-0.035 Y-0.768 F180.000
G1 X-0.035 Y-0.792 F180.000
G1 X-0.304 Y-1.061 F180.000
G1 X-1.514 Y-11.266 F180.000
G1 X-1.514 Y-1.685 E0.13044 F90.000
G1 X-11.095 Y-1.685 E0.13044
G1 X-11.095 Y-11.266 E0.13044
G1 X-1.538 Y-11.266 E0.13011
G1 X-1.384 Y-11.396 F180.000
G1 X-1.384 Y-1.556 E0.12595 F90.000
G1 X-11.224 Y-1.556 E0.12595
G1 X-11.224 Y-11.396 E0.12595
G1 X-1.408 Y-11.396 E0.12564
G1 X-1.464 Y-11.257 F180.000
G1 X-2.231 Y-10.415 F180.000
G1 X-1.681 Y-10.415 E0.00749 F90.000
G1 X-1.681 Y-10.214 E0.00274
G1 X-2.231 Y-10.214 E0.00749
G1 X-2.695 Y-9.410 E0.01264
G1 X-3.972 Y-9.410 E0.01739
G1 X-4.437 Y-10.214 E0.01264
G1 X-5.714 Y-10.214 E0.01739
G1 X-6.178 Y-9.410 E0.01264
G1 X-7.455 Y-9.410 E0.01739
G1 X-7.919 Y-10.214 E0.01264
G1 X-9.196 Y-10.214 E0.01739
G1 X-9.660 Y-9.410 E0.01264
G1 X-10.927 Y-9.410 E0.01725
G1 X-10.927 Y-11.099 E0.02299
G1 X-9.591 Y-11.099 E0.01820

G1 X-9.196 Y-10.415 E0.01074
G1 X-7.919 Y-10.415 E0.01739
G1 X-7.525 Y-11.099 E0.01074
G1 X-6.108 Y-11.099 E0.01929
G1 X-5.714 Y-10.415 E0.01074
G1 X-4.437 Y-10.415 E0.01739
G1 X-4.042 Y-11.099 E0.01074
G1 X-2.626 Y-11.099 E0.01929
G1 X-2.231 Y-10.415 E0.01074
G1 X-9.196 Y-8.405 F180.000
G1 X-7.919 Y-8.405 E0.01739 F90.000
G1 X-7.455 Y-9.209 E0.01264
G1 X-6.178 Y-9.209 E0.01739
G1 X-5.714 Y-8.405 E0.01264
G1 X-4.437 Y-8.405 E0.01739
G1 X-3.972 Y-9.209 E0.01264
G1 X-2.695 Y-9.209 E0.01739
G1 X-2.231 Y-8.405 E0.01264
G1 X-1.681 Y-8.405 E0.00749
G1 X-1.681 Y-8.204 E0.00274
G1 X-2.231 Y-8.204 E0.00749
G1 X-2.695 Y-7.399 E0.01264
G1 X-3.972 Y-7.399 E0.01739
G1 X-4.437 Y-8.204 E0.01264
G1 X-5.714 Y-8.204 E0.01739
G1 X-6.178 Y-7.399 E0.01264
G1 X-7.455 Y-7.399 E0.01739
G1 X-7.919 Y-8.204 E0.01264
G1 X-9.196 Y-8.204 E0.01739
G1 X-9.660 Y-7.399 E0.01264
G1 X-10.927 Y-7.399 E0.01725
G1 X-10.927 Y-9.209 E0.02464
G1 X-9.660 Y-9.209 E0.01725
G1 X-9.196 Y-8.405 E0.01264
G1 X-9.196 Y-6.394 F180.000
G1 X-7.919 Y-6.394 E0.01739 F90.000
G1 X-7.455 Y-7.198 E0.01264
G1 X-6.178 Y-7.198 E0.01739
G1 X-5.714 Y-6.394 E0.01264
G1 X-4.437 Y-6.394 E0.01739
G1 X-3.972 Y-7.198 E0.01264
G1 X-2.695 Y-7.198 E0.01739
G1 X-2.231 Y-6.394 E0.01264
G1 X-1.681 Y-6.394 E0.00749
G1 X-1.681 Y-6.193 E0.00274
G1 X-2.231 Y-6.193 E0.00749
G1 X-2.695 Y-5.389 E0.01264
G1 X-3.972 Y-5.389 E0.01739
G1 X-4.437 Y-6.193 E0.01264
G1 X-5.714 Y-6.193 E0.01739
G1 X-6.178 Y-5.389 E0.01264
G1 X-7.455 Y-5.389 E0.01739
G1 X-7.919 Y-6.193 E0.01264
G1 X-9.196 Y-6.193 E0.01739
G1 X-9.660 Y-5.389 E0.01264
G1 X-10.927 Y-5.389 E0.01725
G1 X-10.927 Y-7.198 E0.02464
G1 X-9.660 Y-7.198 E0.01725
G1 X-9.196 Y-6.394 E0.01264
G1 X-9.196 Y-4.383 F180.000
G1 X-7.919 Y-4.383 E0.01739 F90.000
G1 X-7.455 Y-5.188 E0.01264
G1 X-6.178 Y-5.188 E0.01739
G1 X-5.714 Y-4.383 E0.01264
G1 X-4.437 Y-4.383 E0.01739
G1 X-3.972 Y-5.188 E0.01264
G1 X-2.695 Y-5.188 E0.01739
G1 X-2.231 Y-4.383 E0.01264
G1 X-1.681 Y-4.383 E0.00749
G1 X-1.681 Y-4.182 E0.00274

G1 X-2.231 Y-4.182 E0.00749
G1 X-2.695 Y-3.378 E0.01264
G1 X-3.972 Y-3.378 E0.01739
G1 X-4.437 Y-4.182 E0.01264
G1 X-5.714 Y-4.182 E0.01739
G1 X-6.178 Y-3.378 E0.01264
G1 X-7.455 Y-3.378 E0.01739
G1 X-7.919 Y-4.182 E0.01264
G1 X-9.196 Y-4.182 E0.01739
G1 X-9.660 Y-3.378 E0.01264
G1 X-10.927 Y-3.378 E0.01725
G1 X-10.927 Y-5.188 E0.02464
G1 X-9.660 Y-5.188 E0.01725
G1 X-9.196 Y-4.383 E0.01264
G1 X-9.196 Y-2.373 F180.000
G1 X-7.919 Y-2.373 E0.01739 F90.000
G1 X-7.455 Y-3.177 E0.01264
G1 X-6.178 Y-3.177 E0.01739
G1 X-5.714 Y-2.373 E0.01264
G1 X-4.437 Y-2.373 E0.01739
G1 X-3.972 Y-3.177 E0.01264
G1 X-2.695 Y-3.177 E0.01739
G1 X-2.231 Y-2.373 E0.01264
G1 X-1.681 Y-2.373 E0.00749
G1 X-1.681 Y-2.172 E0.00274
G1 X-2.231 Y-2.172 E0.00749
G1 X-2.415 Y-1.853 E0.00502
G1 X-4.252 Y-1.853 E0.02501
G1 X-4.437 Y-2.172 E0.00502
G1 X-5.714 Y-2.172 E0.01739
G1 X-5.898 Y-1.853 E0.00502
G1 X-7.735 Y-1.853 E0.02501
G1 X-7.919 Y-2.172 E0.00502
G1 X-9.196 Y-2.172 E0.01739
G1 X-9.380 Y-1.853 E0.00502
G1 X-10.927 Y-1.853 E0.02106
G1 X-10.927 Y-3.177 E0.01803
G1 X-9.660 Y-3.177 E0.01725
G1 X-9.196 Y-2.373 E0.01264
G1 X-0.304 Y-11.890 F180.000
G1 X-0.023 Y-12.171 F180.000
G1 X-0.002 Y-13.297 F180.000
G1 X0.831 Y-12.464 F180.000
G1 X11.036 Y-11.254 F180.000
G1 X11.036 Y-1.673 E0.13044 F90.000
G1 X1.455 Y-1.673 E0.13044
G1 X1.455 Y-11.254 E0.13044
G1 X11.012 Y-11.254 E0.13011
G1 X11.166 Y-11.384 F180.000
G1 X11.166 Y-1.544 E0.12595 F90.000
G1 X1.326 Y-1.544 E0.12595
G1 X1.326 Y-11.384 E0.12595
G1 X11.142 Y-11.384 E0.12564
G1 X11.086 Y-11.245 F180.000
G1 X10.319 Y-10.403 F180.000
G1 X10.869 Y-10.403 E0.00749 F90.000
G1 X10.869 Y-10.202 E0.00274
G1 X10.319 Y-10.202 E0.00749
G1 X9.854 Y-9.398 E0.01264
G1 X8.577 Y-9.398 E0.01739
G1 X8.113 Y-10.202 E0.01264
G1 X6.836 Y-10.202 E0.01739
G1 X6.372 Y-9.398 E0.01264
G1 X5.095 Y-9.398 E0.01739
G1 X4.631 Y-10.202 E0.01264
G1 X3.354 Y-10.202 E0.01739
G1 X2.889 Y-9.398 E0.01264
G1 X1.623 Y-9.398 E0.01725
G1 X1.623 Y-11.087 E0.02299

G1 X2.959 Y-11.087 E0.01820
G1 X3.354 Y-10.403 E0.01074
G1 X4.631 Y-10.403 E0.01739
G1 X5.025 Y-11.087 E0.01074
G1 X6.442 Y-11.087 E0.01929
G1 X6.836 Y-10.403 E0.01074
G1 X8.113 Y-10.403 E0.01739
G1 X8.508 Y-11.087 E0.01074
G1 X9.924 Y-11.087 E0.01929
G1 X10.319 Y-10.403 E0.01074
G1 X3.354 Y-8.393 F180.000
G1 X4.631 Y-8.393 E0.01739 F90.000
G1 X5.095 Y-9.197 E0.01264
G1 X6.372 Y-9.197 E0.01739
G1 X6.836 Y-8.393 E0.01264
G1 X8.113 Y-8.393 E0.01739
G1 X8.577 Y-9.197 E0.01264
G1 X9.854 Y-9.197 E0.01739
G1 X10.319 Y-8.393 E0.01264
G1 X10.869 Y-8.393 E0.00749
G1 X10.869 Y-8.192 E0.00274
G1 X10.319 Y-8.192 E0.00749
G1 X9.854 Y-7.387 E0.01264
G1 X8.577 Y-7.387 E0.01739
G1 X8.113 Y-8.192 E0.01264
G1 X6.836 Y-8.192 E0.01739
G1 X6.372 Y-7.387 E0.01264
G1 X5.095 Y-7.387 E0.01739
G1 X4.631 Y-8.192 E0.01264
G1 X3.354 Y-8.192 E0.01739
G1 X2.889 Y-7.387 E0.01264
G1 X1.623 Y-7.387 E0.01725
G1 X1.623 Y-9.197 E0.02464
G1 X2.889 Y-9.197 E0.01725
G1 X3.354 Y-8.393 E0.01264
G1 X3.354 Y-6.382 F180.000
G1 X4.631 Y-6.382 E0.01739 F90.000
G1 X5.095 Y-7.186 E0.01264
G1 X6.372 Y-7.186 E0.01739
G1 X6.836 Y-6.382 E0.01264
G1 X8.113 Y-6.382 E0.01739
G1 X8.577 Y-7.186 E0.01264
G1 X9.854 Y-7.186 E0.01739
G1 X10.319 Y-6.382 E0.01264
G1 X10.869 Y-6.382 E0.00749
G1 X10.869 Y-6.181 E0.00274
G1 X10.319 Y-6.181 E0.00749
G1 X9.854 Y-5.377 E0.01264
G1 X8.577 Y-5.377 E0.01739
G1 X8.113 Y-6.181 E0.01264
G1 X6.836 Y-6.181 E0.01739
G1 X6.372 Y-5.377 E0.01264
G1 X5.095 Y-5.377 E0.01739
G1 X4.631 Y-6.181 E0.01264
G1 X3.354 Y-6.181 E0.01739
G1 X2.889 Y-5.377 E0.01264
G1 X1.623 Y-5.377 E0.01725
G1 X1.623 Y-7.186 E0.02464
G1 X2.889 Y-7.186 E0.01725
G1 X3.354 Y-6.382 E0.01264
G1 X3.354 Y-4.371 F180.000
G1 X4.631 Y-4.371 E0.01739 F90.000
G1 X5.095 Y-5.176 E0.01264
G1 X6.372 Y-5.176 E0.01739
G1 X6.836 Y-4.371 E0.01264
G1 X8.113 Y-4.371 E0.01739
G1 X8.577 Y-5.176 E0.01264
G1 X9.854 Y-5.176 E0.01739
G1 X10.319 Y-4.371 E0.01264
G1 X10.869 Y-4.371 E0.00749

G1 X10.869 Y-4.170 E0.00274
G1 X10.319 Y-4.170 E0.00749
G1 X9.854 Y-3.366 E0.01264
G1 X8.577 Y-3.366 E0.01739
G1 X8.113 Y-4.170 E0.01264
G1 X6.836 Y-4.170 E0.01739
G1 X6.372 Y-3.366 E0.01264
G1 X5.095 Y-3.366 E0.01739
G1 X4.631 Y-4.170 E0.01264
G1 X3.354 Y-4.170 E0.01739
G1 X2.889 Y-3.366 E0.01264
G1 X1.623 Y-3.366 E0.01725
G1 X1.623 Y-5.176 E0.02464
G1 X2.889 Y-5.176 E0.01725
G1 X3.354 Y-4.371 E0.01264
G1 X3.354 Y-2.361 F180.000
G1 X4.631 Y-2.361 E0.01739 F90.000
G1 X5.095 Y-3.165 E0.01264
G1 X6.372 Y-3.165 E0.01739
G1 X6.836 Y-2.361 E0.01264
G1 X8.113 Y-2.361 E0.01739
G1 X8.577 Y-3.165 E0.01264
G1 X9.854 Y-3.165 E0.01739
G1 X10.319 Y-2.361 E0.01264
G1 X10.869 Y-2.361 E0.00749
G1 X10.869 Y-2.160 E0.00274
G1 X10.319 Y-2.160 E0.00749
G1 X10.134 Y-1.841 E0.00502
G1 X8.297 Y-1.841 E0.02501
G1 X8.113 Y-2.160 E0.00502
G1 X6.836 Y-2.160 E0.01739
G1 X6.652 Y-1.841 E0.00502
G1 X4.815 Y-1.841 E0.02501
G1 X4.631 Y-2.160 E0.00502
G1 X3.354 Y-2.160 E0.01739
G1 X3.169 Y-1.841 E0.00502
G1 X1.623 Y-1.841 E0.02106
G1 X1.623 Y-3.165 E0.01803
G1 X2.889 Y-3.165 E0.01725
G1 X3.354 Y-2.361 E0.01264
G1 Z0.260 F180.000
G1 X11.660 Y-0.464 F180.000
G1 X12.042 Y-0.081 F180.000
G1 X12.319 Y-0.103 F180.000
G1 X12.513 Y0.050 F180.000
G1 X12.529 Y1.407 E0.01266 F180.000
G1 X12.529 Y11.407 E0.09329
G1 X12.146 Y12.256 E0.00869
G1 X11.401 Y12.540 E0.00744
G1 X-1.389 Y12.609 E0.11932
G1 X-11.395 Y12.609 E0.09335
G1 X-12.244 Y12.227 E0.00869
G1 X-12.529 Y11.476 E0.00750
G1 X-12.529 Y1.468 E0.09336
G1 X-12.438 Y-11.484 E0.12082
G1 X-12.050 Y-12.330 E0.00869
G1 X-11.304 Y-12.609 E0.00743
G1 X-1.303 Y-12.609 E0.09330
G1 X11.247 Y-12.597 E0.11708 F180.000
G1 X12.095 Y-12.214 E0.00869
G1 X12.379 Y-11.477 E0.00737
G1 X12.513 Y0.026 E0.10732
G1 X12.319 Y-0.103 F180.000
G1 X12.319 Y-0.103 F180.000
G1 X11.809 Y0.407 F180.000
G1 X11.145 Y1.656 F180.000
G1 X11.145 Y11.157 E0.12161 F180.000
G1 X1.645 Y11.157 E0.12161

G1 X1.645 Y1.656 E0.12161
G1 X11.121 Y1.656 E0.12130
G1 X11.315 Y1.487 F180.000
G1 X11.315 Y11.327 E0.08679 F180.000
G1 X1.475 Y11.327 E0.08679
G1 X1.475 Y1.487 E0.08679
G1 X11.291 Y1.487 E0.08657
G1 X11.235 Y1.625 F180.000
G1 X10.944 Y2.567 F180.000
G1 X10.642 Y2.567 E0.00386 F180.000
G1 X10.004 Y3.673 E0.01634
G1 X10.468 Y4.477 E0.01189
G1 X9.830 Y5.583 E0.01634
G1 X8.901 Y5.583 E0.01189
G1 X8.263 Y6.689 E0.01634
G1 X8.727 Y7.493 E0.01189
G1 X8.088 Y8.599 E0.01634
G1 X7.160 Y8.599 E0.01189
G1 X6.521 Y9.705 E0.01634
G1 X6.986 Y10.509 E0.01189
G1 X6.728 Y10.956 E0.00660
G1 X6.960 Y10.956 E0.00297
G1 X7.160 Y10.610 E0.00511
G1 X8.088 Y10.610 E0.01189
G1 X8.727 Y9.504 E0.01634
G1 X8.263 Y8.700 E0.01189
G1 X8.901 Y7.594 E0.01634
G1 X9.830 Y7.594 E0.01189
G1 X10.468 Y6.488 E0.01634
G1 X10.004 Y5.684 E0.01189
G1 X10.642 Y4.578 E0.01634
G1 X10.944 Y4.578 E0.00386
G1 X10.944 Y2.567 E0.02574
G1 X10.468 Y2.467 F180.000
G1 X10.116 Y1.857 E0.00901 F180.000
G1 X8.731 Y1.857 E0.01774
G1 X8.263 Y2.668 E0.01198
G1 X8.727 Y3.472 E0.01189
G1 X8.088 Y4.578 E0.01634
G1 X7.160 Y4.578 E0.01189
G1 X6.521 Y5.684 E0.01634
G1 X6.986 Y6.488 E0.01189
G1 X6.347 Y7.594 E0.01634
G1 X5.419 Y7.594 E0.01189
G1 X4.780 Y8.700 E0.01634
G1 X5.244 Y9.504 E0.01189
G1 X4.606 Y10.610 E0.01634
G1 X3.677 Y10.610 E0.01189
G1 X3.478 Y10.956 E0.00511
G1 X4.922 Y10.956 E0.01848
G1 X4.780 Y10.710 E0.00363
G1 X5.419 Y9.605 E0.01634
G1 X6.347 Y9.605 E0.01189
G1 X6.986 Y8.499 E0.01634
G1 X6.521 Y7.694 E0.01189
G1 X7.160 Y6.589 E0.01634
G1 X8.088 Y6.589 E0.01189
G1 X8.727 Y5.483 E0.01634
G1 X8.263 Y4.679 E0.01189
G1 X8.901 Y3.573 E0.01634
G1 X9.830 Y3.573 E0.01189
G1 X10.468 Y2.467 E0.01634
G1 X8.088 Y2.567 F180.000
G1 X8.498 Y1.857 E0.01049 F180.000
G1 X6.634 Y1.857 E0.02387
G1 X6.986 Y2.467 E0.00901
G1 X6.347 Y3.573 E0.01634
G1 X5.419 Y3.573 E0.01189
G1 X4.780 Y4.679 E0.01634

G1 X5.244 Y5.483 E0.01189
G1 X4.606 Y6.589 E0.01634
G1 X3.677 Y6.589 E0.01189
G1 X3.039 Y7.694 E0.01634
G1 X3.503 Y8.499 E0.01189
G1 X2.865 Y9.605 E0.01634
G1 X1.936 Y9.605 E0.01189
G1 X1.846 Y9.761 E0.00231
G1 X1.846 Y10.956 E0.01530
G1 X3.245 Y10.956 E0.01791
G1 X3.503 Y10.509 E0.00660
G1 X3.039 Y9.705 E0.01189
G1 X3.677 Y8.599 E0.01634
G1 X4.606 Y8.599 E0.01189
G1 X5.244 Y7.493 E0.01634
G1 X4.780 Y6.689 E0.01189
G1 X5.419 Y5.583 E0.01634
G1 X6.347 Y5.583 E0.01189
G1 X6.986 Y4.477 E0.01634
G1 X6.521 Y3.673 E0.01189
G1 X7.160 Y2.567 E0.01634
G1 X8.088 Y2.567 E0.01189
G1 X4.780 Y2.668 F180.000
G1 X5.248 Y1.857 E0.01198 F180.000
G1 X5.016 Y1.857 E0.00297
G1 X4.606 Y2.567 E0.01049
G1 X3.677 Y2.567 E0.01189
G1 X3.039 Y3.673 E0.01634
G1 X3.503 Y4.477 E0.01189
G1 X2.865 Y5.583 E0.01634
G1 X1.936 Y5.583 E0.01189
G1 X1.846 Y5.739 E0.00231
G1 X1.846 Y7.750 E0.02574
G1 X1.936 Y7.594 E0.00231
G1 X2.865 Y7.594 E0.01189
G1 X3.503 Y6.488 E0.01634
G1 X3.039 Y5.684 E0.01189
G1 X3.677 Y4.578 E0.01634
G1 X4.606 Y4.578 E0.01189
G1 X5.244 Y3.472 E0.01634
G1 X4.780 Y2.668 E0.01189
G1 X3.503 Y2.467 F180.000
G1 X3.151 Y1.857 E0.00901 F180.000
G1 X1.846 Y1.857 E0.01671
G1 X1.846 Y3.729 E0.02395
G1 X1.936 Y3.573 E0.00231
G1 X2.865 Y3.573 E0.01189
G1 X3.503 Y2.467 E0.01634
G1 X10.944 Y8.599 F180.000
G1 X10.944 Y6.589 E0.02574 F180.000
G1 X10.642 Y6.589 E0.00386
G1 X10.004 Y7.694 E0.01634
G1 X10.468 Y8.499 E0.01189
G1 X9.830 Y9.605 E0.01634
G1 X8.901 Y9.605 E0.01189
G1 X8.263 Y10.710 E0.01634
G1 X8.404 Y10.956 E0.00363
G1 X10.210 Y10.956 E0.02312
G1 X10.468 Y10.509 E0.00660
G1 X10.004 Y9.705 E0.01189
G1 X10.642 Y8.599 E0.01634
G1 X10.944 Y8.599 E0.00386
G1 X10.944 Y10.956 F180.000
G1 X10.944 Y10.610 E0.00443 F180.000
G1 X10.642 Y10.610 E0.00386
G1 X10.443 Y10.956 E0.00511
G1 X10.944 Y10.956 E0.00642
G1 X0.395 Y0.992 F180.000
G1 X-0.003 Y0.992 F180.000

G1 X0.000 Y1.061 F180.000
G1 X-0.395 Y1.061 F180.000
G1 X-1.645 Y1.725 F180.000
G1 X-1.645 Y11.226 E0.12161 F180.000
G1 X-11.145 Y11.226 E0.12161
G1 X-11.145 Y1.725 E0.12161
G1 X-1.669 Y1.725 E0.12130
G1 X-1.475 Y1.556 F180.000
G1 X-1.475 Y11.396 E0.08679 F180.000
G1 X-11.315 Y11.396 E0.08679
G1 X-11.315 Y1.556 E0.08679
G1 X-1.499 Y1.556 E0.08657
G1 X-1.555 Y1.694 F180.000
G1 X-1.846 Y2.636 F180.000
G1 X-2.148 Y2.636 F180.000
G1 X-2.786 Y3.742 E0.01634
G1 X-2.322 Y4.547 E0.01189
G1 X-2.960 Y5.652 E0.01634
G1 X-3.889 Y5.652 E0.01189
G1 X-4.528 Y6.758 E0.01634
G1 X-4.063 Y7.562 E0.01189
G1 X-4.702 Y8.668 E0.01634
G1 X-5.630 Y8.668 E0.01189
G1 X-6.269 Y9.774 E0.01634
G1 X-5.804 Y10.578 E0.01189
G1 X-6.062 Y11.025 E0.00660
G1 X-5.830 Y11.025 E0.00297
G1 X-5.630 Y10.679 E0.00511
G1 X-4.702 Y10.679 E0.01189
G1 X-4.063 Y9.573 E0.01634
G1 X-4.528 Y8.769 E0.01189
G1 X-3.889 Y7.663 E0.01634
G1 X-2.960 Y7.663 E0.01189
G1 X-2.322 Y6.557 E0.01634
G1 X-2.786 Y5.753 E0.01189
G1 X-2.148 Y4.647 E0.01634
G1 X-1.846 Y4.647 E0.00386
G1 X-1.846 Y2.636 E0.02574
G1 X-2.322 Y2.536 F180.000
G1 X-2.674 Y1.926 E0.00901 F180.000
G1 X-4.060 Y1.926 E0.01774
G1 X-4.528 Y2.737 E0.01198
G1 X-4.063 Y3.541 E0.01189
G1 X-4.702 Y4.647 E0.01634
G1 X-5.630 Y4.647 E0.01189
G1 X-6.269 Y5.753 E0.01634
G1 X-5.804 Y6.557 E0.01189
G1 X-6.443 Y7.663 E0.01634
G1 X-7.372 Y7.663 E0.01189
G1 X-8.010 Y8.769 E0.01634
G1 X-7.546 Y9.573 E0.01189
G1 X-8.184 Y10.679 E0.01634
G1 X-9.113 Y10.679 E0.01189
G1 X-9.313 Y11.025 E0.00511
G1 X-7.868 Y11.025 E0.01848
G1 X-8.010 Y10.779 E0.00363
G1 X-7.372 Y9.674 E0.01634
G1 X-6.443 Y9.674 E0.01189
G1 X-5.804 Y8.568 E0.01634
G1 X-6.269 Y7.764 E0.01189
G1 X-5.630 Y6.658 E0.01634
G1 X-4.702 Y6.658 E0.01189
G1 X-4.063 Y5.552 E0.01634
G1 X-4.528 Y4.748 E0.01189
G1 X-3.889 Y3.642 E0.01634
G1 X-2.960 Y3.642 E0.01189
G1 X-2.322 Y2.536 E0.01634
G1 X-4.702 Y2.636 F180.000

G1 X-4.292 Y1.926 E0.01049 F180.000
G1 X-6.156 Y1.926 E0.02387
G1 X-5.804 Y2.536 E0.00901
G1 X-6.443 Y3.642 E0.01634
G1 X-7.372 Y3.642 E0.01189
G1 X-8.010 Y4.748 E0.01634
G1 X-7.546 Y5.552 E0.01189
G1 X-8.184 Y6.658 E0.01634
G1 X-9.113 Y6.658 E0.01189
G1 X-9.751 Y7.763 E0.01634
G1 X-9.287 Y8.568 E0.01189
G1 X-9.925 Y9.674 E0.01634
G1 X-10.854 Y9.674 E0.01189
G1 X-10.944 Y9.830 E0.00231
G1 X-10.944 Y11.025 E0.01530
G1 X-9.545 Y11.025 E0.01791
G1 X-9.287 Y10.578 E0.00660
G1 X-9.751 Y9.774 E0.01189
G1 X-9.113 Y8.668 E0.01634
G1 X-8.184 Y8.668 E0.01189
G1 X-7.546 Y7.562 E0.01634
G1 X-8.010 Y6.758 E0.01189
G1 X-7.372 Y5.652 E0.01634
G1 X-6.443 Y5.652 E0.01189
G1 X-5.804 Y4.547 E0.01634
G1 X-6.269 Y3.742 E0.01189
G1 X-5.630 Y2.636 E0.01634
G1 X-4.702 Y2.636 E0.01189
G1 X-8.010 Y2.737 F180.000
G1 X-7.542 Y1.926 E0.01198 F180.000
G1 X-7.774 Y1.926 E0.00297
G1 X-8.184 Y2.636 E0.01049
G1 X-9.113 Y2.636 E0.01189
G1 X-9.751 Y3.742 E0.01634
G1 X-9.287 Y4.547 E0.01189
G1 X-9.925 Y5.652 E0.01634
G1 X-10.854 Y5.652 E0.01189
G1 X-10.944 Y5.808 E0.00231
G1 X-10.944 Y7.819 E0.02574
G1 X-10.854 Y7.663 E0.00231
G1 X-9.925 Y7.663 E0.01189
G1 X-9.287 Y6.557 E0.01634
G1 X-9.751 Y5.753 E0.01189
G1 X-9.113 Y4.647 E0.01634
G1 X-8.184 Y4.647 E0.01189
G1 X-7.546 Y3.541 E0.01634
G1 X-8.010 Y2.737 E0.01189
G1 X-9.287 Y2.536 F180.000
G1 X-9.639 Y1.926 E0.00901 F180.000
G1 X-10.944 Y1.926 E0.01671
G1 X-10.944 Y3.798 E0.02395
G1 X-10.854 Y3.642 E0.00231
G1 X-9.925 Y3.642 E0.01189
G1 X-9.287 Y2.536 E0.01634
G1 X-1.846 Y8.668 F180.000
G1 X-1.846 Y6.658 E0.02574 F180.000
G1 X-2.148 Y6.658 E0.00386
G1 X-2.786 Y7.764 E0.01634
G1 X-2.322 Y8.568 E0.01189
G1 X-2.960 Y9.674 E0.01634
G1 X-3.889 Y9.674 E0.01189
G1 X-4.528 Y10.779 E0.01634
G1 X-4.386 Y11.025 E0.00363
G1 X-2.580 Y11.025 E0.02312
G1 X-2.322 Y10.578 E0.00660
G1 X-2.786 Y9.774 E0.01189
G1 X-2.148 Y8.668 E0.01634
G1 X-1.846 Y8.668 E0.00386
G1 X-1.846 Y11.025 F180.000

G1 X-1.846 Y10.679 E0.00443 F180.000
G1 X-2.148 Y10.679 E0.00386
G1 X-2.348 Y11.025 E0.00511
G1 X-1.846 Y11.025 E0.00642
G1 X-0.981 Y0.476 F180.000
G1 X-0.369 Y0.045 F180.000
G1 X-0.035 Y-0.768 F180.000
G1 X-0.035 Y-0.792 F180.000
G1 X-0.304 Y-1.061 F180.000
G1 X-1.554 Y-11.226 F180.000
G1 X-1.554 Y-1.725 E0.12161 F180.000
G1 X-11.054 Y-1.725 E0.12161
G1 X-11.054 Y-11.226 E0.12161
G1 X-1.578 Y-11.226 E0.12130
G1 X-1.384 Y-11.396 F180.000
G1 X-1.384 Y-11.556 E0.08679 F180.000
G1 X-11.224 Y-1.556 E0.08679
G1 X-11.224 Y-11.396 E0.08679
G1 X-1.408 Y-11.396 E0.08657
G1 X-1.464 Y-11.257 F180.000
G1 X-1.755 Y-10.315 F180.000
G1 X-2.057 Y-10.315 E0.00386 F180.000
G1 X-2.695 Y-9.209 E0.01634
G1 X-2.231 Y-8.405 E0.01189
G1 X-2.870 Y-7.299 E0.01634
G1 X-3.798 Y-7.299 E0.01189
G1 X-4.437 Y-6.193 E0.01634
G1 X-3.972 Y-5.389 E0.01189
G1 X-4.611 Y-4.283 E0.01634
G1 X-5.539 Y-4.283 E0.01189
G1 X-6.178 Y-3.177 E0.01634
G1 X-5.714 Y-2.373 E0.01189
G1 X-5.971 Y-1.926 E0.00660
G1 X-5.739 Y-1.926 E0.00297
G1 X-5.539 Y-2.272 E0.00511
G1 X-4.611 Y-2.272 E0.01189
G1 X-3.972 Y-3.378 E0.01634
G1 X-4.437 Y-4.182 E0.01189
G1 X-3.798 Y-5.288 E0.01634
G1 X-2.870 Y-5.288 E0.01189
G1 X-2.231 Y-6.394 E0.01634
G1 X-2.695 Y-7.198 E0.01189
G1 X-2.057 Y-8.304 E0.01634
G1 X-1.755 Y-8.304 E0.00386
G1 X-1.755 Y-10.315 E0.02574
G1 X-2.231 Y-10.415 F180.000
G1 X-2.583 Y-11.025 E0.00901 F180.000
G1 X-3.969 Y-11.025 E0.01774
G1 X-4.437 Y-10.214 E0.01198
G1 X-3.972 Y-9.410 E0.01189
G1 X-4.611 Y-8.304 E0.01634
G1 X-5.539 Y-8.304 E0.01189
G1 X-6.178 Y-7.198 E0.01634
G1 X-5.714 Y-6.394 E0.01189
G1 X-6.352 Y-5.288 E0.01634
G1 X-7.281 Y-5.288 E0.01189
G1 X-7.919 Y-4.182 E0.01634
G1 X-7.455 Y-3.378 E0.01189
G1 X-8.093 Y-2.272 E0.01634
G1 X-9.022 Y-2.272 E0.01189
G1 X-9.222 Y-1.926 E0.00511
G1 X-7.778 Y-1.926 E0.01848
G1 X-7.919 Y-2.172 E0.00363
G1 X-7.281 Y-3.278 E0.01634
G1 X-6.352 Y-3.278 E0.01189
G1 X-5.714 Y-4.383 E0.01634
G1 X-6.178 Y-5.188 E0.01189

G1 X-5.539 Y-6.294 E0.01634
G1 X-4.611 Y-6.294 E0.01189
G1 X-3.972 Y-7.399 E0.01634
G1 X-4.437 Y-8.204 E0.01189
G1 X-3.798 Y-9.309 E0.01634
G1 X-2.870 Y-9.309 E0.01189
G1 X-2.231 Y-10.415 E0.01634
G1 X-4.611 Y-10.315 F180.000
G1 X-4.201 Y-11.025 E0.01049 F180.000
G1 X-6.065 Y-11.025 E0.02387
G1 X-5.714 Y-10.415 E0.00901
G1 X-6.352 Y-9.309 E0.01634
G1 X-7.281 Y-9.309 E0.01189
G1 X-7.919 Y-8.204 E0.01634
G1 X-7.455 Y-7.399 E0.01189
G1 X-8.093 Y-6.294 E0.01634
G1 X-9.022 Y-6.294 E0.01189
G1 X-9.660 Y-5.188 E0.01634
G1 X-9.196 Y-4.383 E0.01189
G1 X-9.835 Y-3.278 E0.01634
G1 X-10.763 Y-3.278 E0.01189
G1 X-10.853 Y-3.121 E0.00231
G1 X-10.853 Y-1.926 E0.01530
G1 X-9.454 Y-1.926 E0.01791
G1 X-9.196 Y-2.373 E0.00660
G1 X-9.660 Y-3.177 E0.01189
G1 X-9.022 Y-4.283 E0.01634
G1 X-8.093 Y-4.283 E0.01189
G1 X-7.455 Y-5.389 E0.01634
G1 X-7.919 Y-6.193 E0.01189
G1 X-7.281 Y-7.299 E0.01634
G1 X-6.352 Y-7.299 E0.01189
G1 X-5.714 Y-8.405 E0.01634
G1 X-6.178 Y-9.209 E0.01189
G1 X-5.539 Y-10.315 E0.01634
G1 X-4.611 Y-10.315 E0.01189
G1 X-7.919 Y-10.214 F180.000
G1 X-7.451 Y-11.025 E0.01198 F180.000
G1 X-7.683 Y-11.025 E0.00297
G1 X-8.093 Y-10.315 E0.01049
G1 X-9.022 Y-10.315 E0.01189
G1 X-9.660 Y-9.209 E0.01634
G1 X-9.196 Y-8.405 E0.01189
G1 X-9.835 Y-7.299 E0.01634
G1 X-10.763 Y-7.299 E0.01189
G1 X-10.853 Y-7.143 E0.00231
G1 X-10.853 Y-5.132 E0.02574
G1 X-10.763 Y-5.288 E0.00231
G1 X-9.835 Y-5.288 E0.01189
G1 X-9.196 Y-6.394 E0.01634
G1 X-9.660 Y-7.198 E0.01189
G1 X-9.022 Y-8.304 E0.01634
G1 X-8.093 Y-8.304 E0.01189
G1 X-7.455 Y-9.410 E0.01634
G1 X-7.919 Y-10.214 E0.01189
G1 X-9.196 Y-10.415 F180.000
G1 X-9.548 Y-11.025 E0.00901 F180.000
G1 X-10.853 Y-11.025 E0.01671
G1 X-10.853 Y-9.153 E0.02395
G1 X-10.763 Y-9.309 E0.00231
G1 X-9.835 Y-9.309 E0.01189
G1 X-9.196 Y-10.415 E0.01634
G1 X-1.755 Y-4.283 F180.000
G1 X-1.755 Y-6.294 E0.02574 F180.000
G1 X-2.057 Y-6.294 E0.00386
G1 X-2.695 Y-5.188 E0.01634
G1 X-2.231 Y-4.383 E0.01189

G1 X-2.870 Y-3.278 E0.01634
G1 X-3.798 Y-3.278 E0.01189
G1 X-4.437 Y-2.172 E0.01634
G1 X-4.295 Y-1.926 E0.00363
G1 X-2.489 Y-1.926 E0.02312
G1 X-2.231 Y-2.373 E0.00660
G1 X-2.695 Y-3.177 E0.01189
G1 X-2.057 Y-4.283 E0.01634
G1 X-1.755 Y-4.283 E0.00386
G1 X-1.755 Y-1.926 F180.000
G1 X-1.755 Y-2.272 E0.00443 F180.000
G1 X-2.057 Y-2.272 E0.00386
G1 X-2.257 Y-1.926 E0.00511
G1 X-1.755 Y-1.926 E0.00642
G1 X-0.304 Y-11.890 F180.000
G1 X-0.023 Y-12.171 F180.000
G1 X-0.002 Y-13.297 F180.000
G1 X0.831 Y-12.464 F180.000
G1 X10.996 Y-11.214 F180.000
G1 X10.996 Y-1.713 E0.12161 F180.000
G1 X1.495 Y-1.713 E0.12161
G1 X1.495 Y-11.214 E0.12161
G1 X10.972 Y-11.214 E0.12130
G1 X11.166 Y-11.384 F180.000
G1 X11.166 Y-1.544 E0.08679 F180.000
G1 X1.326 Y-1.544 E0.08679
G1 X1.326 Y-11.384 E0.08679
G1 X11.142 Y-11.384 E0.08657
G1 X11.086 Y-11.245 F180.000
G1 X10.795 Y-10.303 F180.000
G1 X10.493 Y-10.303 E0.00386 F180.000
G1 X9.854 Y-9.197 E0.01634
G1 X10.319 Y-8.393 E0.01189
G1 X9.680 Y-7.287 E0.01634
G1 X8.751 Y-7.287 E0.01189
G1 X8.113 Y-6.181 E0.01634
G1 X8.577 Y-5.377 E0.01189
G1 X7.939 Y-4.271 E0.01634
G1 X7.010 Y-4.271 E0.01189
G1 X6.372 Y-3.165 E0.01634
G1 X6.836 Y-2.361 E0.01189
G1 X6.578 Y-1.914 E0.00660
G1 X6.811 Y-1.914 E0.00297
G1 X7.010 Y-2.260 E0.00511
G1 X7.939 Y-2.260 E0.01189
G1 X8.577 Y-3.366 E0.01634
G1 X8.113 Y-4.170 E0.01189
G1 X8.751 Y-5.276 E0.01634
G1 X9.680 Y-5.276 E0.01189
G1 X10.319 Y-6.382 E0.01634
G1 X9.854 Y-7.186 E0.01189
G1 X10.493 Y-8.292 E0.01634
G1 X10.795 Y-8.292 E0.00386
G1 X10.795 Y-10.303 E0.02574
G1 X10.319 Y-10.403 F180.000
G1 X9.967 Y-11.013 E0.00901 F180.000
G1 X8.581 Y-11.013 E0.01774
G1 X8.113 Y-10.202 E0.01198
G1 X8.577 Y-9.398 E0.01189
G1 X7.939 Y-8.292 E0.01634
G1 X7.010 Y-8.292 E0.01189
G1 X6.372 Y-7.186 E0.01634
G1 X6.836 Y-6.382 E0.01189
G1 X6.198 Y-5.276 E0.01634
G1 X5.269 Y-5.276 E0.01189
G1 X4.631 Y-4.170 E0.01634

G1 X5.095 Y-3.366 E0.01189
G1 X4.456 Y-2.260 E0.01634
G1 X3.528 Y-2.260 E0.01189
G1 X3.328 Y-1.914 E0.00511
G1 X4.772 Y-1.914 E0.01848
G1 X4.631 Y-2.160 E0.00363
G1 X5.269 Y-3.266 E0.01634
G1 X6.198 Y-3.266 E0.01189
G1 X6.836 Y-4.371 E0.01634
G1 X6.372 Y-5.176 E0.01189
G1 X7.010 Y-6.281 E0.01634
G1 X7.939 Y-6.281 E0.01189
G1 X8.577 Y-7.387 E0.01634
G1 X8.113 Y-8.192 E0.01189
G1 X8.751 Y-9.297 E0.01634
G1 X9.680 Y-9.297 E0.01189
G1 X10.319 Y-10.403 E0.01634
G1 X7.939 Y-10.303 F180.000
G1 X8.349 Y-11.013 E0.01049
F180.000
G1 X6.484 Y-11.013 E0.02387
G1 X6.836 Y-10.403 E0.00901
G1 X6.198 Y-9.297 E0.01634
G1 X5.269 Y-9.297 E0.01189
G1 X4.631 Y-8.192 E0.01634
G1 X5.095 Y-7.387 E0.01189
G1 X4.456 Y-6.281 E0.01634
G1 X3.528 Y-6.281 E0.01189
G1 X2.889 Y-5.176 E0.01634
G1 X3.354 Y-4.371 E0.01189
G1 X2.715 Y-3.266 E0.01634
G1 X1.786 Y-3.266 E0.01189
G1 X1.696 Y-3.109 E0.00231
G1 X1.696 Y-1.914 E0.01530
G1 X3.096 Y-1.914 E0.01791
G1 X3.354 Y-2.361 E0.00660
G1 X2.889 Y-3.165 E0.01189
G1 X3.528 Y-4.271 E0.01634
G1 X4.456 Y-4.271 E0.01189
G1 X5.095 Y-5.377 E0.01634
G1 X4.631 Y-6.181 E0.01189
G1 X5.269 Y-7.287 E0.01634
G1 X6.198 Y-7.287 E0.01189
G1 X6.836 Y-8.393 E0.01634
G1 X6.372 Y-9.197 E0.01189
G1 X7.010 Y-10.303 E0.01634
G1 X7.939 Y-10.303 E0.01189
G1 X4.631 Y-10.202 F180.000
G1 X5.098 Y-11.013 E0.01198
F180.000
G1 X4.866 Y-11.013 E0.00297
G1 X4.456 Y-10.303 E0.01049
G1 X3.528 Y-10.303 E0.01189
G1 X2.889 Y-9.197 E0.01634
G1 X3.354 Y-8.393 E0.01189
G1 X2.715 Y-7.287 E0.01634
G1 X1.786 Y-7.287 E0.01189
G1 X1.696 Y-7.131 E0.00231
G1 X1.696 Y-5.120 E0.02574
G1 X1.786 Y-5.276 E0.00231
G1 X2.715 Y-5.276 E0.01189
G1 X3.354 Y-6.382 E0.01634
G1 X2.889 Y-7.186 E0.01189
G1 X3.528 Y-8.292 E0.01634
G1 X4.456 Y-8.292 E0.01189
G1 X5.095 Y-9.398 E0.01634
G1 X4.631 Y-10.202 E0.01189
G1 X3.354 Y-10.403 F180.000
G1 X3.002 Y-11.013 E0.00901
F180.000

G1 X1.696 Y-11.013 E0.01671
G1 X1.696 Y-9.141 E0.02395
G1 X1.786 Y-9.297 E0.00231
G1 X2.715 Y-9.297 E0.01189
G1 X3.354 Y-10.403 E0.01634
G1 X10.795 Y-4.271 F180.000
G1 X10.795 Y-6.281 E0.02574
F180.000
G1 X10.493 Y-6.281 E0.00386
G1 X9.854 Y-5.176 E0.01634
G1 X10.319 Y-4.371 E0.01189
G1 X9.680 Y-3.266 E0.01634
G1 X8.751 Y-3.266 E0.01189
G1 X8.113 Y-2.160 E0.01634
G1 X8.255 Y-1.914 E0.00363
G1 X10.061 Y-1.914 E0.02312
G1 X10.319 Y-2.361 E0.00660
G1 X9.854 Y-3.165 E0.01189
G1 X10.493 Y-4.271 E0.01634
G1 X10.795 Y-4.271 E0.00386
G1 X10.795 Y-1.914 F180.000
G1 X10.795 Y-2.260 E0.00443
F180.000
G1 X10.493 Y-2.260 E0.00386
G1 X10.293 Y-1.914 E0.00511
G1 X10.795 Y-1.914 E0.00642
G1 Z0.360 F180.000
G1 X11.660 Y-0.464 F180.000
G1 X11.660 Y-0.028 F180.000
G1 X11.809 Y-0.041 F180.000
G1 X11.809 Y0.407 F180.000
G1 X11.145 Y1.656 F180.000
G1 X11.145 Y11.157 E0.12161
F180.000
G1 X1.645 Y11.157 E0.12161
G1 X1.645 Y1.656 E0.12161
G1 X11.121 Y1.656 E0.12130
G1 X11.315 Y1.487 F180.000
G1 X11.315 Y11.327 E0.08679
F180.000
G1 X1.475 Y11.327 E0.08679
G1 X1.475 Y1.487 E0.08679
G1 X11.291 Y1.487 E0.08657
G1 X11.235 Y1.625 F180.000
G1 X10.642 Y2.567 F180.000
G1 X10.232 Y1.857 E0.01049 F180.000
G1 X10.944 Y1.857 E0.00911
G1 X10.944 Y2.567 E0.00909
G1 X10.642 Y2.567 E0.00386
G1 X10.004 Y3.472 F180.000
G1 X10.642 Y4.578 E0.01634 F180.000
G1 X10.944 Y4.578 E0.00386
G1 X10.944 Y6.589 E0.02574
G1 X10.642 Y6.589 E0.00386
G1 X10.004 Y5.483 E0.01634
G1 X10.468 Y4.679 E0.01189
G1 X9.830 Y3.573 E0.01634
G1 X8.901 Y3.573 E0.01189
G1 X8.263 Y2.467 E0.01634
G1 X8.614 Y1.857 E0.00901
G1 X10.000 Y1.857 E0.01774
G1 X10.468 Y2.668 E0.01198
G1 X10.004 Y3.472 E0.01189
G1 X7.160 Y2.567 F180.000
G1 X8.088 Y2.567 E0.01189 F180.000
G1 X8.727 Y3.673 E0.01634
G1 X8.263 Y4.477 E0.01189
G1 X8.901 Y5.583 E0.01634
G1 X9.830 Y5.583 E0.01189
G1 X10.468 Y6.689 E0.01634

G1 X10.004 Y7.493 E0.01189
G1 X10.642 Y8.599 E0.01634
G1 X10.944 Y8.599 E0.00386
G1 X10.944 Y10.610 E0.02574
G1 X10.642 Y10.610 E0.00386
G1 X10.004 Y9.504 E0.01634
G1 X10.468 Y8.700 E0.01189
G1 X9.830 Y7.594 E0.01634
G1 X8.901 Y7.594 E0.01189
G1 X8.263 Y6.488 E0.01634
G1 X8.727 Y5.684 E0.01189
G1 X8.088 Y4.578 E0.01634
G1 X7.160 Y4.578 E0.01189
G1 X6.521 Y3.472 E0.01634
G1 X6.986 Y2.668 E0.01189
G1 X6.518 Y1.857 E0.01198
G1 X6.750 Y1.857 E0.00297
G1 X7.160 Y2.567 E0.01049
G1 X4.780 Y2.467 F180.000
G1 X5.419 Y3.573 E0.01634 F180.000
G1 X6.347 Y3.573 E0.01189
G1 X6.986 Y4.679 E0.01634
G1 X6.521 Y5.483 E0.01189
G1 X7.160 Y6.589 E0.01634
G1 X8.088 Y6.589 E0.01189
G1 X8.727 Y7.694 E0.01634
G1 X8.263 Y8.499 E0.01189
G1 X8.901 Y9.605 E0.01634
G1 X9.830 Y9.605 E0.01189
G1 X10.468 Y10.710 E0.01634
G1 X10.327 Y10.956 E0.00363
G1 X8.520 Y10.956 E0.02312
G1 X8.263 Y10.509 E0.00660
G1 X8.727 Y9.705 E0.01189
G1 X8.088 Y8.599 E0.01634
G1 X7.160 Y8.599 E0.01189
G1 X6.521 Y7.493 E0.01634
G1 X6.986 Y6.689 E0.01189
G1 X6.347 Y5.583 E0.01634
G1 X5.419 Y5.583 E0.01189
G1 X4.780 Y4.477 E0.01634
G1 X5.244 Y3.673 E0.01189
G1 X4.606 Y2.567 E0.01634
G1 X3.677 Y2.567 E0.01189
G1 X3.267 Y1.857 E0.01049
G1 X5.132 Y1.857 E0.02387
G1 X4.780 Y2.467 E0.00901
G1 X3.503 Y2.668 F180.000
G1 X3.039 Y3.472 E0.01189 F180.000
G1 X3.677 Y4.578 E0.01634
G1 X4.606 Y4.578 E0.01189
G1 X5.244 Y5.684 E0.01634
G1 X4.780 Y6.488 E0.01189
G1 X5.419 Y7.594 E0.01634
G1 X6.347 Y7.594 E0.01189
G1 X6.986 Y8.700 E0.01634
G1 X6.521 Y9.504 E0.01189
G1 X7.160 Y10.610 E0.01634
G1 X8.088 Y10.610 E0.01189
G1 X8.288 Y10.956 E0.00511
G1 X6.844 Y10.956 E0.01848
G1 X6.986 Y10.710 E0.00363
G1 X6.347 Y9.605 E0.01634
G1 X5.419 Y9.605 E0.01189
G1 X4.780 Y8.499 E0.01634
G1 X5.244 Y7.694 E0.01189
G1 X4.606 Y6.589 E0.01634
G1 X3.677 Y6.589 E0.01189
G1 X3.039 Y5.483 E0.01634
G1 X3.503 Y4.679 E0.01189

G1 X2.865 Y3.573 E0.01634
G1 X1.936 Y3.573 E0.01189
G1 X1.846 Y3.417 E0.00231
G1 X1.846 Y1.857 E0.01996
G1 X3.035 Y1.857 E0.01522
G1 X3.503 Y2.668 E0.01198
G1 X1.936 Y5.583 F180.000
G1 X2.865 Y5.583 E0.01189 F180.000
G1 X3.503 Y6.689 E0.01634
G1 X3.039 Y7.493 E0.01189
G1 X3.677 Y8.599 E0.01634
G1 X4.606 Y8.599 E0.01189
G1 X5.244 Y9.705 E0.01634
G1 X4.780 Y10.509 E0.01189
G1 X5.038 Y10.956 E0.00660
G1 X4.806 Y10.956 E0.00297
G1 X4.606 Y10.610 E0.00511
G1 X3.677 Y10.610 E0.01189
G1 X3.039 Y9.504 E0.01634
G1 X3.503 Y8.700 E0.01189
G1 X2.865 Y7.594 E0.01634
G1 X1.936 Y7.594 E0.01189
G1 X1.846 Y7.438 E0.00231
G1 X1.846 Y5.427 E0.02574
G1 X1.936 Y5.583 E0.00231
G1 X1.936 Y9.605 F180.000
G1 X2.865 Y9.605 E0.01189 F180.000
G1 X3.503 Y10.710 E0.01634
G1 X3.362 Y10.956 E0.00363
G1 X1.846 Y10.956 E0.01940
G1 X1.846 Y9.448 E0.01929
G1 X1.936 Y9.605 E0.00231
G1 X0.395 Y0.992 F180.000
G1 X-0.003 Y0.992 F180.000
G1 X0.000 Y1.061 F180.000
G1 X-0.395 Y1.061 F180.000
G1 X-1.645 Y1.725 F180.000
G1 X-1.645 Y11.226 E0.12161
F180.000
G1 X-11.145 Y11.226 E0.12161
G1 X-11.145 Y1.725 E0.12161
G1 X-1.669 Y1.725 E0.12130
G1 X-1.475 Y1.556 F180.000
G1 X-1.475 Y11.396 E0.08679
F180.000
G1 X-11.315 Y11.396 E0.08679
G1 X-11.315 Y1.556 E0.08679
G1 X-1.499 Y1.556 E0.08657
G1 X-1.555 Y1.694 F180.000
G1 X-2.148 Y2.636 F180.000
G1 X-2.558 Y1.926 E0.01049 F180.000
G1 X-1.846 Y1.926 E0.00911
G1 X-1.846 Y2.636 E0.00909
G1 X-2.148 Y2.636 E0.00386
G1 X-2.786 Y3.541 F180.000
G1 X-2.148 Y4.647 E0.01634 F180.000
G1 X-1.846 Y4.647 E0.00386
G1 X-1.846 Y6.658 E0.02574
G1 X-2.148 Y6.658 E0.00386
G1 X-2.786 Y5.552 E0.01634
G1 X-2.322 Y4.748 E0.01189
G1 X-2.960 Y3.642 E0.01634
G1 X-3.889 Y3.642 E0.01189
G1 X-4.528 Y2.536 E0.01634
G1 X-4.176 Y1.926 E0.00901
G1 X-2.790 Y1.926 E0.01774
G1 X-2.322 Y2.737 E0.01198
G1 X-2.786 Y3.541 E0.01189
G1 X-5.630 Y2.636 F180.000
G1 X-4.702 Y2.636 E0.01189 F180.000

G1 X-4.063 Y3.742 E0.01634
G1 X-4.528 Y4.547 E0.01189
G1 X-3.889 Y5.652 E0.01634
G1 X-2.960 Y5.652 E0.01189
G1 X-2.322 Y6.758 E0.01634
G1 X-2.786 Y7.562 E0.01189
G1 X-2.148 Y8.668 E0.01634
G1 X-1.846 Y8.668 E0.00386
G1 X-1.846 Y10.679 E0.02574
G1 X-2.148 Y10.679 E0.00386
G1 X-2.786 Y9.573 E0.01634
G1 X-2.322 Y8.769 E0.01189
G1 X-2.960 Y7.663 E0.01634
G1 X-3.889 Y7.663 E0.01189
G1 X-4.528 Y6.557 E0.01634
G1 X-4.063 Y5.753 E0.01189
G1 X-4.702 Y4.647 E0.01634
G1 X-5.630 Y4.647 E0.01189
G1 X-6.269 Y3.541 E0.01634
G1 X-5.804 Y2.737 E0.01189
G1 X-6.272 Y1.926 E0.01198
G1 X-6.040 Y1.926 E0.00297
G1 X-5.630 Y2.636 E0.01049
G1 X-8.010 Y2.536 F180.000
G1 X-7.372 Y3.642 E0.01634 F180.000
G1 X-6.443 Y3.642 E0.01189
G1 X-5.804 Y4.748 E0.01634
G1 X-6.269 Y5.552 E0.01189
G1 X-5.630 Y6.658 E0.01634
G1 X-4.702 Y6.658 E0.01189
G1 X-4.063 Y7.764 E0.01634
G1 X-4.528 Y8.568 E0.01189
G1 X-3.889 Y9.674 E0.01634
G1 X-2.960 Y9.674 E0.01189
G1 X-2.322 Y10.779 E0.01634
G1 X-2.464 Y11.025 E0.00363
G1 X-4.270 Y11.025 E0.02312
G1 X-4.528 Y10.578 E0.00660
G1 X-4.063 Y9.774 E0.01189
G1 X-4.702 Y8.668 E0.01634
G1 X-5.630 Y8.668 E0.01189
G1 X-6.269 Y7.562 E0.01634
G1 X-5.804 Y6.758 E0.01189
G1 X-6.443 Y5.652 E0.01634
G1 X-7.372 Y5.652 E0.01189
G1 X-8.010 Y4.547 E0.01634
G1 X-7.546 Y3.742 E0.01189
G1 X-8.184 Y2.636 E0.01634
G1 X-9.113 Y2.636 E0.01189
G1 X-9.523 Y1.926 E0.01049
G1 X-7.658 Y1.926 E0.02387
G1 X-8.010 Y2.536 E0.00901
G1 X-9.287 Y2.737 F180.000
G1 X-9.751 Y3.541 E0.01189 F180.000
G1 X-9.113 Y4.647 E0.01634
G1 X-8.184 Y4.647 E0.01189
G1 X-7.546 Y5.753 E0.01634
G1 X-8.010 Y6.557 E0.01189
G1 X-7.372 Y7.663 E0.01634
G1 X-6.443 Y7.663 E0.01189
G1 X-5.804 Y8.769 E0.01634
G1 X-6.269 Y9.573 E0.01189
G1 X-5.630 Y10.679 E0.01634
G1 X-4.702 Y10.679 E0.01189
G1 X-4.502 Y11.025 E0.00511
G1 X-5.946 Y11.025 E0.01848
G1 X-5.804 Y10.779 E0.00363
G1 X-6.443 Y9.674 E0.01634
G1 X-7.372 Y9.674 E0.01189
G1 X-8.010 Y8.568 E0.01634

G1 X-7.546 Y7.764 E0.01189
G1 X-8.184 Y6.658 E0.01634
G1 X-9.113 Y6.658 E0.01189
G1 X-9.751 Y5.552 E0.01634
G1 X-9.287 Y4.748 E0.01189
G1 X-9.925 Y3.642 E0.01634
G1 X-10.854 Y3.642 E0.01189
G1 X-10.944 Y3.486 E0.00231
G1 X-10.944 Y1.926 E0.01996
G1 X-9.755 Y1.926 E0.01522
G1 X-9.287 Y2.737 E0.01198
G1 X-10.854 Y5.652 F180.000
G1 X-9.925 Y5.652 E0.01189 F180.000
G1 X-9.287 Y6.758 E0.01634
G1 X-9.751 Y7.562 E0.01189
G1 X-9.113 Y8.668 E0.01634
G1 X-8.184 Y8.668 E0.01189
G1 X-7.546 Y9.774 E0.01634
G1 X-8.010 Y10.578 E0.01189
G1 X-7.752 Y11.025 E0.00660
G1 X-7.985 Y11.025 E0.00297
G1 X-8.184 Y10.679 E0.00511
G1 X-9.113 Y10.679 E0.01189
G1 X-9.751 Y9.573 E0.01634
G1 X-9.287 Y8.769 E0.01189
G1 X-9.925 Y7.663 E0.01634
G1 X-10.854 Y7.663 E0.01189
G1 X-10.944 Y7.507 E0.00231
G1 X-10.944 Y5.496 E0.02574
G1 X-10.854 Y5.652 E0.00231
G1 X-10.854 Y9.674 F180.000
G1 X-9.925 Y9.674 E0.01189 F180.000
G1 X-9.287 Y10.779 E0.01634
G1 X-9.429 Y11.025 E0.00363
G1 X-10.944 Y11.025 E0.01940
G1 X-10.944 Y9.517 E0.01929
G1 X-10.854 Y9.674 E0.00231
G1 X-0.981 Y0.476 F180.000
G1 X-0.369 Y0.045 F180.000
G1 X-0.035 Y-0.768 F180.000
G1 X-0.035 Y-0.792 F180.000
G1 X-0.304 Y-1.061 F180.000
G1 X-1.554 Y-11.226 F180.000
G1 X-1.554 Y-1.725 E0.12161 F180.000
G1 X-11.054 Y-1.725 E0.12161
G1 X-11.054 Y-11.226 E0.12161
G1 X-1.578 Y-11.226 E0.12130
G1 X-1.384 Y-11.396 F180.000
G1 X-1.384 Y-1.556 E0.08679 F180.000
G1 X-11.224 Y-1.556 E0.08679
G1 X-11.224 Y-11.396 E0.08679
G1 X-1.408 Y-11.396 E0.08657
G1 X-1.464 Y-11.257 F180.000
G1 X-2.057 Y-10.315 F180.000
G1 X-2.467 Y-11.025 E0.01049
F180.000
G1 X-1.755 Y-11.025 E0.00911
G1 X-1.755 Y-10.315 E0.00909
G1 X-2.057 Y-10.315 E0.00386
G1 X-2.695 Y-9.410 F180.000
G1 X-2.057 Y-8.304 E0.01634 F180.000
G1 X-1.755 Y-8.304 E0.00386
G1 X-1.755 Y-6.294 E0.02574
G1 X-2.057 Y-6.294 E0.00386
G1 X-2.695 Y-7.399 E0.01634
G1 X-2.231 Y-8.204 E0.01189
G1 X-2.870 Y-9.309 E0.01634
G1 X-3.798 Y-9.309 E0.01189
G1 X-4.437 Y-10.415 E0.01634
G1 X-4.085 Y-11.025 E0.00901

G1 X-2.699 Y-11.025 E0.01774
G1 X-2.231 Y-10.214 E0.01198
G1 X-2.695 Y-9.410 E0.01189
G1 X-5.539 Y-10.315 F180.000
G1 X-4.611 Y-10.315 E0.01189
F180.000
G1 X-3.972 Y-9.209 E0.01634
G1 X-4.437 Y-8.405 E0.01189
G1 X-3.798 Y-7.299 E0.01634
G1 X-2.870 Y-7.299 E0.01189
G1 X-2.231 Y-6.193 E0.01634
G1 X-2.695 Y-5.389 E0.01189
G1 X-2.057 Y-4.283 E0.01634
G1 X-1.755 Y-4.283 E0.00386
G1 X-1.755 Y-2.272 E0.02574
G1 X-2.057 Y-2.272 E0.00386
G1 X-2.695 Y-3.378 E0.01634
G1 X-2.231 Y-4.182 E0.01189
G1 X-2.870 Y-5.288 E0.01634
G1 X-3.798 Y-5.288 E0.01189
G1 X-4.437 Y-6.394 E0.01634
G1 X-3.972 Y-7.198 E0.01189
G1 X-4.611 Y-8.304 E0.01634
G1 X-5.539 Y-8.304 E0.01189
G1 X-6.178 Y-9.410 E0.01634
G1 X-5.714 Y-10.214 E0.01189
G1 X-6.182 Y-11.025 E0.01198
G1 X-5.949 Y-11.025 E0.00297
G1 X-5.539 Y-10.315 E0.01049
G1 X-7.919 Y-10.415 F180.000
G1 X-7.281 Y-9.309 E0.01634 F180.000
G1 X-6.352 Y-9.309 E0.01189
G1 X-5.714 Y-8.204 E0.01634
G1 X-6.178 Y-7.399 E0.01189
G1 X-5.539 Y-6.294 E0.01634
G1 X-4.611 Y-6.294 E0.01189
G1 X-3.972 Y-5.188 E0.01634
G1 X-4.437 Y-4.383 E0.01189
G1 X-3.798 Y-3.278 E0.01634
G1 X-2.870 Y-3.278 E0.01189
G1 X-2.231 Y-2.172 E0.01634
G1 X-2.373 Y-1.926 E0.00363
G1 X-4.179 Y-1.926 E0.02312
G1 X-4.437 Y-2.373 E0.00660
G1 X-3.972 Y-3.177 E0.01189
G1 X-4.611 Y-4.283 E0.01634
G1 X-5.539 Y-4.283 E0.01189
G1 X-6.178 Y-5.389 E0.01634
G1 X-5.714 Y-6.193 E0.01189
G1 X-6.352 Y-7.299 E0.01634
G1 X-7.281 Y-7.299 E0.01189
G1 X-7.919 Y-8.405 E0.01634
G1 X-7.455 Y-9.209 E0.01189
G1 X-8.093 Y-10.315 E0.01634
G1 X-9.022 Y-10.315 E0.01189
G1 X-9.432 Y-11.025 E0.01049
G1 X-7.567 Y-11.025 E0.02387
G1 X-7.919 Y-10.415 E0.00901
G1 X-9.196 Y-10.214 F180.000
G1 X-9.660 Y-9.410 E0.01189 F180.000
G1 X-9.022 Y-8.304 E0.01634
G1 X-8.093 Y-8.304 E0.01189
G1 X-7.455 Y-7.198 E0.01634
G1 X-7.919 Y-6.394 E0.01189
G1 X-7.281 Y-5.288 E0.01634
G1 X-6.352 Y-5.288 E0.01189
G1 X-5.714 Y-4.182 E0.01634
G1 X-6.178 Y-3.378 E0.01189
G1 X-5.539 Y-2.272 E0.01634
G1 X-4.611 Y-2.272 E0.01189

G1 X-4.411 Y-1.926 E0.00511
G1 X-5.855 Y-1.926 E0.01848
G1 X-5.714 Y-2.172 E0.00363
G1 X-6.352 Y-3.278 E0.01634
G1 X-7.281 Y-3.278 E0.01189
G1 X-7.919 Y-4.383 E0.01634
G1 X-7.455 Y-5.188 E0.01189
G1 X-8.093 Y-6.294 E0.01634
G1 X-9.022 Y-6.294 E0.01189
G1 X-9.660 Y-7.399 E0.01634
G1 X-9.196 Y-8.204 E0.01189
G1 X-9.835 Y-9.309 E0.01634
G1 X-10.763 Y-9.309 E0.01189
G1 X-10.853 Y-9.466 E0.00231
G1 X-10.853 Y-11.025 E0.01996
G1 X-9.664 Y-11.025 E0.01522
G1 X-9.196 Y-10.214 E0.01189
G1 X-10.763 Y-7.299 F180.000
G1 X-9.835 Y-7.299 E0.01189 F180.000
G1 X-9.196 Y-6.193 E0.01634
G1 X-9.660 Y-5.389 E0.01189
G1 X-9.022 Y-4.283 E0.01634
G1 X-8.093 Y-4.283 E0.01189
G1 X-7.455 Y-3.177 E0.01634
G1 X-7.919 Y-2.373 E0.01189
G1 X-7.661 Y-1.926 E0.00660
G1 X-7.894 Y-1.926 E0.00297
G1 X-8.093 Y-2.272 E0.00511
G1 X-9.022 Y-2.272 E0.01189
G1 X-9.660 Y-3.378 E0.01634
G1 X-9.196 Y-4.182 E0.01189
G1 X-9.835 Y-5.288 E0.01634
G1 X-10.763 Y-5.288 E0.01189
G1 X-10.853 Y-5.444 E0.00231
G1 X-10.853 Y-7.455 E0.02574
G1 X-10.763 Y-7.299 E0.00231
G1 X-10.763 Y-3.278 F180.000
G1 X-9.835 Y-3.278 E0.01189 F180.000
G1 X-9.196 Y-2.172 E0.01634
G1 X-9.338 Y-1.926 E0.00363
G1 X-10.853 Y-1.926 E0.01940
G1 X-10.853 Y-3.434 E0.01929
G1 X-10.763 Y-3.278 E0.00231
G1 X-0.304 Y-11.890 F180.000
G1 X-0.023 Y-12.171 F180.000
G1 X-0.002 Y-13.297 F180.000
G1 X0.831 Y-12.464 F180.000
G1 X10.996 Y-11.214 F180.000
G1 X10.996 Y-1.713 E0.12161
F180.000
G1 X1.495 Y-1.713 E0.12161
G1 X1.495 Y-11.214 E0.12161
G1 X10.972 Y-11.214 E0.12130
G1 X11.166 Y-11.384 F180.000
G1 X11.166 Y-1.544 E0.08679
F180.000
G1 X1.326 Y-1.544 E0.08679
G1 X1.326 Y-11.384 E0.08679
G1 X11.142 Y-11.384 E0.08657
G1 X11.086 Y-11.245 F180.000
G1 X10.493 Y-10.303 F180.000
G1 X10.083 Y-11.013 E0.01049
F180.000
G1 X10.795 Y-11.013 E0.00911
G1 X10.795 Y-10.303 E0.00909
G1 X10.493 Y-10.303 E0.00386
G1 X9.854 Y-9.398 F180.000
G1 X10.493 Y-8.292 E0.01634
F180.000
G1 X10.795 Y-8.292 E0.00386

G1 X10.795 Y-6.281 E0.02574
G1 X10.493 Y-6.281 E0.00386
G1 X9.854 Y-7.387 E0.01634
G1 X10.319 Y-8.192 E0.01189
G1 X9.680 Y-9.297 E0.01634
G1 X8.751 Y-9.297 E0.01189
G1 X8.113 Y-10.403 E0.01634
G1 X8.465 Y-11.013 E0.00901
G1 X9.851 Y-11.013 E0.01774
G1 X10.319 Y-10.202 E0.01198
G1 X9.854 Y-9.398 E0.01189
G1 X7.010 Y-10.303 F180.000
G1 X7.939 Y-10.303 E0.01189
F180.000
G1 X8.577 Y-9.197 E0.01634
G1 X8.113 Y-8.393 E0.01189
G1 X8.751 Y-7.287 E0.01634
G1 X9.680 Y-7.287 E0.01189
G1 X10.319 Y-6.181 E0.01634
G1 X9.854 Y-5.377 E0.01189
G1 X10.493 Y-4.271 E0.01634
G1 X10.795 Y-4.271 E0.00386
G1 X10.795 Y-2.260 E0.02574
G1 X10.493 Y-2.260 E0.00386
G1 X9.854 Y-3.366 E0.01634
G1 X10.319 Y-4.170 E0.01189
G1 X9.680 Y-5.276 E0.01634
G1 X8.751 Y-5.276 E0.01189
G1 X8.113 Y-6.382 E0.01634
G1 X8.577 Y-7.186 E0.01189
G1 X7.939 Y-8.292 E0.01634
G1 X7.010 Y-8.292 E0.01189
G1 X6.372 Y-9.398 E0.01634
G1 X6.836 Y-10.202 E0.01189
G1 X6.368 Y-11.013 E0.01198
G1 X6.600 Y-11.013 E0.00297
G1 X7.010 Y-10.303 E0.01049
G1 X4.631 Y-10.403 F180.000
G1 X5.269 Y-9.297 E0.01634 F180.000
G1 X6.198 Y-9.297 E0.01189
G1 X6.836 Y-8.192 E0.01634
G1 X6.372 Y-7.387 E0.01189
G1 X7.010 Y-6.281 E0.01634
G1 X7.939 Y-6.281 E0.01189
G1 X8.577 Y-5.176 E0.01634
G1 X8.113 Y-4.371 E0.01189
G1 X8.751 Y-3.266 E0.01634
G1 X9.680 Y-3.266 E0.01189
G1 X10.319 Y-2.160 E0.01634
G1 X10.177 Y-1.914 E0.00363
G1 X8.371 Y-1.914 E0.02312
G1 X8.113 Y-2.361 E0.00660
G1 X8.577 Y-3.165 E0.01189
G1 X7.939 Y-4.271 E0.01634
G1 X7.010 Y-4.271 E0.01189
G1 X6.372 Y-5.377 E0.01634
G1 X6.836 Y-6.181 E0.01189
G1 X6.198 Y-7.287 E0.01634
G1 X5.269 Y-7.287 E0.01189
G1 X4.631 Y-8.393 E0.01634
G1 X5.095 Y-9.197 E0.01189
G1 X4.456 Y-10.303 E0.01634
G1 X3.528 Y-10.303 E0.01189
G1 X3.118 Y-11.013 E0.01049
G1 X4.982 Y-11.013 E0.02387
G1 X4.631 Y-10.403 E0.00901
G1 X3.354 Y-10.202 F180.000
G1 X2.889 Y-9.398 E0.01189 F180.000
G1 X3.528 Y-8.292 E0.01634
G1 X4.456 Y-8.292 E0.01189

G1 X5.095 Y-7.186 E0.01634
G1 X4.631 Y-6.382 E0.01189
G1 X5.269 Y-5.276 E0.01634
G1 X6.198 Y-5.276 E0.01189
G1 X6.836 Y-4.170 E0.01634
G1 X6.372 Y-3.366 E0.01189
G1 X7.010 Y-2.260 E0.01634
G1 X7.939 Y-2.260 E0.01189
G1 X8.139 Y-1.914 E0.00511
G1 X6.694 Y-1.914 E0.01848
G1 X6.836 Y-2.160 E0.00363
G1 X6.198 Y-3.266 E0.01634
G1 X5.269 Y-3.266 E0.01189
G1 X4.631 Y-4.371 E0.01634
G1 X5.095 Y-5.176 E0.01189
G1 X4.456 Y-6.281 E0.01634
G1 X3.528 Y-6.281 E0.01189
G1 X2.889 Y-7.387 E0.01634
G1 X3.354 Y-8.192 E0.01189
G1 X2.715 Y-9.297 E0.01634
G1 X1.786 Y-9.297 E0.01189
G1 X1.696 Y-9.454 E0.00231
G1 X1.696 Y-11.013 E0.01996
G1 X2.886 Y-11.013 E0.01522
G1 X3.354 Y-10.202 E0.01198
G1 X1.786 Y-7.287 F180.000
G1 X2.715 Y-7.287 E0.01189 F180.000
G1 X3.354 Y-6.181 E0.01634
G1 X2.889 Y-5.377 E0.01189
G1 X3.528 Y-4.271 E0.01634
G1 X4.456 Y-4.271 E0.01189
G1 X5.095 Y-3.165 E0.01634
G1 X4.631 Y-2.361 E0.01189
G1 X4.888 Y-1.914 E0.00660
G1 X4.656 Y-1.914 E0.00297
G1 X4.456 Y-2.260 E0.00511
G1 X3.528 Y-2.260 E0.01189
G1 X2.889 Y-3.366 E0.01634
G1 X3.354 Y-4.170 E0.01189
G1 X2.715 Y-5.276 E0.01634
G1 X1.786 Y-5.276 E0.01189
G1 X1.696 Y-5.432 E0.00231
G1 X1.696 Y-7.443 E0.02574
G1 X1.786 Y-7.287 E0.00231
G1 X1.786 Y-3.266 F180.000
G1 X2.715 Y-3.266 E0.01189 F180.000
G1 X3.354 Y-2.160 E0.01634
G1 X3.212 Y-1.914 E0.00363
G1 X1.696 Y-1.914 E0.01940
G1 X1.696 Y-3.422 E0.01929
G1 X1.786 Y-3.266 E0.00231
G1 Z0.460 F180.000
G1 X11.660 Y-0.464 F180.000
G1 X11.660 Y-0.028 F180.000
G1 X11.809 Y-0.041 F180.000
G1 X11.809 Y0.407 F180.000
G1 X11.145 Y1.656 F180.000
G1 X11.145 Y11.157 E0.12161
F180.000
G1 X1.645 Y11.157 E0.12161
G1 X1.645 Y1.656 E0.12161
G1 X11.121 Y1.656 E0.12130
G1 X11.315 Y1.487 F180.000
G1 X11.315 Y11.327 E0.08679
F180.000
G1 X1.475 Y11.327 E0.08679
G1 X1.475 Y1.487 E0.08679
G1 X11.291 Y1.487 E0.08657
G1 X11.235 Y1.625 F180.000
G1 X10.468 Y2.467 F180.000

G1 X10.944 Y2.467 E0.00609 F180.000
G1 X10.944 Y2.668 E0.00257
G1 X10.468 Y2.668 E0.00609
G1 X10.004 Y3.472 E0.01189
G1 X8.727 Y3.472 E0.01634
G1 X8.263 Y2.668 E0.01189
G1 X6.986 Y2.668 E0.01634
G1 X6.521 Y3.472 E0.01189
G1 X5.244 Y3.472 E0.01634
G1 X4.780 Y2.668 E0.01189
G1 X3.503 Y2.668 E0.01634
G1 X3.039 Y3.472 E0.01189
G1 X1.846 Y3.472 E0.01527
G1 X1.846 Y1.857 E0.02067
G1 X3.151 Y1.857 E0.01671
G1 X3.503 Y2.467 E0.00901
G1 X4.780 Y2.467 E0.01634
G1 X5.132 Y1.857 E0.00901
G1 X6.634 Y1.857 E0.01922
G1 X6.986 Y2.467 E0.00901
G1 X8.263 Y2.467 E0.01634
G1 X8.614 Y1.857 E0.00901
G1 X10.116 Y1.857 E0.01922
G1 X10.468 Y2.467 E0.00901
G1 X3.503 Y4.477 F180.000
G1 X4.780 Y4.477 E0.01634 F180.000
G1 X5.244 Y3.673 E0.01189
G1 X6.521 Y3.673 E0.01634
G1 X6.986 Y4.477 E0.01189
G1 X8.263 Y4.477 E0.01634
G1 X8.727 Y3.673 E0.01189
G1 X10.004 Y3.673 E0.01634
G1 X10.468 Y4.477 E0.01189
G1 X10.944 Y4.477 E0.00609
G1 X10.944 Y4.679 E0.00257
G1 X10.468 Y4.679 E0.00609
G1 X10.004 Y5.483 E0.01189
G1 X8.727 Y5.483 E0.01634
G1 X8.263 Y4.679 E0.01189
G1 X6.986 Y4.679 E0.01634
G1 X6.521 Y5.483 E0.01189
G1 X5.244 Y5.483 E0.01634
G1 X4.780 Y4.679 E0.01189
G1 X3.503 Y4.679 E0.01634
G1 X3.039 Y5.483 E0.01189
G1 X1.846 Y5.483 E0.01527
G1 X1.846 Y3.673 E0.02316
G1 X3.039 Y3.673 E0.01527
G1 X3.503 Y4.477 E0.01189
G1 X3.503 Y6.488 F180.000
G1 X4.780 Y6.488 E0.01634 F180.000
G1 X5.244 Y5.684 E0.01189
G1 X6.521 Y5.684 E0.01634
G1 X6.986 Y6.488 E0.01189
G1 X8.263 Y6.488 E0.01634
G1 X8.727 Y5.684 E0.01189
G1 X10.004 Y5.684 E0.01634
G1 X10.468 Y6.488 E0.01189
G1 X10.944 Y6.488 E0.00609
G1 X10.944 Y6.689 E0.00257
G1 X10.468 Y6.689 E0.00609
G1 X10.004 Y7.493 E0.01189
G1 X8.727 Y7.493 E0.01634
G1 X8.263 Y6.689 E0.01189
G1 X6.986 Y6.689 E0.01634
G1 X6.521 Y7.493 E0.01189
G1 X5.244 Y7.493 E0.01634
G1 X4.780 Y6.689 E0.01189
G1 X3.503 Y6.689 E0.01634
G1 X3.039 Y7.493 E0.01189

G1 X1.846 Y7.493 E0.01527
G1 X1.846 Y5.684 E0.02316
G1 X3.039 Y5.684 E0.01527
G1 X3.503 Y6.488 E0.01189
G1 X3.503 Y8.499 F180.000
G1 X4.780 Y8.499 E0.01634 F180.000
G1 X5.244 Y7.694 E0.01189
G1 X6.521 Y7.694 E0.01634
G1 X6.986 Y8.499 E0.01189
G1 X8.263 Y8.499 E0.01634
G1 X8.727 Y7.694 E0.01189
G1 X10.004 Y7.694 E0.01634
G1 X10.468 Y8.499 E0.01189
G1 X10.944 Y8.700 E0.00257
G1 X10.468 Y8.700 E0.00609
G1 X10.004 Y9.504 E0.01189
G1 X8.727 Y9.504 E0.01634
G1 X8.263 Y8.700 E0.01189
G1 X6.986 Y8.700 E0.01634
G1 X6.521 Y9.504 E0.01189
G1 X5.244 Y9.504 E0.01634
G1 X4.780 Y8.700 E0.01189
G1 X3.503 Y8.700 E0.01634
G1 X3.039 Y9.504 E0.01189
G1 X1.846 Y9.504 E0.01527
G1 X1.846 Y7.694 E0.02316
G1 X3.039 Y7.694 E0.01527
G1 X3.503 Y8.499 E0.01189
G1 X3.503 Y10.509 F180.000
G1 X4.780 Y10.509 E0.01634 F180.000
G1 X5.244 Y9.705 E0.01189
G1 X6.521 Y9.705 E0.01634
G1 X6.986 Y10.509 E0.01189
G1 X8.263 Y10.509 E0.01634
G1 X8.727 Y9.705 E0.01189
G1 X10.004 Y9.705 E0.01634
G1 X10.468 Y10.509 E0.01189
G1 X10.944 Y10.509 E0.00609
G1 X10.944 Y10.710 E0.00257
G1 X10.468 Y10.710 E0.00609
G1 X10.327 Y10.956 E0.00363
G1 X8.404 Y10.956 E0.02461
G1 X8.263 Y10.710 E0.00363
G1 X6.986 Y10.710 E0.01634
G1 X6.844 Y10.956 E0.00363
G1 X4.922 Y10.956 E0.02461
G1 X4.780 Y10.710 E0.00363
G1 X3.503 Y10.710 E0.01634
G1 X3.362 Y10.956 E0.00363
G1 X1.846 Y10.956 E0.01940
G1 X1.846 Y9.705 E0.01601
G1 X3.039 Y9.705 E0.01527
G1 X3.503 Y10.509 E0.01189
G1 X0.395 Y0.992 F180.000
G1 X-0.003 Y0.992 F180.000
G1 X0.000 Y1.061 F180.000
G1 X-0.395 Y1.061 F180.000
G1 X-1.645 Y1.725 F180.000
G1 X-1.645 Y11.226 E0.12161
F180.000
G1 X-11.145 Y11.226 E0.12161
G1 X-11.145 Y1.725 E0.12161
G1 X-1.669 Y1.725 E0.12130
G1 X-1.475 Y1.556 F180.000
G1 X-1.475 Y11.396 E0.08679
F180.000
G1 X-11.315 Y11.396 E0.08679
G1 X-11.315 Y1.556 E0.08679
G1 X-1.499 Y1.556 E0.08657

G1 X-1.555 Y1.694 F180.000
G1 X-2.322 Y2.536 F180.000
G1 X-1.846 Y2.536 E0.00609 F180.000
G1 X-1.846 Y2.737 E0.00257
G1 X-2.322 Y2.737 E0.00609
G1 X-2.786 Y3.541 E0.01189
G1 X-4.063 Y3.541 E0.01634
G1 X-4.528 Y2.737 E0.01189
G1 X-5.804 Y2.737 E0.01634
G1 X-6.269 Y3.541 E0.01189
G1 X-7.546 Y3.541 E0.01634
G1 X-8.010 Y2.737 E0.01189
G1 X-9.287 Y2.737 E0.01634
G1 X-9.751 Y3.541 E0.01189
G1 X-10.944 Y3.541 E0.01527
G1 X-10.944 Y1.926 E0.02067
G1 X-9.639 Y1.926 E0.01671
G1 X-9.287 Y2.536 E0.00901
G1 X-8.010 Y2.536 E0.01634
G1 X-7.658 Y1.926 E0.00901
G1 X-6.156 Y1.926 E0.01922
G1 X-5.804 Y2.536 E0.00901
G1 X-4.528 Y2.536 E0.01634
G1 X-4.176 Y1.926 E0.00901
G1 X-2.674 Y1.926 E0.01922
G1 X-2.322 Y2.536 E0.00901
G1 X-9.287 Y4.547 F180.000
G1 X-8.010 Y4.547 E0.01634 F180.000
G1 X-7.546 Y3.742 E0.01189
G1 X-6.269 Y3.742 E0.01634
G1 X-5.804 Y4.547 E0.01189
G1 X-4.528 Y4.547 E0.01634
G1 X-4.063 Y3.742 E0.01189
G1 X-2.786 Y3.742 E0.01634
G1 X-2.322 Y4.547 E0.01189
G1 X-1.846 Y4.547 E0.00609
G1 X-1.846 Y4.748 E0.00257
G1 X-2.322 Y4.748 E0.00609
G1 X-2.786 Y5.552 E0.01189
G1 X-4.063 Y5.552 E0.01634
G1 X-4.528 Y4.748 E0.01189
G1 X-5.804 Y4.748 E0.01634
G1 X-6.269 Y5.552 E0.01189
G1 X-7.546 Y5.552 E0.01634
G1 X-8.010 Y4.748 E0.01189
G1 X-9.287 Y4.748 E0.01634
G1 X-9.751 Y5.552 E0.01189
G1 X-10.944 Y5.552 E0.01527
G1 X-10.944 Y3.742 E0.02316
G1 X-9.751 Y3.742 E0.01527
G1 X-9.287 Y4.547 E0.01189
G1 X-9.287 Y6.557 F180.000
G1 X-8.010 Y6.557 E0.01634 F180.000
G1 X-7.546 Y5.753 E0.01189
G1 X-6.269 Y5.753 E0.01634
G1 X-5.804 Y6.557 E0.01189
G1 X-4.528 Y6.557 E0.01634
G1 X-4.063 Y5.753 E0.01189
G1 X-2.786 Y5.753 E0.01634
G1 X-2.322 Y6.557 E0.01189
G1 X-1.846 Y6.557 E0.00609
G1 X-1.846 Y6.758 E0.00257
G1 X-2.322 Y6.758 E0.00609
G1 X-2.786 Y7.562 E0.01189
G1 X-4.063 Y7.562 E0.01634
G1 X-4.528 Y6.758 E0.01189
G1 X-5.804 Y6.758 E0.01634
G1 X-6.269 Y7.562 E0.01189
G1 X-7.546 Y7.562 E0.01634
G1 X-8.010 Y6.758 E0.01189

G1 X-9.287 Y6.758 E0.01634
G1 X-9.751 Y7.562 E0.01189
G1 X-10.944 Y7.562 E0.01527
G1 X-10.944 Y5.753 E0.02316
G1 X-9.751 Y5.753 E0.01527
G1 X-9.287 Y6.557 E0.01189
G1 X-9.287 Y8.568 F180.000
G1 X-8.010 Y8.568 E0.01634 F180.000
G1 X-7.546 Y7.764 E0.01189
G1 X-6.269 Y7.764 E0.01634
G1 X-5.804 Y8.568 E0.01189
G1 X-4.528 Y8.568 E0.01634
G1 X-4.063 Y7.764 E0.01189
G1 X-2.786 Y7.764 E0.01634
G1 X-2.322 Y8.568 E0.01189
G1 X-1.846 Y8.568 E0.00609
G1 X-1.846 Y8.769 E0.00257
G1 X-2.322 Y8.769 E0.00609
G1 X-2.786 Y9.573 E0.01189
G1 X-4.063 Y9.573 E0.01634
G1 X-4.528 Y8.769 E0.01189
G1 X-5.804 Y8.769 E0.01634
G1 X-6.269 Y9.573 E0.01189
G1 X-7.546 Y9.573 E0.01634
G1 X-8.010 Y8.769 E0.01189
G1 X-9.287 Y8.769 E0.01634
G1 X-9.751 Y9.573 E0.01189
G1 X-10.944 Y9.573 E0.01527
G1 X-10.944 Y7.764 E0.02316
G1 X-9.751 Y7.764 E0.01527
G1 X-9.287 Y8.568 E0.01189
G1 X-9.287 Y10.578 F180.000
G1 X-8.010 Y10.578 E0.01634 F180.000
G1 X-7.546 Y9.774 E0.01189
G1 X-6.269 Y9.774 E0.01634
G1 X-5.804 Y10.578 E0.01189
G1 X-4.528 Y10.578 E0.01634
G1 X-4.063 Y9.774 E0.01189
G1 X-2.786 Y9.774 E0.01634
G1 X-2.322 Y10.578 E0.01189
G1 X-1.846 Y10.578 E0.00609
G1 X-1.846 Y10.779 E0.00257
G1 X-2.322 Y10.779 E0.00609
G1 X-2.464 Y11.025 E0.00363
G1 X-4.386 Y11.025 E0.02461
G1 X-4.528 Y10.779 E0.00363
G1 X-5.804 Y10.779 E0.01634
G1 X-5.946 Y11.025 E0.00363
G1 X-7.868 Y11.025 E0.02461
G1 X-8.010 Y10.779 E0.00363
G1 X-9.287 Y10.779 E0.01634
G1 X-9.429 Y11.025 E0.00363
G1 X-10.944 Y11.025 E0.01940
G1 X-10.944 Y9.774 E0.01601
G1 X-9.751 Y9.774 E0.01527
G1 X-9.287 Y10.578 E0.01189
G1 X-0.981 Y0.476 F180.000
G1 X-0.369 Y0.045 F180.000
G1 X-0.035 Y-0.768 F180.000
G1 X-0.035 Y-0.792 F180.000
G1 X-0.304 Y-1.061 F180.000
G1 X-1.554 Y-11.226 F180.000
G1 X-1.554 Y-1.725 E0.12161 F180.000
G1 X-11.054 Y-1.725 E0.12161
G1 X-11.054 Y-11.226 E0.12161
G1 X-1.578 Y-11.226 E0.12130
G1 X-1.384 Y-11.396 F180.000
G1 X-1.384 Y-1.556 E0.08679 F180.000
G1 X-11.224 Y-1.556 E0.08679

G1 X-11.224 Y-11.396 E0.08679
G1 X-1.408 Y-11.396 E0.08657
G1 X-1.464 Y-11.257 F180.000
G1 X-2.231 Y-10.415 F180.000
G1 X-1.755 Y-10.415 E0.00609 F180.000
G1 X-1.755 Y-10.214 E0.00257
G1 X-2.231 Y-10.214 E0.00609
G1 X-2.695 Y-9.410 E0.01189
G1 X-3.972 Y-9.410 E0.01634
G1 X-4.437 Y-10.214 E0.01189
G1 X-5.714 Y-10.214 E0.01634
G1 X-6.178 Y-9.410 E0.01189
G1 X-7.455 Y-9.410 E0.01634
G1 X-7.919 Y-10.214 E0.01189
G1 X-9.196 Y-10.214 E0.01634
G1 X-9.660 Y-10.415 E0.01189
G1 X-10.853 Y-9.410 E0.01527
G1 X-10.853 Y-11.025 E0.02067
G1 X-9.548 Y-11.025 E0.01671
G1 X-9.196 Y-10.415 E0.00901
G1 X-7.919 Y-10.415 E0.01634
G1 X-7.567 Y-11.025 E0.00901
G1 X-6.065 Y-11.025 E0.01922
G1 X-5.714 Y-10.415 E0.00901
G1 X-4.437 Y-10.415 E0.01634
G1 X-4.085 Y-11.025 E0.00901
G1 X-2.583 Y-11.025 E0.01922
G1 X-2.231 Y-10.415 E0.00901
G1 X-9.196 Y-8.405 F180.000
G1 X-7.919 Y-8.405 E0.01634 F180.000
G1 X-7.455 Y-9.209 E0.01189
G1 X-6.178 Y-9.209 E0.01634
G1 X-5.714 Y-8.405 E0.01189
G1 X-4.437 Y-8.405 E0.01634
G1 X-3.972 Y-9.209 E0.01189
G1 X-2.695 Y-9.209 E0.01634
G1 X-2.231 Y-8.405 E0.01189
G1 X-1.755 Y-8.405 E0.00609
G1 X-1.755 Y-8.204 E0.00257
G1 X-2.231 Y-8.204 E0.00609
G1 X-2.695 Y-7.399 E0.01189
G1 X-3.972 Y-7.399 E0.01634
G1 X-4.437 Y-8.204 E0.01189
G1 X-5.714 Y-8.204 E0.01634
G1 X-6.178 Y-7.399 E0.01189
G1 X-7.455 Y-7.399 E0.01634
G1 X-7.919 Y-8.204 E0.01189
G1 X-9.196 Y-8.204 E0.01634
G1 X-9.660 Y-7.399 E0.01189
G1 X-10.853 Y-7.399 E0.01527
G1 X-10.853 Y-9.209 E0.02316
G1 X-9.660 Y-9.209 E0.01527
G1 X-9.196 Y-8.405 E0.01189
G1 X-9.196 Y-6.394 F180.000
G1 X-7.919 Y-6.394 E0.01634 F180.000
G1 X-7.455 Y-7.198 E0.01189
G1 X-6.178 Y-7.198 E0.01634
G1 X-5.714 Y-6.394 E0.01189
G1 X-4.437 Y-6.394 E0.01634
G1 X-3.972 Y-7.198 E0.01189
G1 X-2.695 Y-7.198 E0.01634
G1 X-2.231 Y-6.394 E0.01189
G1 X-1.755 Y-6.394 E0.00609
G1 X-1.755 Y-6.193 E0.00257
G1 X-2.231 Y-6.193 E0.00609
G1 X-2.695 Y-5.389 E0.01189
G1 X-3.972 Y-5.389 E0.01634
G1 X-4.437 Y-6.193 E0.01189
G1 X-5.714 Y-6.193 E0.01634

G1 X-6.178 Y-5.389 E0.01189
 G1 X-7.455 Y-5.389 E0.01634
 G1 X-7.919 Y-6.193 E0.01189
 G1 X-9.196 Y-6.193 E0.01634
 G1 X-9.660 Y-5.389 E0.01189
 G1 X-10.853 Y-5.389 E0.01527
 G1 X-10.853 Y-7.198 E0.02316
 G1 X-9.660 Y-7.198 E0.01527
 G1 X-9.196 Y-6.394 E0.01189
 G1 X-9.196 Y-4.383 F180.000
 G1 X-7.919 Y-4.383 E0.01634 F180.000
 G1 X-7.455 Y-5.188 E0.01189
 G1 X-6.178 Y-5.188 E0.01634
 G1 X-5.714 Y-4.383 E0.01189
 G1 X-4.437 Y-4.383 E0.01634
 G1 X-3.972 Y-5.188 E0.01189
 G1 X-2.695 Y-5.188 E0.01634
 G1 X-2.231 Y-4.383 E0.01189
 G1 X-1.755 Y-4.383 E0.00609
 G1 X-1.755 Y-4.182 E0.00257
 G1 X-2.231 Y-4.182 E0.00609
 G1 X-2.695 Y-3.378 E0.01189
 G1 X-3.972 Y-3.378 E0.01634
 G1 X-4.437 Y-4.182 E0.01189
 G1 X-5.714 Y-4.182 E0.01634
 G1 X-6.178 Y-3.378 E0.01189
 G1 X-7.455 Y-3.378 E0.01634
 G1 X-7.919 Y-4.182 E0.01189
 G1 X-9.196 Y-4.182 E0.01634
 G1 X-9.660 Y-3.378 E0.01189
 G1 X-10.853 Y-3.378 E0.01527
 G1 X-10.853 Y-5.188 E0.02316
 G1 X-9.660 Y-5.188 E0.01527
 G1 X-9.196 Y-4.383 E0.01189
 G1 X-9.196 Y-2.373 F180.000
 G1 X-7.919 Y-2.373 E0.01634 F180.000

G1 X-7.455 Y-3.177 E0.01189
 G1 X-6.178 Y-3.177 E0.01634
 G1 X-5.714 Y-2.373 E0.01189
 G1 X-4.437 Y-2.373 E0.01634
 G1 X-3.972 Y-3.177 E0.01189
 G1 X-2.695 Y-3.177 E0.01634
 G1 X-2.231 Y-2.373 E0.01189
 G1 X-1.755 Y-2.373 E0.00609
 G1 X-1.755 Y-2.172 E0.00257
 G1 X-2.231 Y-2.172 E0.00609
 G1 X-2.373 Y-1.926 E0.00363
 G1 X-4.295 Y-1.926 E0.02461
 G1 X-4.437 Y-2.172 E0.00363
 G1 X-5.714 Y-2.172 E0.01634
 G1 X-5.855 Y-1.926 E0.00363
 G1 X-7.778 Y-1.926 E0.02461
 G1 X-7.919 Y-2.172 E0.00363
 G1 X-9.196 Y-2.172 E0.01634
 G1 X-9.338 Y-1.926 E0.00363
 G1 X-10.853 Y-1.926 E0.01940
 G1 X-10.853 Y-3.177 E0.01601
 G1 X-9.660 Y-3.177 E0.01527
 G1 X-9.196 Y-2.373 E0.01189
 G1 X-0.304 Y-11.890 F180.000
 G1 X-0.023 Y-12.171 F180.000
 G1 X-0.002 Y-13.297 F180.000
 G1 X0.831 Y-12.464 F180.000
 G1 X10.996 Y-11.214 F180.000
 G1 X10.996 Y-1.713 E0.12161 F180.000
 G1 X1.495 Y-1.713 E0.12161
 G1 X1.495 Y-11.214 E0.12161
 G1 X10.972 Y-11.214 E0.12130
 G1 X11.166 Y-11.384 F180.000
 G1 X11.166 Y-1.544 E0.08679 F180.000

G1 X1.326 Y-1.544 E0.08679
 G1 X1.326 Y-11.384 E0.08679
 G1 X11.142 Y-11.384 E0.08657
 G1 X11.086 Y-11.245 F180.000
 G1 X10.319 Y-10.403 F180.000
 G1 X10.795 Y-10.403 E0.00609 F180.000
 G1 X10.795 Y-10.202 E0.00257
 G1 X10.319 Y-10.202 E0.00609
 G1 X9.854 Y-9.398 E0.01189
 G1 X8.577 Y-9.398 E0.01634
 G1 X8.113 Y-10.202 E0.01189
 G1 X6.836 Y-10.202 E0.01634
 G1 X6.372 Y-9.398 E0.01189
 G1 X5.095 Y-9.398 E0.01634
 G1 X4.631 Y-10.202 E0.01189
 G1 X3.354 Y-10.202 E0.01634
 G1 X2.889 Y-9.398 E0.01189
 G1 X1.696 Y-9.398 E0.01527
 G1 X1.696 Y-11.013 E0.02067
 G1 X3.002 Y-11.013 E0.01671
 G1 X3.354 Y-10.403 E0.00901
 G1 X4.631 Y-10.403 E0.01634
 G1 X4.982 Y-11.013 E0.00901
 G1 X6.484 Y-11.013 E0.01922
 G1 X6.836 Y-10.403 E0.00901
 G1 X8.113 Y-10.403 E0.01634
 G1 X8.465 Y-11.013 E0.00901
 G1 X9.967 Y-11.013 E0.01922
 G1 X10.319 Y-10.403 E0.00901
 G1 X3.354 Y-8.393 F180.000
 G1 X4.631 Y-8.393 E0.01634 F180.000
 G1 X5.095 Y-9.197 E0.01189
 G1 X6.372 Y-9.197 E0.01634
 G1 X6.836 Y-8.393 E0.01189
 G1 X8.113 Y-8.393 E0.01634

PCL Rectilinear Scaffolds

```
<?xml version="1.0"?>
<profile name="Default" version="2017-03-01 08:00:00" app="S3D-Software 4.0.0">
  <printMaterial>PLA</printMaterial>
  <printQuality>Medium</printQuality>
  <printExtruders></printExtruders>
  <extruder name="Primary Extruder">
    <toolheadNumber>0</toolheadNumber>
    <diagrameter>0.35</diagrameter>
    <autoWidth>0</autoWidth>
    <width>0.4</width>
    <extrusionMultiplier>0.9</extrusionMultiplier>
    <useRetract>1</useRetract>
    <retractionDistance>1</retractionDistance>
    <extraRestartDistance>0</extraRestartDistance>
    <retractionZLift>0</retractionZLift>
    <retractionSpeed>1800</retractionSpeed>
    <useCoasting>0</useCoasting>
    <coastingDistance>0.2</coastingDistance>
    <useWipe>0</useWipe>
    <wipeDistance>5</wipeDistance>
    </extruder>
    <primaryExtruder>0</primaryExtruder>
    <layerHeight>0.2</layerHeight>
    <topSolidLayers>3</topSolidLayers>
    <bottomSolidLayers>3</bottomSolidLayers>
    <perimeterOutlines>2</perimeterOutlines>
    <printPerimetersInsideOut>1</printPerimetersInsideOut>
    <startPointOption>2</startPointOption>
    <startPointOriginX>0</startPointOriginX>
    <startPointOriginY>0</startPointOriginY>
    <startPointOriginZ>300</startPointOriginZ>
    <sequentialIslands>0</sequentialIslands>
    <spiralVaseMode>0</spiralVaseMode>
    <firstLayerHeightPercentage>100</firstLayerHeightPercentage>
    <firstLayerWidthPercentage>100</firstLayerWidthPercentage>
    <firstLayerUnderspeed>0.5</firstLayerUnderspeed>
    <useRaft>0</useRaft>
    <raftExtruder>0</raftExtruder>
    <raftTopLayers>3</raftTopLayers>
    <raftBaseLayers>2</raftBaseLayers>
    <raftOffset>3</raftOffset>
  </profile>
</xml>
```

```

<raftSeparationDistance>0.14</raftSeparationDistance>
<raftTopInfill>100</raftTopInfill>

<aboveRaftSpeedMultiplier>0.3</aboveRaftSpeedMultiplier>
<useSkirt>1</useSkirt>
<skirtExtruder>0</skirtExtruder>
<skirtLayers>1</skirtLayers>
<skirtOutlines>2</skirtOutlines>
<skirtOffset>4</skirtOffset>
<usePrimePillar>0</usePrimePillar>

<primePillarExtruder>999</primePillarExtruder>

<primePillarWidth>12</primePillarWidth>

<primePillarLocation>7</primePillarLocation>

<primePillarSpeedMultiplier>1</primePillarSpeedMultiplier>
<useOozeShield>0</useOozeShield>

<oozeShieldExtruder>999</oozeShieldExtruder>

<oozeShieldOffset>2</oozeShieldOffset>

<oozeShieldOutlines>1</oozeShieldOutlines>

<oozeShieldSidewallShape>1</oozeShieldSidewallShape>

<oozeShieldSidewallAngle>30</oozeShieldSidewallAngle>

<oozeShieldSpeedMultiplier>1</oozeShieldSpeedMultiplier>
<infillExtruder>0</infillExtruder>

<internalInfillPattern>Rectilinear</internalInfillPattern>

<externalInfillPattern>Rectilinear</externalInfillPattern>
<infillPercentage>20</infillPercentage>

<outlineOverlapPercentage>15</outlineOverlapPercentage>

<infillExtrusionWidthPercentage>100</infillExtrusionWidthPercentage>
<minInfillLength>5</minInfillLength>

<infillLayerInterval>1</infillLayerInterval>
<internalInfillAngles>45,-45</internalInfillAngles>

```

```

<overlapInternalInfillAngles>0</overlapInternalInfillAngles>
<externalInfillAngles>45,-45</externalInfillAngles>

<generateSupport>0</generateSupport>

<supportExtruder>0</supportExtruder>

<supportInfillPercentage>30</supportInfillPercentage>

<supportExtraInflation>0</supportExtraInflation>

<supportBaseLayers>0</supportBaseLayers>

<denseSupportExtruder>0</denseSupportExtruder>

<denseSupportLayers>0</denseSupportLayers>

<denseSupportInfillPercentage>70</denseSupportInfillPercentage>

<supportLayerInterval>1</supportLayerInterval>

<supportHorizontalPartOffset>0.3</supportHorizontalPartOffset>

<supportUpperSeparationLayers>1</supportUpperSeparationLayers>

<supportLowerSeparationLayers>1</supportLowerSeparationLayers>
<supportType>0</supportType>

<supportGridSpacing>4</supportGridSpacing>

<maxOverhangAngle>45</maxOverhangAngle>
<supportAngles>0</supportAngles>
<temperatureController name="Primary Extruder">

<temperatureNumber>0</temperatureNumber>
<isHeatedBed>0</isHeatedBed>

<stabilizeAtStartup>1</stabilizeAtStartup>
<setpoint layer="1" temperature="190"/>
</temperatureController>
<fanSpeed>
<setpoint layer="1" speed="0"/>
<setpoint layer="2" speed="100"/>
</fanSpeed>

```

```

<blipFanToFullPower>0</blipFanToFullPower>

<adjustSpeedForCooling>1</adjustSpeedForCooling>

<minSpeedLayerTime>15</minSpeedLayerTime>

<minCoolingSpeedSlowdown>20</minCoolingSpeedSlowdown>

<increaseFanForCooling>0</increaseFanForCooling>

<minFanLayerTime>45</minFanLayerTime>

<maxCoolingFanSpeed>100</maxCoolingFanSpeed>

<increaseFanForBridging>0</increaseFanForBridging>

<bridgingFanSpeed>100</bridgingFanSpeed>
<use5D>1</use5D>

<relativeDistances>0</relativeDistances>

<allowEaxisZeroing>1</allowEaxisZeroing>

<independentExtruderAxes>0</independentExtruderAxes>
<includeM10123>0</includeM10123>
<stickySupport>1</stickySupport>

<applyToolheadOffsets>0</applyToolheadOffsets>
<gcodeXoffset>0</gcodeXoffset>
<gcodeYoffset>0</gcodeYoffset>
<gcodeZoffset>0</gcodeZoffset>

<overrideMachineDefinition>0</overrideMachineDefinition>

<machineTypeOverride>0</machineTypeOverride>

<strokeXoverride>200</strokeXoverride>

<strokeYoverride>200</strokeYoverride>

<strokeZoverride>200</strokeZoverride>

<originOffsetXoverride>0</originOffsetXoverride>

<originOffsetYoverride>0</originOffsetYoverride>

```

```

<originOffsetZoverride>0</originOffsetZ
override>
  <homeXdirOverride>
1</homeXdirOverride>
  <homeYdirOverride>
1</homeYdirOverride>
  <homeZdirOverride>
1</homeZdirOverride>
  <flipXoverride>1</flipXoverride>
  <flipYoverride>-1</flipYoverride>
  <flipZoverride>1</flipZoverride>

<toolheadOffsets>0,0|0,0|0,0|0,0|0,0|
0,0</toolheadOffsets>

<overrideFirmwareConfiguration>0</ov
errideFirmwareConfiguration>
  <firmwareTypeOverride>RepRap
(Marlin/Repetier/Sprinter)</firmwareTy
peOverride>

<GPXconfigOverride>r2</GPXconfigOve
rride>

<baudRateOverride>115200</baudRate
Override>

<overridePrinterModels>0</overridePri
nterModels>

<printerModelsOverride></printerMode
lsOverride>
  <startingGcode>G28 ; home all
axes</startingGcode>

<layerChangeGcode></layerChangeGco
de>
  <retractionGcode></retractionGcode>

<toolChangeGcode></toolChangeGcode
>
  <endingGcode>M104 S0 ; turn off
extruder,M140 S0 ; turn off bed,M84 ;
disable motors</endingGcode>

<exportFileFormat>gcode</exportFileFo
rmat>
  <celebration>0</celebration>
  <celebrationSong>Random
Song</celebrationSong>
  <postProcessing></postProcessing>
  <defaultSpeed>3600</defaultSpeed>

<outlineUnderspeed>0.5</outlineUnde
rspeed>

<solidInfillUnderspeed>0.8</solidInfillU
nderspeed>

<supportUnderspeed>0.8</supportUnde
rspeed>
  <rapidXYspeed>4800</rapidXYspeed>
  <rapidZspeed>1000</rapidZspeed>

```

```

<minBridgingArea>50</minBridgingArea
>

<bridgingExtraInflation>0</bridgingExtr
ainflation>

<bridgingExtrusionMultiplier>1</bridgin
gExtrusionMultiplier>

<bridgingSpeedMultiplier>1</bridgingSp
eedMultiplier>

<useFixedBridgingAngle>0</useFixedBri
dgingAngle>

<fixedBridgingAngle>0</fixedBridgingAn
gle>

<applyBridgingToPerimeters>0</applyBr
idgingToPerimeters>

<filamentDiameters>1.75|1.75|1.75|1.
75|1.75|1.75</filamentDiameters>

<filamentPricesPerKg>46|46|46|46|46|
46</filamentPricesPerKg>

<filamentDensities>1.25|1.25|1.25|1.2
5|1.25|1.25</filamentDensities>

<useMinPrintHeight>0</useMinPrintHei
ght>
  <minPrintHeight>0</minPrintHeight>

<useMaxPrintHeight>0</useMaxPrintHei
ght>
  <maxPrintHeight>0</maxPrintHeight>
  <useDiaphragm>0</useDiaphragm>

<diaphragmLayerInterval>20</diaphrag
mLayerInterval>
  <robustSlicing>1</robustSlicing>

<mergeAllIntoSolid>0</mergeAllIntoSoli
d>

<onlyRetractWhenCrossingOutline>1</o
nlyRetractWhenCrossingOutline>

<retractBetweenLayers>1</retractBetw
eenLayers>

<useRetractionMinTravel>0</useRetract
ionMinTravel>

<retractionMinTravel>3</retractionMin
Travel>

<retractWhileWiping>0</retractWhileW
iping>

<onlyWipeOutlines>1</onlyWipeOutline
s>

```

```

<avoidCrossingOutline>0</avoidCrossin
gOutline>

<maxMovementDetourFactor>3</max
MovementDetourFactor>

<toolChangeRetractionDistance>12</to
olChangeRetractionDistance>
  <toolChangeExtraRestartDistance>-
0.5</toolChangeExtraRestartDistance>

<toolChangeRetractionSpeed>600</tool
ChangeRetractionSpeed>

<externalThinWallType>0</externalThin
WallType>

<internalThinWallType>2</internalThin
WallType>

<thinWallAllowedOverlapPercentage>10
</thinWallAllowedOverlapPercentage>

<singleExtrusionMinLength>1</singleExt
rusionMinLength>

<singleExtrusionMinPrintingWidthPerce
ntage>50</singleExtrusionMinPrintingW
idthPercentage>

<singleExtrusionMaxPrintingWidthPerce
ntage>200</singleExtrusionMaxPrinting
WidthPercentage>

<singleExtrusionEndpointExtension>0.2<
/singleExtrusionEndpointExtension>

<horizontalSizeCompensation>0</horizo
ntalSizeCompensation>
  <autoConfigureMaterial name="PLA">

<globalExtruderTemperature>190</glob
alExtruderTemperature>

<globalBedTemperature>60</globalBed
Temperature>

<globalExtrusionMultiplier>0.9</globa
lExtrusionMultiplier>
  <fanSpeed>
    <setpoint layer="1" speed="0"/>
    <setpoint layer="2" speed="100"/>
  </fanSpeed>
</autoConfigureMaterial>
  <autoConfigureMaterial name="ABS">

<globalExtruderTemperature>225</glob
alExtruderTemperature>

<globalBedTemperature>100</globalBe
dTemperature>

<globalExtrusionMultiplier>1</globalExt
rusionMultiplier>
  <fanSpeed>

```



```

    <setpoint layer="1" speed="0"/>
  </fanSpeed>
</autoConfigureMaterial>
<autoConfigureMaterial name="PVA">

<globalExtruderTemperature>195</globalExtruderTemperature>

<globalBedTemperature>80</globalBedTemperature>

<globalExtrusionMultiplier>1</globalExtrusionMultiplier>
  <fanSpeed>
    <setpoint layer="1" speed="0"/>
    <setpoint layer="2" speed="100"/>
  </fanSpeed>
</autoConfigureMaterial>
<autoConfigureMaterial name="Nylon">

<globalExtruderTemperature>220</globalExtruderTemperature>

</profile>

```

```

<globalBedTemperature>80</globalBedTemperature>

<globalExtrusionMultiplier>1</globalExtrusionMultiplier>
  <fanSpeed>
    <setpoint layer="1" speed="0"/>
  </fanSpeed>
</autoConfigureMaterial>
<autoConfigureQuality name="Fast">
  <layerHeight>0.3</layerHeight>
  <topSolidLayers>3</topSolidLayers>

<bottomSolidLayers>3</bottomSolidLayers>
  <skirtLayers>1</skirtLayers>

<infillPercentage>15</infillPercentage>

<supportInfillPercentage>25</supportInfillPercentage>
  </autoConfigureQuality>
<autoConfigureQuality name="Medium">

```

```

  <layerHeight>0.2</layerHeight>
  <topSolidLayers>3</topSolidLayers>

<bottomSolidLayers>3</bottomSolidLayers>
  <skirtLayers>1</skirtLayers>

<infillPercentage>20</infillPercentage>

<supportInfillPercentage>30</supportInfillPercentage>
  </autoConfigureQuality>
  <autoConfigureQuality name="High">
    <layerHeight>0.1</layerHeight>
    <topSolidLayers>4</topSolidLayers>

<bottomSolidLayers>4</bottomSolidLayers>
  <skirtLayers>2</skirtLayers>

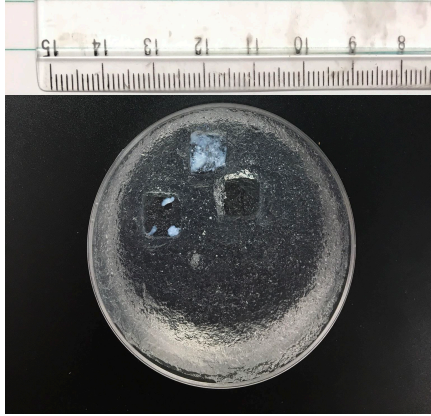
<infillPercentage>30</infillPercentage>

<supportInfillPercentage>40</supportInfillPercentage>
  </autoConfigureQuality>

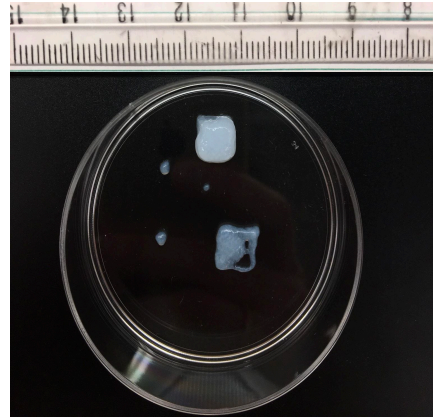
```

Appendix C: Summary of Early Embedded Printing Attempts

Variable	Settings Attempted
Needle	30G 18G
Print Speed	5% - 100%
First Layer Print Speed	10% 20% 50%
Extrusion Multiplier	0.45 0.5 0.6 0.9
Bioink Dilution	None 5:2 2:1
Infill Density	20% 40% 70% 100%
Infill Pattern	Line Rectilinear Hexagonal
Infill/Perimeter Overlap	0% 10%
Support	Gelatin blended microparticle slurry Dry culture plastic
Gelatin Slurry Preparation	Blend: 60 s, 90 s, 120 s Centrifugation: 225G for 5 min, 300G for 5 min, 3800G for 4 min, 4000G for 5 min Temperature: room temperature preparation, kept on ice and centrifuged at 4°C



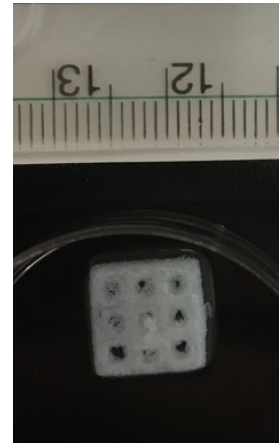
18 G print nozzle and unoptimized support slurry preparation displaced gelatin microparticles during printing



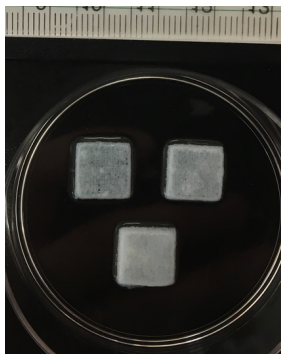
Unoptimized printing parameters resulted in bioink ejection issues



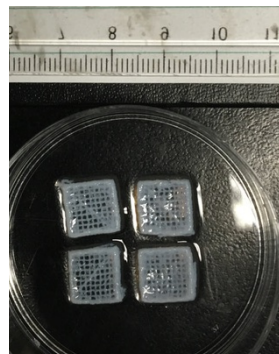
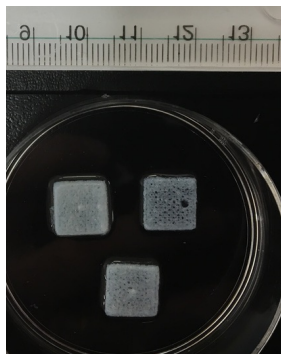
Compromised print resolution was observed when a gelatin slurry blended for 60 s was employed



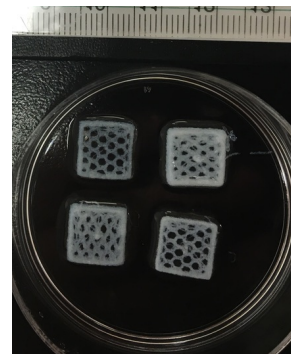
Higher print resolution was achieved when gelatin slurry was blended for 120 s



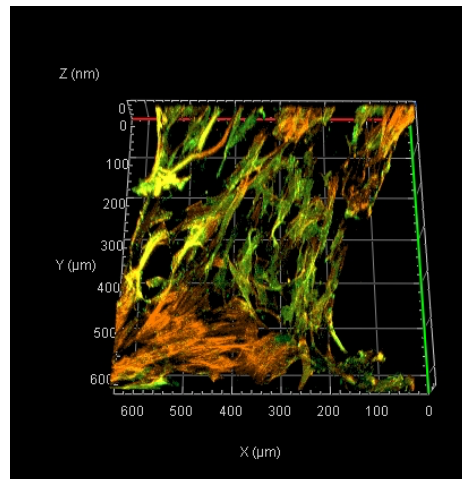
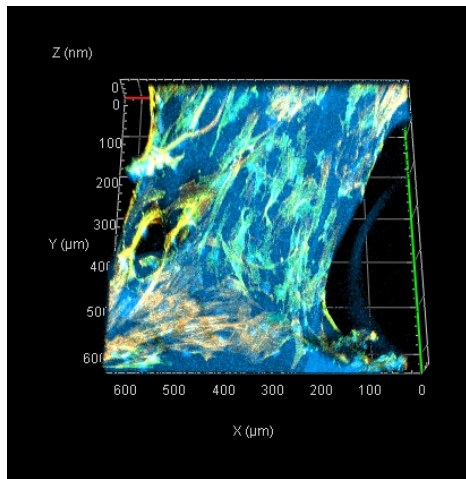
Rectilinear (L) and hexagonal (R) 40% infill density was too dense



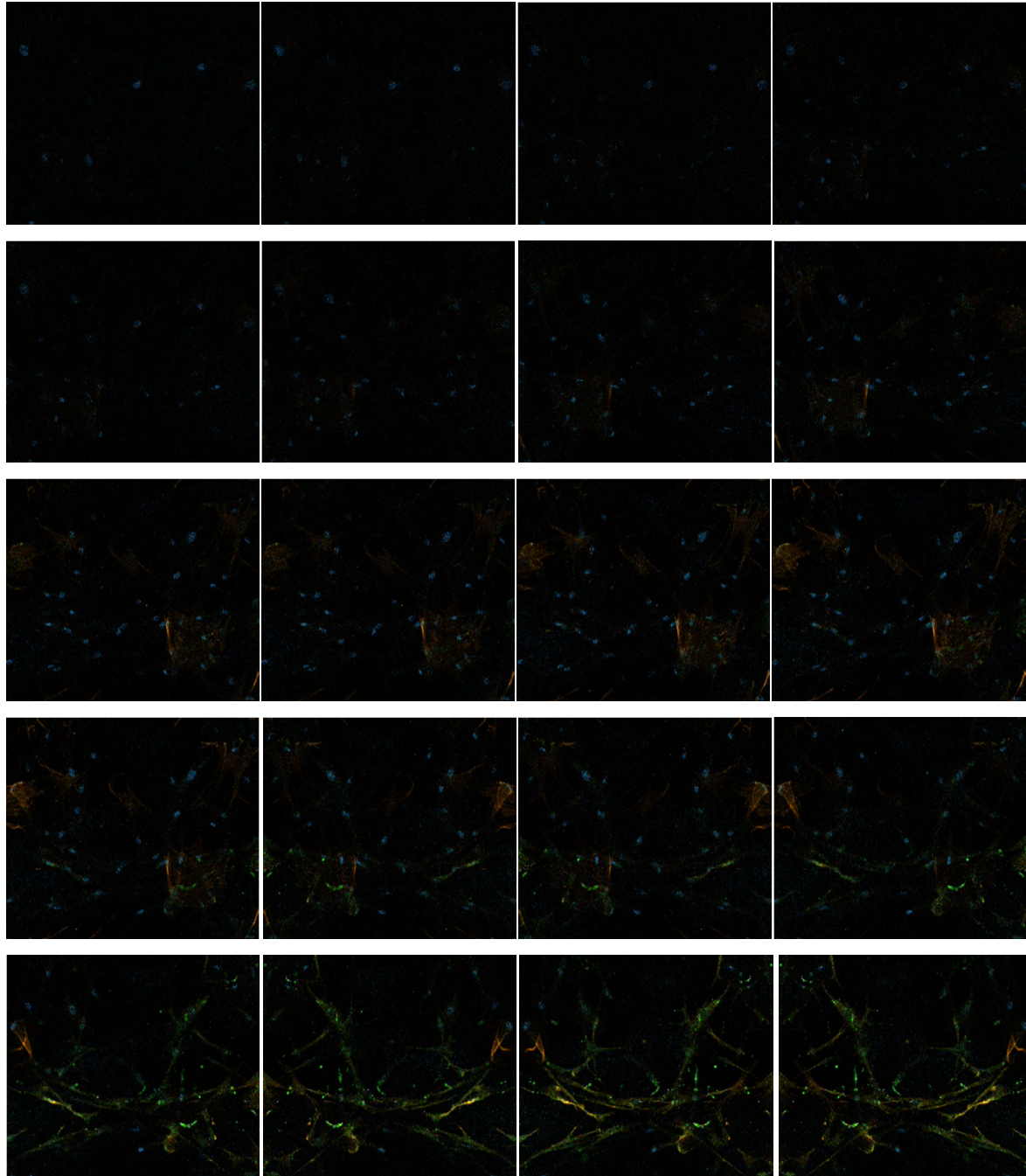
Rectilinear (L) and hexagonal (R) 20% infill resulted in reproducible porosity



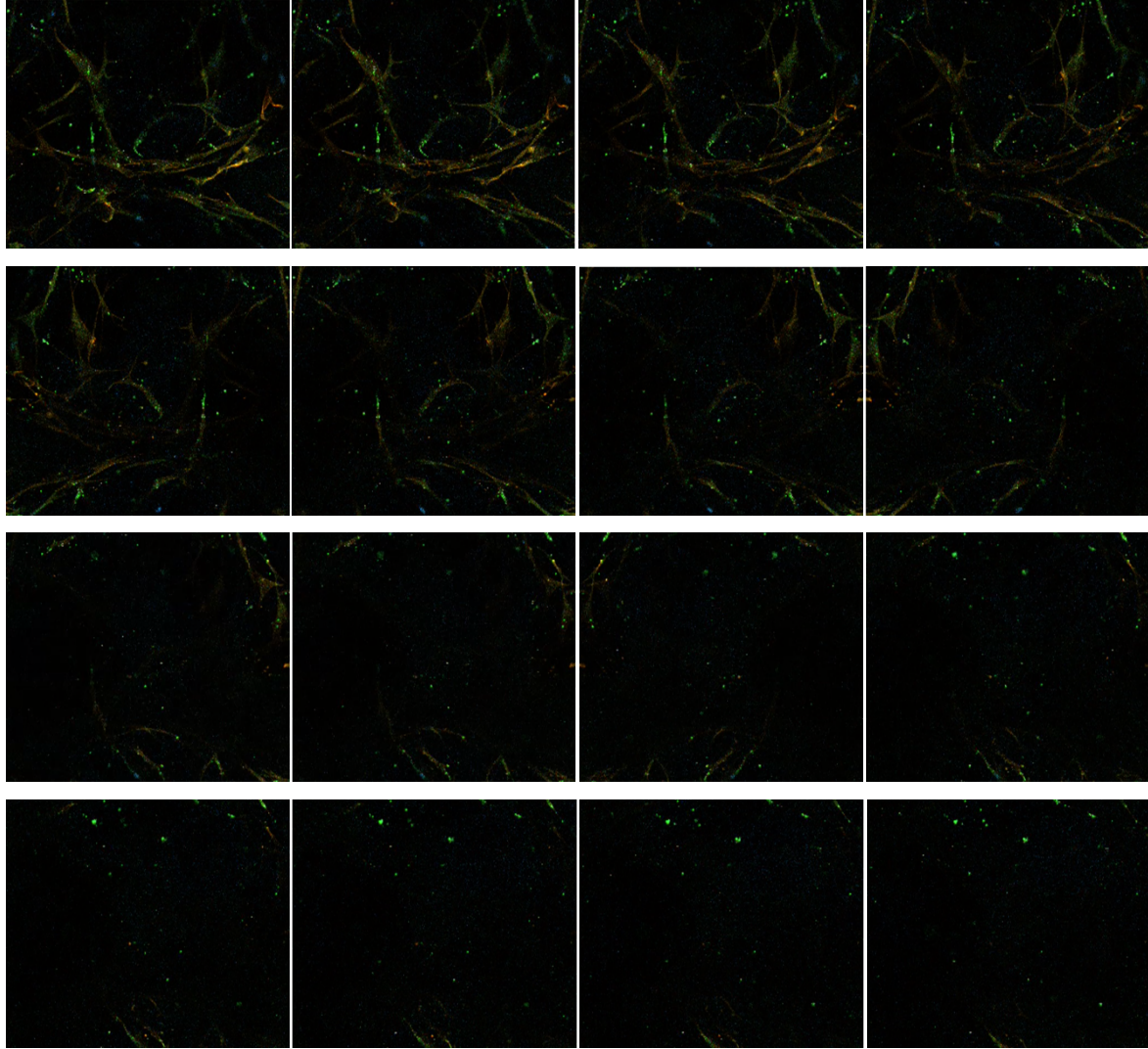
Appendix D: Autofluorescence of PCL Scaffolds



Appendix E: Example of the Appearance of Individual Z Slices for Scaffold
Confocal Microscopy

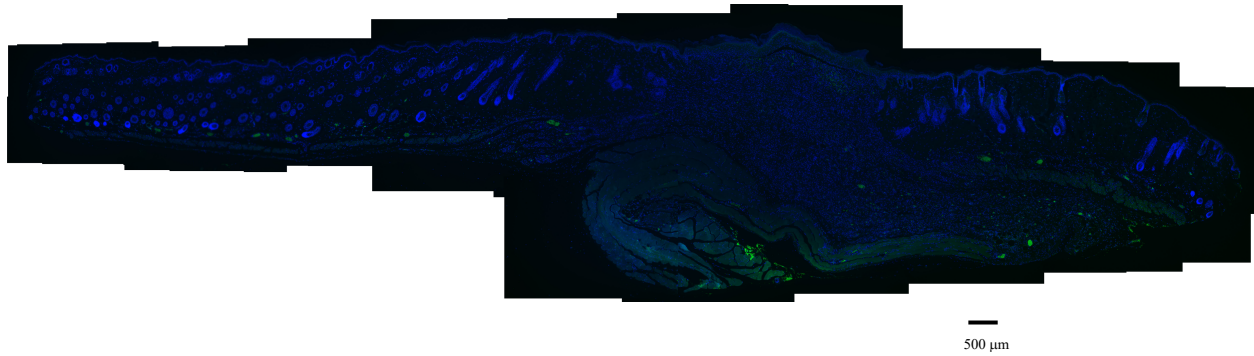


600 μm



600 μm

Appendix F: Arginase-I Immunofluorescent Staining of Day 9 Murine Wound
Sections No Primary Antibody Negative Control



Appendix G: Research Ethics Approvals



PI :	Hamilton, Doug
Protocol #	2016-085
Status :	Approved (w/o Stipulation)
Approved :	01/09/2017
Expires :	01/01/2021
Title :	Influence of biomaterials and material physiochemical properties on cell behaviour in vitro and in vivo.

Table of Contents

- [Animal Use Protocol Overview](#)
- [Funding Source List](#)
- [Purpose of Animal Use](#)
- [Hazardous Materials](#)
- [Animal Movement Between Sites](#)
- [Animal Groups and Experimental Timelines Overview](#)
- Mouse**
 - [Tissue Collection](#)
 - [Justification for Choice of Species](#)
 - [the 3Rs: Replace, Reduce, Refine](#)
 - [Species Strains](#)
 - [Animal Transfers](#)
 - [Environmental Enrichment](#)
 - [Animal Holding/Housing and Use Location Information](#)
 - [Holding beyond 12 hours](#)
 - [Acclimatization Period & Quarantine](#)
 - [Breeding Information](#)
 - [Experimental Agents Information](#)
 - [SOP List](#)
 - [Procedures Checklist for Reporting and Training](#)
 - [Procedures Narrative](#)
 - [Procedural Consequences & Monitoring](#)
 - [Endpoint Method Information](#)
 - [Animal Numbers Requested](#)
- Rabbit**
 - [Tissue Collection](#)
 - [Justification for Choice of Species](#)
 - [the 3Rs: Replace, Reduce, Refine](#)
 - [Species Strains](#)
 - [Animal Transfers](#)
 - [Environmental Enrichment](#)
 - [Animal Holding/Housing and Use Location Information](#)
 - [Holding beyond 12 hours](#)
 - [Acclimatization Period & Quarantine](#)
 - [SOP List](#)
 - [Procedures Narrative](#)
 - [Procedural Consequences & Monitoring](#)
 - [Animal Numbers Requested](#)
- Rat**
 - [Tissue Collection](#)
 - [Justification for Choice of Species](#)
 - [the 3Rs: Replace, Reduce, Refine](#)
 - [Species Strains](#)
 - [Animal Transfers](#)
 - [Environmental Enrichment](#)
 - [Animal Holding/Housing and Use Location Information](#)
 - [Holding beyond 12 hours](#)
 - [Acclimatization Period & Quarantine](#)
 - [Experimental Agents Information](#)



Western Research

Date: 27 June 2019

To: Dr. Douglas Hamilton

Project ID: 6311

Study Title: Role of periostin in the repair of skin - 16245E

Application Type: Continuing Ethics Review (CER) Form

Review Type: Delegated

REB Meeting Date: 02/Jul/2019

Date Approval Issued: 27/Jun/2019

REB Approval Expiry Date: 24/Jun/2020

Lapse in Approval: June 25, 2019 to June 27, 2019

Dear Dr. Douglas Hamilton,

The Western University Research Ethics Board has reviewed the application. This study, including all currently approved documents, has been re-approved until the expiry date noted above.

REB members involved in the research project do not participate in the review, discussion or decision.

Western University REB operates in compliance with, and is constituted in accordance with, the requirements of the TriCouncil Policy Statement: Ethical Conduct for Research Involving Humans (TCPS 2); the International Conference on Harmonisation Good Clinical Practice Consolidated Guideline (ICH GCP); Part C, Division 5 of the Food and Drug Regulations; Part 4 of the Natural Health Products Regulations; Part 3 of the Medical Devices Regulations and the provisions of the Ontario Personal Health Information Protection Act (PHIPA 2004) and its applicable regulations. The REB is registered with the U.S. Department of Health & Human Services under the IRB registration number IRB 00000940.

Please do not hesitate to contact us if you have any questions.

Sincerely,

Daniel Wyzynski, Research Ethics Coordinator, on behalf of Dr. Joseph Gilbert, HSREB Chair

Note: This correspondence includes an electronic signature (validation and approval via an online system that is compliant with all regulations).

Curriculum Vitae

Name Madeleine Di Gregorio

Post-Secondary Education and Degrees University of Toronto
Toronto, Ontario, Canada
2013-2017 BSc

The University of Western Ontario
London, Ontario, Canada
2017-2019 MEd

Related Work Experience Teaching Assistant
The University of Western Ontario
2018

Publications

PD Arora, **M Di Gregorio**, P He, CA McCulloch. 2017. TRPV4 mediates the Ca²⁺ influx required for the interaction between flightless-1 and non-muscle myosin, and collagen remodeling. J Cell Sci 130: 2196-2208; doi: 10.1242/jcs.201665.